

AD634137

UNCLASSIFIED
TECHNICAL REPORT VU-65-4A

AIR FORCE TECHNICAL APPLICATIONS CENTER
HEADQUARTERS UNITED STATES AIR FORCE
WASHINGTON DC 20333

MAGNITUDE DETERMINATION
AT
REGIONAL AND NEAR-REGIONAL DISTANCES
IN THE UNITED STATES
UNCLASSIFIED VERSION

CLEARINGHOUSE FOR FEDERAL SCIENTIFIC AND TECHNICAL INFORMATION		
Hardcopy	Microfiche	
\$4.00	\$1.00	145 pp as
ARCHIVE COPY		

30 AUGUST 65

PREPARED FOR
ARPA PROJECT VELA-UNIFORM

BY

AF TECHNICAL APPLICATIONS CENTER
VELA SEISMOLOGICAL CENTER

DDC
RECEIVED
JUN 23 1966
C

DISTRIBUTION OF THIS
DOCUMENT IS UNLIMITED.

**Best
Available
Copy**

AIR FORCE TECHNICAL APPLICATIONS CENTER
HEADQUARTERS UNITED STATES AIR FORCE
WASHINGTON DC 20333


MAJOR GENERAL J. F. RODENHAUSER, CHIEF

MAGNITUDE DETERMINATION AT REGIONAL AND NEAR-REGIONAL
DISTANCES IN THE UNITED STATES

AFTAC/VELA SEISMOLOGICAL CENTER
TECHNICAL REPORT VU-65-4A
PROJECT VELA-UNIFORM

30 August 1965

PREPARED BY: JACK F. EVERNDEN
Research Associate

APPROVED BY: 
CARL F. ROMNEY
Assistant Technical Director
AF Technical Applications Center

DISTRIBUTION OF THIS
DOCUMENT IS UNLIMITED

NOTICE

This report is the unclassified version of Technical Report VU-65-4. All figures and discussions revealing classified data on weapons tests at the Nevada Test Site have been deleted. Such data in no way influences the seismological conclusions of this report.

ABSTRACT

1. This report deals with the problems of variation of P_n amplitudes in the regional and near-regional distance ranges (200-2100 kilometers). The data used were recorded by Long Range Seismic Measurement (LRSM) vans of the VELA Seismological Center as a result of earthquakes throughout the United States and numerous nuclear and chemical explosions in the same region.
2. It is shown that the patterns of P_n amplitudes versus Δ in Western and Eastern United States (WUS and EUS) are markedly different and that these differences are related to different velocity structures in the two regions. These differences extend to at least 150 kilometers depth.
3. Neither the WUS nor EUS patterns conform even approximately to that predicted or suggested by Gutenberg and Richter in the 1000-2000 kilometer range. The hypothesized shadow-zone does not exist and over-estimation of magnitude by as much as 1.5 magnitude units is frequently done because of failure to properly understand the patterns of radiation.
4. By proper calibration of WUS by use of numerous events, it is now possible to get consistent estimates of magnitude at all distance ranges for most explosions and earthquakes. This is very important when body wave magnitudes are used as an essential element in an identification criterion.
5. Obtaining consistent estimates of amplitude as a function of distance for a particular event requires a knowledge of the energy distribution between the several refracted phases used between 200 and 2500 kilometers distance. Data on hand show that the energy partition function is reasonably uniform throughout the regions investigated but that locally it may vary radically, resulting in a ten-fold change in relative excitation of two refracted phases.
6. Patterns of energy radiation, such as those for EUS and WUS, are probably approximately determinable from knowledge of velocity structure and vice versa but are not determinable from earthquake investigations. They are only determinable from explosion data where origin time and focus are accurately known.

CONTENTS

	Page
INTRODUCTION	1
EASTERN UNITED STATES	3
1. Travel-Time Curves for EUS	
2. Magnitudes as Computed by the Shot Report for EUS Events	4
3. The Dependence of A/T on Δ and the Computation of Magnitude for EUS Events	
WESTERN UNITED STATES	9
1. Travel-Time Curves for WUS	
2. Travel-Time Curves of FORE	10
3. Travel-Time Curves of MISSISSIPPI	
4. Travel-Time Curves of BILBY and CLEARWATER	11
5. Regional Variations of Travel-Time Curves in WUS	
6. Conclusion	
ESTABLISHMENT OF A/T VERSUS Δ CURVES FOR WESTERN UNITED STATES	12
1. P _{7.9} Arrivals	
2. P _{10.5} Arrivals	14
3. P _{8.5} Arrivals	
4. P _{8.1} Arrivals	
DETAILED ANALYSES OF STATION MAGNITUDE VALUES FOR MISSISSIPPI, BILBY, AND HARDHAT	15
1. Introduction	
2. MISSISSIPPI	16
3. BILBY	17
4. HARDHAT	18
COMPARISON OF MAGNITUDES COMPUTED BY m_{sr} AND THE SEVERAL CURVES OF THIS REPORT	20
RECALCULATION OF ALL SHOTS PREVIOUSLY ANALYZED IN SHOT REPORTS	20
RELATIVE MAGNITUDE BY USE OF DATA OF FIXED STATIONS	25
APPLICATION OF THE PHASE CURVES TO EARTHQUAKES OF WESTERN UNITED STATES	26
1. General	
2. Earthquakes Studied	27
3. Small Earthquakes	28
4. Libyan Earthquake of 21 February 1963	
USE OF P PHASES AS DIAGNOSTIC AIDS	28

	Page
VELOCITY STRUCTURE OF CRUST OR CRUST AND UPPER MANTLE IN EASTERN UNITED STATES AND WESTERN UNITED STATES	28
1. EUS	
2. WUS	29
APPLICATION OF IDEAS OF THIS PAPER TO REGIONS OUTSIDE THE UNITED STATES	30
1. General	
2. Europe	31
3. Asia	
CONCLUSIONS	31
APPENDIX - ANALYSIS OF P_g DATA	34
1. General	
2. Analysis of P_g Data from Shot Reports	
3. P_g Data for WUS Earthquakes	35

FIGURES

1. Epicenters of Events Studied
2. Reduced Travel-Time Data for SS VILLAGE
3. Reduced Travel-Time Data for SALMON
4. Reduced Travel-Time Data for GNOME - EASTERN PROFILE
5. Reduced Travel-Time Data for West Virginia Earthquake
6. Reduced Travel-Time Data for New Madrid Earthquake
7. Reduced Travel-Time Data for Poplar Bluff Earthquake
8. Magnitude versus Epicentral Distance for SS VILLAGE
9. Magnitude versus Epicentral Distance for SALMON
10. Magnitude versus Epicentral Distance for GNOME - EAST
11. Magnitude versus Epicentral Distance for Texas-Louisiana
Earthquake
12. Magnitude versus Epicentral Distance for West Virginia
Earthquake
13. Magnitude versus Epicentral Distance for New Madrid Earthquake
14. Magnitude versus Epicentral Distance for Poplar Bluff Earthquake
15. Magnitude versus Epicentral Distance for South Dakota-Nebraska
Earthquake
16. Magnitude versus Epicentral Distance for Western Vermont
Earthquake
17. Reduced Travel-Time Data and Curves for FORE
18. Reduced Travel-Time data and Curves for MISSISSIPPI
19. Reduced Travel-Time Data and Curves for BILBY
20. Reduced Travel-Time Data and Curves for CLEARWATER
21. Reduced Travel-Time Data and Curves for CLIMAX

22. Reduced Travel-Time Data and Curves for GNOME - WESTERN PROFILE
23. Reduced Travel-Time Curves for EUS, WUS, and Europe
24. Magnitude versus Epicentral Distance for SHREW
25. Deleted
26. Magnitude versus Epicentral Distance for MAD
27. Magnitude versus Epicentral Distance for MINK
28. Deleted
29. Magnitude versus Epicentral Distance for CHINCHILLA II
30. Magnitude versus Epicentral Distance for ROANOKE
31. Magnitude versus Epicentral Distance for CHINCHILLA
32. Deleted
33. Magnitude versus Epicentral Distance for ALLEGHENY
34. Magnitude versus Epicentral Distance for KAWEAH
35. Magnitude versus Epicentral Distance for STILLWATER
36. Magnitude versus Epicentral Distance for CODSAW
37. Magnitude versus Epicentral Distance for BOBAC
38. Magnitude versus Epicentral Distance for RINGTAIL
39. Magnitude versus Epicentral Distance for SACRAMENTO
40. Magnitude versus Epicentral Distance for STOAT
41. Magnitude versus Epicentral Distance for WICHITA
42. Magnitude versus Epicentral Distance for AGOUTI
43. Magnitude versus Epicentral Distance for SANTEE
44. Magnitude versus Epicentral Distance for ARMADILLO
45. Magnitude versus Epicentral Distance for PACKRAT
46. Magnitude versus Epicentral Distance for CASSELMAN
47. Magnitude versus Epicentral Distance for HYRAX
48. Deleted
49. Magnitude versus Epicentral Distance for ACUSHI
50. Magnitude versus Epicentral Distance for DORMOUSE PRIME
51. Magnitude versus Epicentral Distance for DORMOUSE
52. Magnitude versus Epicentral Distance for CIMARRON
53. Magnitude versus Epicentral Distance for YORK
54. Magnitude versus Epicentral Distance for PEBA
55. Magnitude versus Epicentral Distance for PASSAIC
56. Magnitude versus Epicentral Distance for FISHER
57. Magnitude versus Epicentral Distance for MERRIMAC
58. Magnitude versus Epicentral Distance for HAYMAKER
59. Magnitude versus Epicentral Distance for SEDAN
60. Magnitude versus Epicentral Distance for AARDVARK
61. Magnitude versus Epicentral Distance for STONES
62. Magnitude versus Epicentral Distance for FORE
63. Magnitude versus Epicentral Distance for WAGTAIL
64. Magnitude versus Epicentral Distance for MISSISSIPPI
65. Magnitude versus Epicentral Distance for BILBY
66. Magnitude versus Epicentral Distance for FEATHER
67. Magnitude versus Epicentral Distance for CHENA
68. Magnitude versus Epicentral Distance for PLATTE

69. Magnitude versus Epicentral Distance for ANTLER
70. Magnitude versus Epicentral Distance for MADISON
71. Magnitude versus Epicentral Distance for DES MOINES
72. Magnitude versus Epicentral Distance for MARSHMALLOW
73. Magnitude versus Epicentral Distance for CLEARWATER
74. Magnitude versus Epicentral Distance for HANDCAR
75. Magnitude versus Epicentral Distance for HARDHAT
76. Magnitude versus Epicentral Distance for SHOAL
77. Magnitude versus Epicentral Distance for DANNY BOY
78. Magnitude versus Epicentral Distance for GNOME - WEST
79. Magnitude versus Epicentral Distance for CLIMAX
80. Magnitude versus Epicentral Distance for SWORDFISH
81. Magnitude versus Epicentral Distance for Earthquake of 2 Feb 1962
82. Magnitude versus Epicentral Distance for Earthquake of 5 Feb 1962
83. Magnitude versus Epicentral Distance for Earthquake of 15 Feb 1962
84. Magnitude versus Epicentral Distance for Earthquake of 15 Feb 1962 (2)
85. Magnitude versus Epicentral Distance for Earthquake of 25 Feb 1962
86. Magnitude versus Epicentral Distance for Earthquake of 14 Apr 1962
87. Magnitude versus Epicentral Distance for Earthquake of 27 May 1962
88. Magnitude versus Epicentral Distance for Earthquake of 20 Jul 1962
89. Magnitude versus Epicentral Distance for Earthquake of 21 Aug 1962
90. Magnitude versus Epicentral Distance for Earthquake of 30 Aug 1962
91. Magnitude versus Epicentral Distance for Earthquake of 5 Sep 1962
92. Magnitude versus Epicentral Distance for Earthquake of 16 Sep 1962
93. Magnitude versus Epicentral Distance for Earthquake of 6 Nov 1962
94. Magnitude versus Epicentral Distance for Earthquake of 18 Nov 1963
95. Magnitude versus Epicentral Distance for Earthquake of 22 Mar 1964
96. Magnitude versus Epicentral Distance for Earthquake of 5 Jul 1964
97. Magnitude versus Epicentral Distance for Earthquake of 24 Oct 1964
98. Magnitude versus Epicentral Distance for Earthquake of 22 Dec 1964
99. Magnitude versus Epicentral Distance for Libyan Earthquake
100. A/T versus Δ for P Phases in the United States
101. Mean A/T versus Distance (10 KT - NTS Shots)
102. m_{ts} versus $\log (A/T)_{500}$ (NTS Shots)
103. A/T versus Δ for P_g for RINGTAIL
104. A/T versus Δ for P_g for FISHER
105. A/T versus Δ for P_g for MISSISSIPPI
106. A/T versus Δ for P_g for ANTLER
107. Deleted
108. $\log (A/T)_{500} P_g$ versus m_b
109. Deleted
110. Deleted

TABLES

	Page
I West Virginia Earthquake, 25 Nov 1964	5
Texas-Louisiana Earthquake, 24 Apr 1964	6
II m_b' versus Distance in EUS	8
III Lake Superior, Oct 1964	8
IV $m_{8.1}$ Magnitude Values	15
V MISSISSIPPI	16
VI BILBY	17
VII HARDHAT	18
VIII Magnitude Data on Selected NTS Shots	21
IX Comparison of m_b' and Individual Station Relative Magnitudes	25

LONG RANGE SEISMIC MEASUREMENT VAN LOCATION DESIGNATORS

APON	Apache, Oklahoma
ARWS	Aurora, Wisconsin
ATNV	Austin, Nevada
AYSD	Academy, South Dakota
AZTX	Amarillo, Texas
BLWV	Beckley, West Virginia
BMSO	Blue Mountains Seismological Observatory
BMTX	Balmorea, Texas
BRPA	Berlin, Pennsylvania
BXUT	Blanding, Utah
CKBC	Cache Creek, British Columbia
CPCL	Campo, California
CPSO	Cumberland Plateau Seismological Observatory
CTOK	Clayton, Oklahoma
CVTN	Centerville, Tennessee
DHNY	Delhi, New York
DRCO	Durango, Colorado
DUOK	Durant, Oklahoma
EBMT	East Braintree, Manitoba
EFIX	Eagle Flat, Texas
EPTX	El Paso, Texas
EUAL	Eutaw, Alabama
FMUT	Fillmore, Utah
FRMA	Forsyth, Montana
PSAZ	Flagstaff, Arizona
CLMA	Glendive, Montana
GNMX	Gnome, New Mexico
GRMN	Grand Rapids, Minnesota
GVTX	Grapevine, Texas
HBOK	Hobart, Oklahoma
HDPA	Howard, Pennsylvania
HETX	Hempstead, Texas
HEND	Hannah, North Dakota
HLID	Hailey, Idaho
HMBC	100 Mile House, British Columbia
HTMN	Hastings, Minnesota
HYMA	Hysham, Montana
JELA	Jena, Louisiana
JUTX	Juno, Texas
KNUT	Kanab, Utah
LCNM	Las Cruces, New Mexico
LPTX	La Pryor, Texas
LSNH	Lisbon, New Hampshire

MLNM	Mogollon, New Mexico
MMTN	McMinnville, Tennessee
MNNV	Mina, Nevada
MFAK	Mountain Pine, Arkansas
MTWA	Mount Baker, Washington
MYCL	Marysville, California
NGWS	Niagara, Wisconsin
PMWY	Pole Mountain, Wyoming
PTOR	Pendleton, Oregon
PJOK	Perkins, Oklahoma
KKON	Red Lake, Ontario
RTNM	Raton, New Mexico
RYND	Ryder, North Dakota
SEMN	Sleepy Eye, Minnesota
SIAZ	Snowflake, Arizona
SIIX	San Jose, Texas
SKTX	Shamrock, Texas
SSIX	Sanderson, Texas
SVAZ	Springerville, Arizona
TDNM	Tres Piedras, New Mexico
TFCL	Taft, California
TISO	Tonto Forest Seismological Observatory
TKWA	Tonasket, Washington
UBSO	Uinta Basin Seismological Observatory
VNUT	Vernal, Utah
VTOR	Venator, Oregon
WINV	Winnemucca, Nevada
WMAZ	Williams, Arizona
WMSO	Wichita Mountains Seismological Observatory
WNSD	Winner, South Dakota

INTRODUCTION

1. Little advance has occurred in our understanding of so-called magnitude values computed at regional or near-regional distances by use of body waves since the work of Richter and Gutenberg (VESIAC Report 4410-71-X, Proceedings of the VESIAC Conference on Seismic Event Magnitude Determination, May 1964). Work done by Romney some time ago and described in detail in this report constitutes one of the few exceptions to this generalization. Seismologists have tended to simply adopt the curves given by Richter, extend them by arbitrary assumptions, or to ignore the whole matter. The most cursory glance at available Amplitude/Period (A/T) versus Epicentral Distance (Δ) data impresses one with the profound control exerted on such data by regional crustal characteristics. Imposition of a "standard" A/T versus Δ curve on data for events east of the Rocky Mountains, hereafter referred to as Eastern United States (EUS), with the associated plotting of magnitude (m) versus Δ rather than A/T versus Δ obscured the simple A/T versus Δ relationship of that region. Even in the Western United States (WUS) the standardized approach to magnitude computations as exemplified by VELA reports dealing with individual Nevada Test Site (NTS) events (so-called "shot reports") effectively obscured significant aspects of travel-time and amplitude data as well as evidence for the vertical velocity structure in the crust and upper mantle. The whole concept of the "crust" of the earth as defined by seismic velocity data may require revision based on data obtained by the VELA program. This report attempts to advance understanding of the problems associated with magnitude determinations at regional and near-regional distances. Corollary problems that became evident during the analysis will be discussed at the appropriate places.

2. Both short and long period amplitude measurements of high quality for both earthquakes and explosions are now available as a result of the ARPA/AFIAC program. They show that the A/T versus Δ relationship in the range 200-2100 kilometers for the first P phase as published in tabulated form in the VELA shot reports represents a comparatively crude attempt to express the observed pattern of variation of P amplitudes with distance. That curve bears no relation to patterns of P energy resulting from events in the EUS. The supposed profound decrease and subsequent increase of amplitude in the neighborhood of 1000 kilometers epicentral distance (the "observational" basis for the "Shadow Zone") in the WUS has little basis in fact. The misconception

arose by unknowingly attempting to analyze the A/T versus Δ data for three independently propagating refracted phases by one curve. It will be shown that magnitudes computed according to the formula appropriate to each phase largely remove the apparently profound dependence of determined magnitude upon distance of observation. Systematic variations of 1.9 magnitude units occur when using the shot report A/T versus Δ table at regional and near-regional distances (for example, see Figures 8, 9, 10, 58, 60, 62, and all plots of data from earthquakes). Such overestimation of magnitude becomes a matter of concern to bomb detection and identification studies as some proposed identification criteria demand a valid and meaningful ordering of seismic events on a body wave magnitude basis. For example, miscalculation of the magnitude of events can effectively garble such a criterion as $AR^{1,2}$ versus body wave magnitude. Most of this report deals with the clarification of the problem of understanding the variation of P amplitudes as a function of distance in the regional and near-regional distance ranges (150-2100 kilometers).

3. The data of this study refute widely held ideas about the functional relationship between amplitudes of P phases and epicentral distance. In so doing, the data clearly show that some current ideas about the proper placement of seismometers for optimum detection capability are grossly misleading for the WUS and are untrue for the EUS and, by extension, for much of the world. The WUS represents only one of many possible areas in terms of velocity structure and, unfortunately, most studies of amplitude as a function of distance have treated WUS events. Misinterpretation of the data resulted in invalid conclusions for even that region. We will demonstrate the complete irrelevancy of the currently accepted A/T versus Δ assumptions to conditions in EUS though many seismologists assume these assumptions to be valid. No shadow zone exists in EUS and amplitudes of the $P_{8.5}$ phase increase continuously from teleseismic distances to the epicenter (that is, to the inner limit of existence of the phase at a hundred or so kilometers). A 10-fold increase in signal-to-noise ratio, relative to that at an epicentral distance of 65° , can be obtained by observing $P_{10.5}$ at 20° or $P_{8.5}$ at 11° .

¹Brune, J. A. Espinosa, J. Oliver, 1963, Relative Excitation of Surface Waves by Earthquakes and Underground Explosions in the California-Nevada Region, J. G. R., Vol 68, pp. 3501-3513.

²Mansfield, R. H., Measurements of P_g/P_n , L_g/P_g , and AR for Nuclear Explosions and Earthquakes, VSC Technical Report VU-64-1.

4. The observed travel-time complications in WUS at distances of less than 2000 kilometers are largely nonexistent for many other areas, the general belief in the universality of such complications results from confusing the problem of multiple refractors with that of regional variations of refraction velocities. Possibly, highly seismic regions have, as a corollary feature, complex velocity structures.

5. This report purports to demonstrate the general statements made above and to present the quantitative relationships between amplitude, distance, and phase for EUS and WUS. We will consider initially EUS because of its remarkable simplicity and will then attempt to explain the major problems inherent in understanding amplitude relationships in the P phases arising from WUS events. Any careful attempt to develop a meaningful A/T versus Δ relationship requires the identification of phases, the determination of their distance dependence, and their average energy content relative to other phases.

6. Magnitude has varied definitions with none universally accepted. Since the important points to consider include relative ordering of events and establishment of their relative magnitude, we can accept any reasonably meaningful point of departure for our definition. The definition of the magnitude we accept is as it is derived by several observations at 20-30°, according to Richter's³ published curve for P body waves. Formulas derived herein yield a uniform estimate of the magnitude by use of data obtained between 200 kilometers and teleseismic distances. We can then use those formulas to determine a meaningful estimate of relative magnitude of events over any distance range.

7. The subscript nomenclature used to characterize particular phases should not be taken too literally. A subscript of (7.9) means that we attempt to treat under one phase and equation profiles with observed velocities in the range (7.7-7.9). The (8.5) subscript should be considered as indication of velocities in the range (8.3-8.7) while (8.1) covers (8.0-8.1) in WUS. The $P_{10.5}$ subscript identifies the first segment of the travel-time curve observed beyond $P_{8.5}$. These phases are distinct and are associated with distinct refractors.

EASTERN UNITED STATES

1. Travel-Time Curves for EUS. The standard (T - $\Delta/8.1$ versus Δ) figures of the shot reports show clearly the essential character of P_n travel-time curves for EUS (Figures 2 through 7). The Jeffreys-Bullen (J-B) travel-time curve is included in all figures. Figures 2 through 7 give

³See, for example, Richter, C. F., 1958, Elementary Seismology, Freeman and Company, San Francisco, p. 688.

the first arrival data observed for the indicated events, numerous figures being presented in order to make it clear that this pattern of travel-time profile typifies epicenters throughout EUS. Figure 1 indicates the epicenters of these events and all others considered in this report. Note that the events of EUS are distributed from Eastern New Mexico to the Western Atlantic Ocean and from the South Dakota-Nebraska Border to the Louisiana Gulf Coast. Clearly, the simple profile of a P_n leg of approximately 8.5 velocity extending from around 150 to about 2100 kilometers typifies the region. At that distance, a deeper refraction becomes first arrival, travel times then following the J-B curve with regional characteristics no longer playing a significant role. A comparison of this travel-time curve pattern with the incomplete pattern of curves of WUS presented in Figure 23 indicates the gross contrast of velocity structures of the two areas. More discussion of this point will follow a discussion of the WUS profile. For the moment, we note only the existence of the contrast with its implications of different patterns of amplitudes as a function of distance from epicenters in the two areas.

2. Magnitudes as Computed by the Shot Report Table for EUS Events.

The half circles on Figures 8 through 16 indicate magnitude values (m_{sr}) based upon the standard shot report A/T versus Δ table in the range of 0-2100 kilometers. Clearly, the magnitude estimates are a function of distance and thus unsatisfactory in estimating the magnitude of EUS events. Not surprisingly, a generalized A/T versus Δ curve attempting to express the complexities of WUS velocity structures fails completely when applied to EUS, a simple region displaying essential phase continuity over the entire interval, 150-2100 kilometers.

3. The Dependence of A/T on Δ and the Computation of Magnitude for EUS Events.

a. It is assumed that the relationship between m , A/T, and Δ is of the form

$$m = a + \log (A/T) + n \log \Delta \quad (1)$$

where m is magnitude, a and n are constants to be determined, A/T is measured in millimicrons per second, and Δ , the epicentral distance, is measured in kilometers. The equation can be rewritten as $C = m - a = \log (A/T) + n \log \Delta$, the correct value of n being that for which C is independent of Δ . After n is determined, a is evaluated by use of the magnitude value determined at teleseismic distances (beyond the $P_{8.5}$ leg of travel-time curve or, in this case, beyond 2100 kilometers).

b. An estimate of n can be obtained by determining a least square fit of $\log A/T$ versus $n \log \Delta$ data for events occurring in EUS. The six events

selected and the computed values of n with their standard deviations are:

West Virginia Earthquakes (25 Nov 1964)	-1.84 ± 0.23
Texas-Louisiana Earthquake (24 Apr 1964)	-2.26 ± 0.33
GNOME - Eastern Profile	-2.07 ± 0.39
SALMON	-2.37 ± 0.34
SS Village	-1.56 ± 0.36
Poplar Bluff Earthquake (3 Mar 1963)	-1.88 ± 0.54
Average	-2.0

As examples of the influence of the value of n on data interpretation, a detailed presentation of the data for the first two events above is given in Table I. Note that, according to VELA custom, all standard deviations indicated are standard deviations of a single determination. Standard deviations of the mean are generally one-third to one-quarter of the standard deviation of a single determination.

TABLE I

West Virginia Earthquake 25 Nov 64 02:50:07.1 $m_{ts} = 3.58 \pm 0.20$

Station	Δ (km)	A/T m/s	$\log \Delta$	$\log A/T$	$\log A/T + \log \Delta$	$\log A/T + 2 \log \Delta$	$\log A/T + 3 \log \Delta$	$m_{8.5}$	m_{sr}
BRPA	377	51.8	2.576	1.714	4.290	6.866	9.442	3.60	4.61
CPSO	403	55.6	2.605	1.745	4.350	6.955	9.560	3.69	4.75
HDP A	537	14.5	2.730	.161	3.891	6.621	9.351	3.35	4.64
DHNY	795	19.7	2.900	1.294	4.194	7.094	9.994	3.82	5.09
LSNH	1122	3.26	3.050	0.513	3.563	6.613	9.663	3.34	4.81
GPMN	1507	2.93	3.178	0.467	3.645	6.823	10.001	3.55	4.27
WMSO	1556	4.36	3.192	0.639	3.831	7.023	10.215	3.75	4.24
RKON	1784	2.87	3.251	0.458	3.719	6.970	10.221	3.70	3.36
RTNM	2022	2.79	3.306	0.433	3.739	7.045	10.351	3.78	3.35
						<u>6.890</u>		<u>3.62</u>	

$$C = 6.890 = 3.58 - a, a = -3.31$$

Texas-Louisiana Earthquake 24 Apr 1964 07:33:53.5 $m_{ts} = 3.85 \pm 0.34$

Station	Δ (km)	A/T	$\log \Delta$	$\log A/T$	$\log A/T$ + $\log \Delta$	$\log A/T$ + 2 $\log \Delta$	$\log A/T$ + 3 $\log \Delta$	$m_{8.5}$	m_{sr}
JELA	170	492.2	2.230	2.692	4.922	7.152	9.382	3.88	4.89
GVTX	333	374.0	2.522	2.573	5.095	7.617	10.139	4.34	5.27
WMSO	365	14.1	2.752	1.149	3.901	6.653	9.405	3.38	4.55
EUAL	574	40.5	2.759	1.607	4.366	7.125	9.884	3.86	5.01
JUTX	715	52.0	2.854	1.716	4.570	7.424	10.278	4.15	5.41
CPSO	883	23.8	2.946	1.377	4.323	7.269	9.466	4.00	5.38
RTNM	1127	(2.04)	3.052	0.310	3.362	6.414	9.980	(3.14)	4.61
LCNM	1212	5.35	3.084	0.728	3.812	6.896	10.249	3.63	4.93
BLWV	1333	7.49	3.125	0.874	3.999	7.124	10.237	3.85	4.98
BRPA	1634	3.96	3.213	0.598	3.811	7.024		3.75	4.00
						7.070		3.80	

$$C = 7.070 = 3.85 - a, a = -3.22$$

c. Columns 6, 7, and 8 give values of C for $n = 1, 2$, and 3 , respectively. The values of Column 7 ($n = 2$) appear independent of Δ while those of Columns 6 and 8 ($n = 1$ and $n = 3$) show a dependence of C upon Δ . The values of "a" follow immediately (-3.31 and -3.22), their average value of -3.27 being adopted. Finally, the formula desired reads

$$m_{eus} = m_{8.5} = -3.27 + \log A/T + 2 \log \Delta. \quad (2)$$

This equation is shown graphically in Figure 100 as the $P_{8.5}$ curves, A/T being measured in millimicrons per second and Δ in kilometers. Column 9 gives the magnitude computed according to this formula as a function of distance. Compare these values with those of Column 10 which were computed according to the shot report table. There is obvious disagreement of m_{sr} values with the teleseismic determination (m_{ts}) while the $m_{8.5}$ values yield the statistically identical estimate of magnitude at both distance ranges. Note that magnitude estimates that differed by 1.74 units (DHNY and RTNM) according to m_{sr} differ by only 0.04 units when computed by $m_{8.5}$.

d. The application of formula (2) to other events in EUS achieves clarification and greater internal consistency of computed magnitudes. Figures 8 through 16 give the relevant data for all events studied. The events studied include surface explosions of zero focal depth, underwater explosions, and earthquakes of unknown but shallow focal depth. The variation of type of event is such that dependence of the observed patterns upon a specific source type cannot be seriously considered. Also, A/T appears little dependent on profile azimuth. The only GNOME data used in this part of the report comprise the profile laid out eastward from the test site. The only event showing marked discrepancy between $m_{8.5}$ and m_{ts} is the Lake Superior 10-ton shot, $m_{8.5}$ being 4.3 ± 0.35 , whereas m_{ts} is 3.5 ± 0.35 . The reason for this discrepancy cannot be demonstrated but

it will be shown under the discussion of the Nevada Test Site (NTS) events that variation in rock type at the source can lead to large variations in the pattern of energy distribution between generated P-wave signals.

e. Note the systematic discrepancy of the m_{sr} values, maximum predicted values by this formula being around 1000 kilometers. Figure 100 shows that m_{sr} overestimates the magnitude by 1.5 units at 1000 kilometers and underestimates it by 0.4 units at 1900 kilometers, a difference of 1.9 units introduced not by the data but by the use of an inappropriate formula.

f. Note also that the A/T versus Δ data of these events indicate the total lack of any obvious shadow zone phenomenon. No shadow zone exists in EUS and the supposed problems of observing at distances of less than 2000 kilometers because of low signal levels do not exist for EUS events. The signal level at 1000 kilometers attains 30 times that predicted by the m_{sr} table and more than 10 times that predicted by m_{sr} at all distances between 400 and 1400 kilometers. The implications for the relative advantage of regional and near-regional stations versus teleseismic stations for regions of the crustal type of EUS appear obvious.

g. The Vermont Earthquake data depicted in Figure 16 provide an excellent example of the misconceptions that can be reached by use of inappropriate formulas. Very few stations recorded this event, no station beyond 2017 kilometers receiving a detectable signal. However, by use of m_{gr} values, one obtains an estimated magnitude of 4.7, an average of 5 values ranging from 5.4 to 3.3. An estimate of 4.7 magnitude on the basis of observations at regional and near-regional distances is in pronounced conflict with the fact of total lack of recordings at teleseismic distances. Such an event should yield an A/T value of 10 m_{gr} at 50° and should be widely recorded at teleseismic distances. The significance of this misevaluation will be pointed out in the forthcoming discussion of AR versus m. Here simply note that, by use of m_{gr} values, the spread of m values for signals clear in both period and amplitude is 0.1 magnitude units as compared with 2.1 for m_{gr} values. The estimated magnitude becomes 3.8 or 3.9, consistent with no recordings beyond 2000 kilometers.

WESTERN UNITED STATES

1. Travel-Time Curves for WUS. In the WUS, the situation becomes much more complicated than in EUS. Several events must be studied in order to appreciate the complexity even to the extent that it is now understood. One could not find a suite of events which would establish the basic uniformity of the WUS as such uniformity does not exist. It seems only possible to appreciate the major patterns resulting from explosions at NTS and to then use the limited data available from other areas to suggest the similarities and dissimilarities with NTS data caused by varying epicentral positions and varying azimuths of profiles. We shall consider GNOME, CLIMAX (the 0.2 KT chemical explosion at Climax, Colorado), 50 shots at NTS, and 17 earthquakes distributed from Central Mexico through WUS to Queen Charlotte Islands.

2. Travel-Time Curves of FORE.

a. It is convenient to begin the discussion with FORE because of the excellent and significant profiles that were installed for this event. See Figure 17. The generally observed $P_{7.9}$ refracted wave was well observed from 200 kilometers out to 1000 kilometers to the south-east, reaching Las Cruces, New Mexico (LCNM). Remember that all arrivals noted on figures of the type of Figure 17 are the first observed arrivals at the several stations. No observed second arrivals are shown. A $P_{8.5}$ leg was received as first arrival at Uinta Basin Seismological Observatory (UBSO), Blue Mountains Seismological Observatory (BMSO), Forsyth, Montana (FRMA), and at Glendive, Montana (GIMA), the positioning of Raton, New Mexico (RTNM), on this line being probably fortuitous. Note that the line through these points appears parallel to the SS Village profile but with a time intercept on the zero distance axis of 14 seconds rather than the 9 seconds of the SS Village profile. The time arrivals along the profile to the ESE provide both complex and interesting data. Blanding, Utah (BXUT), and Durango, Colorado (DRCO), lie well below the two previously mentioned refractions and cannot be related to either of them. More discussion of these arrivals will be presented later. RTNM probably did not actually receive a $P_{8.5}$ arrival consistent with the 8.5 profile through FRMA and GIMA but we cannot identify the phase measured at this time. The next stations on this profile appear to have recorded a signal with a slope of about 8.5 but with a time intercept on the zero distance axis of nearly 20 seconds. At least, they did not record the phase seen at BXUT and DRCO but something much later and with a higher refracted velocity.

b. Finally, the P phase generally received as first arrival beyond 2000 kilometers is well observed at EBMT and RKON, 2148 and 2338 kilometers respectively, as well as at Hempstead, Texas (HETX), Hannah, North Dakota (HHND), and Ryder, North Dakota (RYND), the latter being at an epicentral distance of 1700 kilometers. Thus RYND failed to observe earlier but less energetic refractions, recording instead the strong $P_{10.5}$ arrival as first arrival.

3. Travel-Time Curves of MISSISSIPPI. MISSISSIPPI (Figure 18) shows similarity to FORE, $P_{7.9}$ being observed towards LCNM to 1200 kilometers and to shorter distances in other azimuths. Hailey, Idaho (HLID), and DRCO received as first arrivals signals preceding the expected $P_{7.9}$ event. The profile across Colorado and the Dakotas follows the previously mentioned 8.5 leg to WNSD but then jumps to $P_{10.5}$ for Academy, South Dakota (AYSD), at 1601 kilometers. Other points are associated, in some cases, with unclarified phases.

4. Travel-Time Curves of BILBY and CLEARWATER. The interpretation of the BXUT, HLID, and DRCO arrivals becomes clear as soon as larger events such as BILBY and CLEARWATER are considered (Figures 19 and 20). These events show the existence of an 8.0 - 8.1 refraction extending eastward from NTS through BXUT, DRCO, TDNM, and RTNM. Shamrock, Texas (SKTX), did not record this phase, a more energetic phase arriving at essentially the predicted time, while the figures show clearly that Apache, Oklahoma (APOK), Grapevine, Texas (CVTX), and Durant, Oklahoma (DUOK), observed other phases as first arrivals. As will be noted below, much of the supposed difference between MISSISSIPPI and BILBY and the inability of a formula based upon MISSISSIPPI data to reasonably interpret BILBY data results from different patterns of observation in a heterogeneous region.

5. Regional Variations of Travel-Time Curves in WUS. Regional variations within the WUS appear when events from other than NTS sites are considered. For CLIMAX (Figure 21), located in Colorado, the first arrivals at most stations in WUS were an 8.1 refraction with no stations measuring a 7.9 event as first arrival. As noted above, the eastern profile from GNOME (Eastern New Mexico) recorded only P_{8.5} while P_{8.1} and P_{7.9} were seen to the west and northwest (Figure 22), the P_{8.1} event being observed only very near GNOME. Note that the intersection of the P_{8.5} segment through Montana with P_{10.5} occurs at approximately 2000 kilometers while for the SS Village profile these two refractions intersect at about 2200 kilometers. The suggested P_{8.5} segment through Texas and Oklahoma for NTS events intersects P_{10.5} at about 1700 kilometers. P_{8.5} and P_{7.9} intersect at a distance of 1250 kilometers to the southeast and approximately 1000 kilometers to the north and northeast.

6. Conclusion. Thus, one may observe at least six different P phases from NTS shots and shots from different localities give rise to different patterns of travel-time curves. Compare this with EUS where essentially one travel-time curve for one phase satisfied all observed profiles. Not surprisingly, amplitude interpretation which does not depend upon phase identification, but which uses a single A/T versus Δ on such complex data as that recorded from NTS and other WUS foci has yielded nearly chaotic results.

ESTABLISHMENT OF A/T VERSUS Δ CURVES FOR WESTERN UNITED STATES

1. P_{7.9} Arrivals. Romney extensively employed P_{7.9} arrivals (VSC Technical Note 10) to determine magnitudes of the smaller NTS events. He observed this phase as first arrival from NTS to LCNM and beyond to a distance of approximately 1050 kilometers. Northward from NTS, another excellent profile extends through Mina, Nevada (MNNV), to Pendleton, Oregon (PTOR), including HLID for events in which P_{8.1} is too small to be recorded. PTOR frequently misses P_{7.9} in favor of P_{8.5}. Beyond PTOR in Washington, Montana, and the Dakotas, either P_{8.5} or P_{10.5} records as first arrival measured. DRCO, to the east of NTS never records P_{7.9} so that the data of that station should be ignored when considering P_{7.9}. The dependence of A/T on Δ for the NTS-LCNM profile (data from FISHER, DORMOUSE, STOAT, etc.), the LCNM-NTS profile (data from GNOME), and the NTS-PTOR profile (numerous events) is identical in all cases. This energy path should serve as an excellent source of internally consistent estimates of magnitude of events within the region. The procedure adopted by Romney for calibrating this energy event against tele-seismic data is as follows (Romney, personal communication):

"a. (U) Since 1961 recordings from numerous underground nuclear explosions at the NTS have been made at mobile stations operated under the VELA LRSM program. These stations have been located at many distances and azimuths from the test site. Some of the stations have operated more or less continuously and have recorded data from many explosions, while others have moved from time to time, recording only a limited number of explosions at a given location. The explosions have included yields smaller than 1 KT and larger than 100 KT. Shot points have been somewhat dispersed within the test site, with the result that the propagation paths to fixed stations, and hence the amplitudes, have been affected somewhat. Variations in coupling which appear to depend upon the characteristics of the rock and other conditions near the explosions have also been noted. It is, therefore, necessary to correct the measurements to common source conditions (explosive yield and coupling factors) before the data can be combined to give a good representation of the amplitude versus distance relationship.

"b. (U) In the course of analyzing recordings from the explosions it was found that, for any given station, the values of log A/T versus log Y (Y = yield) fit an approximate straight line if the measurements were restricted to explosions in Yucca Flats. This made it possible to find A/T at a standard yield for each station by fitting the best straight line to a plot of amplitude versus yield. The amplitude of 10 KT was read from this line and used to represent the best value of A/T at the average distance of the station from its recorded shots.

It was required that at least four shots which bracket 10 KT be recorded before the data were used. This procedure tends to smooth out scatter in the data caused by small variations in coupling or in the path of propagation and by noise.

"c. (U) The average values of $\log A/T$ at 10 KT for each station were plotted as a function of distance (figure 101). These points define a line given by

$$\log A/T = 9.50 \pm 0.72 - (3.04 \pm 0.26) \log \Delta \quad (3)$$

where Δ is measured in kilometers, T in seconds, and A in millimicrons. First arrivals at stations between 200 and 1050 kilometers were used. The slope of this curve is almost identical with that found in LOGAN and BLANCA.

"d. (U) The amplitudes of $P_{7.9}$ can be associated with teleseismic magnitudes by comparison with the signals recorded at long ranges from the LRSM stations. The basic data used came from the 13 explosions which were recorded at five or more stations at teleseismic distance ($\Delta > 16^\circ$) as well as in the P_n range. These shots were generally larger than 10 KT since only these larger shots can be satisfactorily recorded at teleseismic ranges. Unified magnitudes were computed for each such explosion from the measured amplitudes and period of P . The average magnitude for each event was then compared with the value of $\log A/T$ at 500 kilometers, as found by a least square fit of the $P_{7.9}$ amplitude versus distance data. Results are shown in Figure 102. It may be seen that the magnitude increases more rapidly than $\log A/T$ at 500 kilometers. The relationship was found by least squares to be

$$m_{7.9} = 2.36 \pm 0.23 + (1.21 \pm 0.11) \log (A/T)_{500} \quad (4)$$

This implies that the teleseismic amplitudes increase more rapidly with yield than does the amplitude at 500 kilometers. This probably results from the shift toward lower frequencies in the source as the yield increases together with the reduced attenuation at low frequencies.

"e. (U) Equations (3) and (4) may be combined to give the $P_{7.9}$ amplitudes as a function of magnitude. The result is

$$m_{7.9} = -7.55 + 1.21 (\log A/T + 3.04 \log \Delta) \quad (5)$$

Note on Figure 100 that a discrepancy between m_{sr} and $m_{7.9}$ of 0.6 occurs at $m_{7.9}$ equal to 5.0, $m_{7.9}$ being smaller than m_{sr} .

2. P_{10.5} Arrivals. We shall fit a smoothed curve through the Gutenberg-Richter curve between 2100 and 3000 kilometers and, in addition, obtain the values of amplitude for P_{10.5} observed at 1600 kilometers in North Dakota at RYND, etc. The equation obtained is

$$m_{10.5} = -10.35 + \log A/T + 4 \log \Delta \quad (6)$$

where A/T is measured in millimicrons per second and Δ in kilometers. The corresponding curve is shown on Figure 100 as P_{10.5}. As far as is known, this dependence of A/T upon Δ occurs independently of azimuth.

3. P_{8.5} Arrivals. As noted above, PTOR, at approximately 1000 kilometers, generally records P_{8.5} as first measured arrival. A phase with this velocity is observed as first arrival in Montana and the Dakotas. To the southeast, stations in Texas, Oklahoma, and beyond observe P_{8.5} as first arrival to 1800-2000 kilometers. The time intercepts for these three P_{8.5} profiles appear quite different, both from each other and from that typical of this refraction in EUS. Even so, we proceed by attempting to employ the m_{eus} formula for these arrivals. The results agree satisfactorily with the magnitude computed for P_{7.9} and tele-seismic distance. Therefore, we adopt the m_{eus} (i. e., $m_{8.5}$) curve for computing magnitudes for arrivals on P_{8.5} profiles in WUS.

4. P_{8.1} Arrivals. When establishing a curve for $m_{8.1}$, a most interesting result appears in this case. A well-observed profile for this refraction for NTS shots requires a large explosion, only DRCO recording this phase for most events. Either this phase possesses very little energy or the energy dissipates rapidly along the refractor. In this connection, remember that for the CLIMAX shot in Colorado, a small event generated a widely observed P_{8.1} refraction. A/T values from CLIMAX measured toward Arizona decreased as about the inverse third power of the distance while along the profile from NTS through Southern Colorado into Northern New Mexico, A/T values for P_{8.1} arrivals decrease as the inverse seventh power of the distance. Note that DRCO occurs on both the CLIMAX-Arizona and the NTS-New Mexico profiles. High amplitudes typify P_{8.1} arrivals at short distances from NTS. The signal decays so rapidly with increasing distance that it disappears into the noise beyond DRCO for small events. When one attempts to derive equations to use along the NTS-New Mexico profile by use of CLEARWATER and BILBY, it becomes apparent that the data of the two events require a 0.9 difference in the leading coefficient of the derived equations. Thus, for CLEARWATER, shot in mesa tuff, one obtains

$$m_{8.1} \text{ (CLEARWATER)} = -17.20 + \log A/T + 7 \log \Delta \quad (7)$$

while for BILBY, shot at 2314 foot depth in valley tuff,

$$m_{8.1} (\text{BILBY}) = -16.30 + \log A/T + 7 \log \Delta. \quad (8)$$

Apparently, CLEARWATER coupled eight times as much energy (relative to that coupled into the other measured refracted phases) into this phase as did BILBY. If one computes DRCO $P_{8.1}$ arrivals for events with varying shot locations according to $P_{8.1}$ (CLEARWATER) and $P_{8.1}$ (BILBY), the following pattern emerges:

TABLE IV

		Depth	Magnitude	DRCO by $m_{8.1}$ (CLEARWATER)	DRCO by $m_{8.1}$ (BILBY)
DORMOUSE	Alluvium (3)	1191 ft	3.64	3.72	-
MISSISSIPPI	Valley Tuff (9)	1615	4.76	-	4.89
CIMARRON	Alluvium (9)	1000	3.98	3.71	-
STILLWATER	Alluvium (9)	625	3.46	3.27	-
CODSAW	Alluvium (9)	696	3.40	3.03	-
MINK	Alluvium (3)	630	2.72	3.06	-
HAYMAKER	Alluvium (12)	1351	4.52	-	4.46
DES MOINES	Mesa Tuff (12)		3.72	3.71	-
MARSHMALLOW	Mesa Tuff (12)		3.99	3.63	-
MADISON	Mesa Tuff (12)		3.71	3.73	-

Thus, all of the mesa tuff shots behaved similarly to CLEARWATER but so did all of the shallow valley shots. Only HAYMAKER and MISSISSIPPI coupled as little energy into this refractor as did BILBY. Thus, the use of data obtained from this refraction throughout WUS requires extensive crustal calibration (CLIMAX profile versus NTS profile) as well as calibration of energy in the phase relative to source location. In other words, this phase does not appear very useful for routine investigations. The very high rate of amplitude decrease eastward from NTS together with the markedly different behavior on another azimuth through the same area imply the disappearance eastward of the velocity contrast requisite for the refraction. Such an azimuth dependent phenomenon requires lateral crustal inhomogeneities.

DETAILED ANALYSES OF STATION MAGNITUDE VALUES FOR MISSISSIPPI, BILBY, AND HARDHAT

1. Introduction. Three events will be discussed in detail. Two of them, MISSISSIPPI and BILBY, illustrate the problem of observing different profiles and thus possibly different phases for different events while interpreting all data by an inadequate generalized formula. All three events illustrate a type of problem that even proper phase assignment

will not defeat. Obtaining the same estimated magnitude from several phases of the same event requires that the energy partition function for the event be identical to that for the event or events used in establishing the function. Otherwise, magnitude becomes a function of phase.

2. MISSISSIPPI. MISSISSIPPI (Figures 18 and 64) probably represents the most significant event used in the establishment of the $m_{7.9}$ formula. Not surprisingly then, $m_{7.9}$ and m_{ts} values agree closely. Use of the standard EUS $m_{8.5}$ formula obtained excellent agreement with m_{ts} . The station-by-station data are as follows:

TABLE V
MISSISSIPPI

	Δ	Magnitude	m_{sr}		Δ	Magnitude	m_{sr}
MNNV	234	5.06 (7.9)	6.0	SSTX	1496	4.33 (8.5)	5.0
KNUT	278	4.68 (7.9)	5.5	WNSD	1507	4.83 (8.5)	5.6
FMUT	408	- ?	4.8	HBOK	1555	4.98 (8.5)	5.5
TFCL	415	3.70 (7.9)	4.5	CKBC	1578	4.52 (8.5)	5.0
WINV	483	4.83 (7.9)	5.8	WMSO	1596	4.55 (8.5)	4.9
FSAZ	485	4.86 (7.9)	5.5	AYSD	1601	4.95 (10.5)	6.0
CPCL	490	5.10 (7.9)	5.7	HMBC	1670	4.84 (8.5)	5.0
MVCL	517	- ?	-	PUOK	1714	?	
TFSO	536	4.67 (7.9)	5.0	CTOK	1910	4.30 (10.5?)	4.3
DRCO	733	4.89 (8.1)	5.5	SJTX	1970	4.86 (10.5)	4.9
HLID	739	4.61 (8.1)	4.6	SEMN	1971	4.42 (10.5)	4.5
BMSO	863	4.47 (7.9)	5.2	MPAR	2083	4.49 (10.5)	4.6
PTOR	971	4.88 (8.5)	5.3	LR 17	2099	4.85 (10.5)	4.9
LCNM	1101	4.41 (7.9)	5.2	HTNM	2120	5.12 (10.5)	5.2
PMWY	1027	4.40 (7.9)	5.2	LR 16	2460	5.11 (10.5)	5.1
HKWY	1126	4.51 (8.5)	6.0	ARWS	2460	5.05 (10.5)	5.1
MUWA	1392	4.27 (8.5)	5.3	CVTN	2565	4.95 (10.5)	5.0

Average of all stations at less than 1900 kilometers - 4.76 (4.3-5.2)

Average of 28 stations between 1900 and 4064 kilometers - 4.69 (4.3-5.1)

Average of all m_{sr} values at less than 1900 kilometers - 5.3 (4.3-6.0)

The figures in parentheses are the extreme values in each group of values.

Apparently, computations based upon phase assignment and appropriate formulas have made the computed magnitude independent of epicentral distance and have also reduced the range of variation of the data. Whereas the range in computed values was 4.3 to 6.0 using the shot report table, the use of phase curves reduced the range to 4.3 to 5.2, i. e., half the previous range. The pairs PMWY - HKWY and WMSO - AYSD clearly show the influence of proper phase identification. For the former pair, m_{sr} values were 5.2 and 6.0, while properly interpreting the PMWY arrival as $P_{7.9}$ and the HKWY arrival as $P_{8.5}$ leads to magnitude estimates of $m_{7.9} = 4.40$ and $m_{8.5} = 4.51$, respectively. The m_{sr} values for WMSO and AYSD are 4.9 and 6.0, while, when making proper phase identifications, $m_{8.5}$ for WMSO is 4.55 and $m_{10.5}$ for AYSD is 4.95. Regarding the rejection of such stations as TFCL and MVCL, we argue that, for interpretation, we require a reasonably clear-cut relationship between data obtained at a given station and that recorded at teleseismic distances. If we have not established as yet such a relationship, the proper mode of interpretation of the data of such stations is unknown and we ignore their recordings. Further investigations than reported here may render the data of such stations meaningful in a magnitude sense, and thus useable.

3. BILBY. For BILBY (Figures 19 and 65), the data are as follows:

TABLE VI

BILBY

	Δ	Magnitude	m_{sr}		Δ	Magnitude	m_{sr}
MNNV	242	5.46 (7.9)	6.0	TDNM	880	5.59 (8.1)	5.3
KNUT	284	5.42 (7.9)	5.9	RTNM	1039	5.32 (8.1)	5.2
CPCL	483	? early		AZTX	1278	5.05 (8.5)	6.2
WINV	493	5.01 (7.9)	5.6	FRMA	1282	5.17 (8.5)	6.3
		5.13 (8.1)		TKWA	1337	?	6.0
MVCL	520	? early		SKTX	1426	5.26 (8.5)	6.2
TFSO	529	5.68 (7.9)	6.2	GIMA	1487	5.05 (8.5)	5.9
BXUT	586	5.68 (8.1)	5.9	WMSO	1593	5.18 (8.5)	5.5
UBSO	668	5.46 (8.5)	6.7	RYND	1705	5.40 (10.5)	6.0
DRCO	732	5.91 (8.1)	5.9	GVTX	1794	5.75 (8.5) ?	5.4
HLID	747	5.51 (8.1)	5.6	DUOK	1831	5.81 (8.5) ?	5.5
BMSO	871 ?	4.24 (8.5) ?	5.6	HHND	1926	5.83 (10.5)	6.0

Average of 18 stations at less than 1900 kilometers - 5.44 (5.1-5.9)

Average of 18 stations beyond 1900 kilometers (1926-9100) - 5.6 (5.2-6.0)

Note that, in the interval 550-1040 kilometers, the only profile observed for BILBY was the NIS - BXUT - DRCO - TDNM - RTNM path, and that $P_{8.1}$ was observed as first arrival at all stations. When calculated according to $m_{7.9}$ (naïvely assuming that all arrivals in this distance range are $P_{7.9}$), magnitude estimates at these stations are 5.33, 4.64, 4.64, and 4.55, respectively, values below estimates made upon $P_{7.9}$ arrivals and values apparently decreasing with distance. The values entered in the tabulation above were found, as described previously, by calibration against the teleseismic data of this event. Note that the $m_{7.9}$ and $m_{8.5}$ values appear systematically low relative to $m_{10.5}$ and m_{ts} values. We obtained, by use of the same formulas, excellent agreement between magnitude estimates at all ranges for MISSISSIPPI. This implies that the energy partition for these two events, BILBY and MISSISSIPPI, differed markedly. The apparent agreement of $m_{8.1}$ and m_{ts} occurs because we calibrated the $m_{8.1}$ formula by use of this event. Probably, calibration against $m_{7.9}$ and $m_{8.5}$ would have had more meaning, making all of the shallow refractions less energetic relative to $m_{10.5}$ and deeper refractions for BILBY than for MISSISSIPPI. Such variation in the energy partition function requires either nonradial symmetry in the source radiation function, varying patterns of vertical velocity structure in the two shot areas sufficient to give the observed differences of energy level in the lunes of the focal sphere giving rise to the several refractions, or frequency and depth dependent attenuation factors.

4. HARDHAT. For HARDHAT (Figure 75), the data are as follows:

TABLE VII

HARDHAT

MNNV	228	4.96 (7.9)	5.96	MLNM	781	3.56 (8.1CL)	4.29
ATNV	263	5.30 (7.9)	6.11	TCNM	902	4.47 (8.1CL)	4.66
KNUT	288	5.12 (7.9)	5.89			5.34 (8.1B')	4.86
INCL	336	4.09 (7.9)	4.92	PTOR	961	4.44 (8.5)	4.86
WMAZ	399	4.90 (7.0)	5.49	LCNM	1017	3.79 (7.9)	4.64
FMUT	403	4.06 (7.9)	4.83	RTNM	1043	Very late	
WINV	474	5.19 (7.9)	5.78	TRWA	1070	4.27 (8.5)	5.74
FSAZ	490	5.18 (7.9)	5.80	EPTX	1095	3.46 (8.5)	4.94
CPCL	500	? early		EFTX	1209	2.89 (8.5*)	4.21
MVCL	512	? early		GNNM	1244	3.30 (8.5*)	4.56
SFAZ	589	5.63 (7.9)	6.13	BMTX	1324	4.05 (8.5')	5.18
VNUT	669	5.19 (7.9)		SSTX	1501	3.60 (8.5')	4.32
VTOR	688	4.90 (7.9)		WNSD	1504	4.24 (8.5')	4.96
SVAZ	711	4.47 (7.9)		HBOK	1557	4.18 (8.5)	
HLID	729	3.48 (8.1CL)	4.34				
		4.08 (8.1B)					
DRCO	734	4.32 (8.1CL)	5.20				
		4.92 (8.1B')					

TABLE VII (Contd)

	Δ	Magnitude	m_{sr}		Δ	Magnitude	m_{sr}
WMSO	1598	?		MPAR	2084	3.90 (10.5)	5.00
LPTX	1765	?		NGWS	2500	4.13 (10.5)	4.13
SEMN	1967	4.41 (8.5)	4.02	MMTN	2728	4.34 (10.5)	4.37
SJTX	1975	4.09 (10.5)	5.37				

The three symbols for $P_{8.5}$ arrivals identify probable 8.5 refractions from different profiles with different intercept times. The identification of the primed events as $P_{8.5}$ is tentative. Uncertainty exists as to the appropriateness of using $m_{8.1}$ (CLEARWATER) or $m_{8.1}$ (BILBY) (prime implying 0.3 adjustment of BILBY formula based upon discussion of BILBY). If the computed magnitudes are grouped according to phase, the following tabulation is obtained:

$m_{7.9}$	$m_{8.1}$ (CL)	$m_{8.1}$ (B')	$m_{8.5}$	$m_{8.5*}$	$m_{8.5'}$	$m_{10.5}$
4.96	3.48	4.08	4.44	4.05	3.46	4.09
5.30	4.32	4.92	4.27	3.60	2.89	3.90
5.12	3.56	4.16	4.24	4.18	3.30	4.13
4.09	4.74	5.35	4.41			4.34
4.90						
4.06						
5.19						
5.18						
5.63						
5.19						
4.90						
4.47						
3.79						

The two arrivals that were 1 second early relative to $P_{7.9}$ and had very low computed $m_{7.9}$ magnitudes (4.09 and 4.06), together with the unusually low estimate at LCNM (3.79) introduce an abnormal spread into the $m_{7.9}$ data. If one ignores these arrivals, the average $m_{7.9} = 5.17$; if they are included, the average $m_{7.9} = 4.87$. The mean $m_{8.1}$ (B') = 4.62, the mean $m_{8.5} = 4.34$, the mean $m_{10.5} = 4.12$, with the $m_{8.5*}$ and $m_{8.5'}$ values even lower. Obviously, the formulas used for MISSISSIPPI do not satisfy HARDHAT. No obvious distance dependence appears in any phase. The path length differences between $P_{7.9}$, $P_{8.5}$, and $P_{10.5}$ represent small fractions of the total path lengths so that one cannot explain a dependence of magnitude upon phase as being due to a higher frequency signal for HARDHAT than for MISSISSIPPI with a more rapid decay of signal with distance. The lack of dependence of magnitude upon distance in each phase also suggests this conclusion. Another explanation seems required. The decrease in $m_{10.5}$ values shown above from those in the shot report largely results from miscalculation in the shot report.

COMPARISON OF MAGNITUDES COMPUTED BY m_{sr} AND THE SEVERAL CURVES OF THIS REPORT

A comparison of the magnitudes computed by m_{sr} and the several curves established here clarifies the significance of employing the proper curve (see Figure 100). At 1900-2000 kilometers, m_{sr} underestimates relative to $m_{8.5}$ by 0.4. At 1600 kilometers, m_{sr} underestimates the magnitude by 0.3 relative to $m_{8.5}$ and 1.0 relative to $m_{10.5}$. Even if using the new curves, an error of 0.7 will be made if one misidentifies the phase measured. At 1100 kilometers, m_{sr} overestimates with respect to both relevant curves, 0.5 relative to $m_{7.9}$ and 1.5 relative to $m_{8.5}$. Again, if $m_{7.9}$ and $m_{8.5}$ are used but misidentification of a phase occurs, an error of 1.0 will be made in magnitude, PTOR providing a perfect example of this phenomenon. This station routinely sees $P_{8.5}$ as first arrival for NTS events though being only 970 kilometers from NTS. Note the gross discrepancy between m_{sr} and $m_{8.5}$ at all distances less than 1400 kilometers. Fortuitously, these curves cross around 1700 kilometers due to the attempt to get by some means from something approximating a mean between $m_{7.9}$ and $m_{8.5}$ at 1000 to $m_{10.5}$ at around 1800 kilometers. Between 1000 and 2000 kilometers the m_{sr} and $m_{7.9}$ curves nearly parallel one another, the difference between the two curves being 0.63 at $m_{sr} = 5$ and 0.95 at $m_{sr} = 3$. We included $m_{8.1}$ (CLEARWATER) on Figure 100 to demonstrate the grossly different behavior of this phase with distance from that of all other curves. Inside 600 kilometers, $P_{8.1}$ (CLEARWATER) appears larger than either $P_{7.9}$ or $P_{8.5}$ for $m = 4$, while it decays to 1.5 m_{μ} at 1000 kilometers for $m = 4$.

RECALCULATION OF ALL SHOTS PREVIOUSLY ANALYZED IN SHOT REPORTS

Subject to the limitations and uncertainties of the type just described, the A/T versus Δ versus magnitude data of all previously analyzed events were recalculated based upon the formulas given above. As none of them, other than SHOAL, were in granite, one does not expect problems of the type met in analyzing the data of HARDHAT. Figures 24 through 79 present the recalculated magnitude values, the figures for selected events (Figures 8, 9, 10, 58, 60, 62, 64, 65, 73, 76, and 78) including shot report values of magnitude for comparison and study purposes. The magnitude of these events was obtained by averaging all recomputed values, the symbol m_b' being adopted for this average value. The values of m_b' are those used throughout the following discussion and tables. It is clear from the indicated figures that the gross dependence of magnitude upon distance which was present in shot report values of magnitude has been largely eliminated by use of the phase formulas. Small events only recorded at less than 1500 kilometers are reduced in magnitude (m_b') from m_{sr} values by as much as a full magnitude. The following tabulation (TABLE VIII) gives all m_b' values computed by procedures of this report for explosions, together with m_{sr} values and values derived by Romney by use of A/T values at 500 kilometers for the smaller events.

TABLE VIII

Magnitude Data on Selected NTS Shots

SHOT	m_b	m_R	m_{gr}
Alluvium			
SHREW	1.2		2.3
MAD	2.37		3.7
MINK	2.72	2.93	3.7
CHINCHILLA II	2.73	2.84	3.8
ROANOKE	2.94	3.21	3.9
CHINCHILLA	3.16	3.33	4.2
ALLEGHENY	3.04	3.31	4.0
KAWEAH	3.15	3.36	4.1
STILLWATER	3.46	3.40	-
CODSAW	3.40	3.54	4.3
BOBAC	3.39	3.60	4.2
RINGTAIL	3.21	3.36	4.1
SACRAMENTO	3.32	3.40	4.1
STOAT	3.38	3.60	4.5
WICHITA	3.47	3.58	4.5
AGOUTI	3.55	3.83	4.5
SANTEE	3.30	3.56	4.2
ARMADILLO	3.51	3.78	-
PACKRAT	3.69	3.73	4.2
CASSELMAN	3.64	3.96	4.6
HYRAX	3.43	3.60	4.4
ACUSHI	3.51	3.75	4.4
DORMOUSE PRIME	3.73	3.91	4.6
DORMOUSE	3.64	3.83	4.5
CIMARRON	3.98	4.38	-
YORK	3.69	3.92	4.4
PEBA	3.54	3.78	4.4
PASSAIC	3.69	4.06	4.3
FISHER	3.45	3.68	4.3
MERRIMAC	3.80	3.87	4.3
HAYMAKER	4.52	4.5	4.9
SEDAN (crater)	4.12	-	4.7

TABLE VIII (Contd)

SHOT	m_b	m_R	m_{sr}
Valley Tuff			
AARDVARK	4.55	4.7	4.9
STONES	4.50	4.6	4.8
FORE	4.85	4.9	5.2
MISSISSIPPI	4.76	4.7	5.1
BILBY	5.61	5.6	5.8
Mesa Tuff			
FEATHER	2.13	-	3.2
CHENA	2.76	-	3.9
PLATTE	3.44	-	-
ANTLER	4.03	-	4.7
MADISON	3.71	-	4.5
DES MOINES	3.72	-	4.5
MARSHMALLOW	3.99	4.0	4.5
CLEARWATER	4.71	4.9	5.3
HANDCAR	4.19	-	4.7
(Dolomite)			
HARDHAT	4.15(m_{ts})	4.6	4.9
(Granite)			
SHOAL	4.62	4.8	4.9
(Granite)			
DANNY BOY	3.06	-	3.6
(Basalt)			
GNOME	4.27	-	4.6
(Salt)			
CLIMAX	3.73	-	4.4
(Granite, Chemical)			
CHASE III	4.7 (m_{ts})	-	-
(Water)			

RELATIVE MAGNITUDE P. USE OF DATA OF FIXED STATIONS

Another approach to establishing relative magnitudes of NTS events is to compare A/T values of the events as recorded at fixed stations. Relative magnitude should be determinable to within several percent by this approach and one measure of the meaningfulness of the overall scheme here employed would be the agreement of relative magnitudes of NTS events as computed by the two methods of analysis. Several events are analyzed by relative amplitudes at fixed stations in Table IX, all stations being restricted to ones receiving P7.9 in WUS from NTS events.

TABLE IX

Comparison of m_b and Individual Station Relative Magnitudes

Event	m_b	Relative m_b (CHIN II)	Relative m (CHIN II)*				Av	δm
			MNNV	WINV	KNUT	FSAZ		
CHINCHILLA II	2.73	2.73*	2.62*	2.35*	3.12*	3.01*	2.78*	+.05
KAWEAH	3.15	.42	.73	1.18	-.10	.03	.51	+.09
STOAT	3.38	.65	.89	-	.59	.62	.70	+.05
CODSAW	3.40	.67	.84	1.10	.34	.19	.62	-.05
FISHER	3.45	.72	1.20	.80	.42	.59	.75	+.03
ACUSHI	3.51	.78	1.11	.96	.35	.84	.82	+.04
DORMOUSE	3.64	.91	1.30	-	.53	.70	.83	-.08
CASSELMAN	3.64	.91	1.16	1.49	.61	.68	.99	+.08
PASSAIC	3.69	.96	1.23	1.34	.72	.75	1.01	+.05
MADISON	3.71	.98	1.08	1.32	1.07	1.09	1.14	+.16

*CHINCHILLA II data are basis of comparison for other events.

In Table IX, the data of CHINCHILLA II are the basis of comparison. Thus, in the row for CHINCHILLA II, values are magnitudes as estimated by $m_{7.9}$ while in the rows for other events, values are differences between magnitude for these events and CHINCHILLA II at the indicated station or stations, based on measured A/T values. Note that such an approach does not necessarily eliminate a full magnitude spread in the data (KAWEAH, for example). Column 8 is an average of the relative magnitude values obtained at the four fixed stations (KNUT, MNNV, FSAZ, and WINV) while Column 9 is the difference between this relative magnitude estimate and that of the magnitude values of this report (m_b). In only one case, MADISON, does a value in Column 9 exceed 0.1 magnitude unit. The conclusion is that the procedural scheme used of averaging values computed by various phase formulas has passed another significant test.

APPLICATION OF THE PHASE CURVES TO EARTHQUAKES OF WESTERN UNITED STATES

1. General. Problems of two sorts expectedly arise in the application of these formulas to data from earthquakes. First, the factor of relative excitation of phases, significant in such a small region as NTS, expectedly introduces inconsistencies in predicted magnitudes of earthquakes. Second, the certain definition of phase for each arrival measured becomes more difficult than for NTS shots. For shots, phase definition is comparatively simple since we know accurately the time of origin and epicenter and 2-second differentials in travel-times are clear and meaningful. However, the programs used in locating earthquakes do not consider the presence of two dominant refracted phases in the distance range 300-1800 kilometers. The attempt to locate epicenters on the basis of a formula that obscures these two arrivals by treating them as one or as an invalid two can lead only to phase confusion and lack of definition on a $T - \Delta/8.1$ plot. SHOAL and the Fallon Earthquake form an excellent demonstration pair of this phenomenon. These two events occurred very near each other and many of the same stations recorded them. The $T - \Delta/8.1$ plot for SHOAL (see shot report) clearly shows the several refracted phases. Time of origin and epicenter were very accurately known and were not derived from the travel-time data. The Fallon Earthquake, however, of necessity was located by use of the travel-time data and by use of an earth model which did not represent the velocity structure of the region. Thus, appreciable uncertainties in the time of origin and epicenter resulted in a confused and virtually undecipherable $T - \Delta/8.1$ plot. In such a situation, one must, almost of necessity, establish arbitrary ranges for the applicability of each phase magnitude formula. We adopt the convention that $m_{7.9}$ applies to all stations with $\Delta \leq 1000$ kilometers, $m_{8.5}$ to all stations with $1000 < \Delta \leq 1800$, and $m_{10.5}$ and m_{ts} beyond 1800 kilometers. The breaking of this rule occurs when obvious reason to do so exists and we note such exceptions. Expectedly, the shadow-zone effects of the Sierra Nevada influence relative amplitudes of these phases. With these limitations in mind, we selected for study a set of WUS earthquakes. Several events

reported by the US Coast and Geodetic Survey (USC&GS) to be of magnitude 5 or greater augment earthquakes previously reported by VELA in shot report style. As an interesting sidelight of this investigation, note that USC&GS or Pasadena often greatly overestimate magnitudes of small earthquakes (5 or less) relative to teleseismic magnitudes. Much of this is clearly due to use of invalid formulas relating magnitude, distance, and A/T.

2. Earthquakes Studied. The earthquakes investigated are those of:

2 Feb 1962	at 18° 12' N 104° 54' W	
5 Feb 1962	38 12	107 36 Colona Earthquake Report
15 Feb 1962	36 51	112 26
15 Feb 1962	37 04	112 58
25 Feb 1962	45 12	111 12 Hebgen Earthquake Report
5 Apr 1962	38 24	119 18 Bridgeport Earthquake Report
14 Apr 1962	41	125
27 May 1962	31.7	115.6
20 Jul 1962	39 30	118 18 Fallon Earthquake Report
21 Aug 1962	42	127
30 Aug 1962	41 54	111 24 Cache Creek Earthquake Report
5 Sep 1962	40 62	112 00 Cache Creek Earthquake Report
16 Sep 1962	36	119
6 Nov 1962	45	123
18 Nov 1963	30	114
22 Mar 1964	38	119
5 Jul 1964	26	111
24 Oct 1964	44.7	129.1
22 Dec 1964	31.5	116.9

Figures 81 through 98 display the m_{sr} values and the phase magnitude values. The general phenomenon of predicting too high a magnitude by use of m_{sr} at less than 1700 kilometers becomes as apparent as for NTS shots. Fallon, in particular, interests us as its pattern of computed magnitude values is so similar to that of SHOAL, implying essentially identical energy partition functions of these two events as regards P-wave energy. The events of 14 April 1962, 27 May 1962, 6 November 1962, and 24 October 1964 display excellent adjustment of the data by use of the phase formulas in contrast to the poor adjustment when using m_{sr} . Events of 2 February 1962, 21 August 1962, 16 September 1962, 22 March 1964, 31 March 1964, and 5 July 1964 give lower estimates of magnitude at less than approximately 1400 kilometers than at greater epicentral distances. Note that these events occurred either immediately west of the Sierra Nevada or in Mexico, or near Queen Charlotte Islands.

3. Small Earthquakes. The quakes of 5, 15, and 25 February 1962, 5 April 1962, and 6 August 1963, i. e., Colona, Kanab aftershock, Hebgen, Bridgeport, and one other, were not recorded at teleseismic distances because of their small size. The first four were used by Mansfield in his discussion of AR. Note that, of all of them, the use of m_{sr} values predicts a teleseismic magnitude completely inconsistent with the short distances over which these events were recorded. Adjustment by the phase formulas brings the individual magnitude data into more reasonable internal agreement and, in addition, yields reasonable magnitudes in light of the short range of recorded signals. A more detailed discussion from a regional pattern point of view seems unwarranted until a large sample of events has been analyzed. It seems obvious, however, that treatment of the A/T data of earthquakes of WUS by the WUS phase formulas yields a more internally consistent body of data than that obtained by use of m_{sr} values.

4. Libyan Earthquake of 21 February 1963. As a final note on this point the two Libyan earthquakes (Figure 99) studied by Gordon⁵ suggest the appropriateness of application of these formulas (or at least $m_{8.5}$) to the Mediterranean area. For the two events reported in the above-mentioned paper, ATU and IST, 5.8° and 10.6° , respectively, yielded excessive magnitude estimates by use of m_{sr} values but yield values consistent with m_{ts} by $m_{8.5}$ for IST and $m_{7.8}$ for ATU.

USE OF P PHASES AS DIAGNOSTIC AIDS

The agreement of $m_{6.0}$ (see Appendix), $m_{7.9}$, $m_{8.5}$, $m_{10.5}$, and m_{ts} values for both explosions and earthquakes means that relative excitation of these phases cannot be used as a diagnostic criterion for distinguishing explosions and earthquakes. Little doubt exists that patterns of variable relative excitation such as observed for BILBY and HARDHAT will occur in earthquakes also but a pattern separating earthquakes and explosions does not exist.

VELOCITY STRUCTURE OF CRUST OR CRUST AND UPPER MANTLE IN EASTERN UNITED STATES AND WESTERN UNITED STATES

1. EUS

a. Limited P_g data indicate that in EUS this phase is never the clearly marked phase that it is in WUS. The events picked as P_g appear to have a zero-distance time-intercept of several seconds and a velocity of about 6.4 kilometers per second. However, the data are exceedingly poor.

b. Figure 23 is the basis of the following discussion, being based upon numerous shot reports. The $P_{8.5}$ event records as first arrival to 2100 kilometers. The SS Village profile (recorded by land stations,

⁵Gordon, David W., 1963, Libyan Earthquake of 21 February 1963, USC&GS Publication.

the nearest being a few hundred kilometers from the shot point) has an intercept of +9 seconds. This represents a path which includes one trip through the EUS crust, one trip through an oceanic crust, and a horizontal leg of a few hundred kilometers to continental structures at about 8.1 kilometers per second rather than the continental velocity. GNOME-East shows an intercept of +11 seconds, this intercept being representative of two trips through the EUS crust. We will assume that 5.5 seconds characterize crustal thickness in EUS, the 3.5 second difference of the SS Village intercept being explained by the two last path segments mentioned above.

c. Very simple crustal models suffice for the discussion which follows. The discussion illustrates the contrast between EUS and WUS, a contrast so gross that slight details of crustal model are of second-order significance. Therefore, we assume a velocity of 6.0 kilometers per second above the P_{8.5} refractor and obtain a thickness of 46 kilometers for the crust in EUS. This thickness varies as other investigations have shown, but an average figure suffices for this discussion.

2. WUS. A cursory glance at Figure 23 reveals immediately the gross contrast between travel-time curves for EUS and WUS in the range 150-2100 kilometers. As we have already illustrated, marked differences occur within WUS itself.

a. P₈ is well observed in WUS out to 1000 kilometers and has a velocity of very nearly 6.0 kilometers per second.

b. P_{7.9} is widely observed in WUS for NTS events. Its intercept does not depend upon azimuth from NTS and is about +5 seconds. Use of a layer velocity of 6.0 kilometers per second indicates a depth of 26 kilometers to this refractor.

c. The P_{8.5} - NTS/Dakotas profile has an intercept of +14 seconds, representing the sum of 1-way trips through WUS and EUS crustal types, all times having been measured in EUS for this phase on this profile. If 5½ seconds represent a 1-way trip through the EUS crust, 8½ seconds characterize a 1-way trip through the WUS crust.

d. For P_{8.5} - NTS/Washington, an observed intercept of about +18 seconds should characterize a 2-way trip through the WUS crust. A value of 9 seconds for a 1-way journey agrees nicely with the value of 8½ found on the NTS/Dakotas profile.

e. If we assume an average value of 8.0 kilometers per second for the velocity in the layer between the P_{7.9} and P_{8.5} refractors in WUS, a thickness of approximately 130 kilometers is found for this.

layer. The $P_{8.5}$ refractor in WUS then occurs at a depth of about 150 kilometers while in EUS it occurs at only approximately 50 kilometers. The question immediately arises as to what to call the crust in these areas. No logical basis exists for calling the $P_{7.9}$ refractor base of crust in WUS and the $P_{8.5}$ refractor the equivalent level in EUS. This customary approach may obscure a fundamental and profoundly significant contrast between these two parts of the United States. No logical explanation of the supposed thinning of the crust from east to west exists. The general conclusion of compensation below the crust has been invoked in order to explain the conflict between gravity and seismic data. Real understanding of the relations between these two types of data may result from the realization that the same velocity surface is present in WUS as is termed base of crust in EUS but is approximately 100 kilometers deeper in WUS. Probably, calling the $P_{8.5}$ refractor in both areas base of crust would constitute a geophysically meaningful definition.

f. $P_{8.1}$ - NTS/Northern New Mexico. On large events at NTS, a clear 8.0 - 8.1 arrival is recorded as far as RINM, the intercept being approximately 7.5 seconds. Detailed inspection of records obtained along this profile indicates absence of a 7.7 - 7.9 refractor. Indefinite recordings of $P_{8.5}$ have been measured at a few hundred kilometers, really good recordings not being obtained until the profile extends into EUS. The $P_{8.1}$ refractor apparently replaced the $P_{7.9}$ refractor in this region and is at a somewhat greater depth, the values given above yielding a depth of 36 kilometers. The $P_{8.5}$ refraction leg observed in Texas and beyond has an intercept of 18 seconds. In light of the fact that the GNOME East profile traversed the same region with an intercept of only 11 seconds, the suggested explanation is that the $P_{8.5}$ energy observed along this profile for NTS shots is the energy that was following the $P_{8.1}$ refractor in WUS.

APPLICATION OF IDEAS OF THIS PAPER TO OTHER AREAS

1. General. The functional relation between A/T and Δ for a given region quite obviously depends upon the velocity structure of the region. A simple velocity structure such as that of EUS will result in a simple dependence of A/T upon Δ . Conversely, the existence of multiple refractors will result in a complex dependence of A/T upon Δ . The general suggestion is that Shield or Cratonal areas of low mean elevation will display a simple A/T versus Δ relationship while regions of high mean elevation on a regional basis will display complex velocity structures and a complicated dependence of A/T upon Δ . Therefore, an investigation of the velocity structure of a region will lead to a basic understanding of the operative A/T versus Δ relationships. Such velocity data cannot be based upon an epicentral location and origin time based in turn upon an assumed velocity structure. Thus, only data for explosions are acceptable for such an analysis.

2. Europe. The Haslach travel-time curve for Europe allows an immediate prediction of the expected A/T versus Δ relationships for this region. The data on which the travel-time curve of Figure 23 is based were obtained as the result of an explosion near Haslach in Southwest Germany ($48^{\circ}16'N$ $08^{\circ}07'E$). Note that a single phase with uniform apparent velocity was recorded from 200 kilometers to 2000 kilometers, a pattern strikingly similar to that observed in EUS. It seems reasonable that A/T will be found proportional to very nearly the inverse second power of Δ in Europe. There seems to be little possibility of a pattern similar to that of WUS. No shadow zone for P phases will be found in this area.

3. Asia. The USSR has not released adequate explosion data to permit a prediction of the expected A/T versus Δ relationships. Obtaining such data is important as it would greatly advance our understanding of the problems to be expected from observatories at specific localities within the area of interest.

CONCLUSIONS

1. Contrary to the curve presented by Richter⁶, P_n amplitudes in WUS in the range 1000-1700 kilometers are not obeying a shadow zone interpretation as envisaged by Gutenberg. There is no evidence for a broad interval of several hundred kilometers in which P amplitudes are very small. There is a large jump in amplitude at approximately 1000 kilometers due to $P_{8.5}$ becoming the first arrival. For some uncertain reason, the $P_{8.5}$ refractor and associated refracted phase were never recognized in WUS by Gutenberg and the high amplitudes of this phase were either missed or misinterpreted. Signal levels decrease continuously from approximately 1000 kilometers outwards except for one or more comparatively small jumps in amplitude associated with the beginning of the first arrival of deeper refractions. These small steps in amplitude (such as from $P_{8.5}$ to $P_{10.5}$) cannot be termed shadow zone phenomena in the Gutenberg sense or in any real sense. Measurement of P amplitudes in the range 1000-2000 kilometers are more desirable than in any more distant.

2. In EUS, amplitudes increase continuously from 1000 kilometers to the epicenter. There is total absence of any phenomenon which could be interpreted as a shadow zone for P.

3. In WUS, the amplitude discontinuity in the neighborhood of 1000 kilometers is abrupt and associated with the first arrival of a deeper refraction ($P_{8.5}$), replacing the weaker $P_{7.9}$ event. The $P_{7.9}$ event can occasionally be followed as second arrival beyond

⁶Richter, loc. cit. and Figure 100, this report.

the point where $P_{g,5}$ becomes first arrival. The $P_{g,5}$ arrival in WUS appears to obey essentially the same decay law with distance as does the $P_{g,5}$ refraction in EUS.

4. The A/T versus Δ table used in the VELA shot reports is grossly inaccurate at distances out to 15° - 20° for virtually all events, even for WUS. Errors in magnitude estimates at single stations of as high as 1.5 magnitude units occur when this law is employed. Extensive confirmation of this failure of the shot report table or for any single curve for both explosions and earthquakes is contained in this report. All previously studied explosions and earthquakes plus several additional earthquakes have been recomputed according to the scheme proposed in this paper. Romney's procedure for computing m for small events by use of $P_{7,9}$ data was calibrated against teleseismic data of large events and thus avoided the inaccuracies of the shot report computations.

5. A/T data for the P_g phase in WUS are as useful and as meaningful for magnitude computations for both earthquakes and explosions as are the refracted P phases (see Appendix).

6. Magnitude computations based on refracted phases can be made essentially independent of distance by proper calibration of the crust and by establishing the correct energy partition function for the several phases generated. Such energy partition functions appear quite variable and must be influenced by focal and near-focus conditions.

7. Epicenter location of unknown events by use of regional and near-regional data will be markedly improved only when crustal models expressing the multiple refractors present in a region are used as the basis of analysis. Any effort to attach regional corrections must fail in general application.

8. Analysis of the amplitude/period data of any region in the range 200-2100 kilometers is only meaningful after elucidation of crustal structure and establishment of the general energy partition function and decay rates of each phase. It appears probable that velocity structure will characterize decay rates. Thus, the Haslach travel-time curve for Europe, based upon surface explosion data, is very similar to that of EUS. The implication is that $m_{g,5}$ may be applicable to A/T data of European seismic events in the regional and near-regional distances but only investigation of A/T data of Europe will indicate the actual relationships. The situation in the USSR is not certain and will not be clarified until data obtained by observing Russian explosions become available.

APPENDIX: ANALYSIS OF P_g DATA

1. General. $P_{6.0}$ (P_g) was observed widely and well throughout WUS to distances of 1000 kilometers with a velocity of 6.0 kilometers per second. P_g gives rise to higher A/T values than other P phases in WUS. In many cases it can be recognized by waveform character even though, at other than very near stations, it is a second arrival. In WUS it decays as the third power of the epicentral distance and its velocity is very near 6.0 kilometers per second. It does not occur beyond WUS and loses definition beyond about 1200 kilometers in any azimuth from NTS. One wishes to know whether one can interpret P_g A/T data in a magnitude sense to the extent that the P_n phases have been successfully interpreted. If so, two useful and significant results accrue. Firstly, one can obtain confirmation of our proposed A/T versus Δ versus m_b interpretive scheme from an independent phase. Secondly, such a uniformity of behavior would imply one could use P_g for estimation of magnitude of earthquakes with as much or more reliability than the P_n phases as the scheme of identification of P_n phases for an unknown epicenter may prove difficult while one can generally identify P_g by record character. If the beginning of P_g is measurable to within two or three seconds, better epicenters probably could be obtained by use of this phase than by use of the P_n phases in WUS. P_n phases as first arrivals are timed to a fraction of a second but the proper classification of the phase measured may be so uncertain and the crustal velocity structure assumed so inaccurate that one can introduce errors of several seconds into the calculations of epicenters. When using P_g in WUS an extremely simple but valid model can be used for computation purposes.

2. Analysis of P_g Data. The procedure followed here begins by estimating the best value of A/T at 500 kilometers from the A/T versus Δ plots for P_g in the shot reports. See Figures 103 through 106 for examples of A/T versus Δ plots of P_g data. We plot these (A/T)₅₀₀ values against radiochemical yield in Figure 107 and against m_b values of this report in Figure 108. Compare Figures 107 and 108 to see that the (A/T)₅₀₀ values of P_g display a linear relationship to the magnitude values of this report, being independent of shot medium. These two figures confirm the usefulness of P_g amplitude data for estimating magnitude and support the relative magnitude determinations of this report. The resulting $P_{6.0}$ equations are:

$$m_{6.0} = 1.28 + 1.14 \log (A/T)_{500} \quad (13)$$

$$m_{6.0} = -8.00 + 1.14 \log A/T + 3.42 \log \Delta \quad (14)$$

The curves of Figure 100 for $P_{7.9}$ can be used for $P_{6.0}$ if magnitude values are decreased by 1.0 units. In other words, $P_{6.0}$ gives A/T values 10 times those of $P_{7.9}$ at the same distance.

3. P_g Data for WUS Earthquakes. A/T data for the P_g phase are available for several earthquakes of WUS. The computed $m_{6.0}$ values follow:

Earthquakes	$(A/T)_{500}$	m_b	$m_{6.0}$
Colona (5 Feb 1962)	40	3.1	3.11
Hebgen (25 Feb 1962)	50	3.2	3.22
Cache Creek (30 Aug 1962)	2500*	4.3	5.16
Cache Creek A/S (5 Sep 1962)	500*	4.1	4.36
Bridgeport (5 Apr 1962)	42	3.03	3.29
Fallon (20 Jul 1962)	240	4.4	4.16

*Based on WUS data.

The P_g data demonstrate their usefulness for the estimation of magnitude of WUS earthquakes. Remember that we derived this scheme for P_g by calibration against m_{ts} values of P phases and noting the linear relationship between $\log Y$ and $\log (A/T)_{500}$. Therefore, the agreement at magnitudes above 4 occurs independently of P_n values inside 2000 kilometers and the agreement at lower magnitudes depends upon control other than previously computed magnitude values.

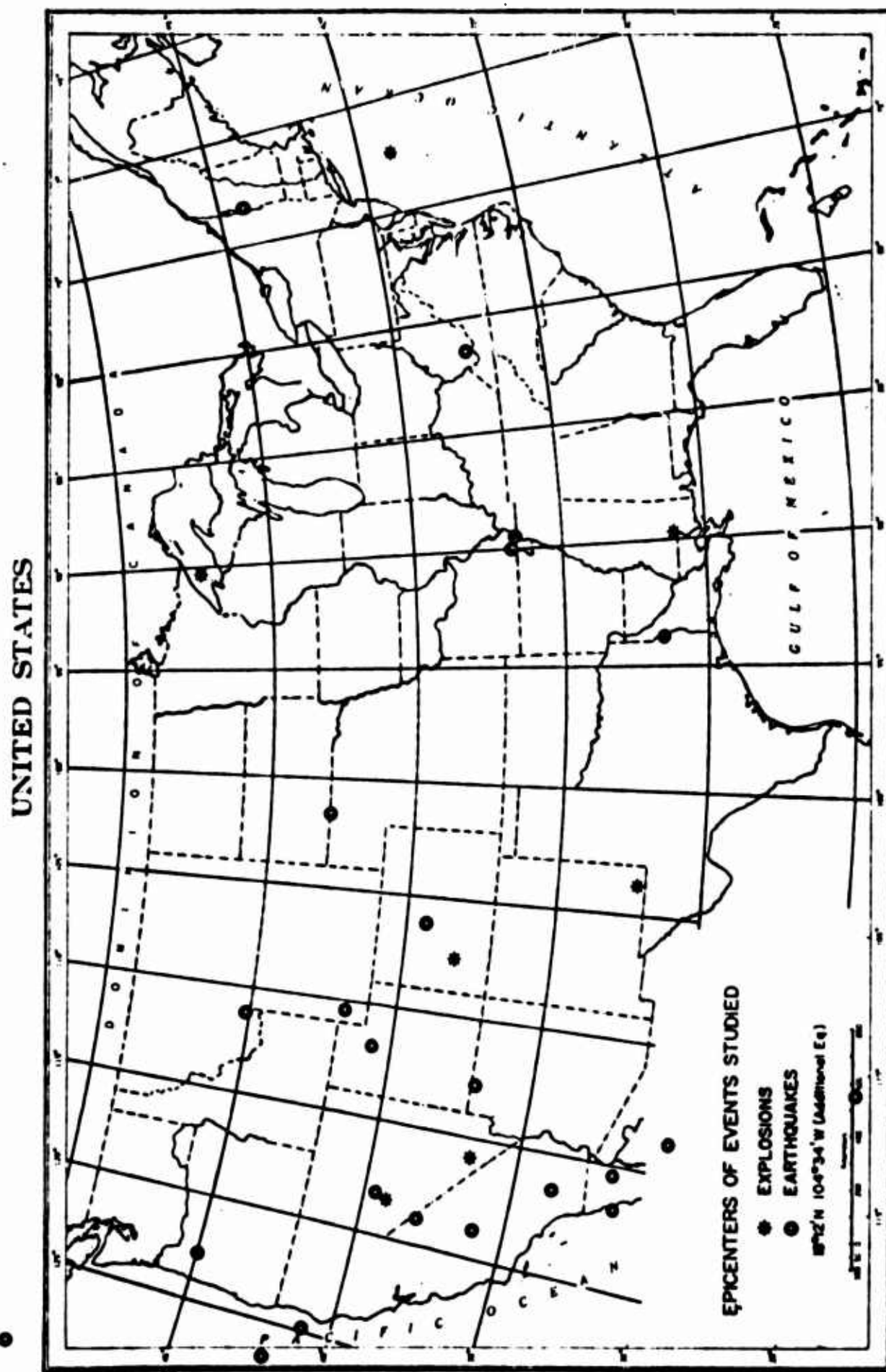


Figure 1
AFTAC/VSC

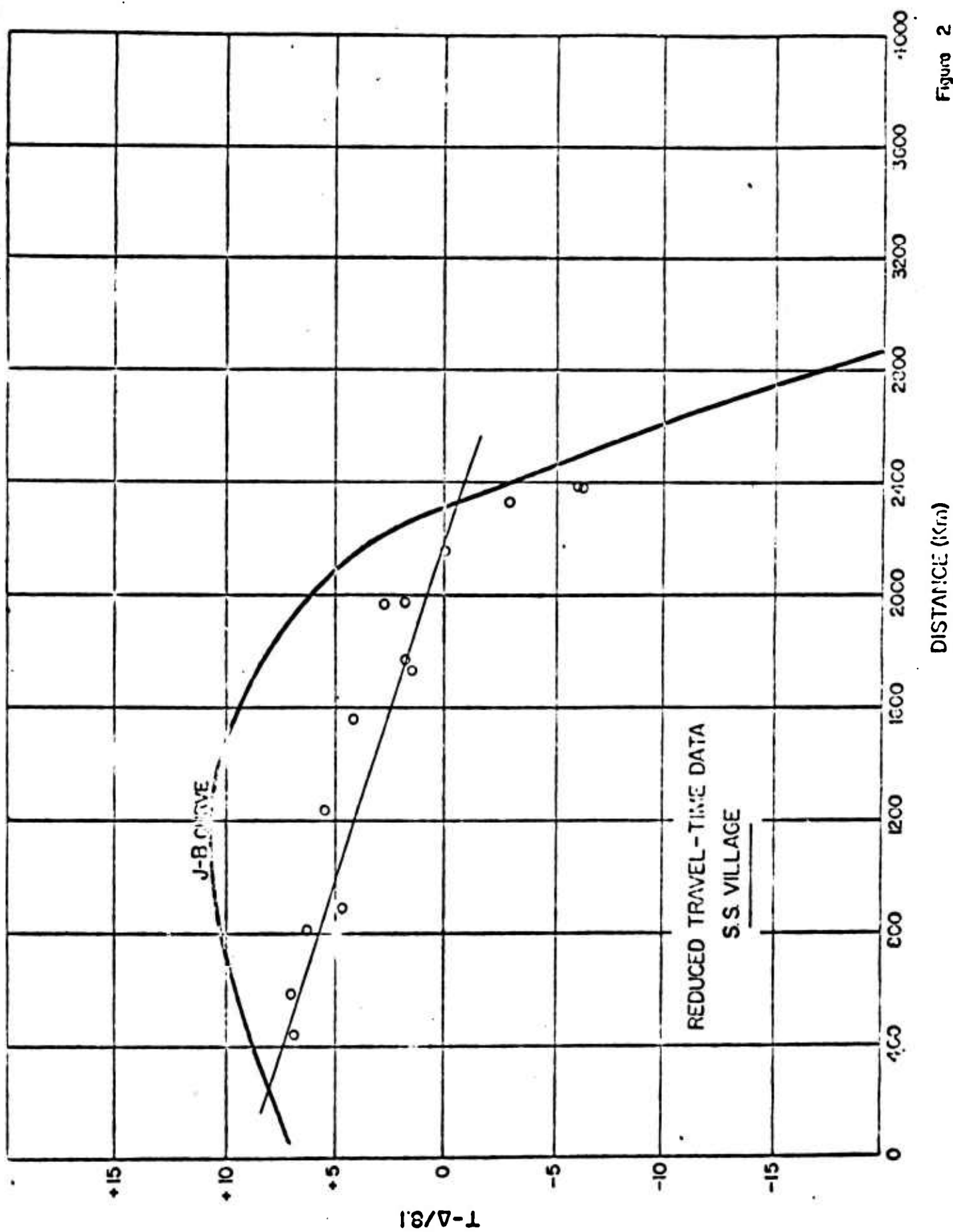


Figure 2
AFTAC/VSC

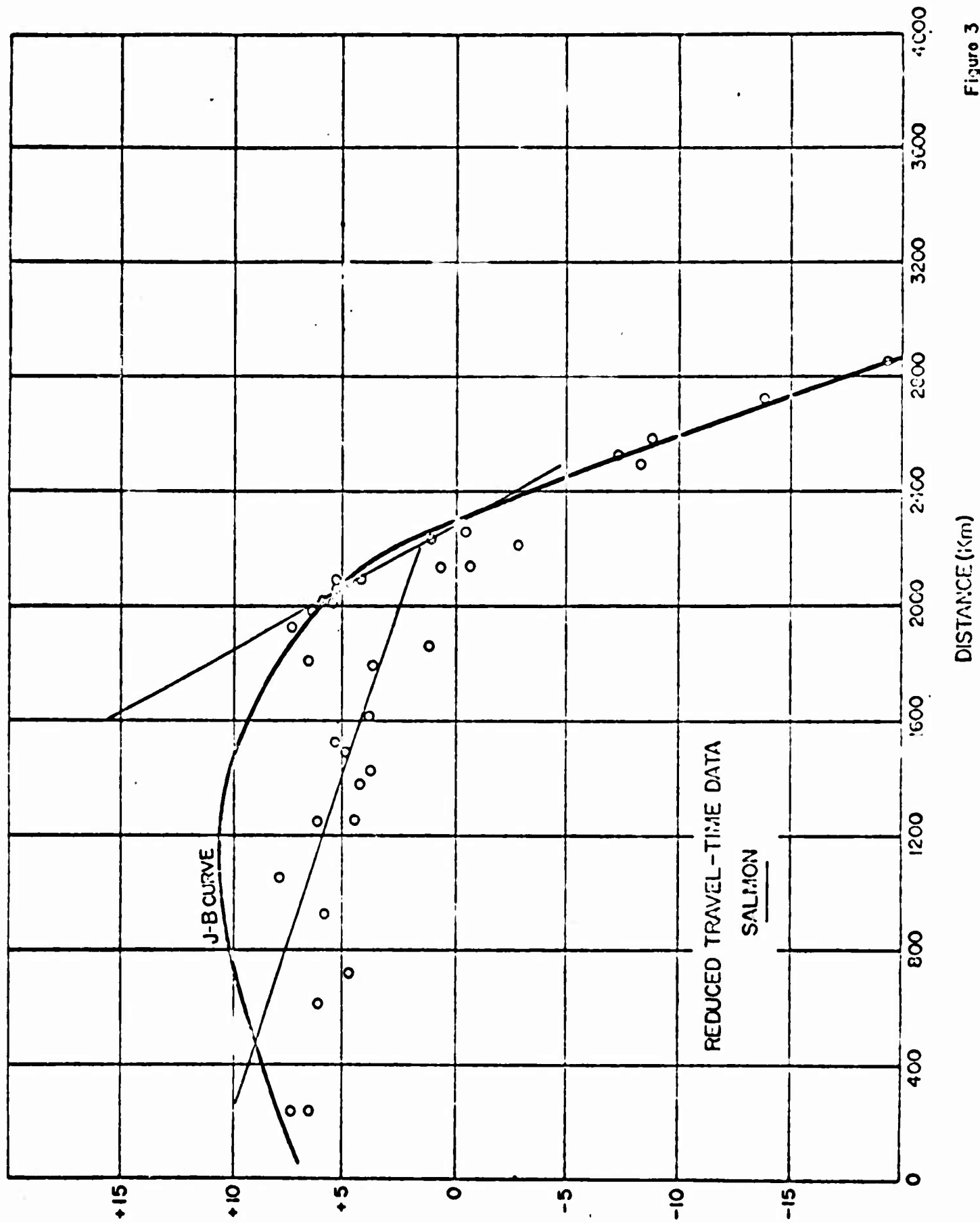


Figure 3

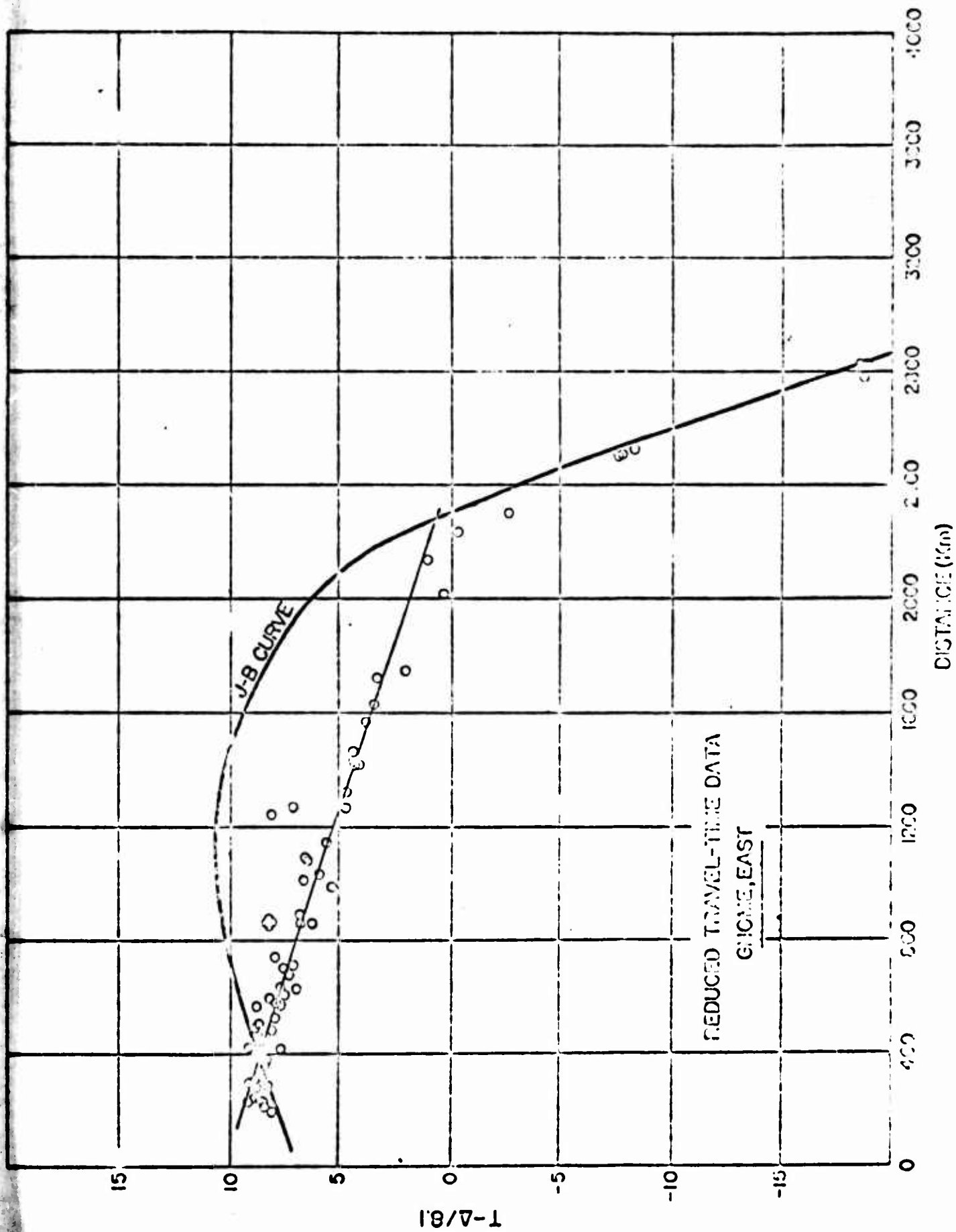


Figure 4
AFTAC/VSC

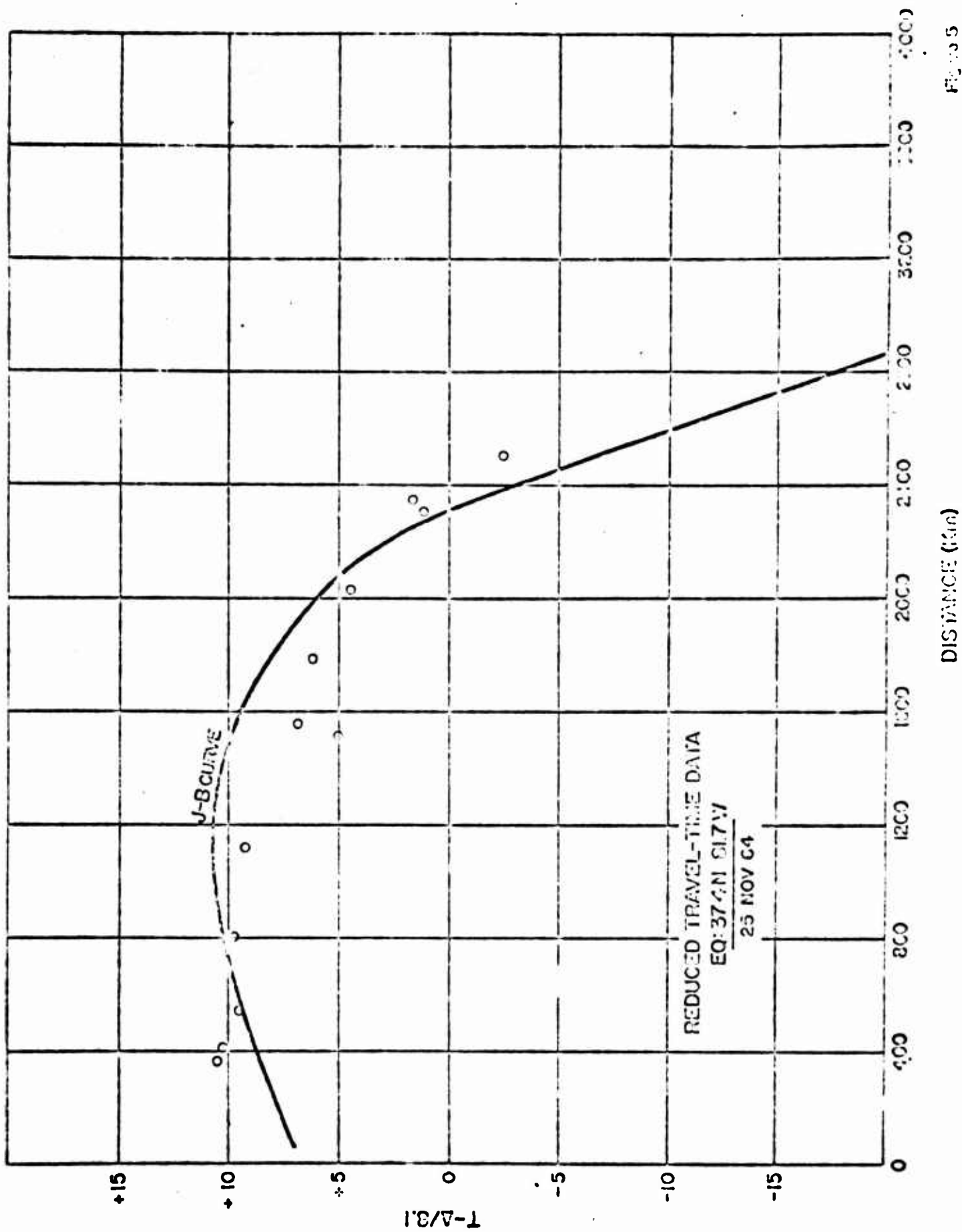


FIGURE 5
AFTER/VCC

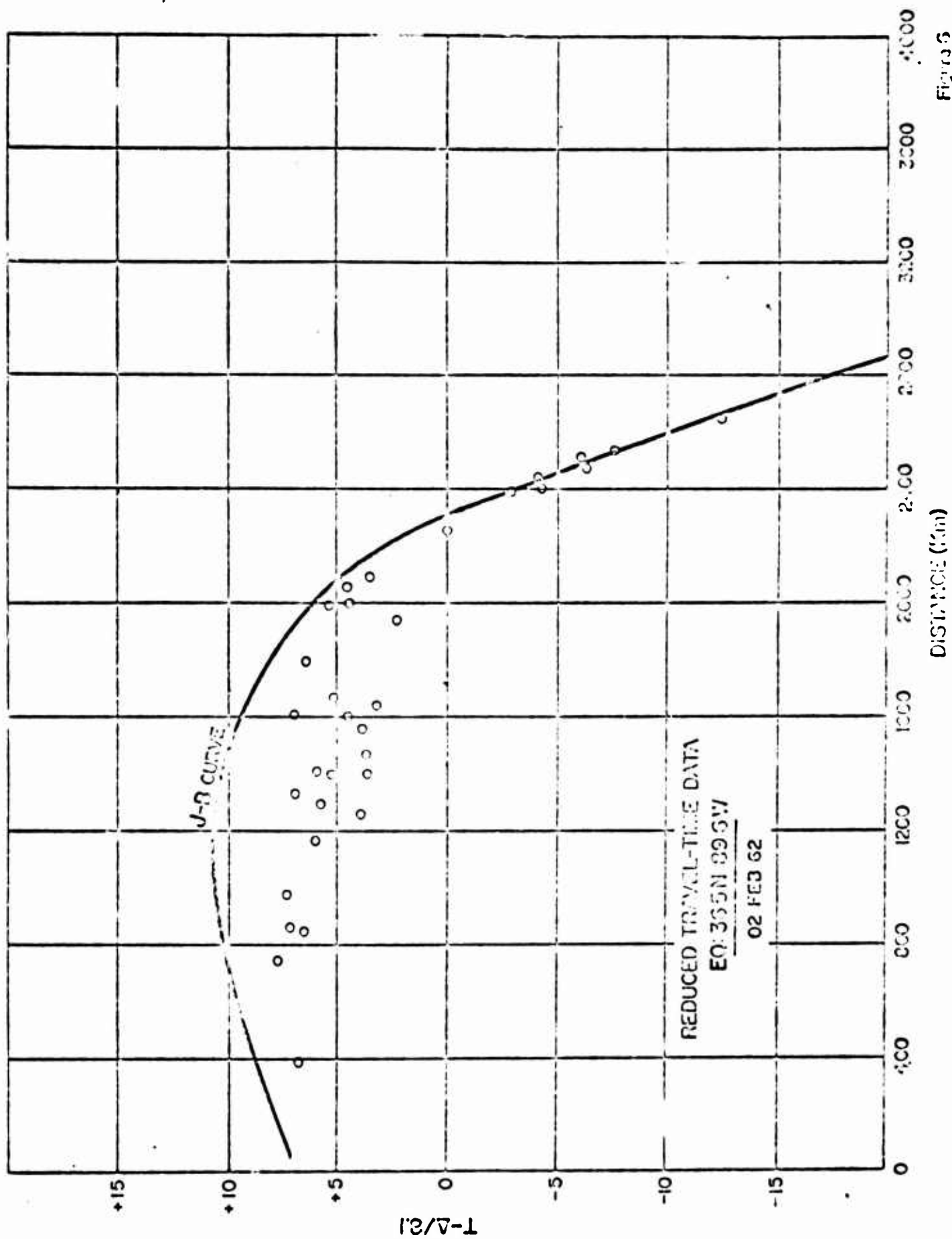
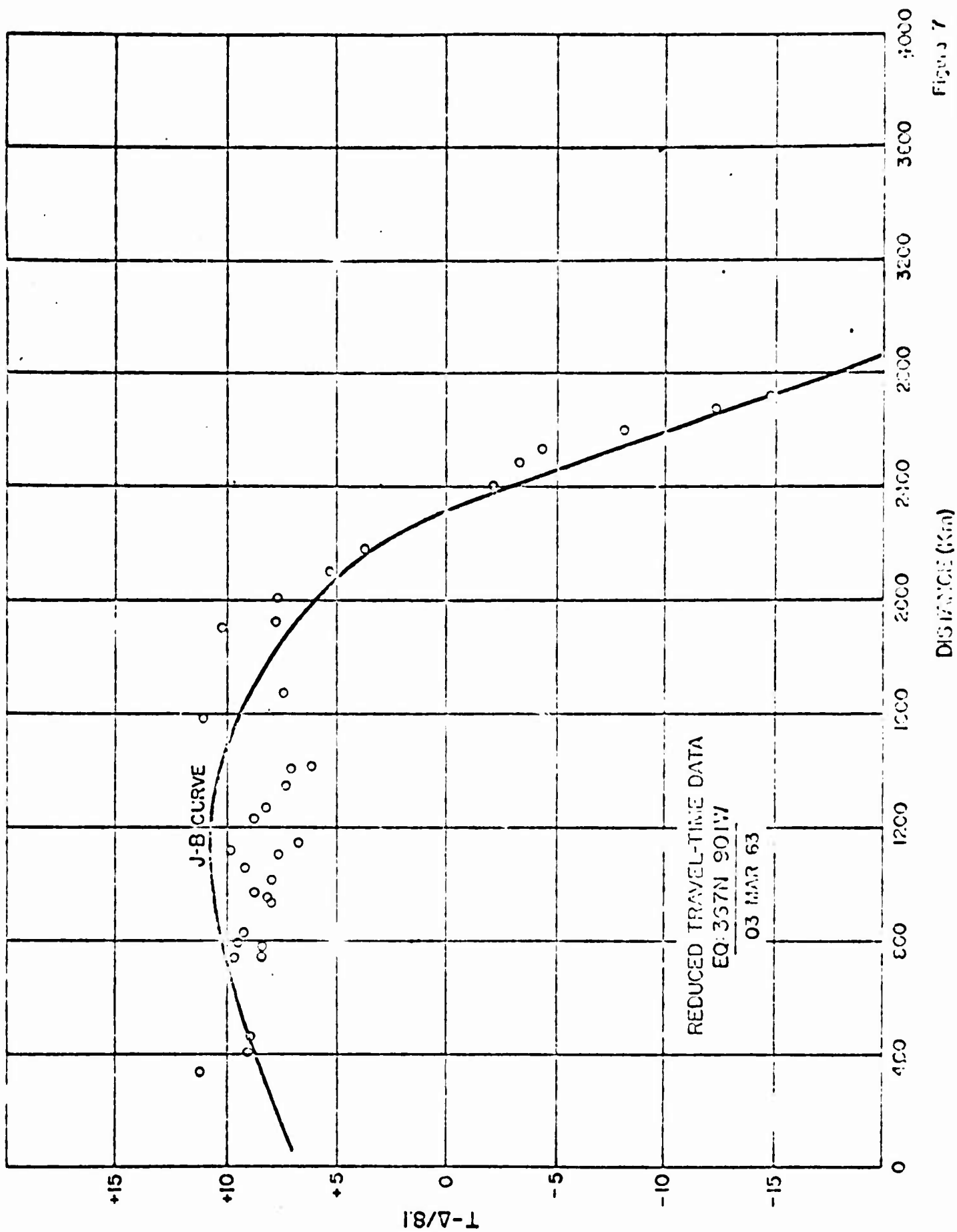


FIGURE 5
AF MAC/VSC



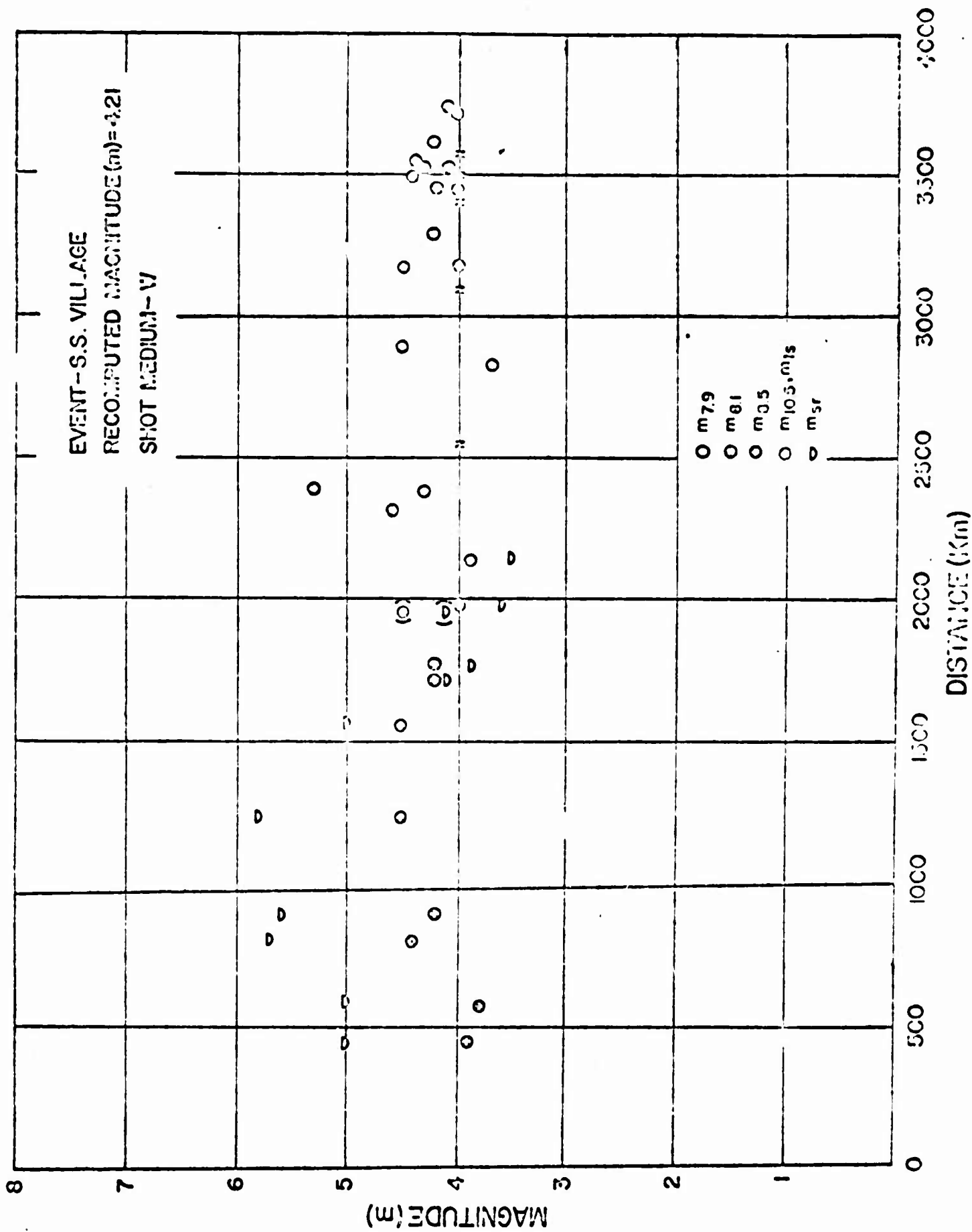


Figure 8
AFINC/VSC

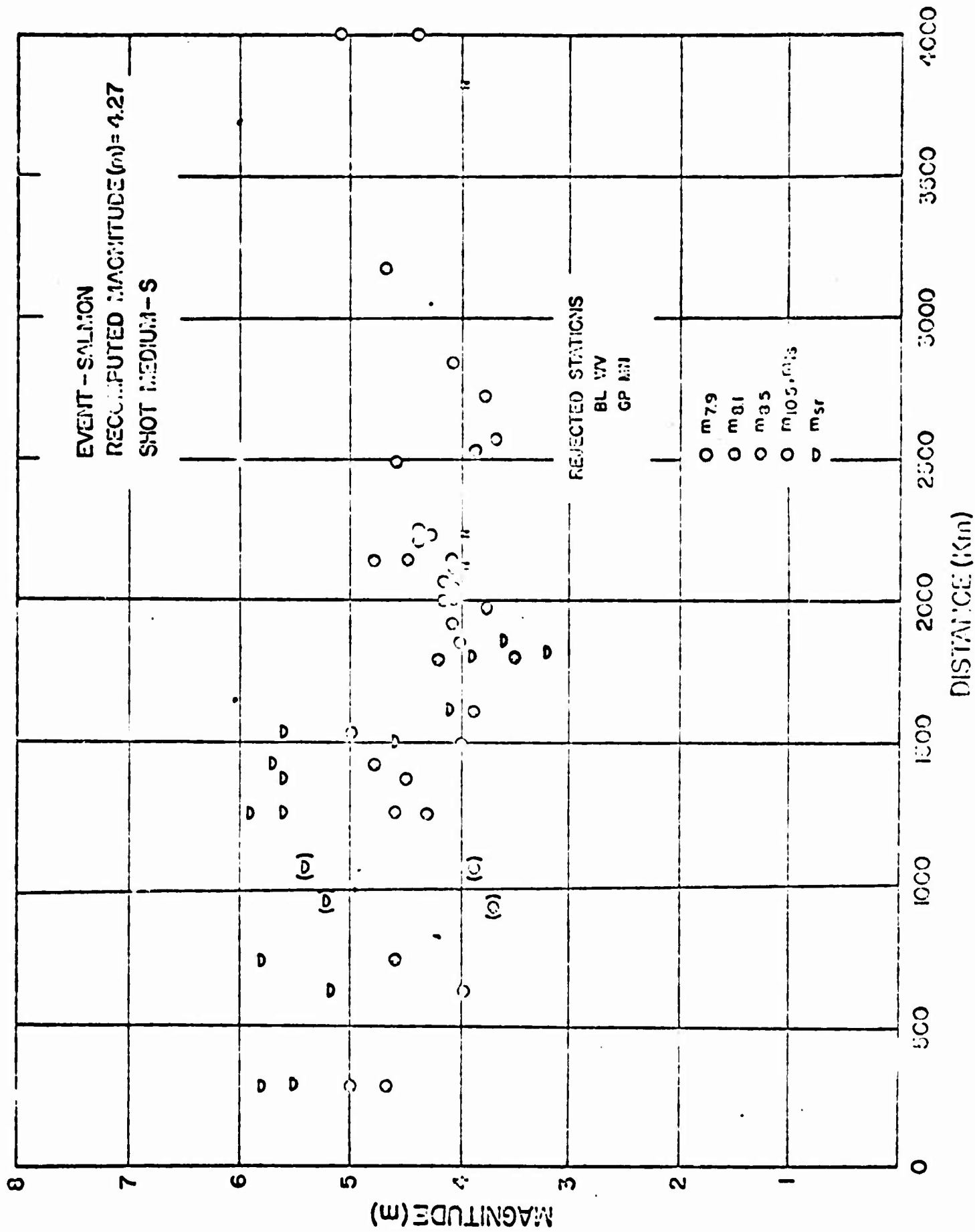


Figure 9

Figure 9

AF IAC/VSC

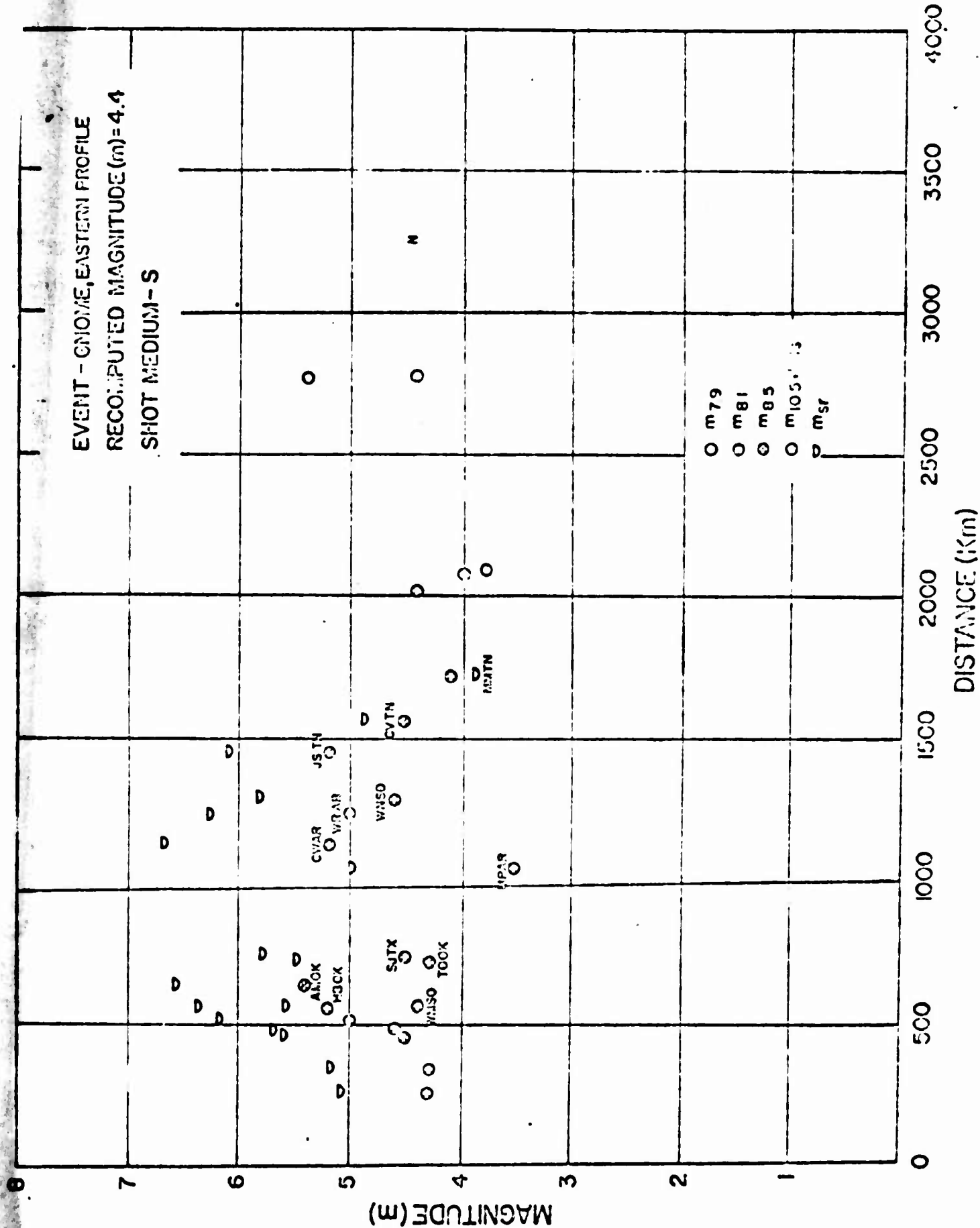


Figure 10

AF IAC/VSC

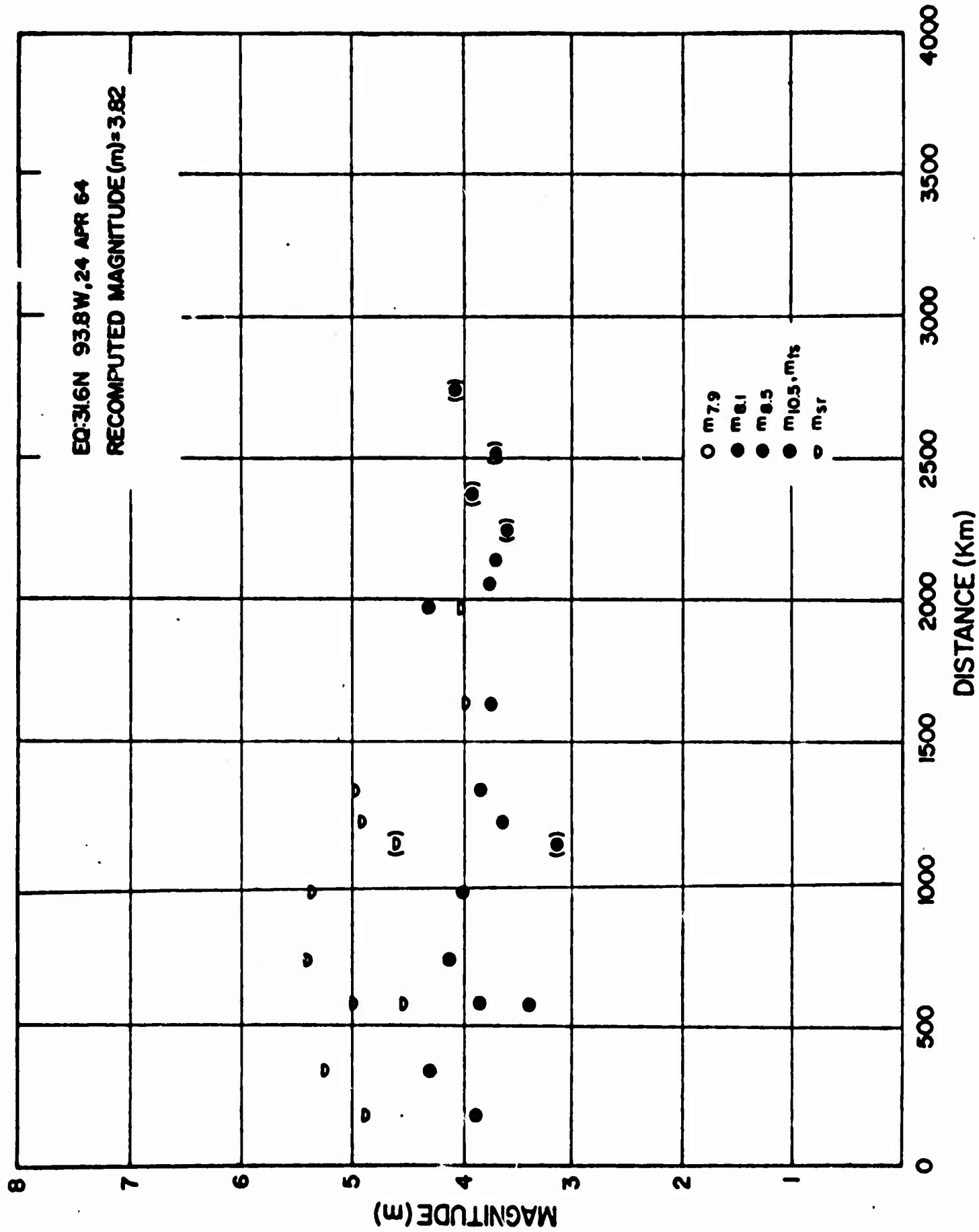


Figure 11
AFTAC/VSC

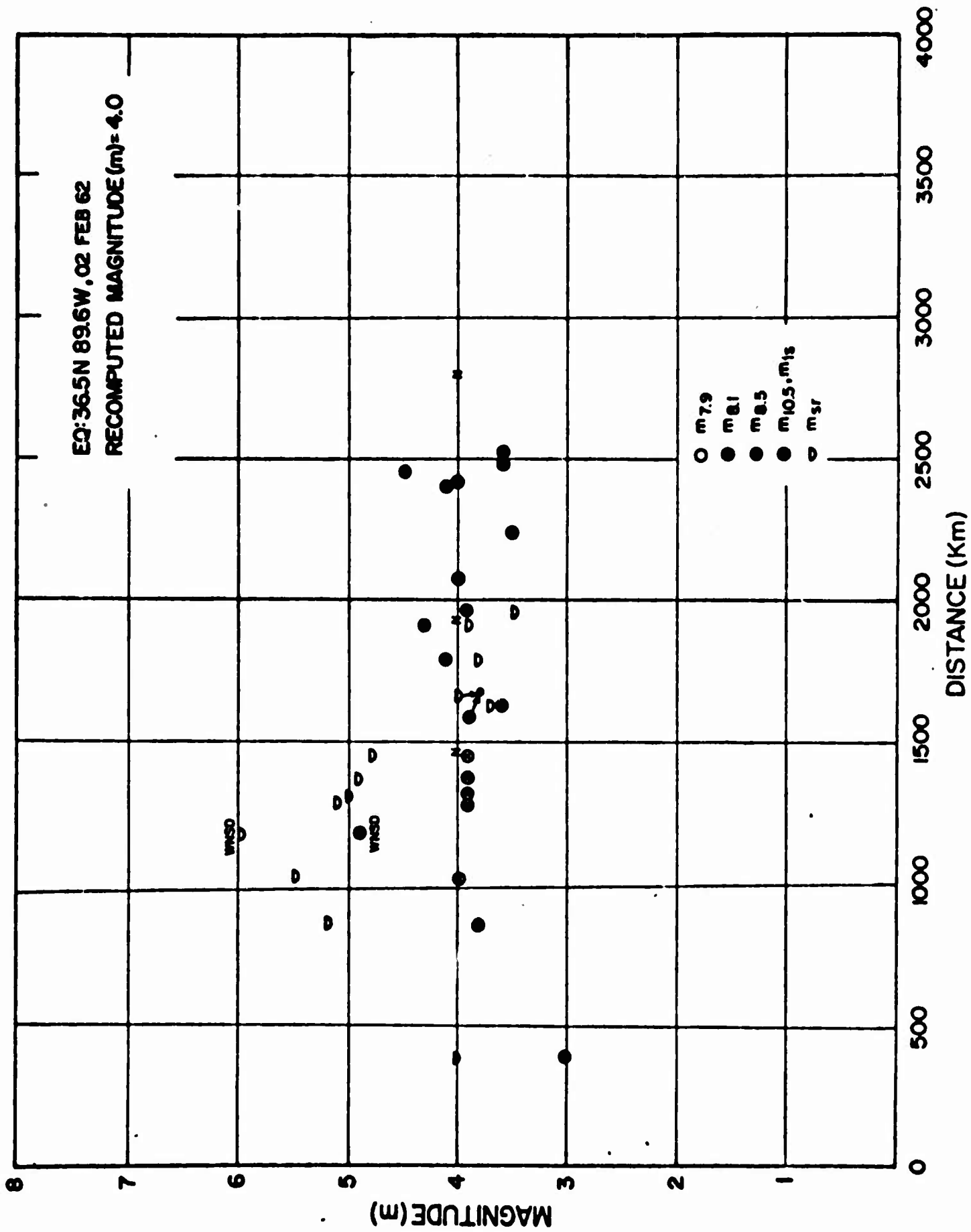


Figure 13
AFTAC/VSC

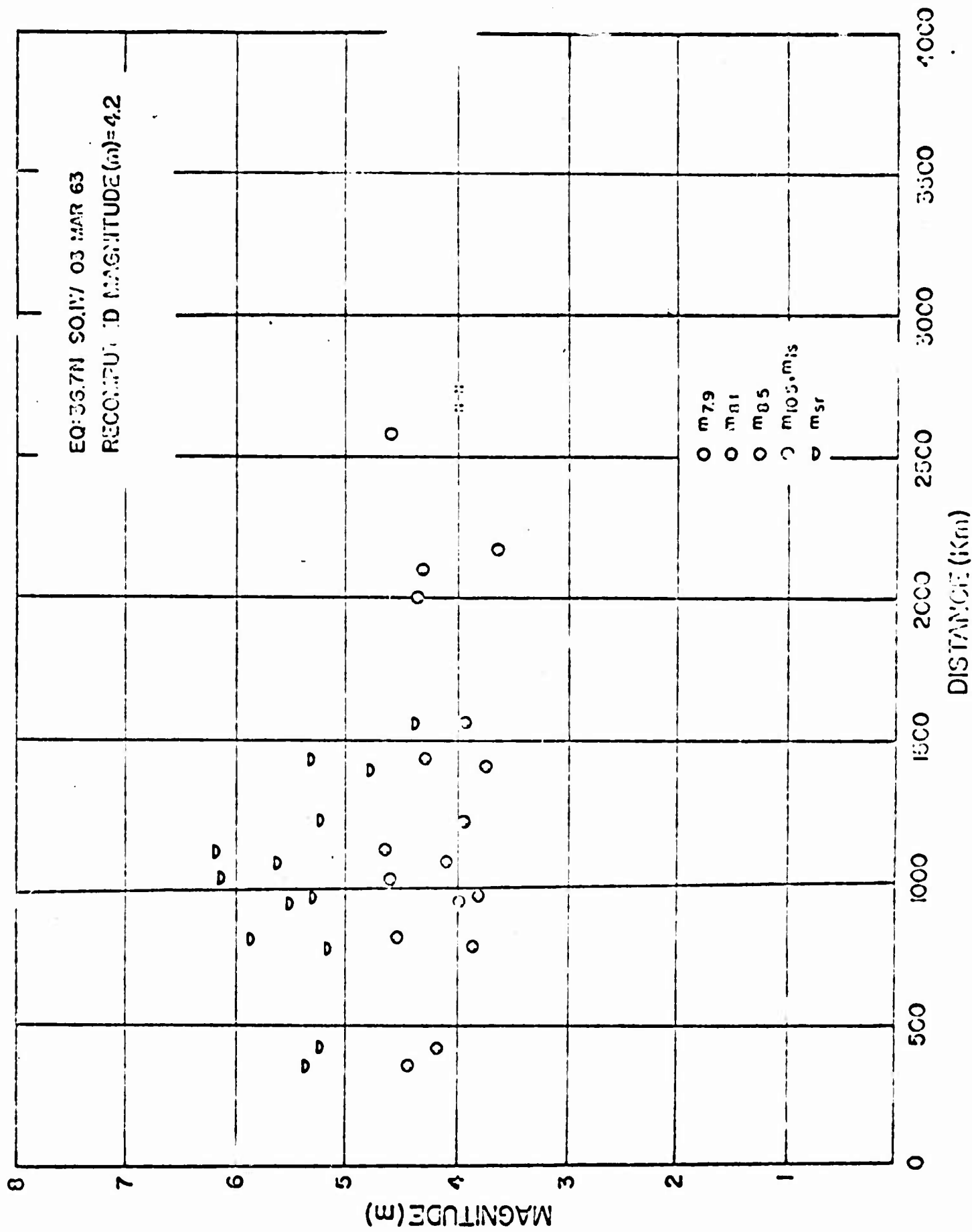


Figure 11
AF TAC/VSC

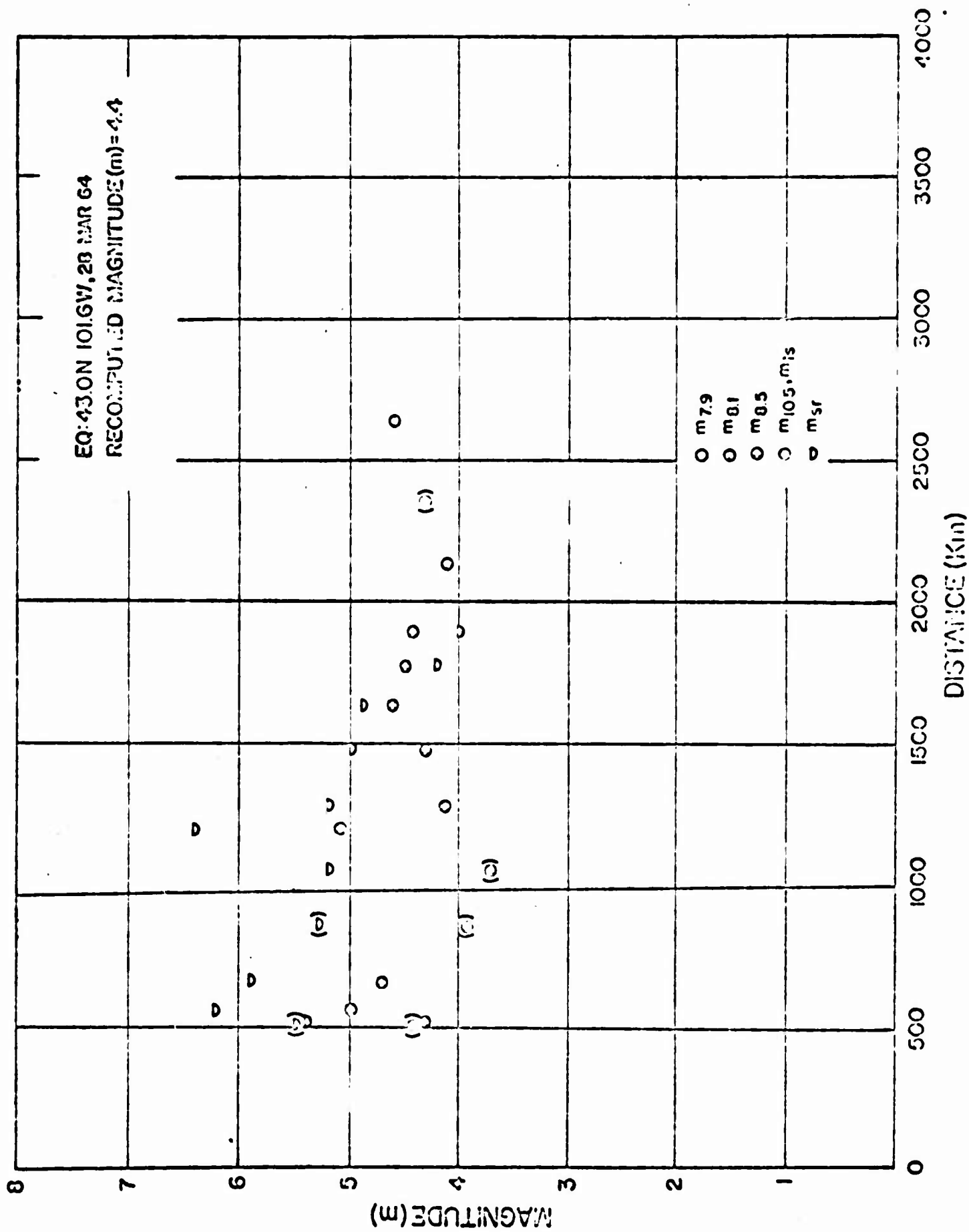


Figure 15
AFTAC/VSC

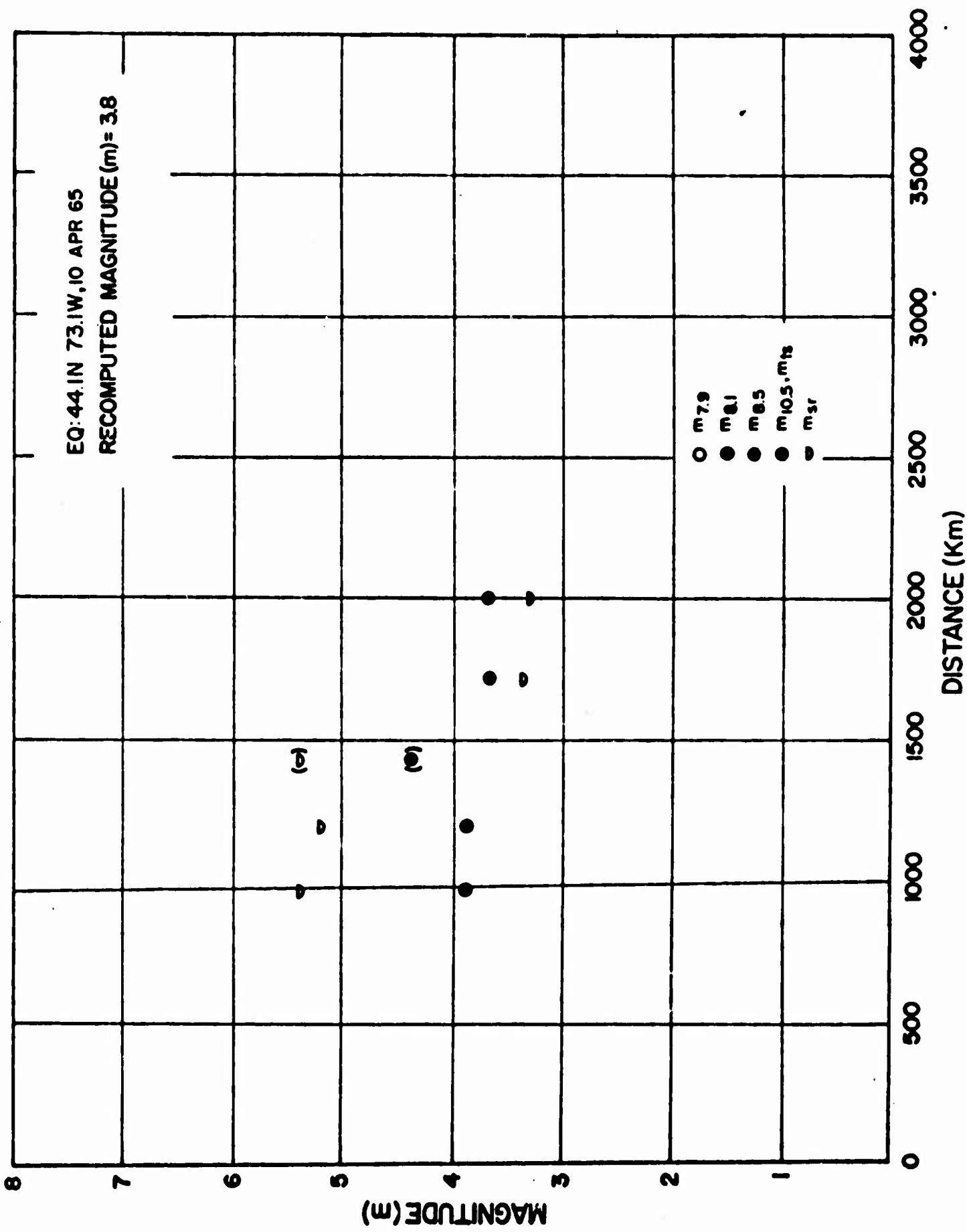


Figure 16
AFTAC/VSC

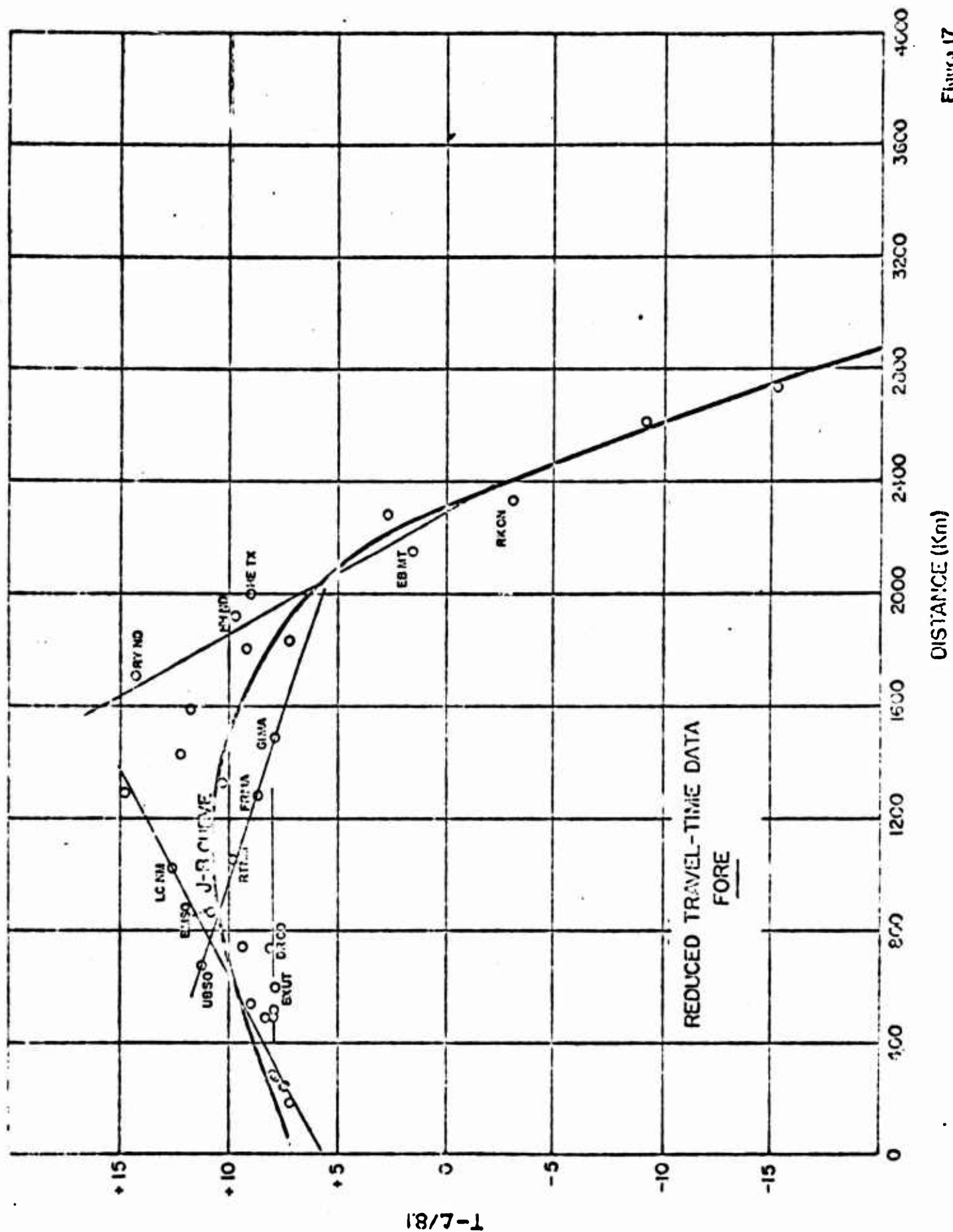


Figure 17
AFTAC/VSC

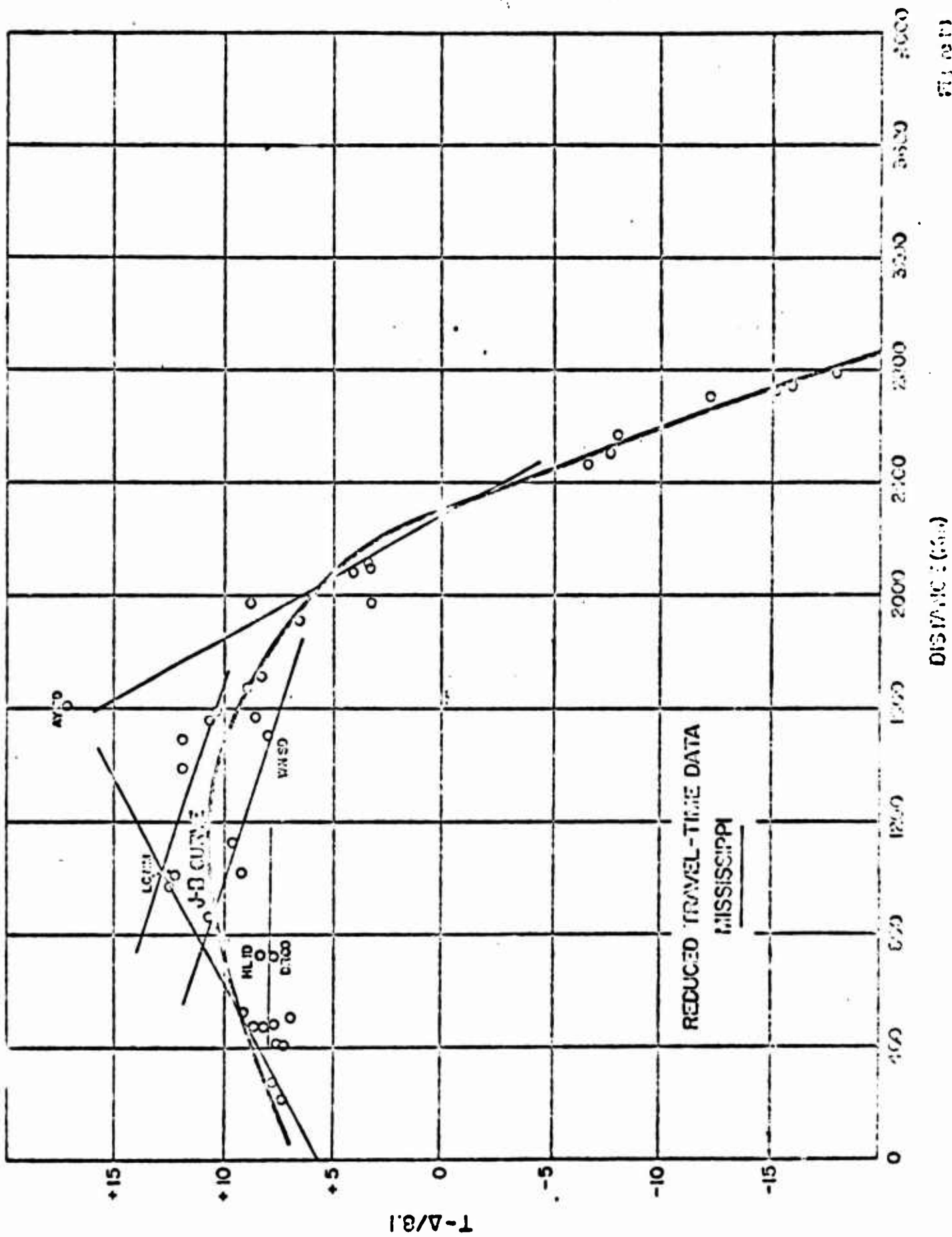


Fig. 10.11
ASCE 1970

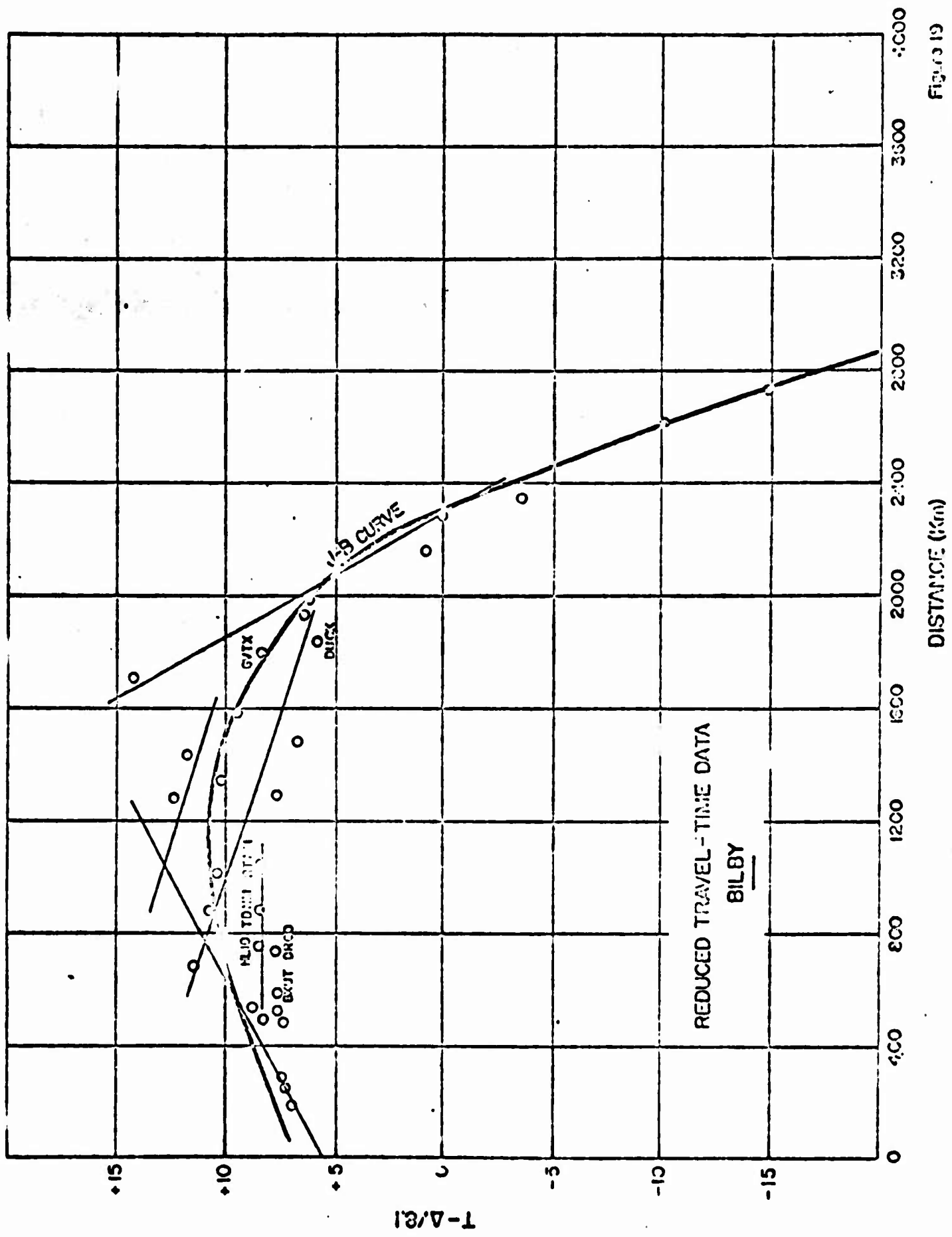


FIGURE 19
AFTAC/VSC

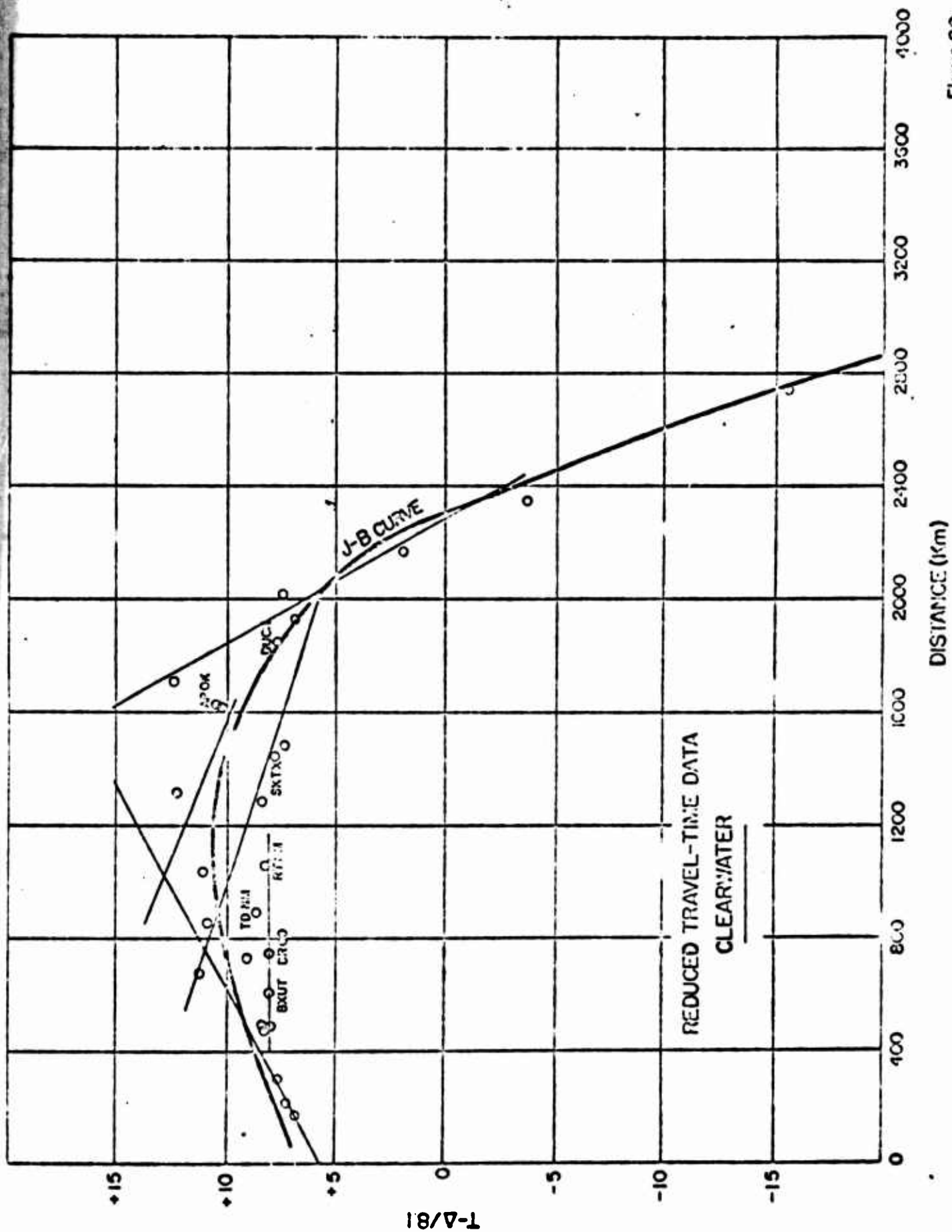


Figure 20
AFTAC/VSC

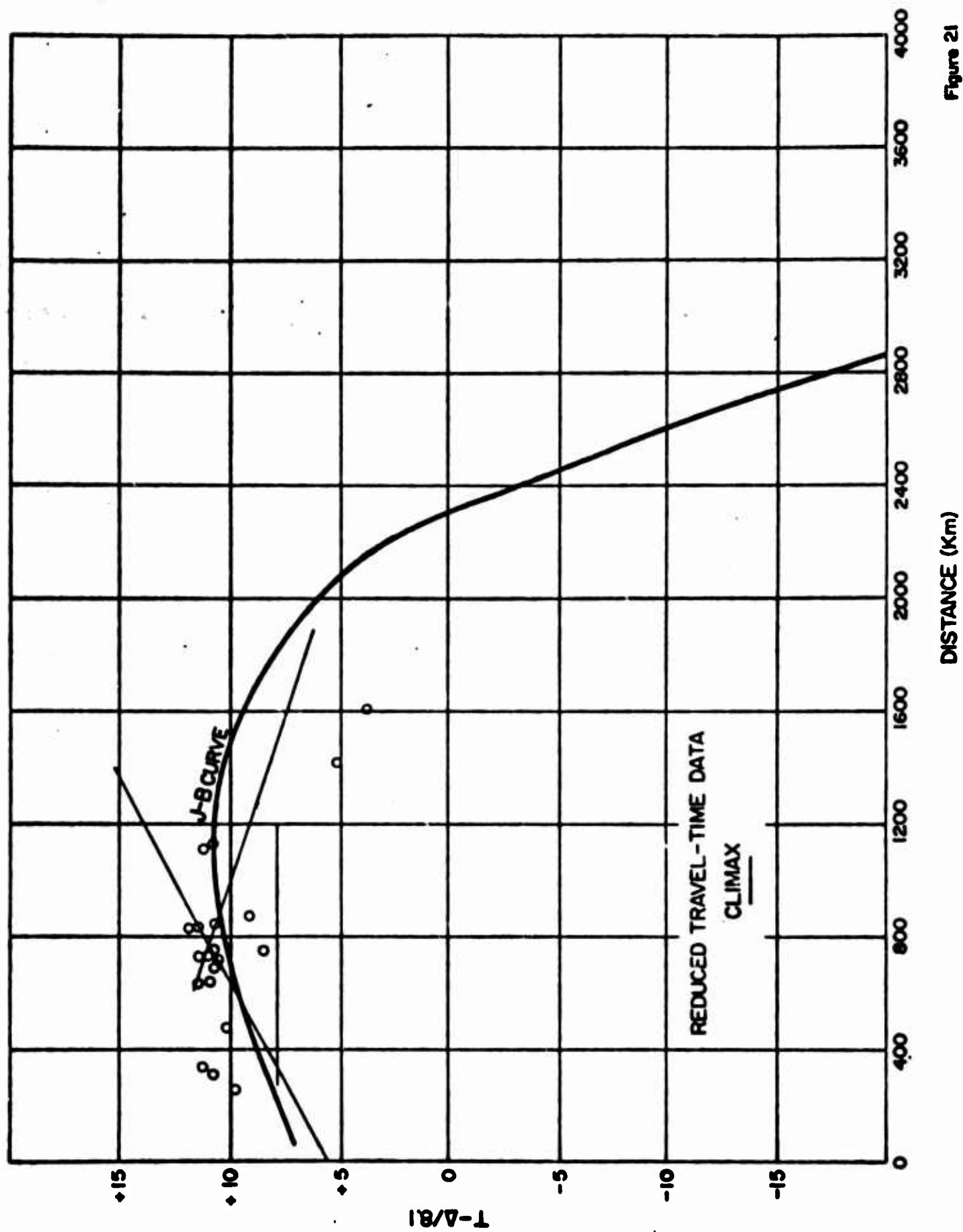


Figure 21
AFTAC/VSC

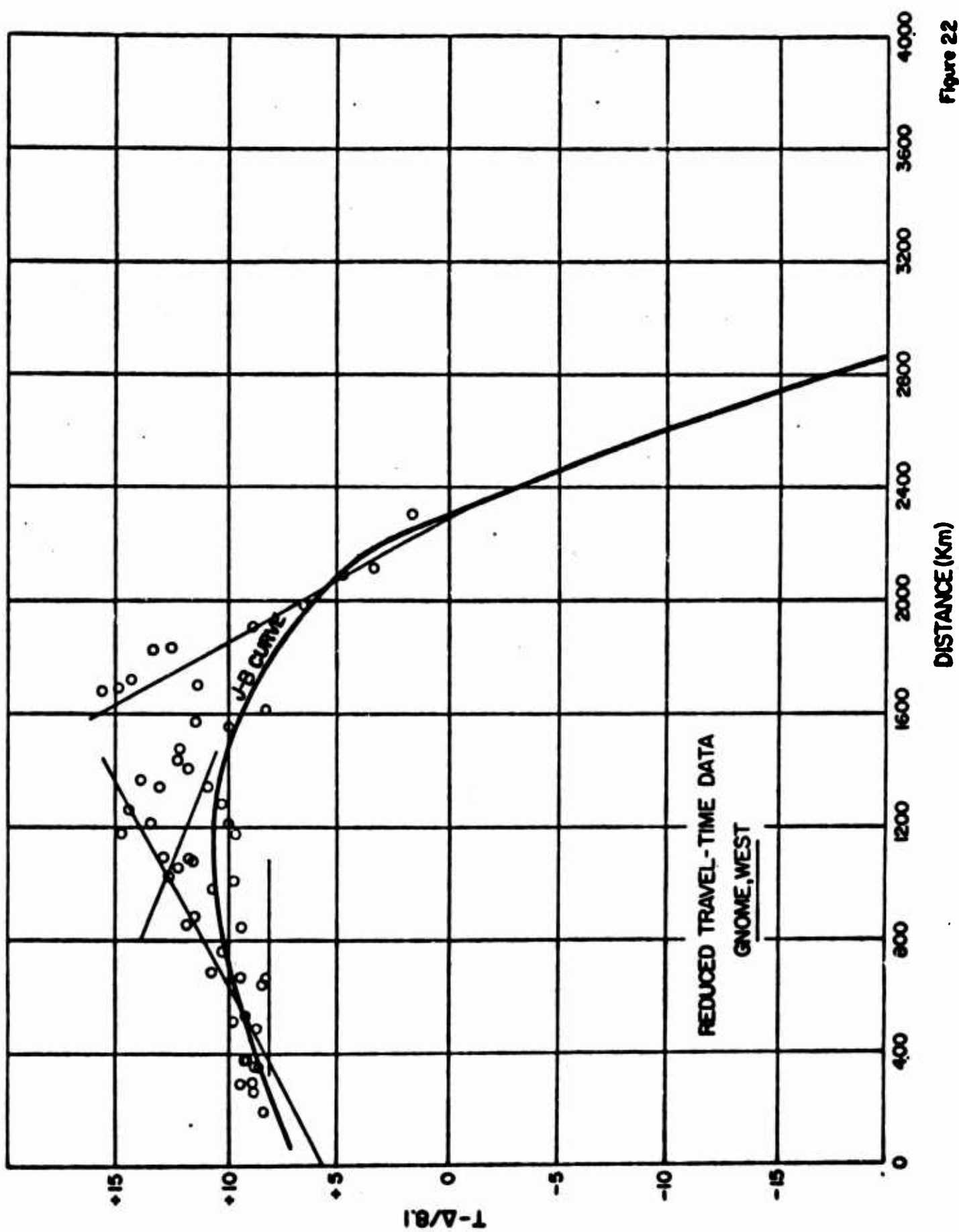
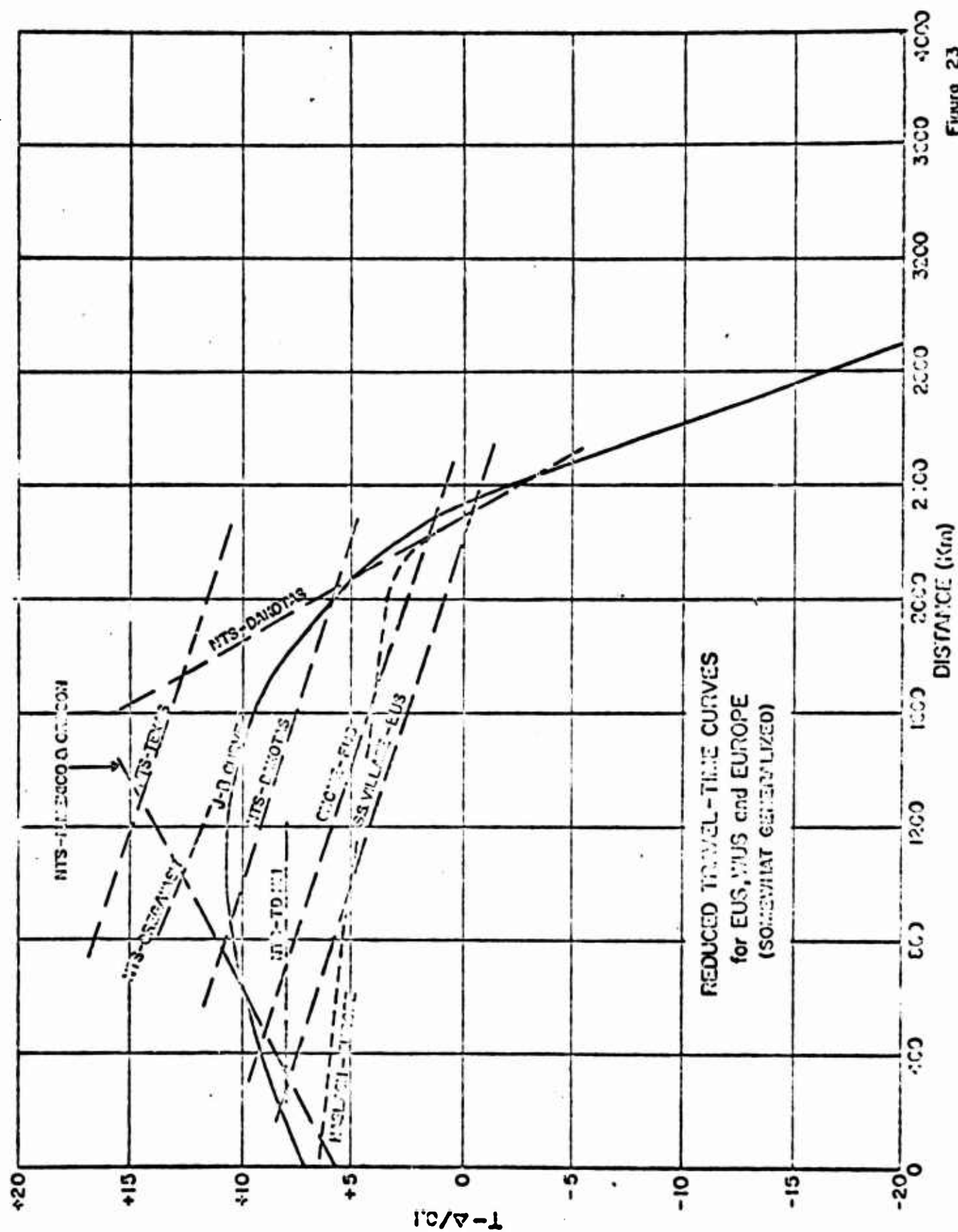


Figure 22
AFTAC/VSC



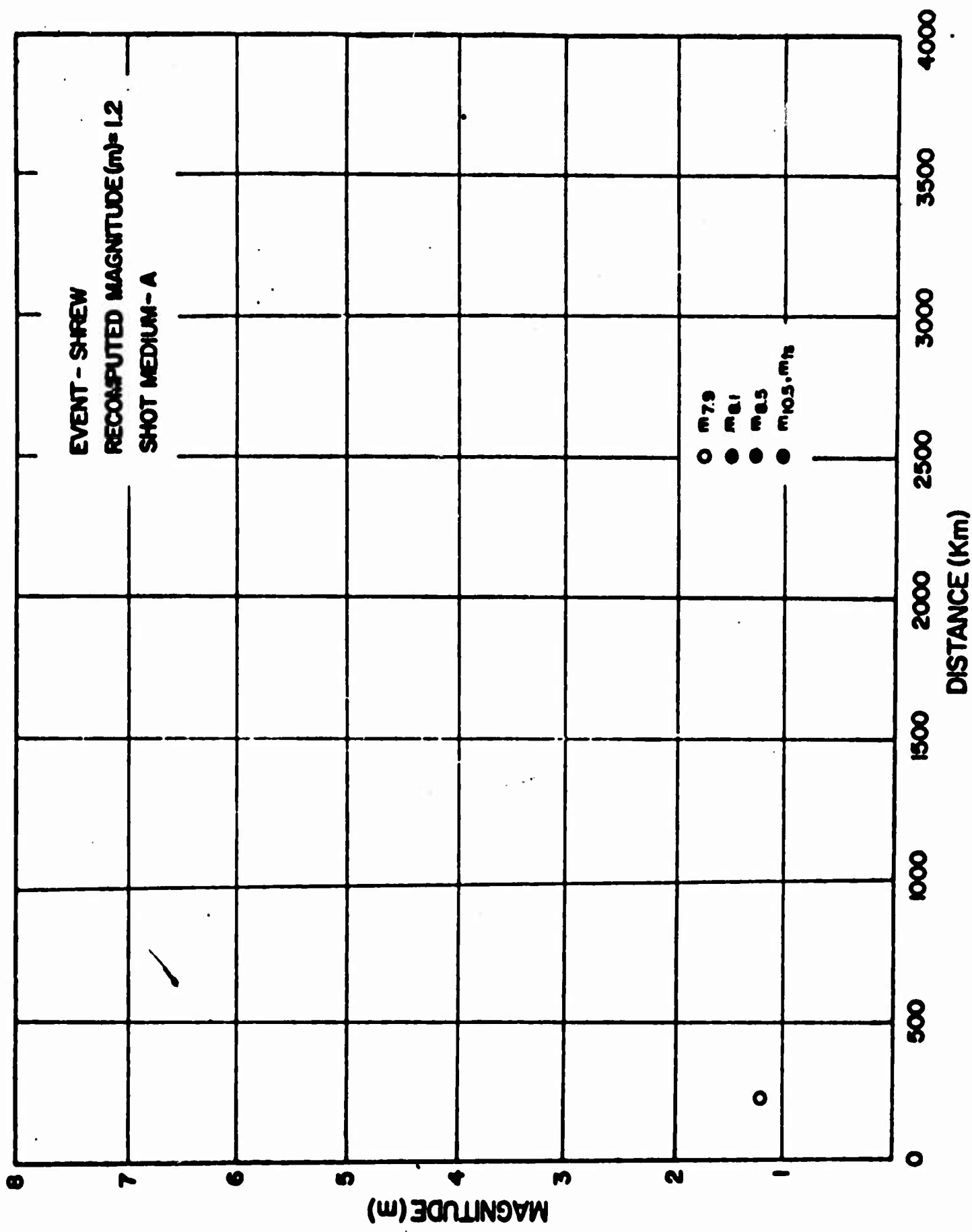


Figure 24
AFTAC/VSC

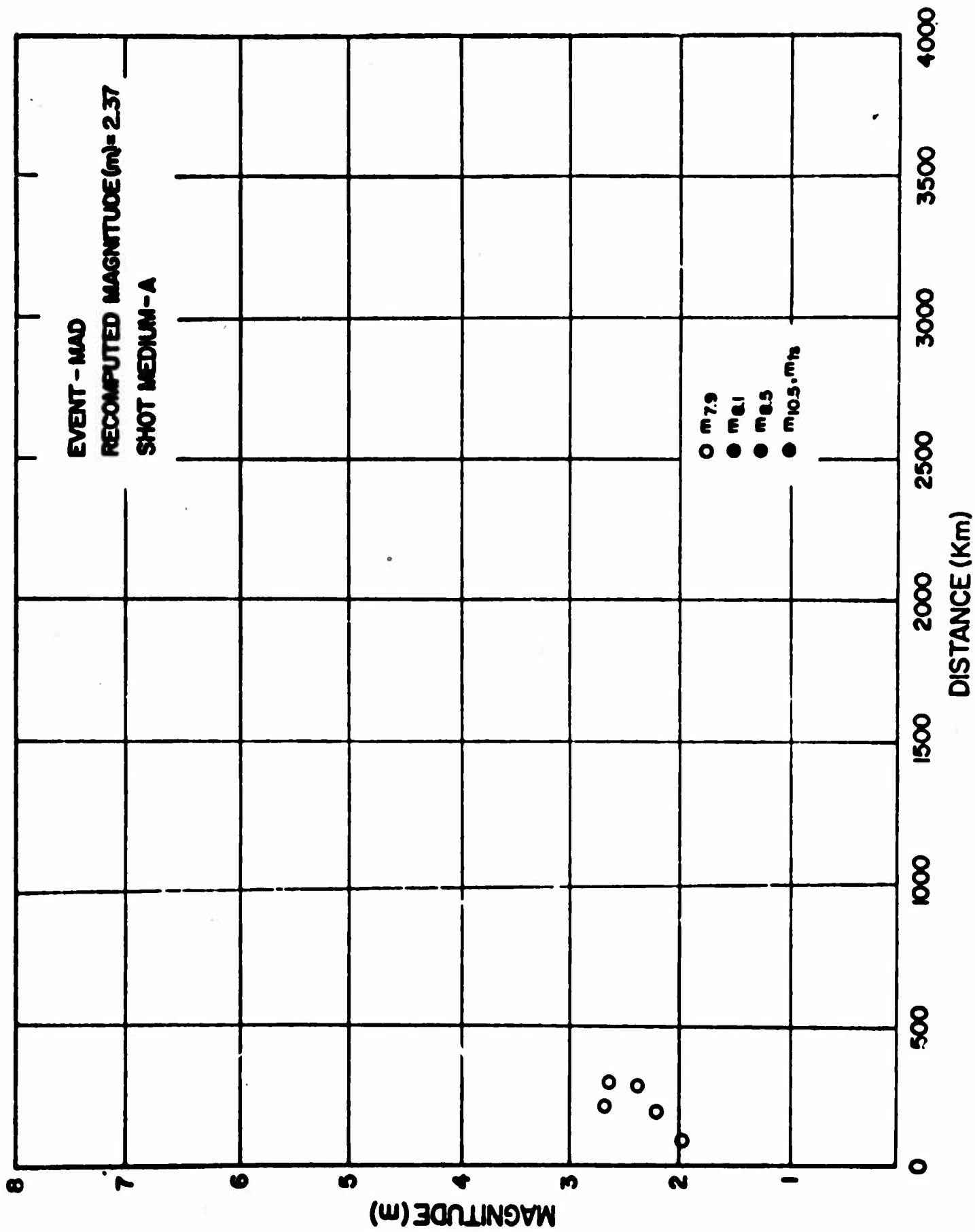


Figure 26
AFTAC/VSC



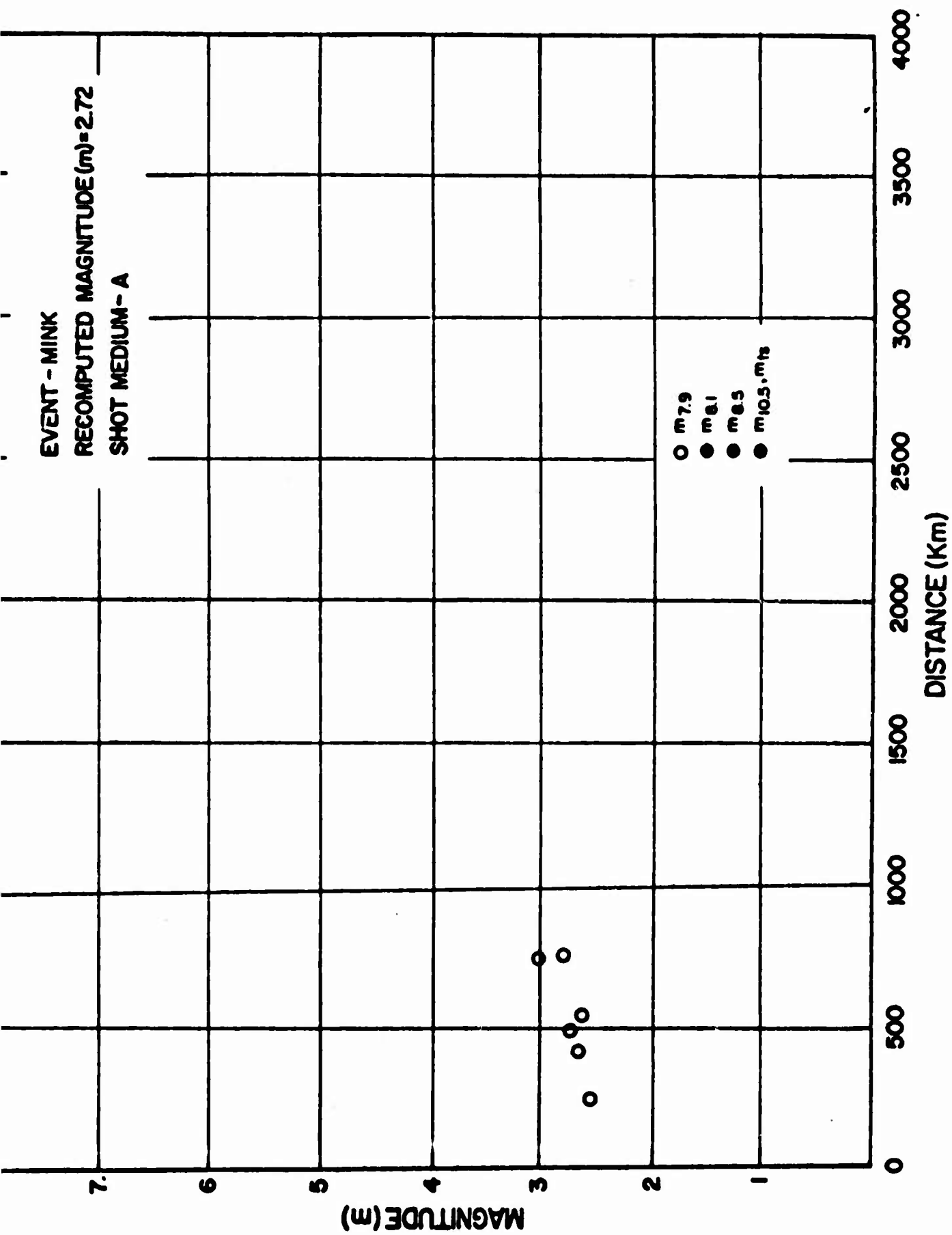


Figure 27
AFTAC/VSC

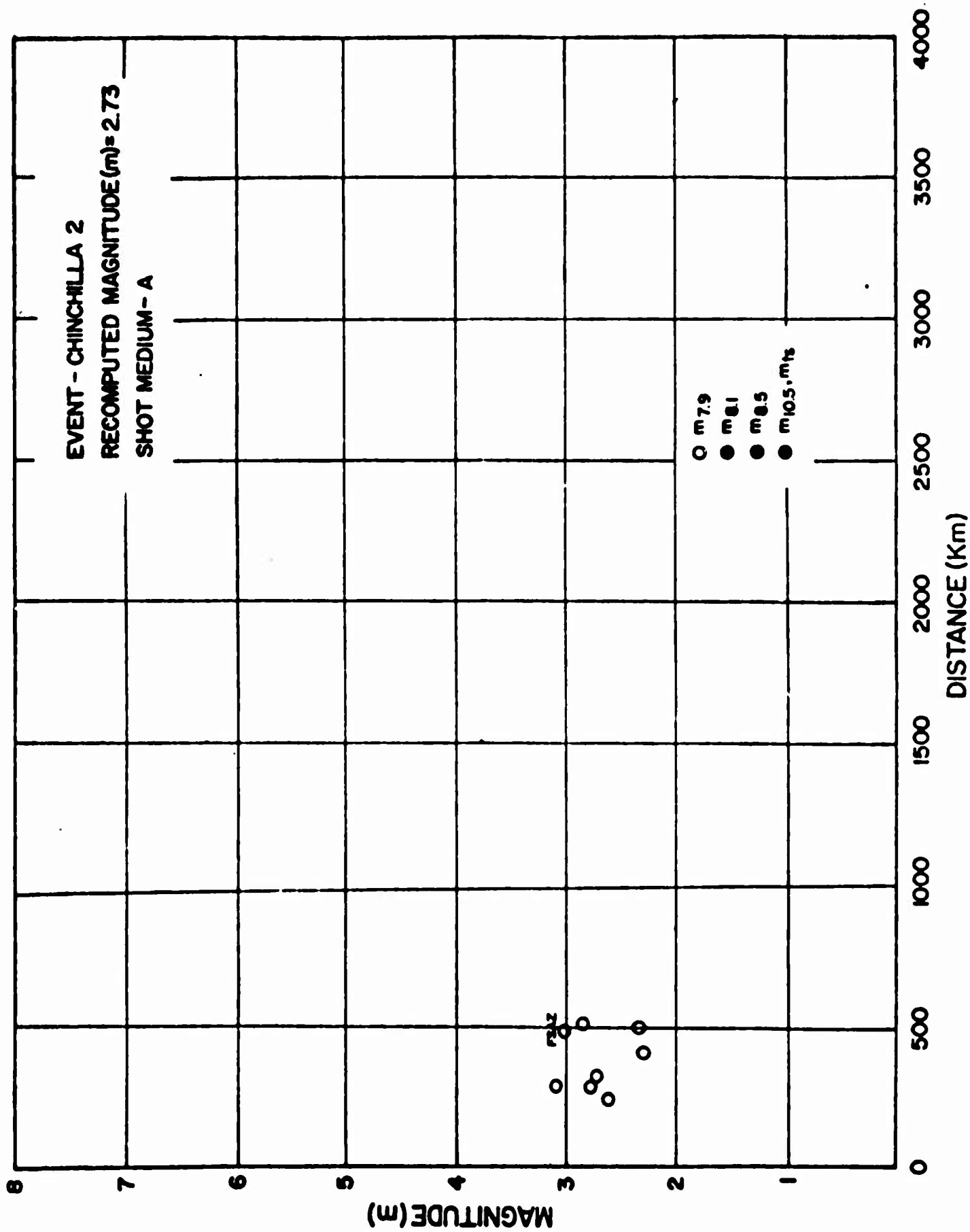


Figure 29
 AFTAC/VSC

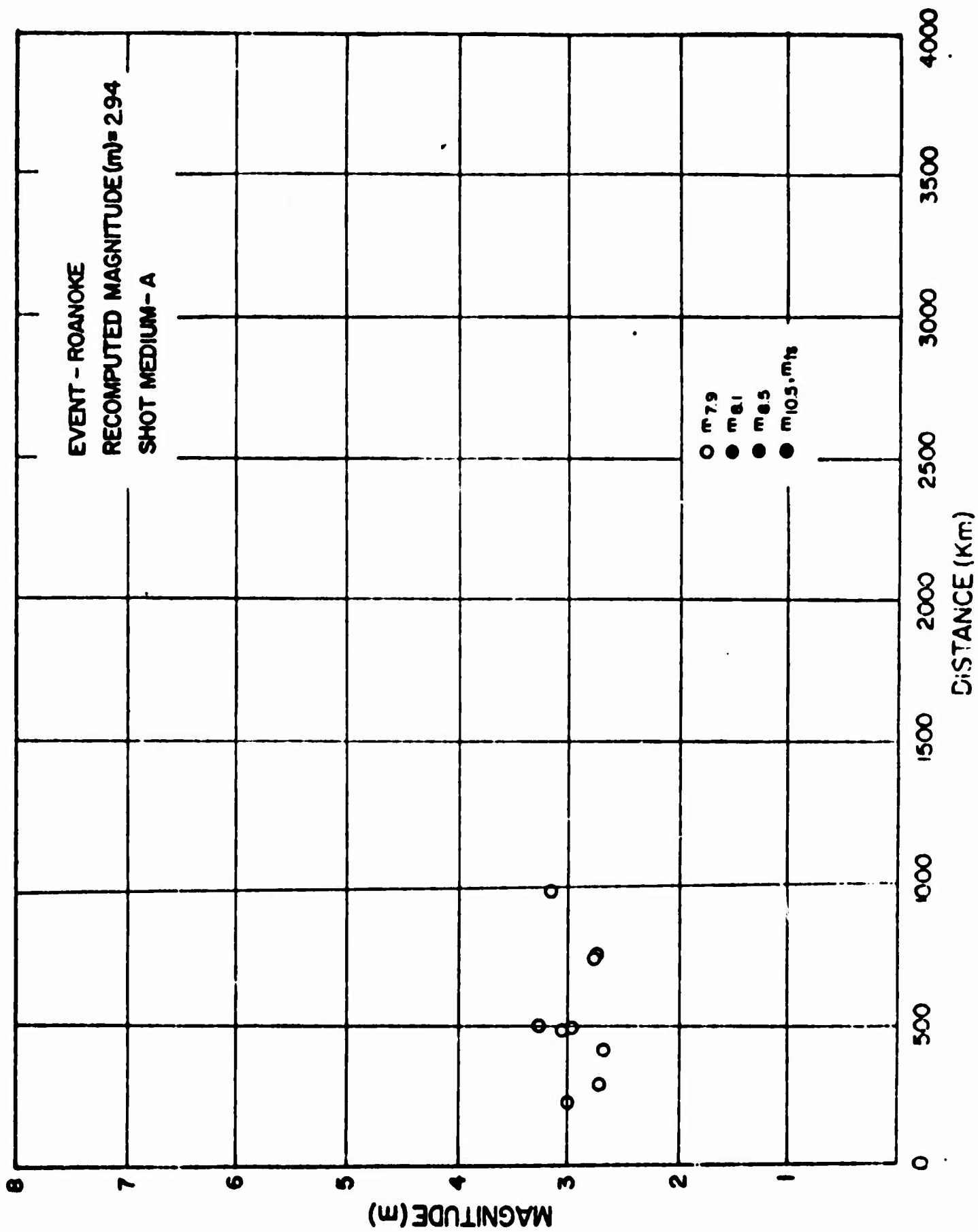


Figure 30
AFTAC/VSC

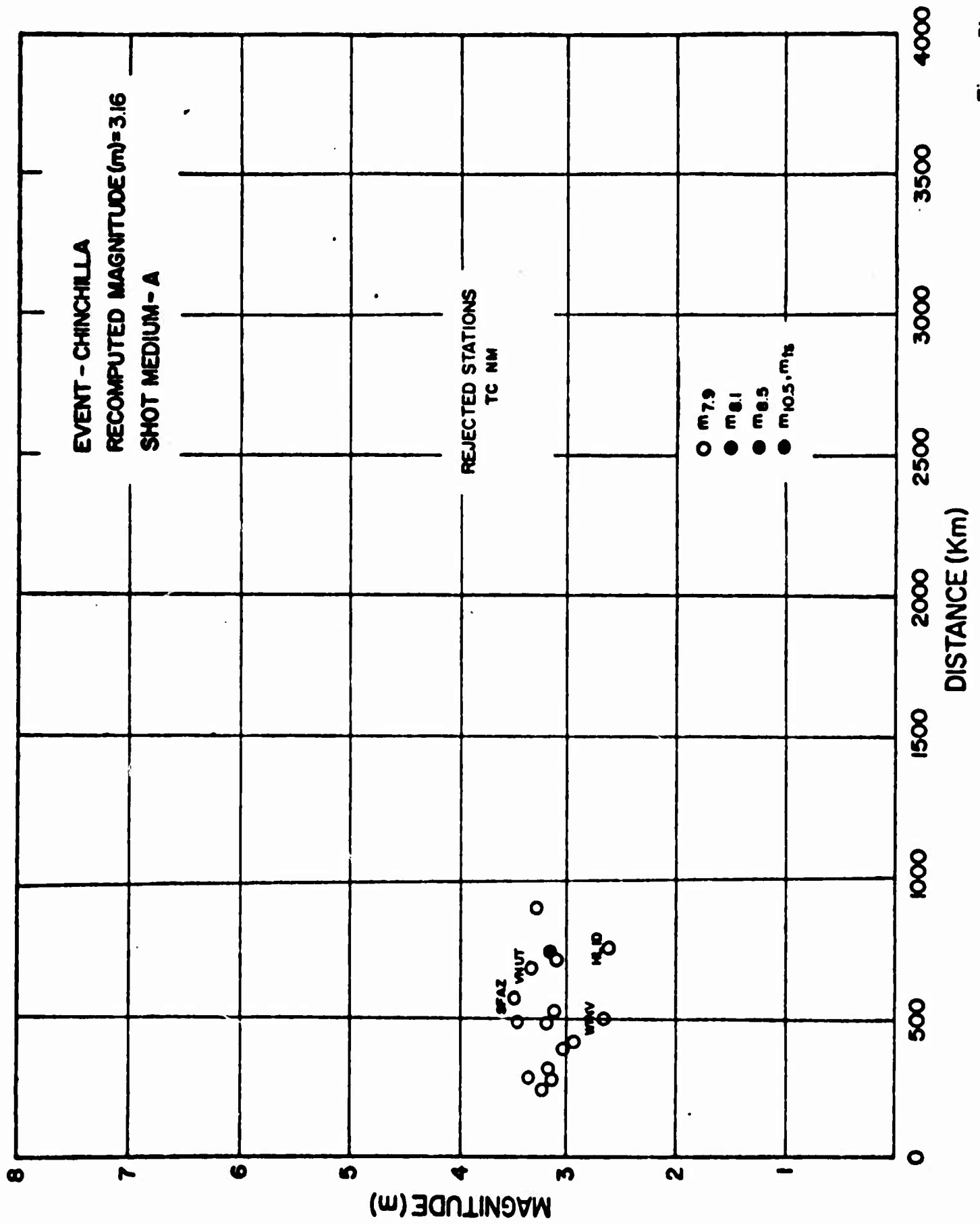


Figure 31
AFTAC/VSC

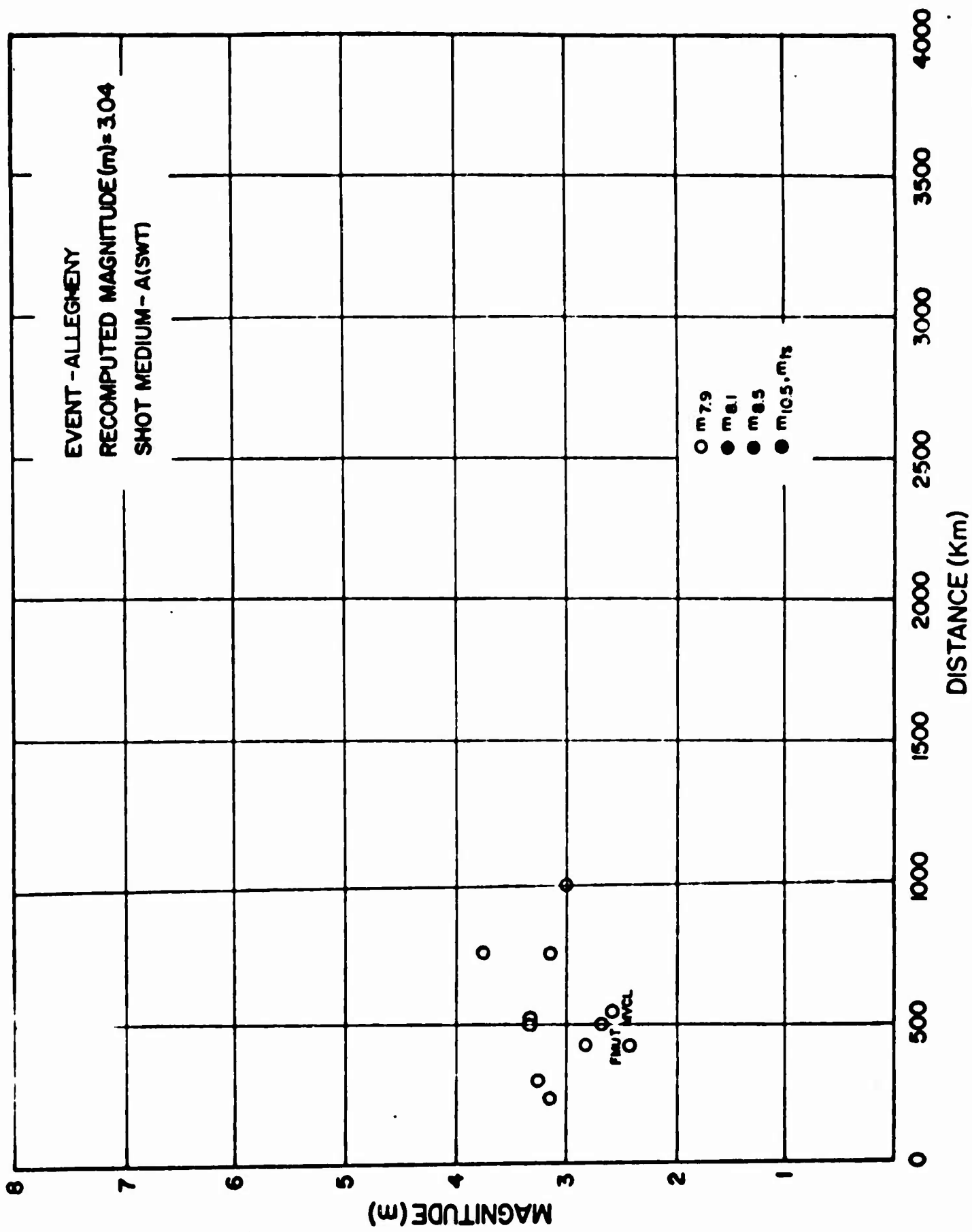


Figure 33
AFTAC/VSC

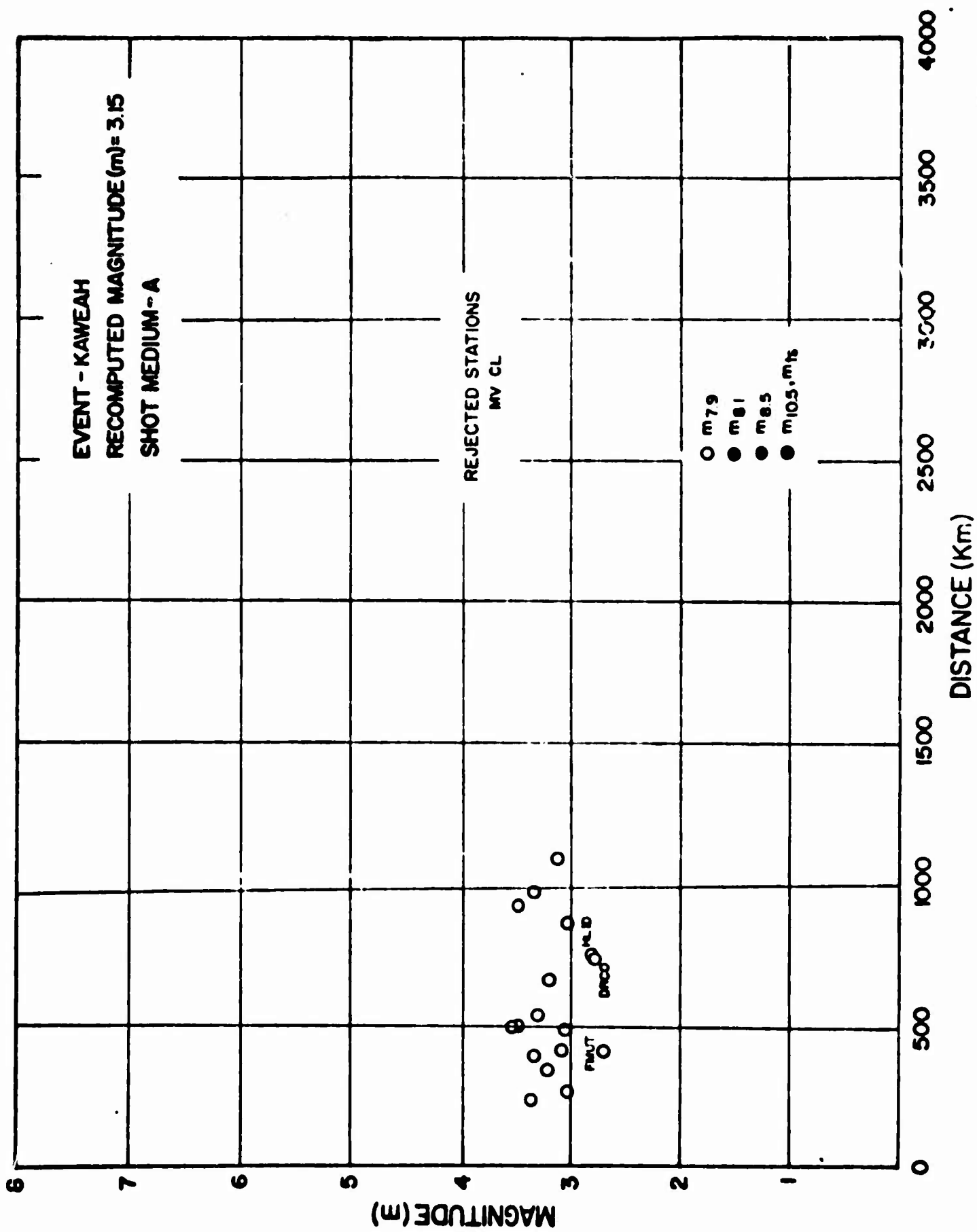


Figure 34
 AFTAC/VSC

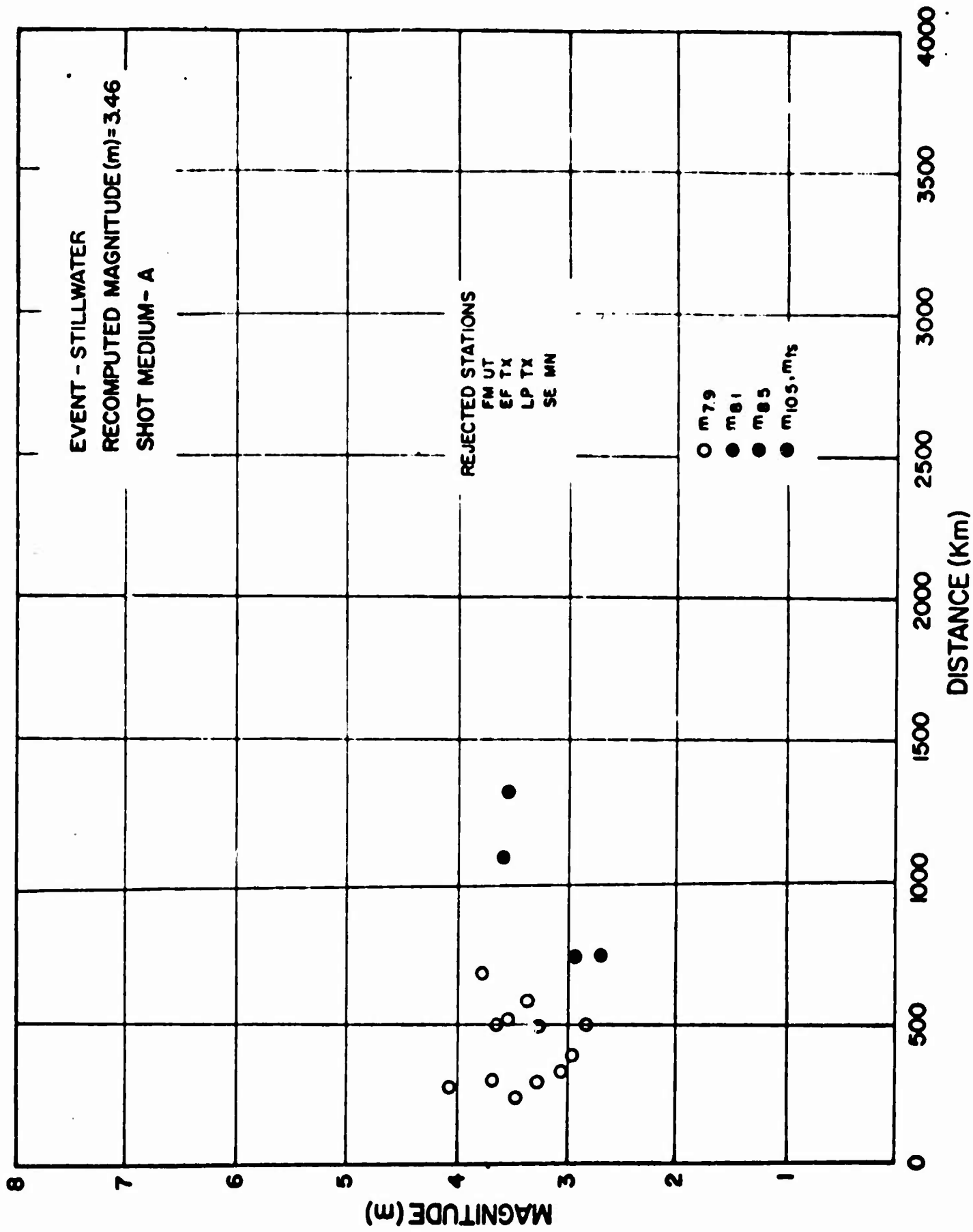


Figure 35
AFTAC/VSC

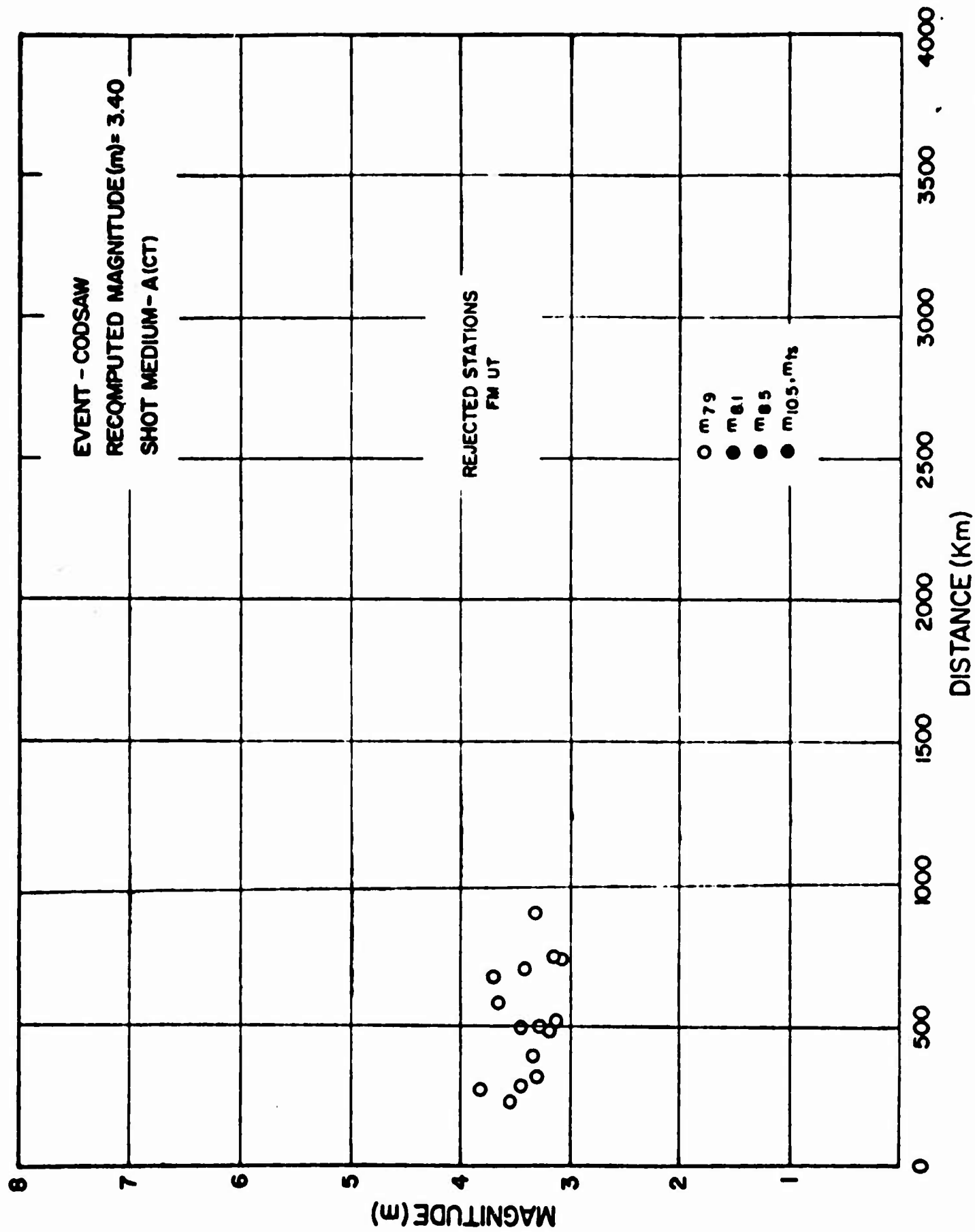


Figure 36
 AFTAC/VSC

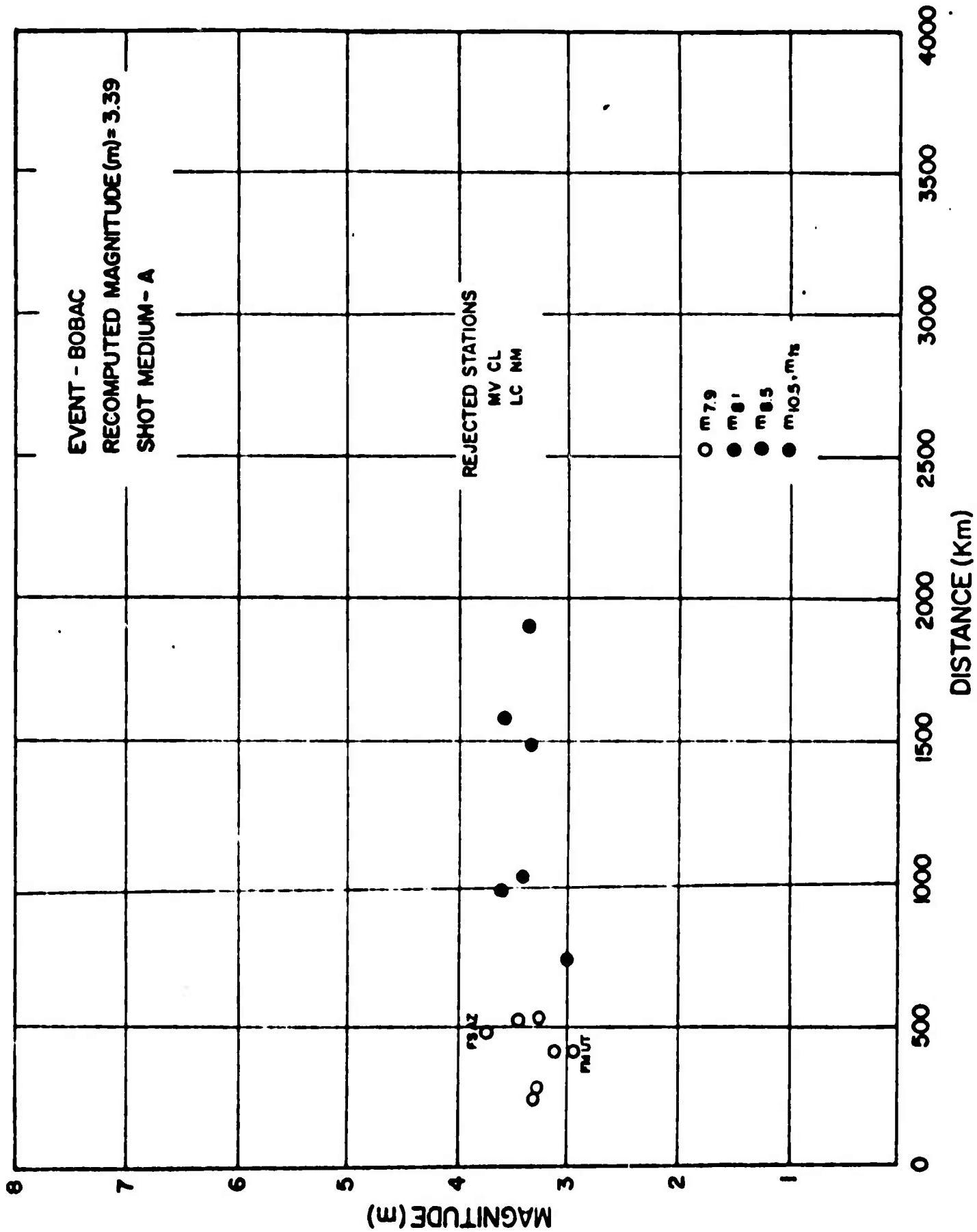


Figure 37
 AFTAC/VSC

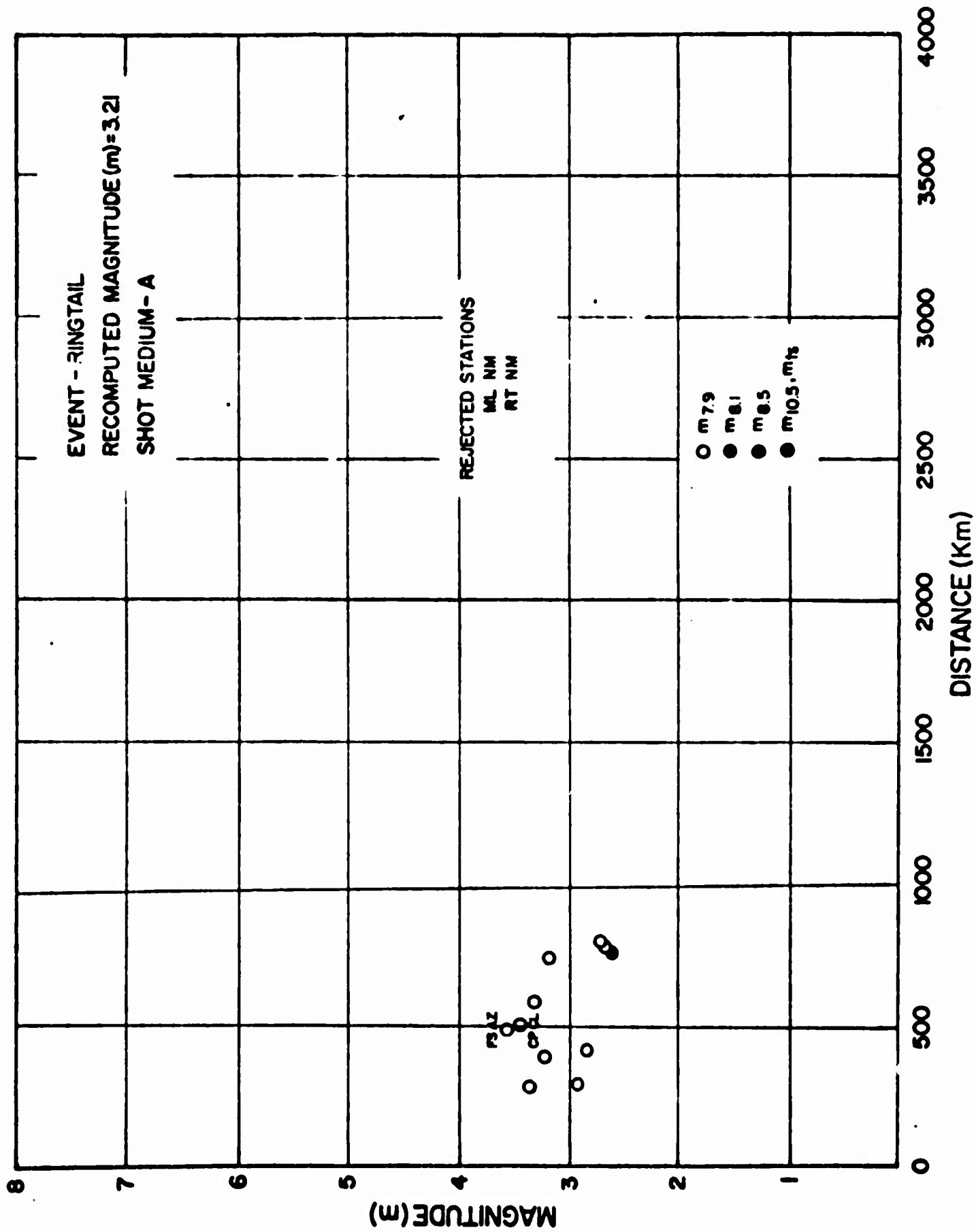


Figure 38
 AFTAC/VSC

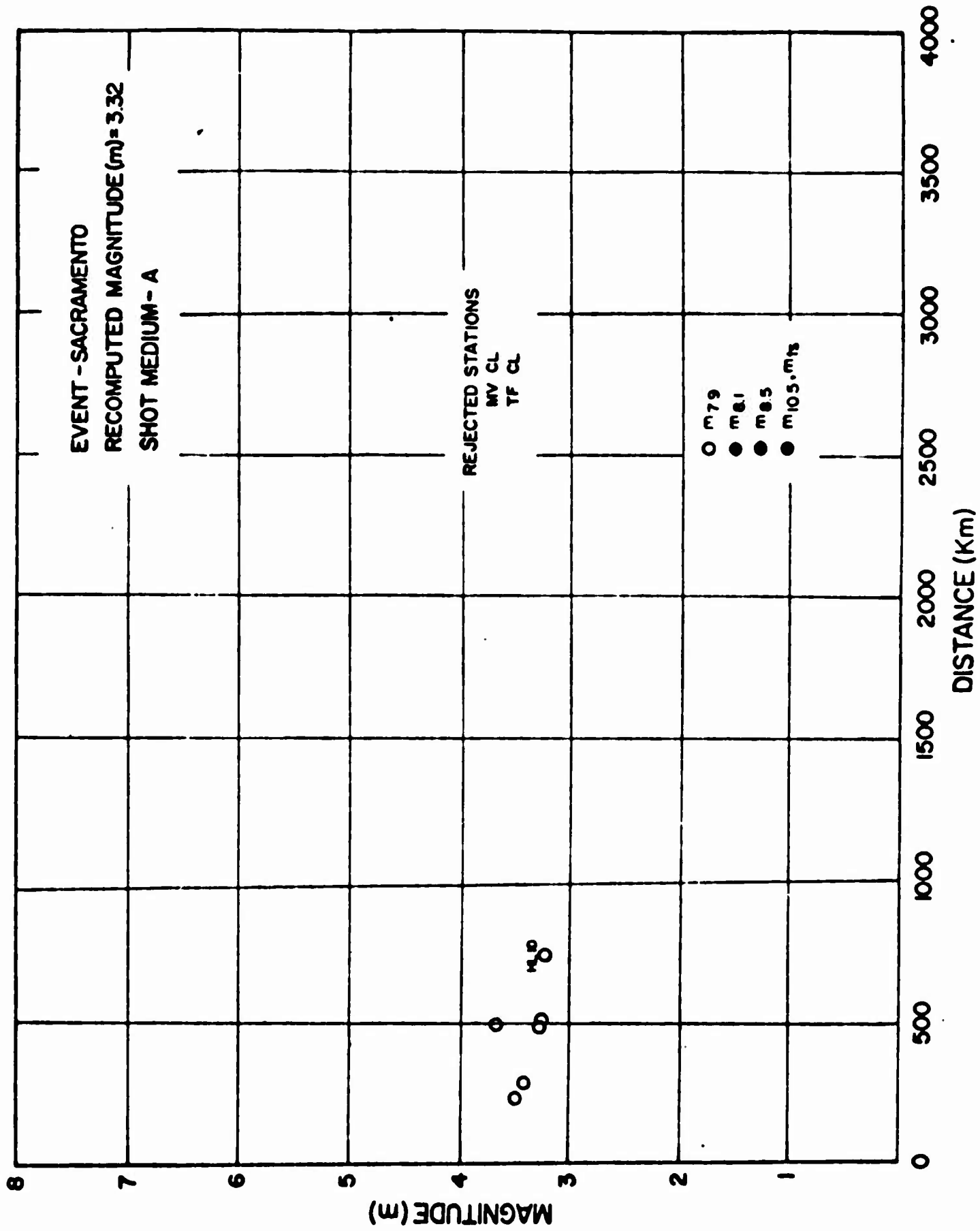


Figure 39
 AFTAC/VSC

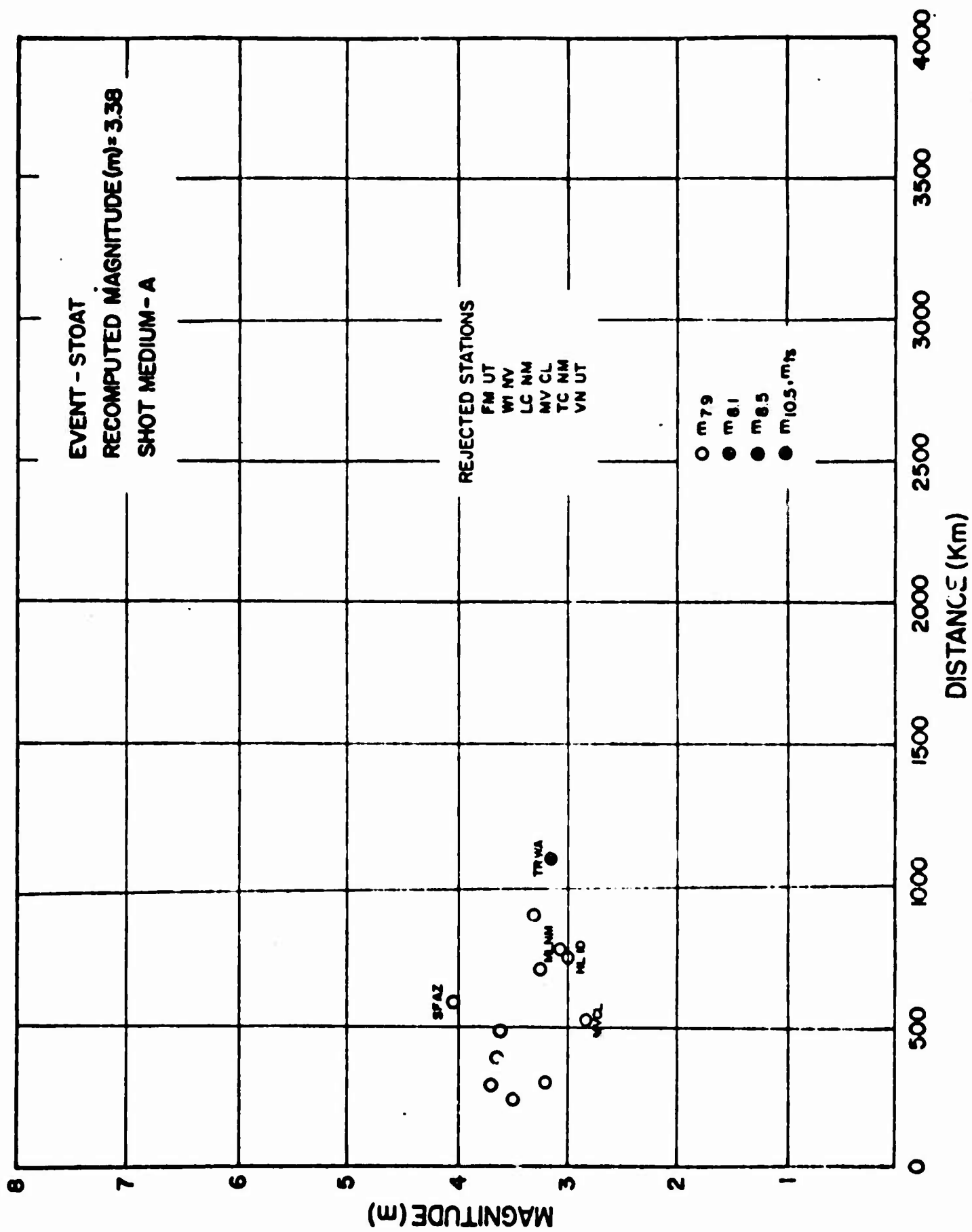


Figure 40
AFTAC/VSC

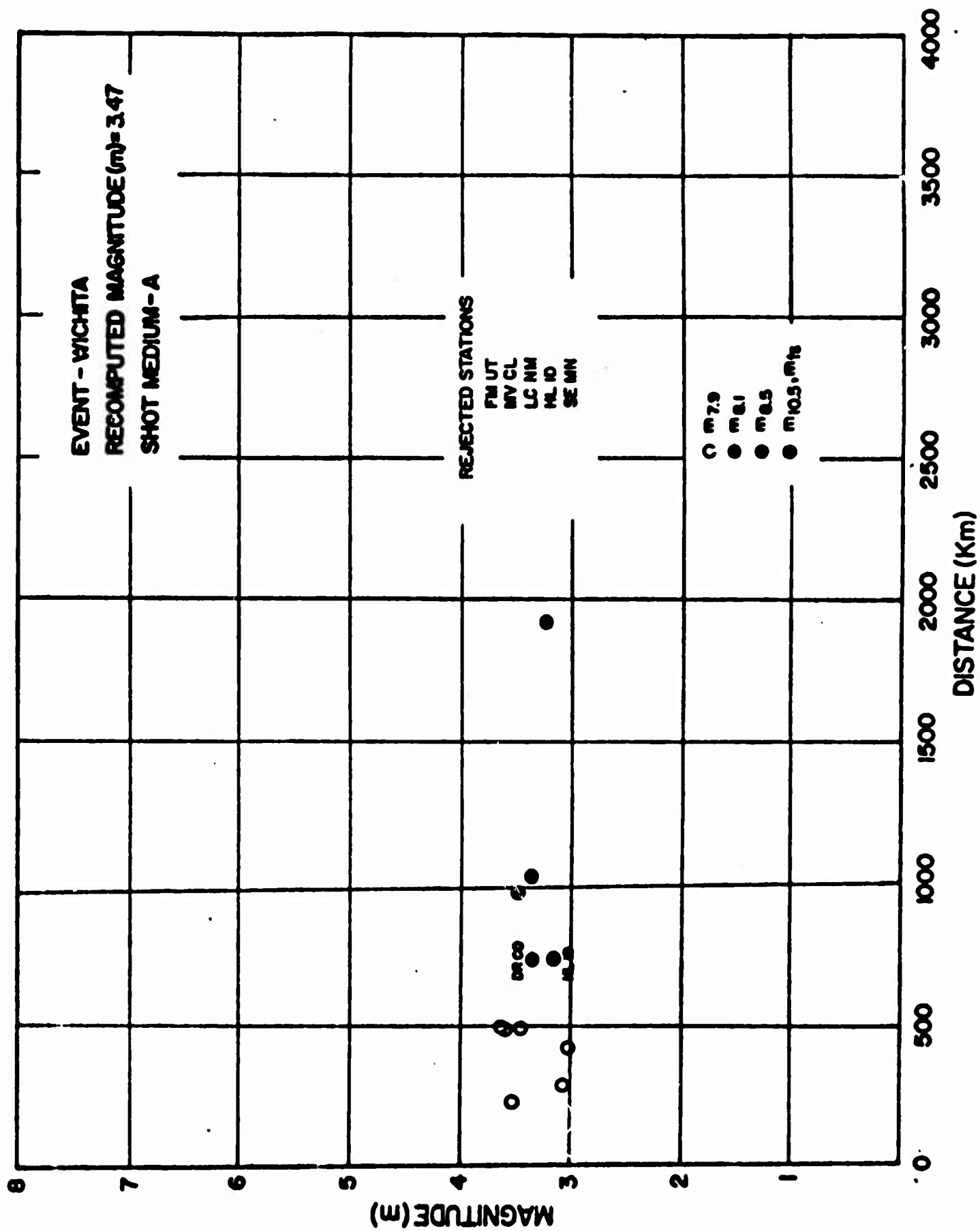


Figure 41
 AFTAC/VSC

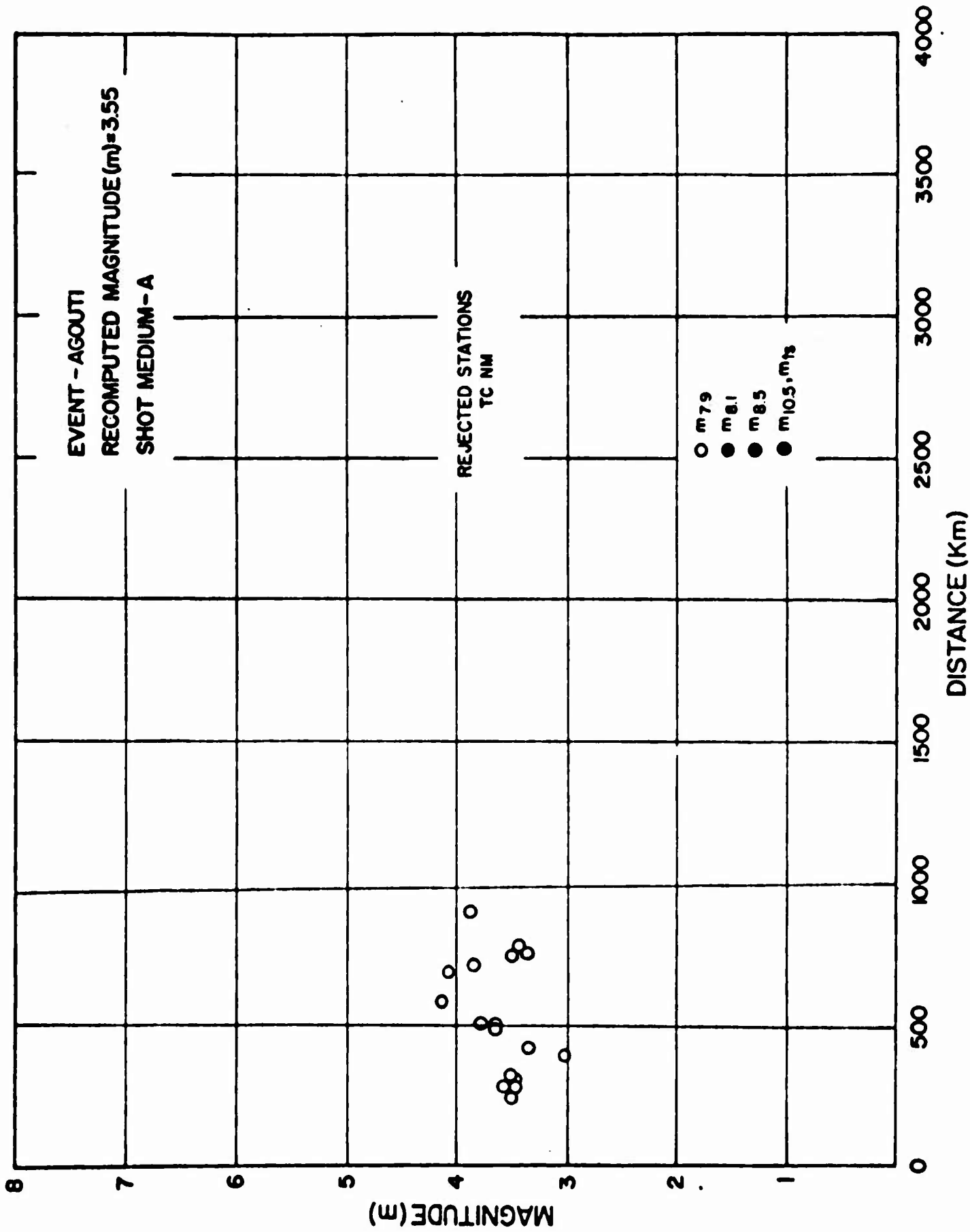


Figure 42
AFTAC/VSC

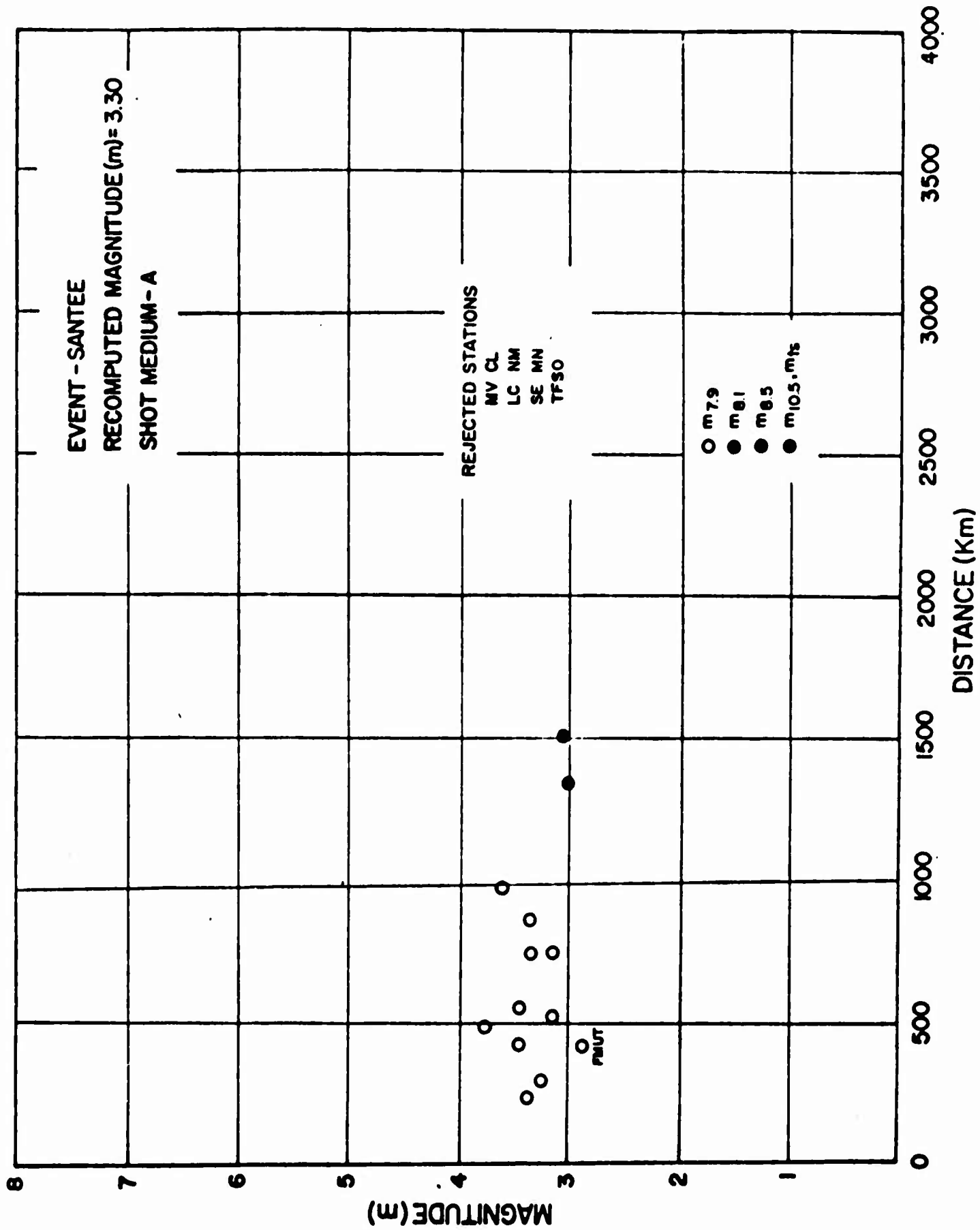


Figure 43
AFTAC/VSC

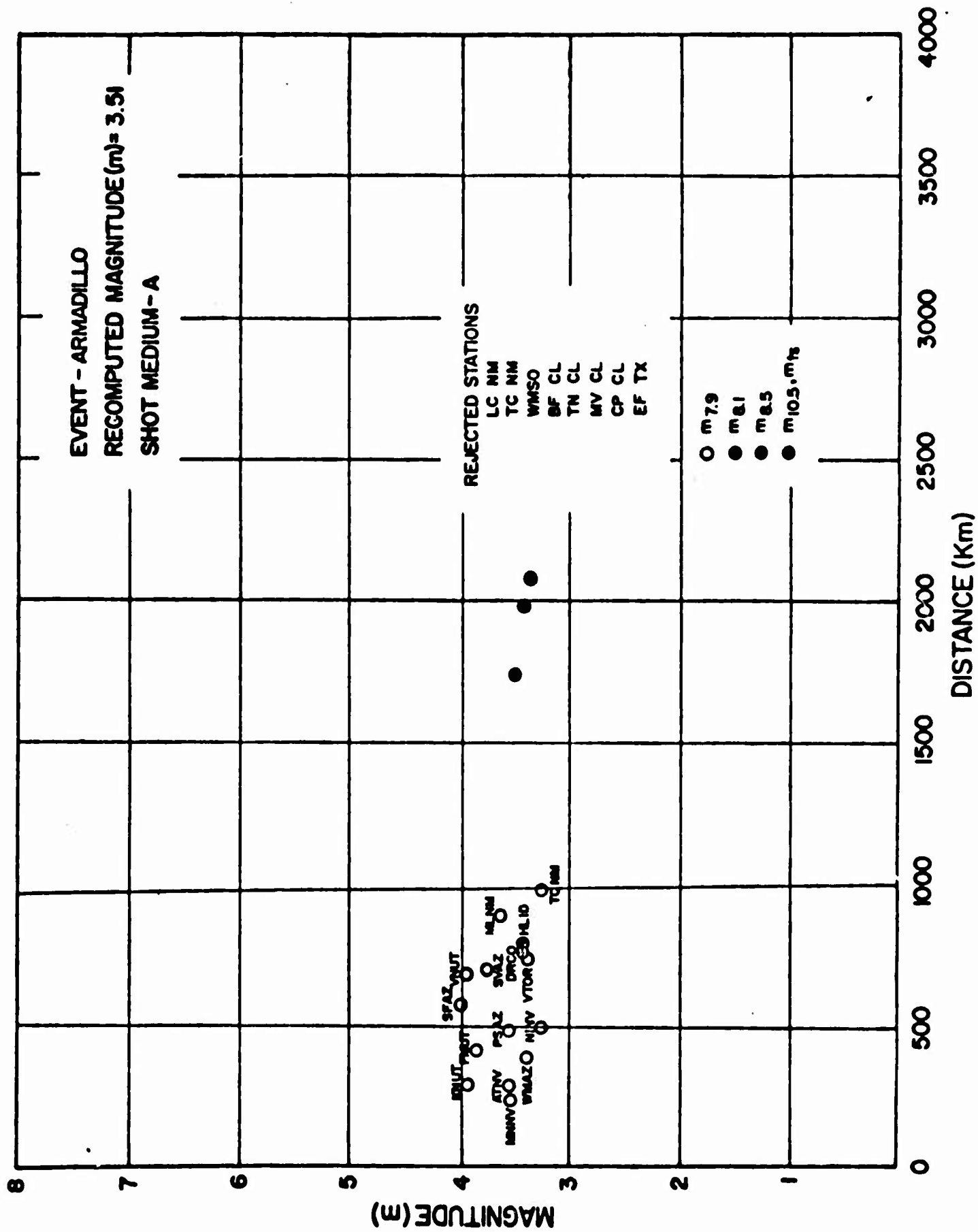


Figure 44
AFTAC/VSC

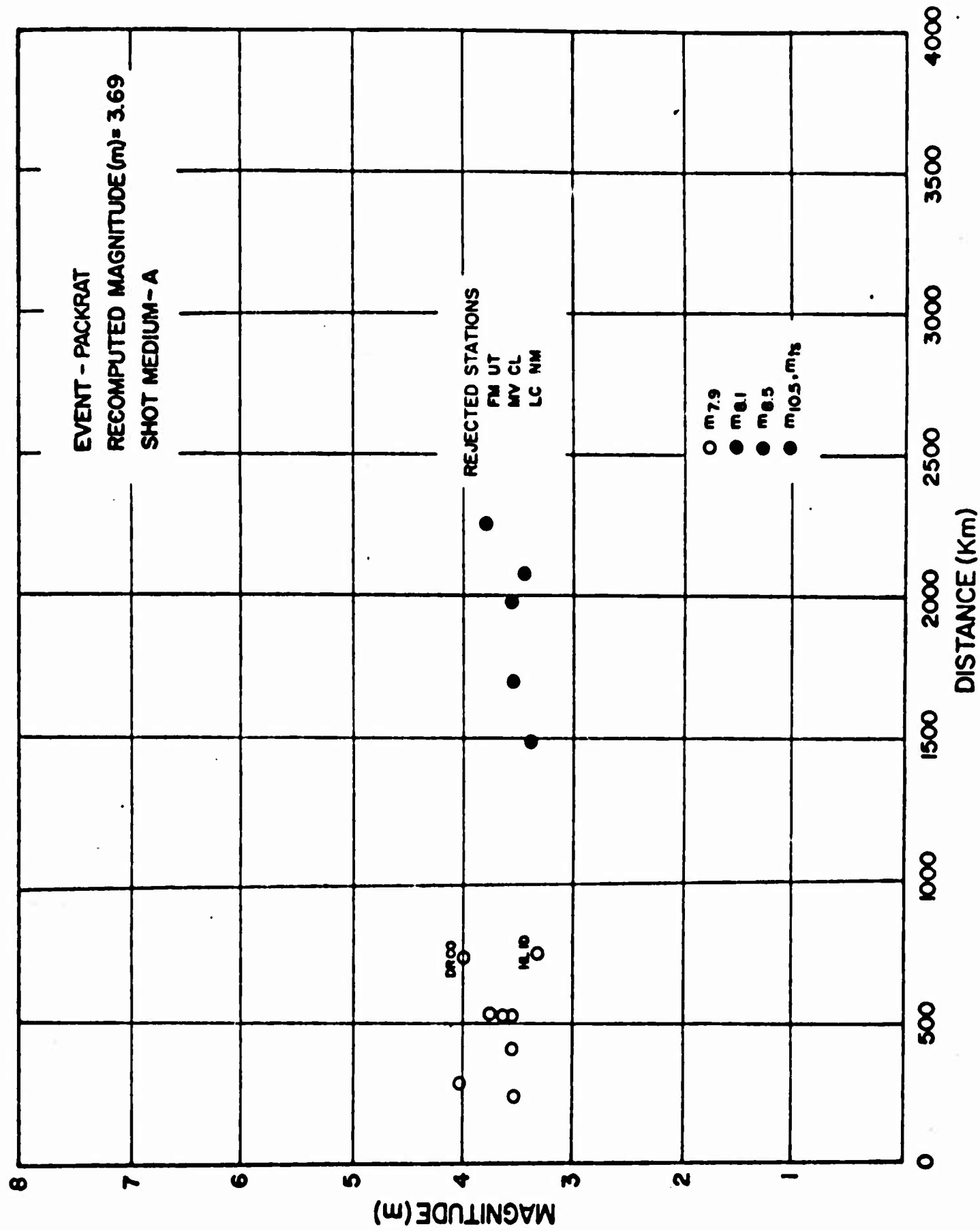


Figure 45
 AFTAC/VSC

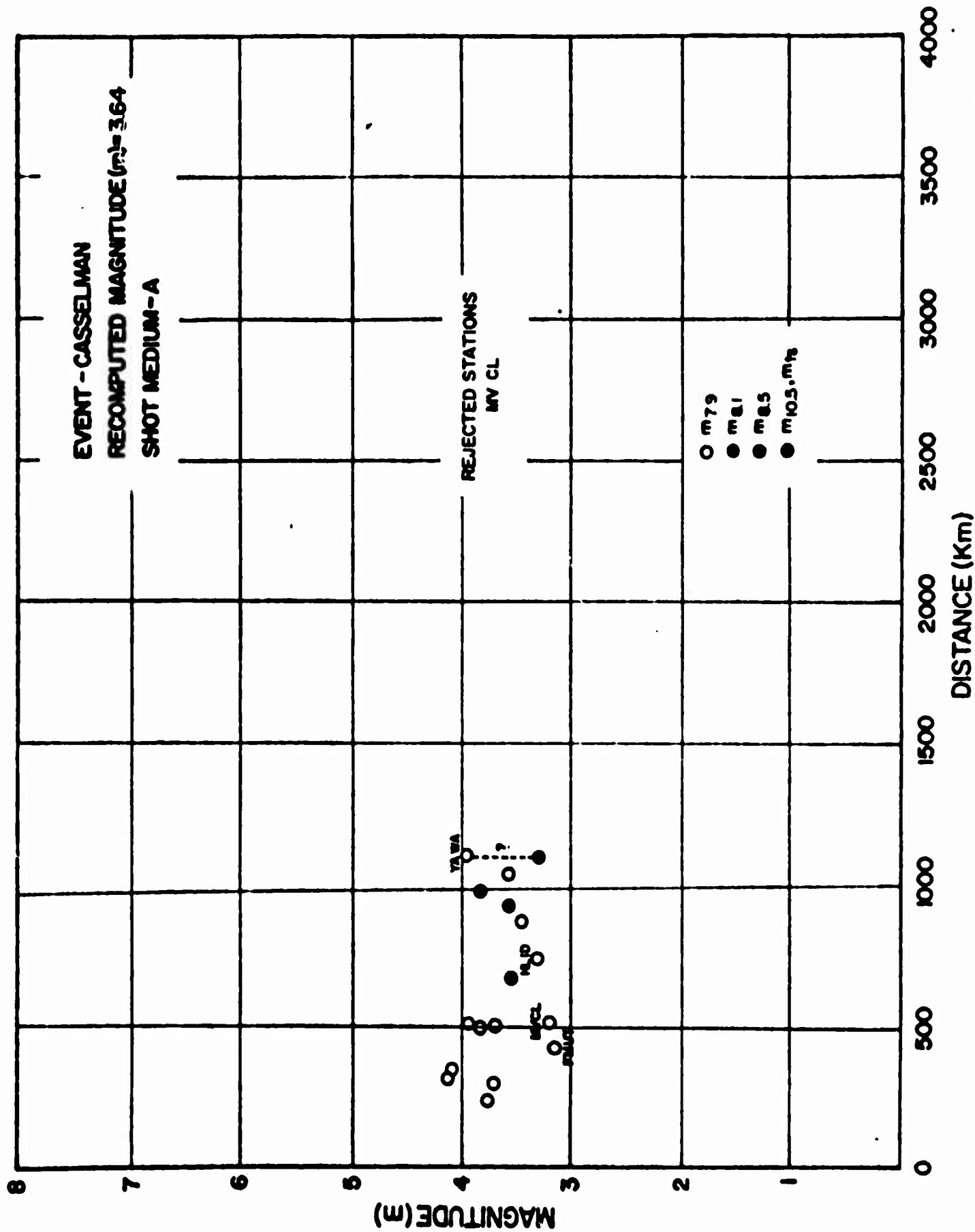


Figure 46
 AFTAC/VSC

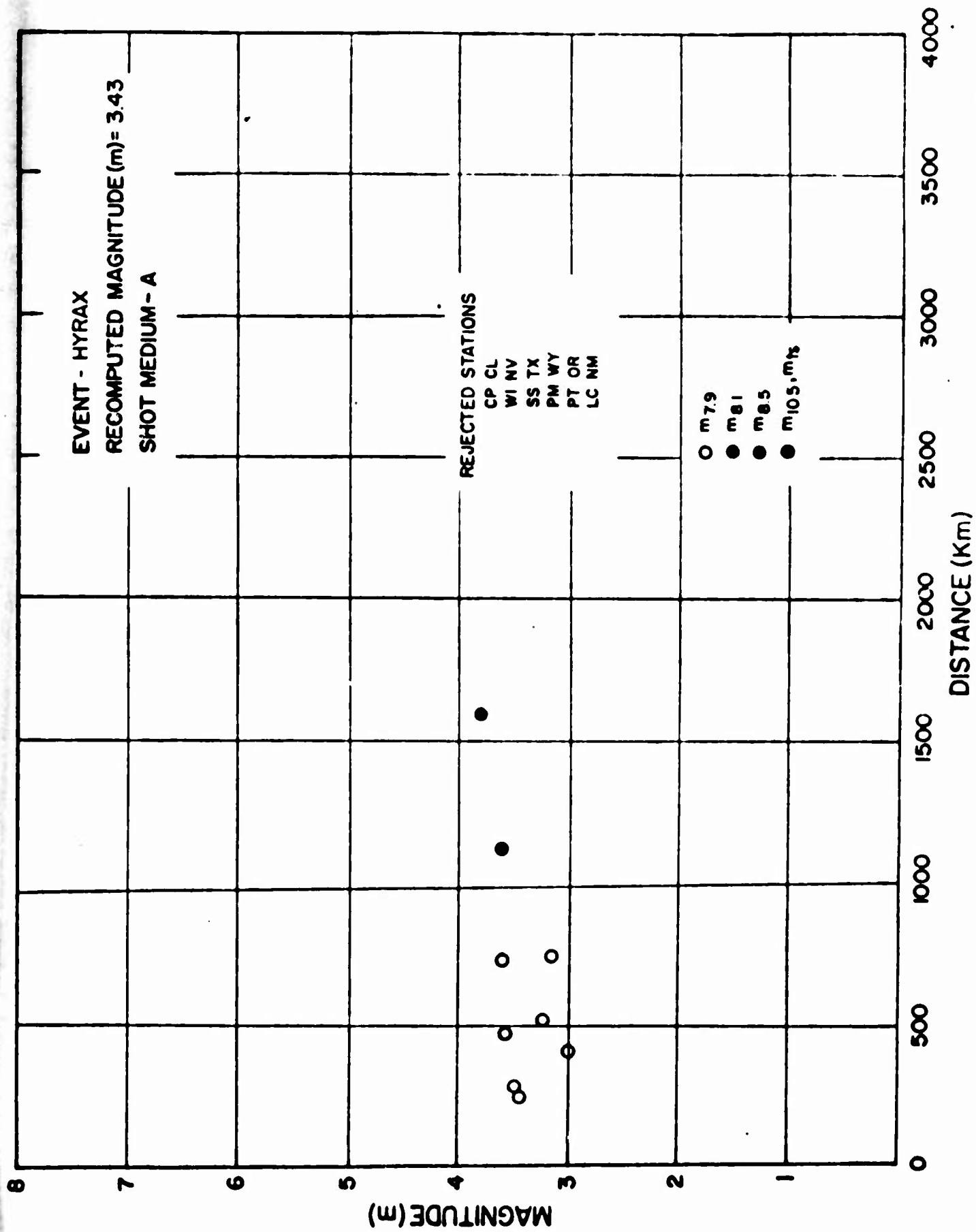


Figure 47
AFTAC/VSC

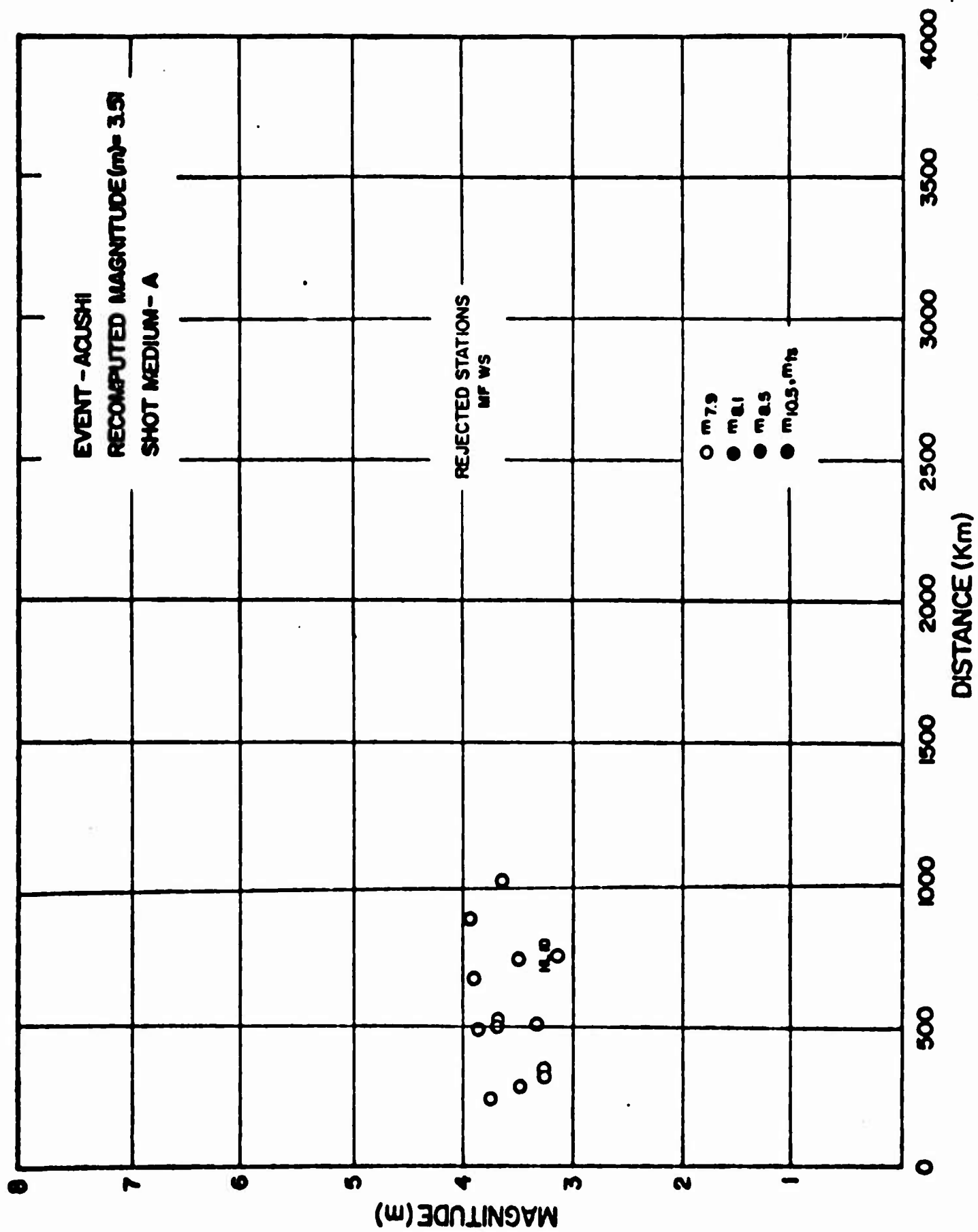


Figure 49
AFTAC/VSC

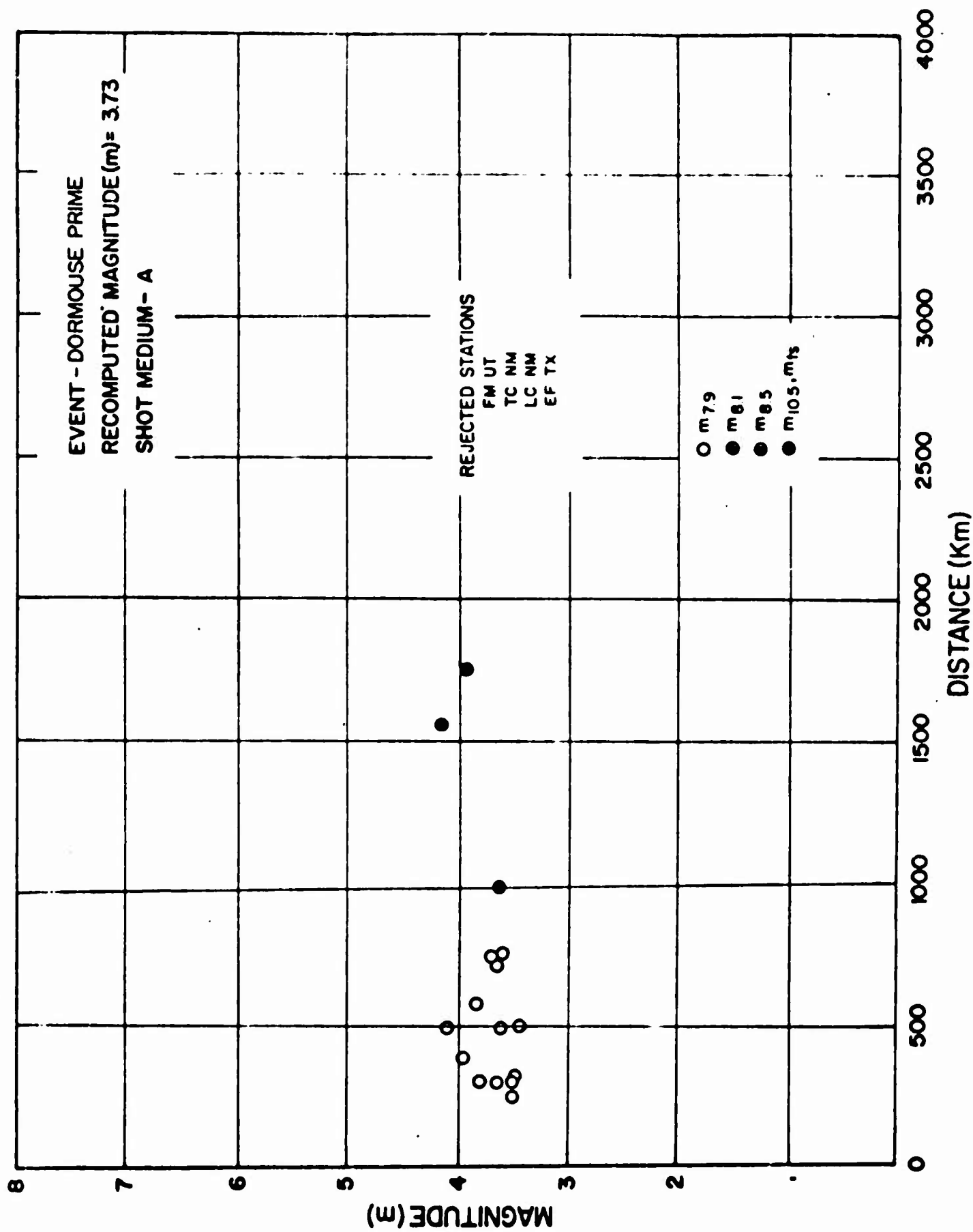


Figure 50
AFTAC/VSC

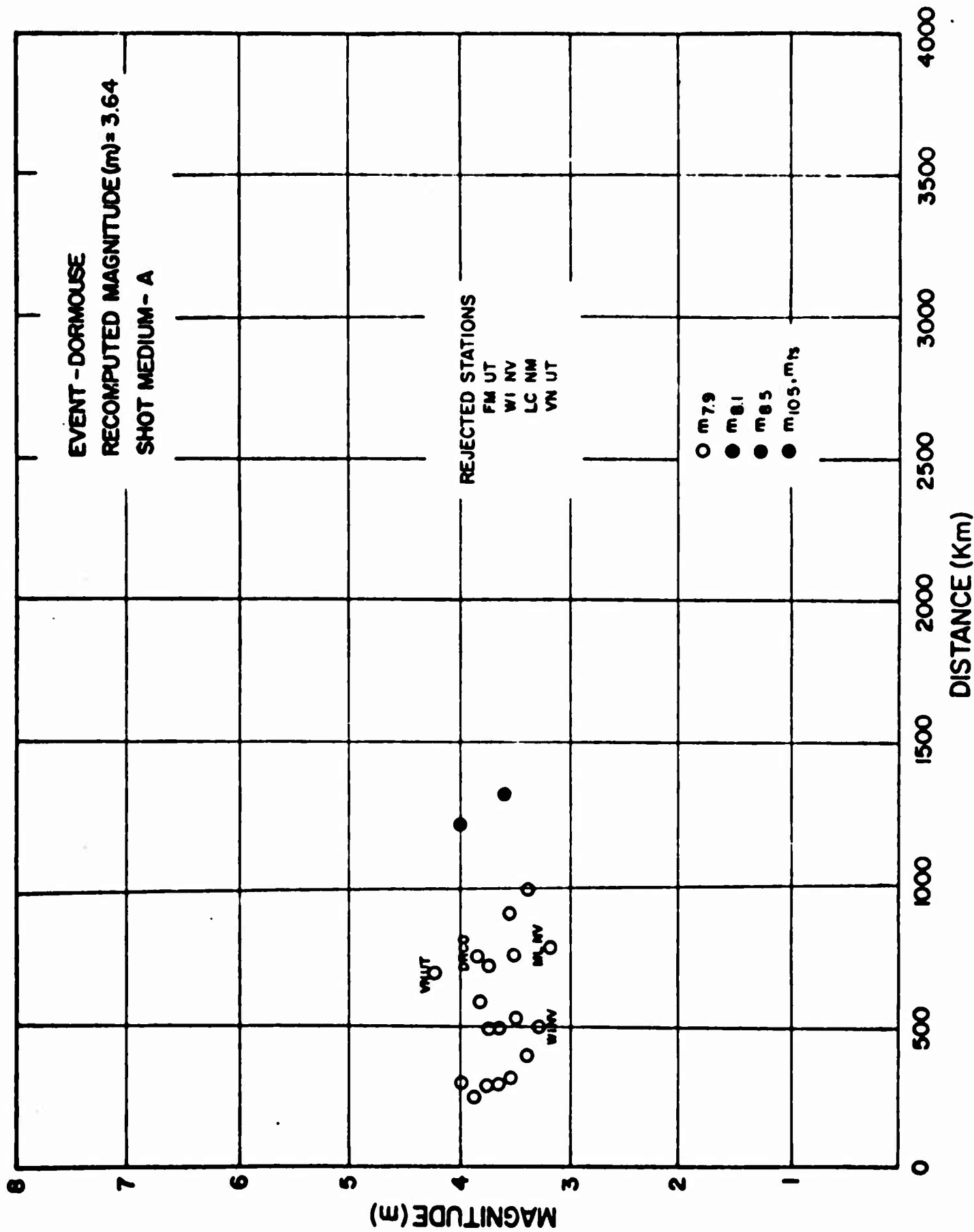


Figure 5i
 AFTAC/VSC

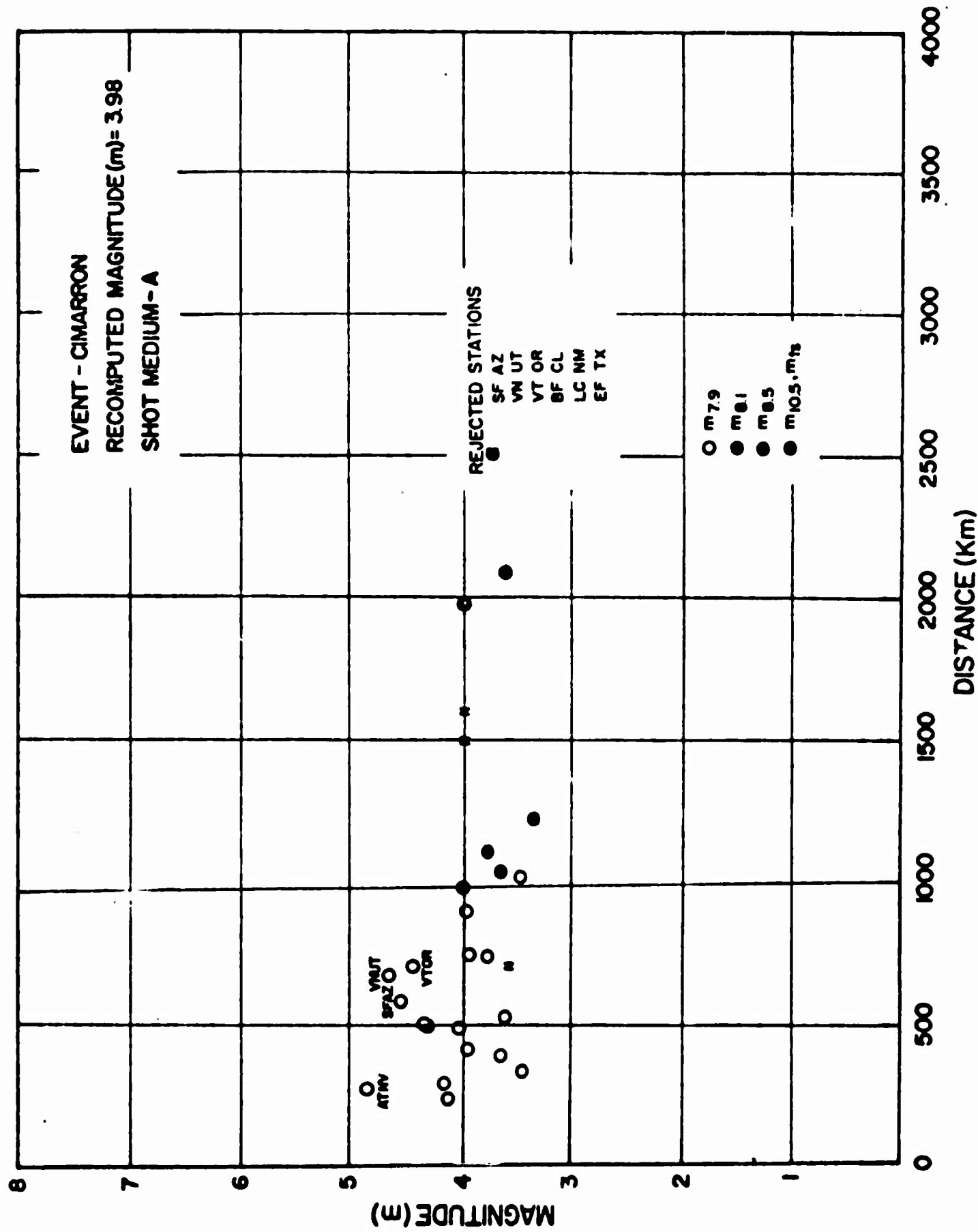


Figure 52
AFTAC/VSC

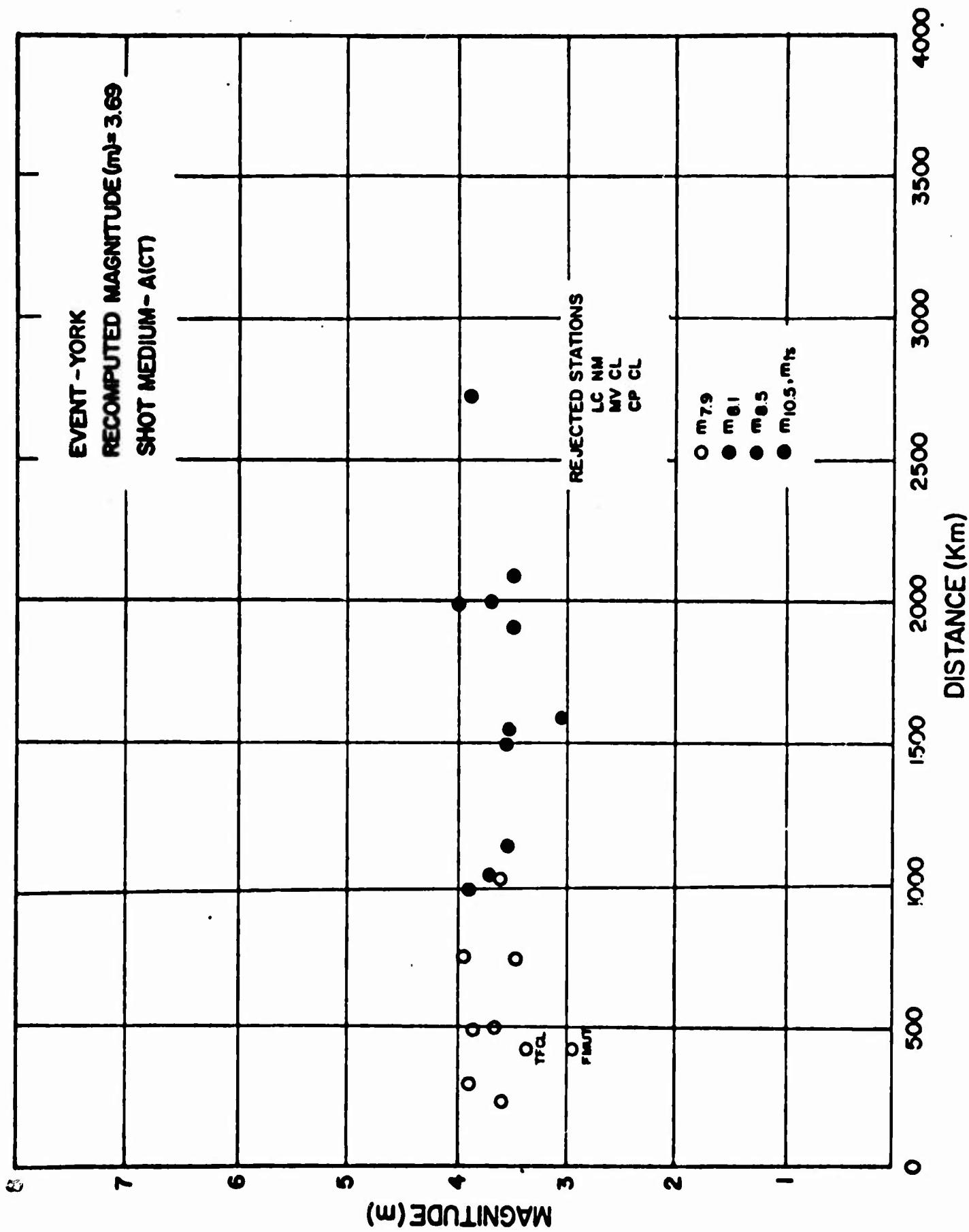


Figure 53
 AFTAC/VSC

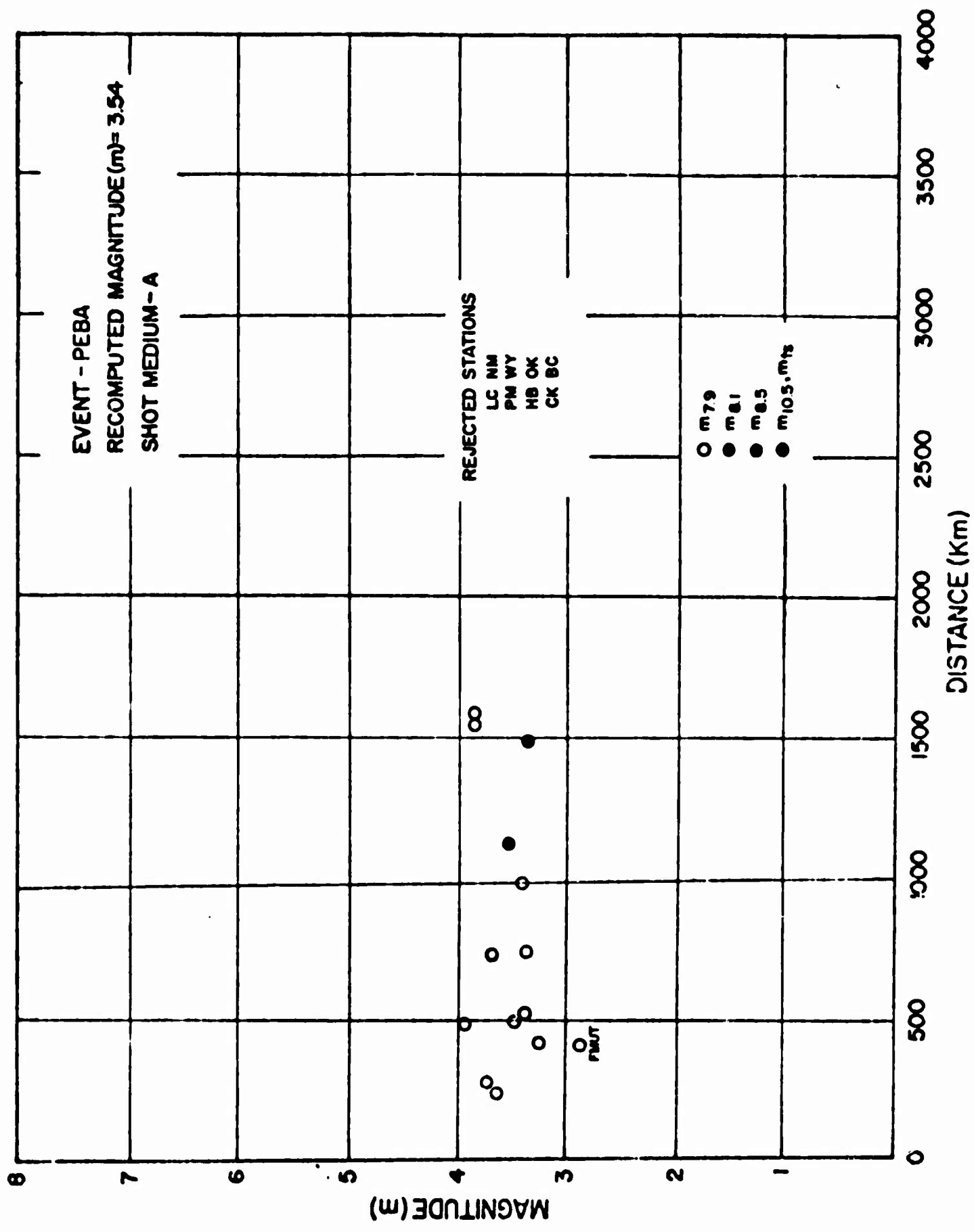


Figure 54
AFTAC/VSC

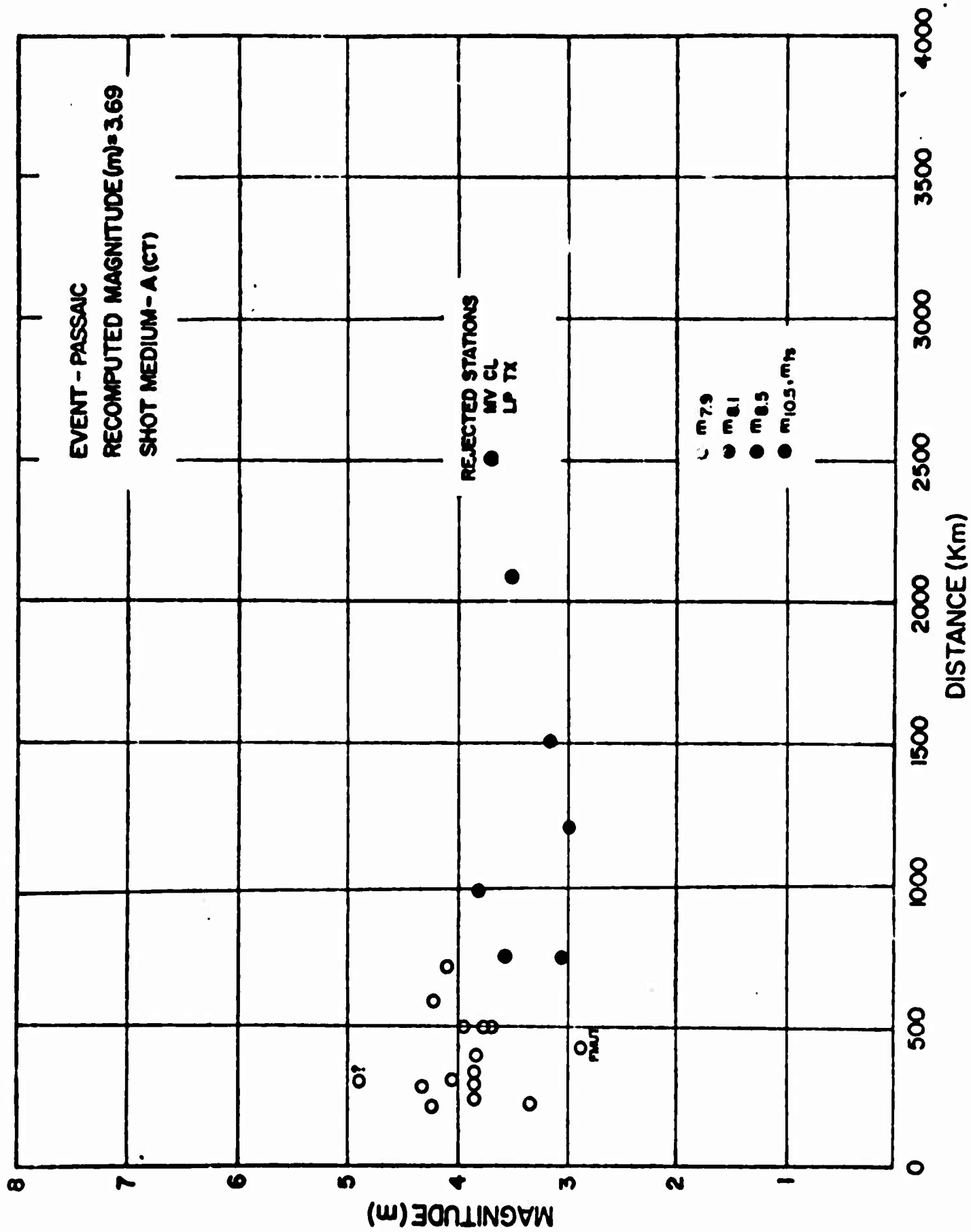


Figure 55
AFTAC/VSC

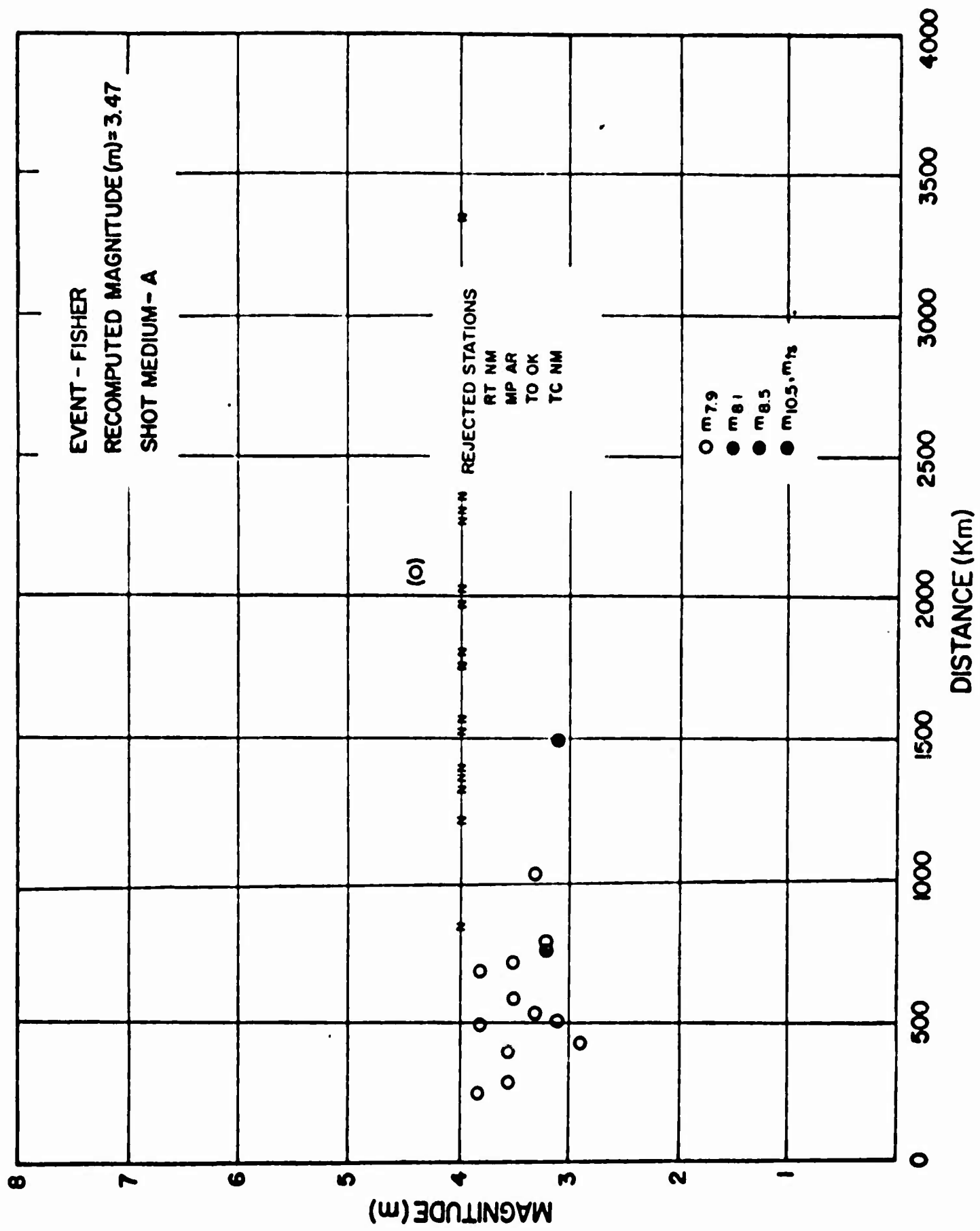


Figure 56
AFTAC/VSC

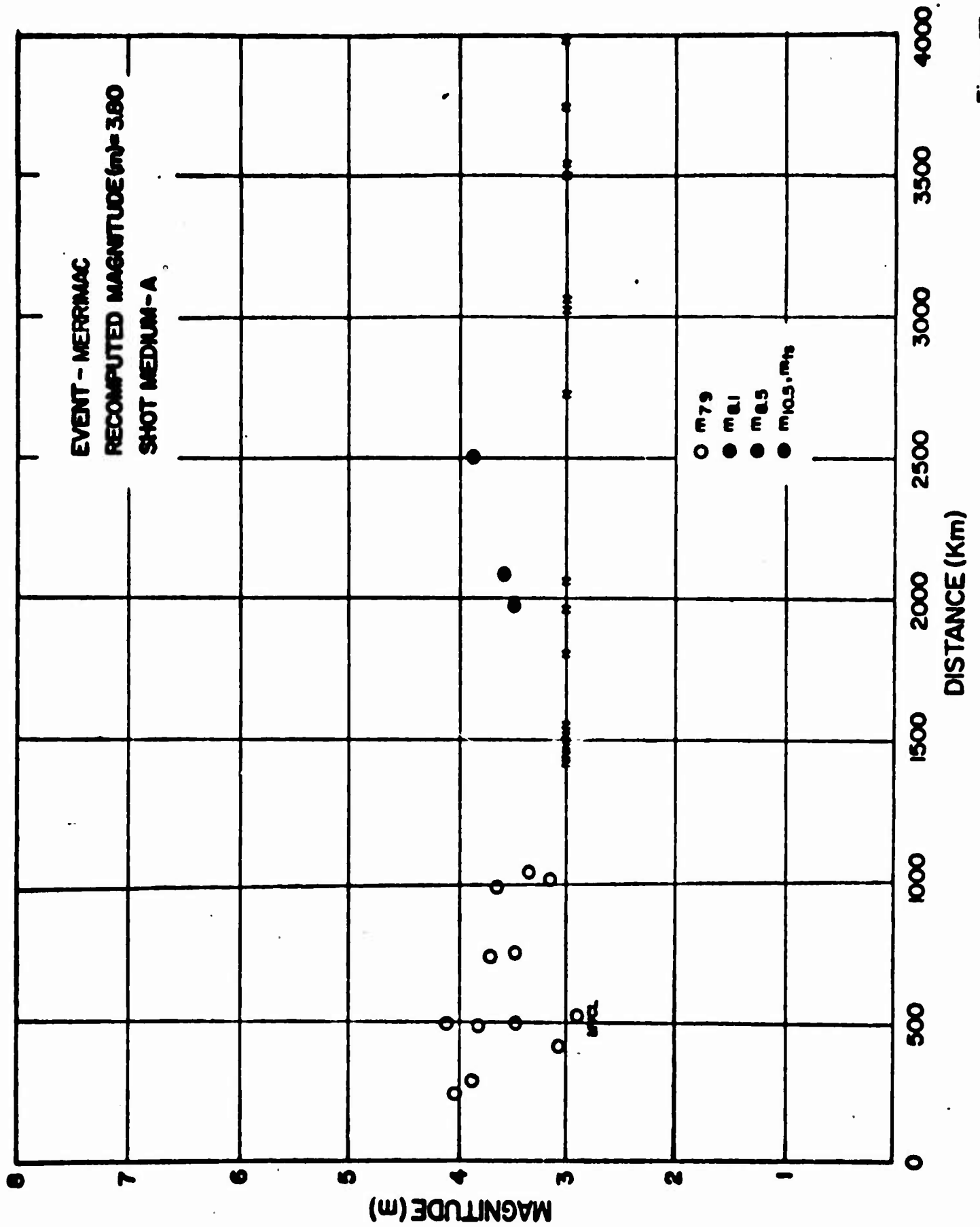


Figure 57
AFTAC/VSC

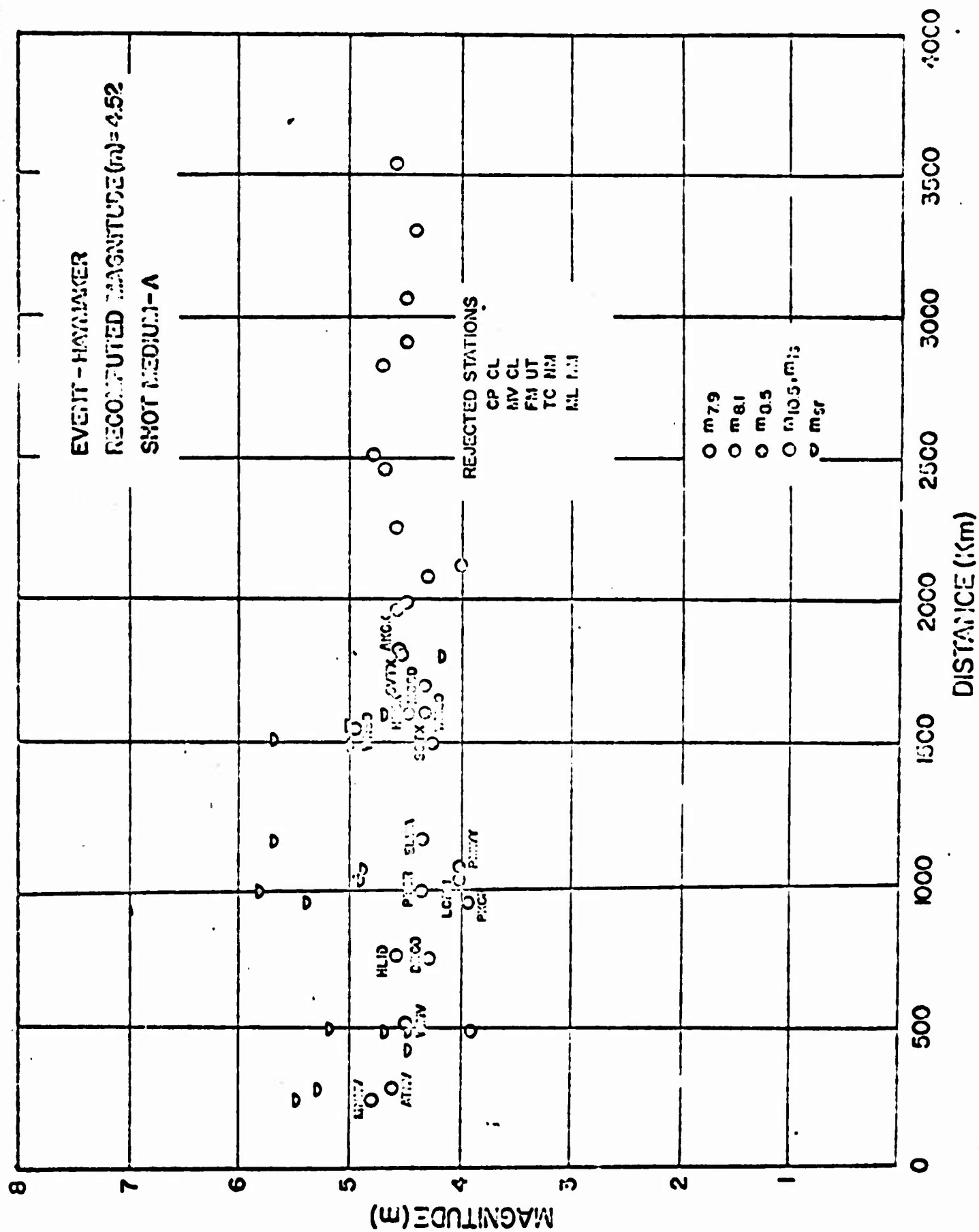


Figure 53
AFTAC/VSC

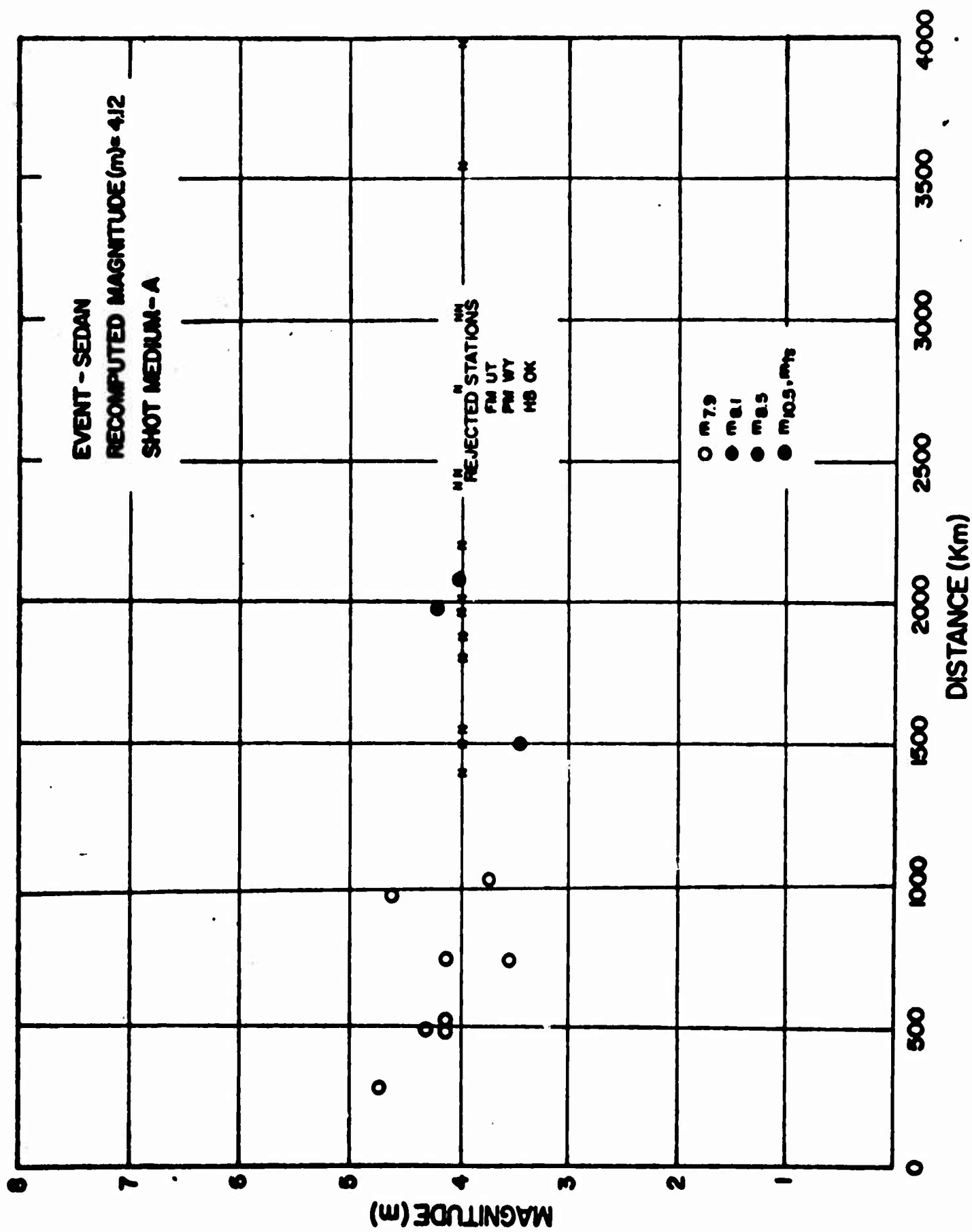


Figure 59
 AFTAC/VSC

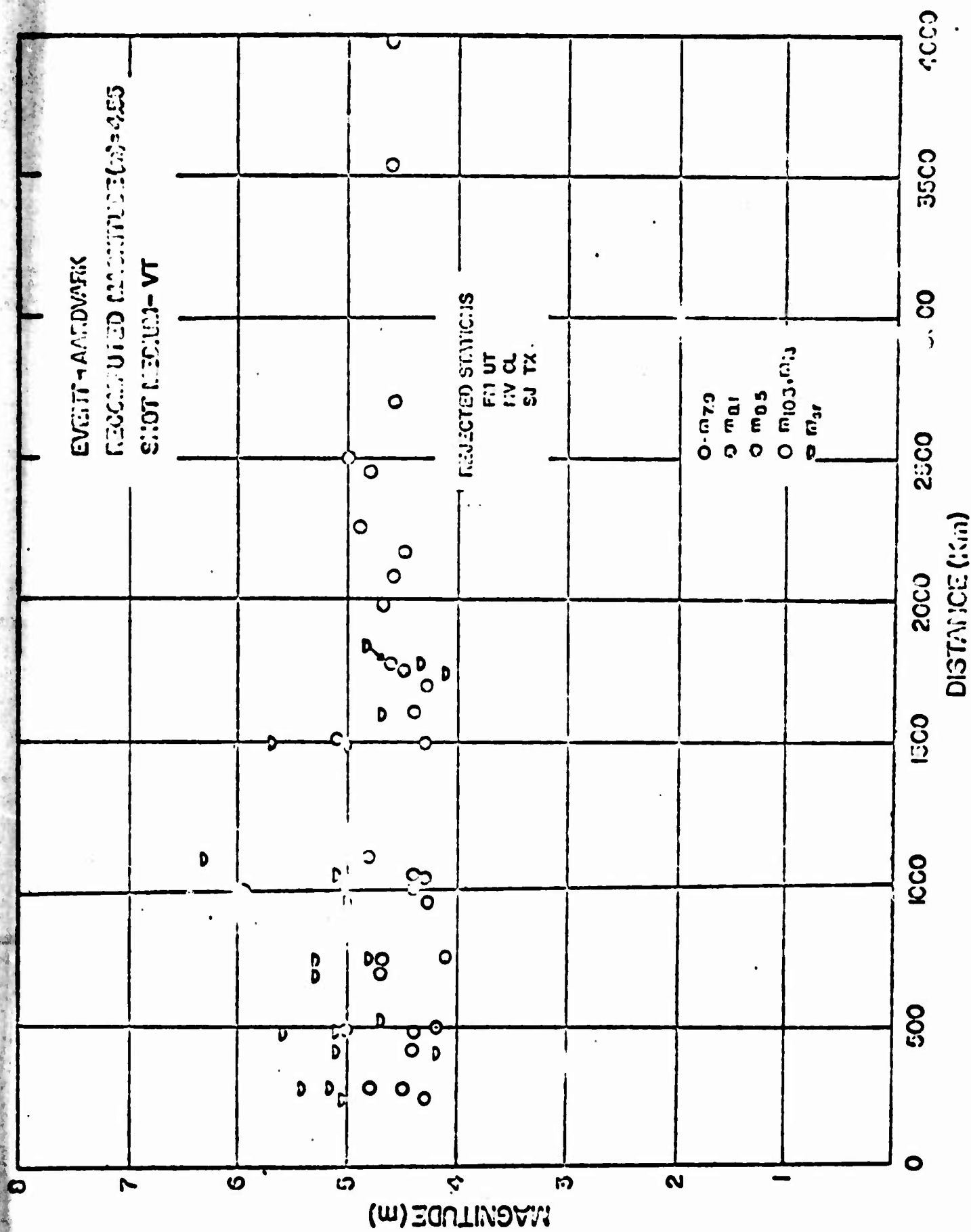


Figure 22
 AFTAC/VSC

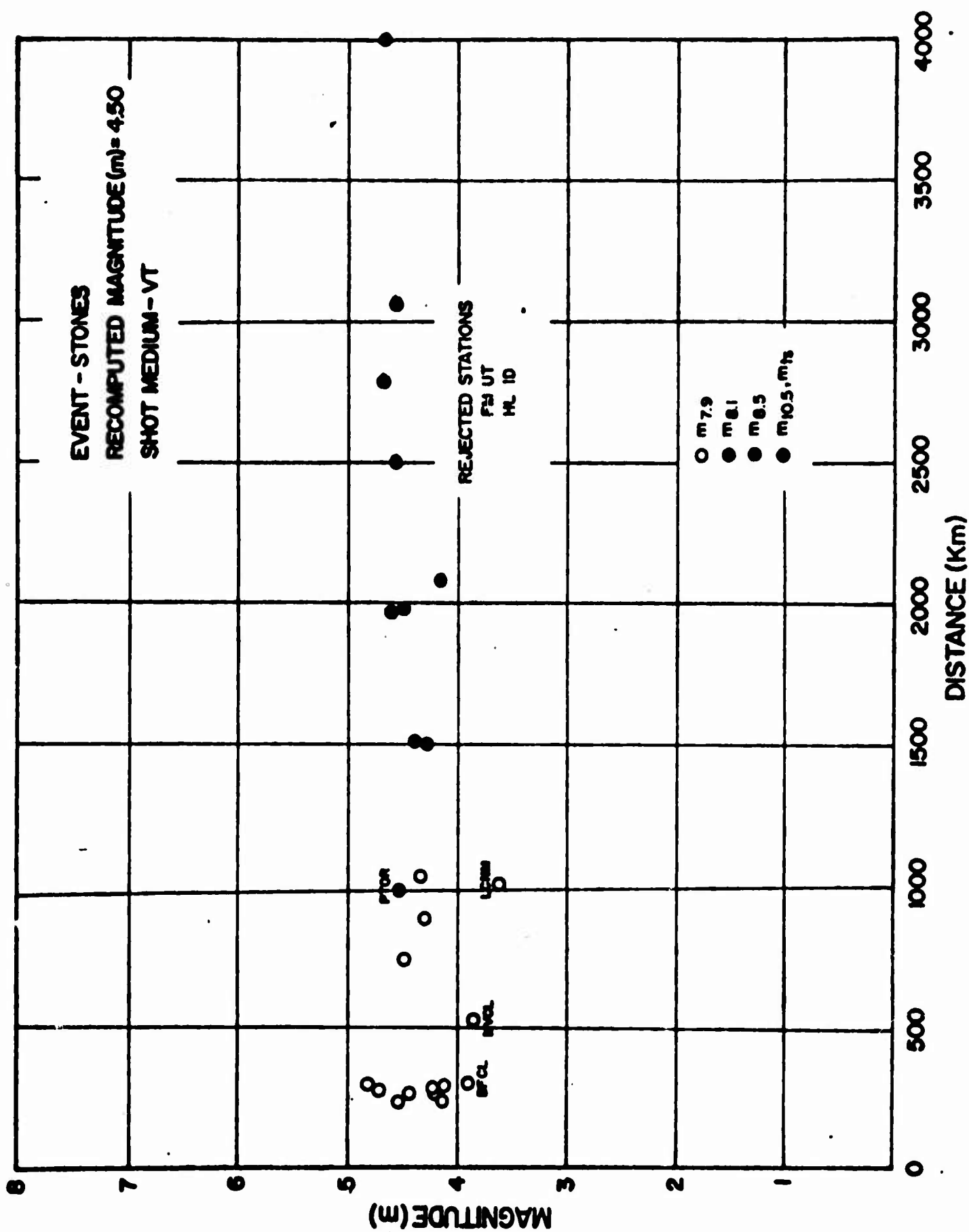


Figure 61
 AFTAC/VSC

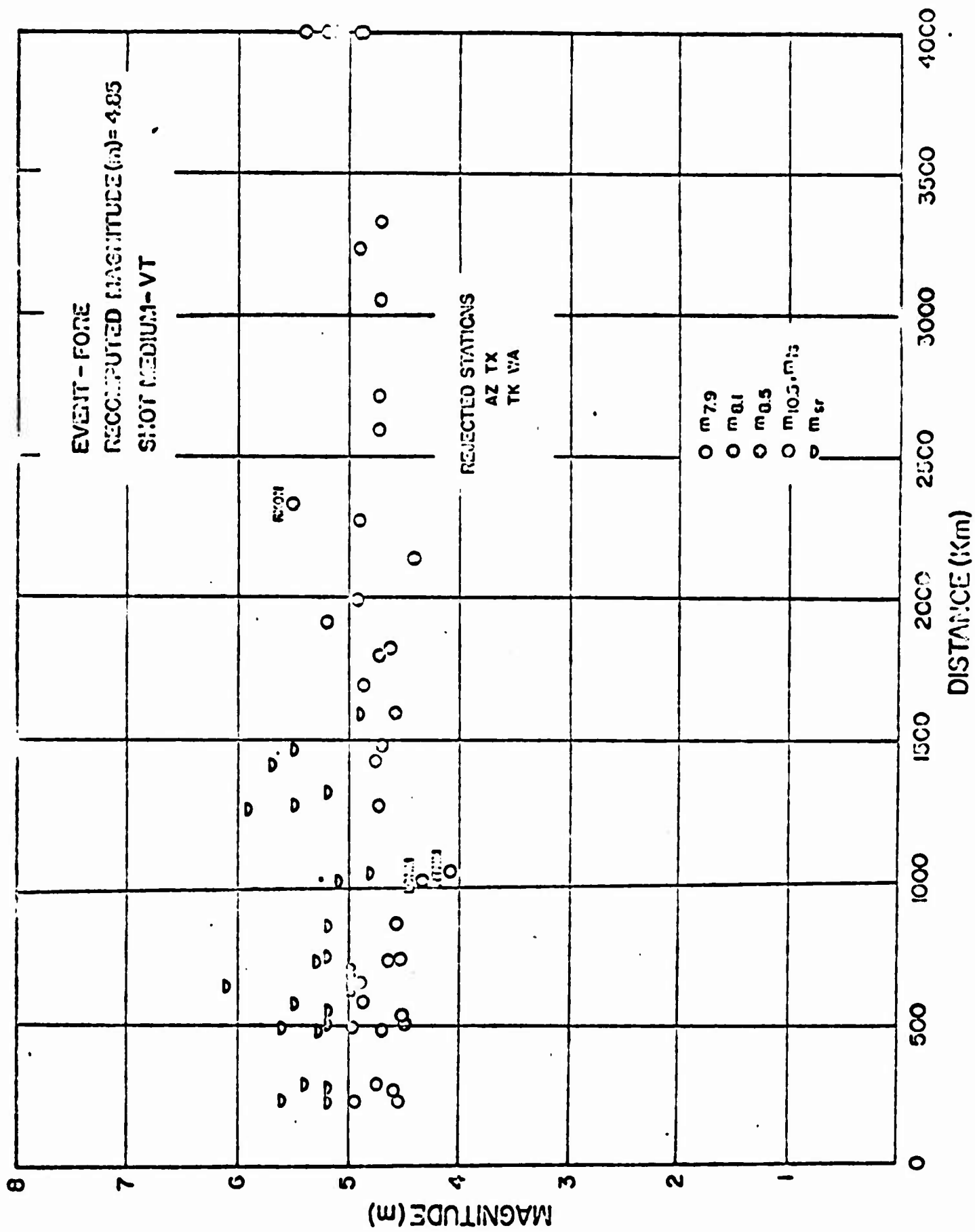


Figure C2
AFTAC/VSC

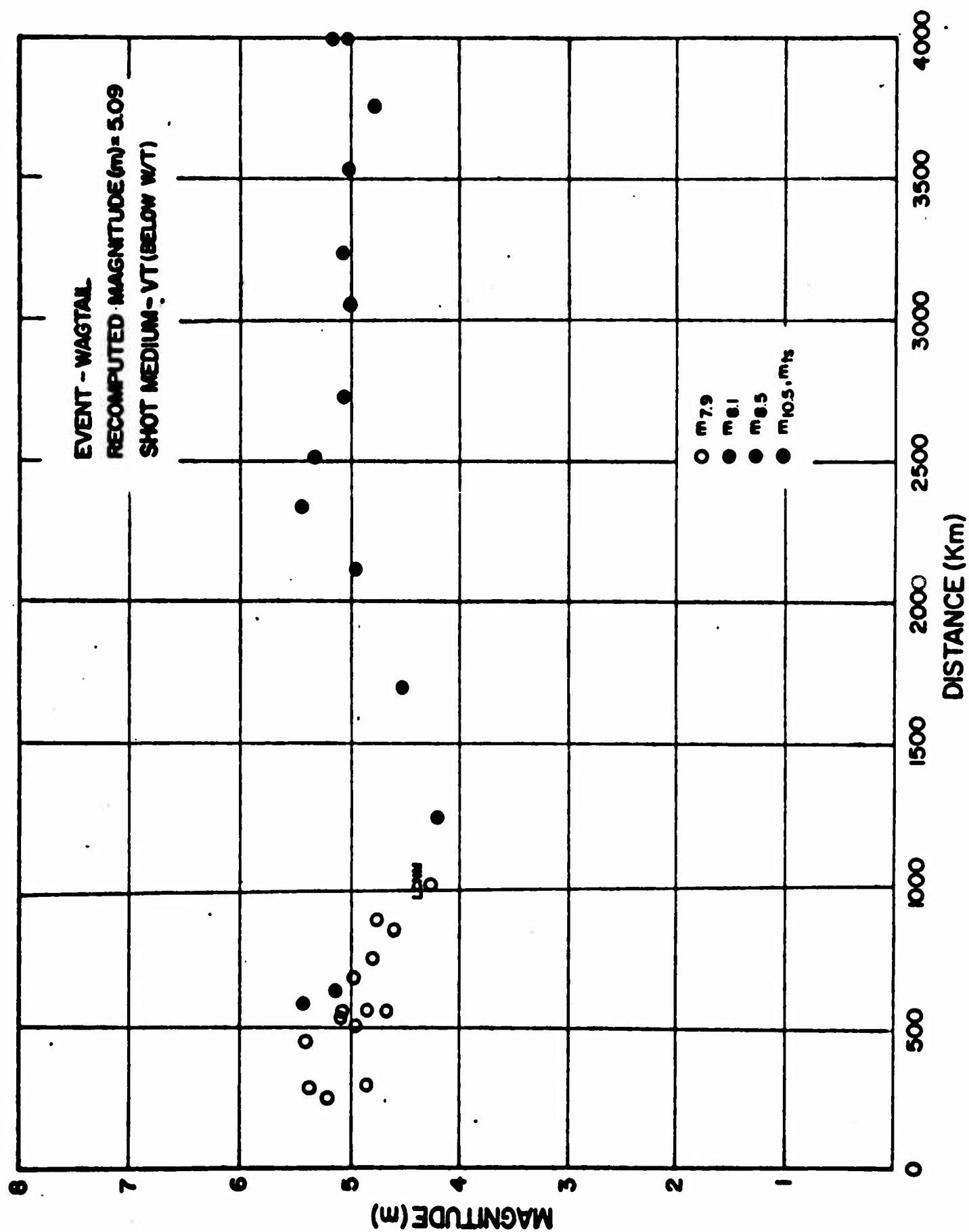


Figure 63
AFTAC/VSC

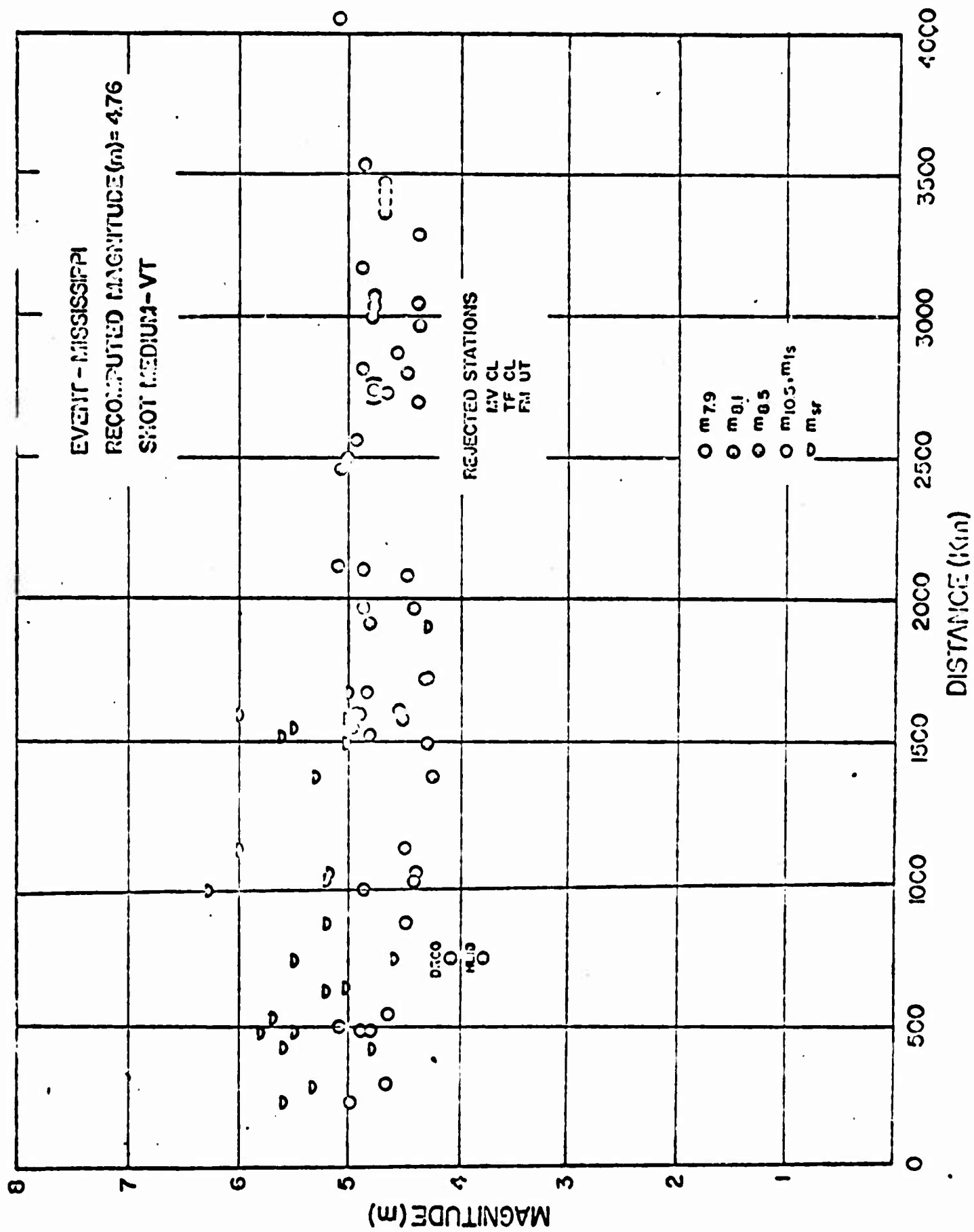


Figure G4
 AFTAC/VSC

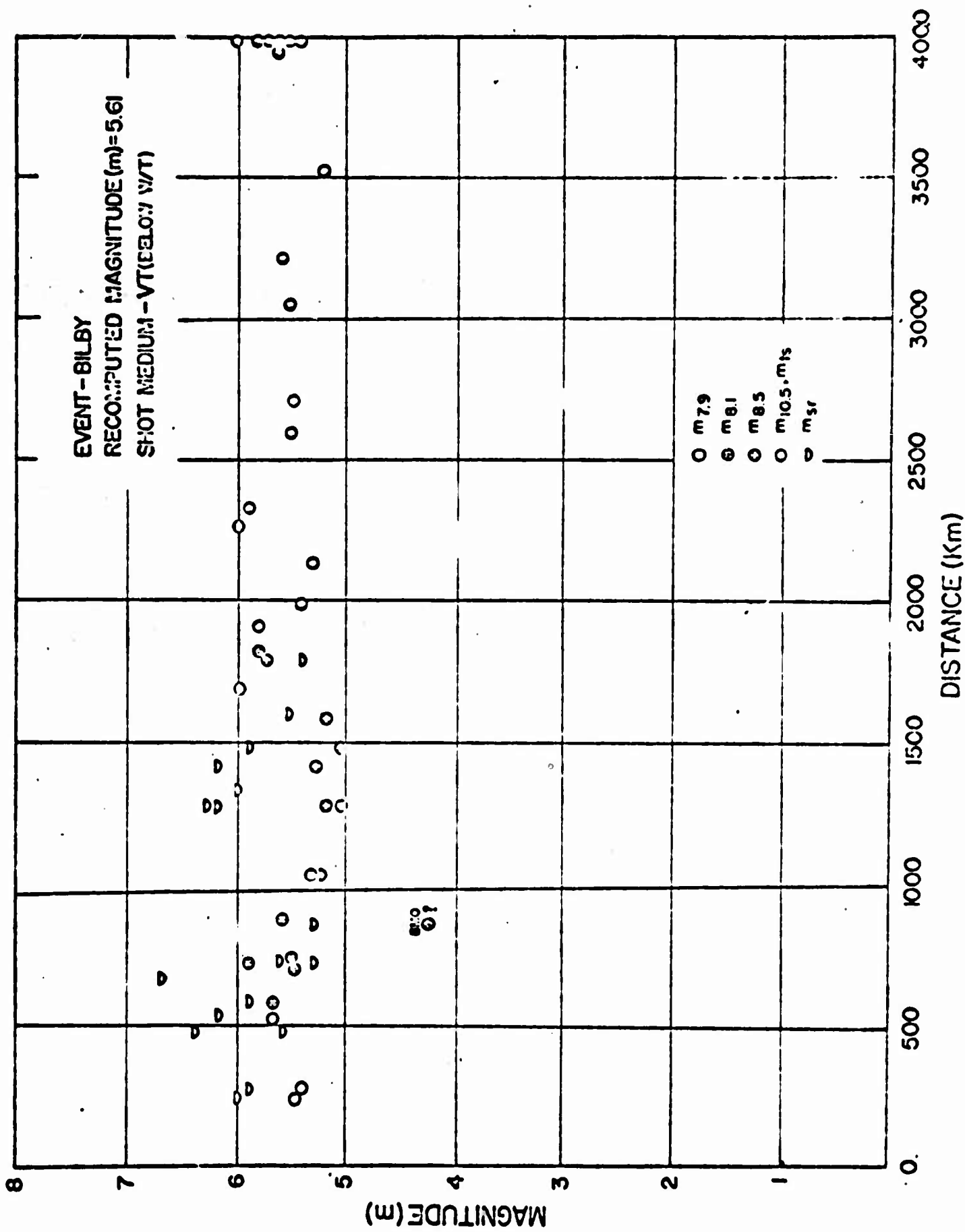


Figure 63
 AFTAC/VSC

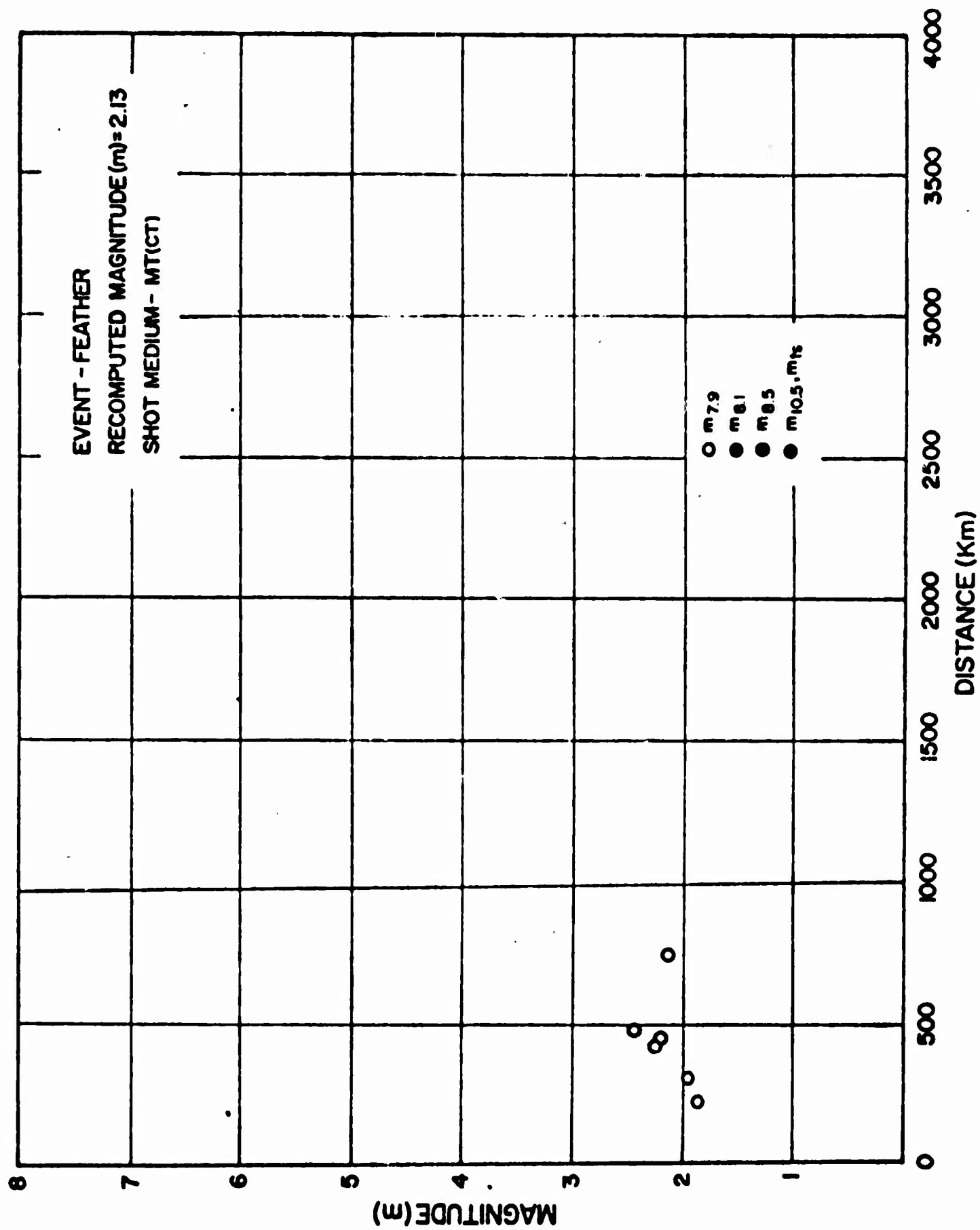


Figure 66
AFTAC/VSC

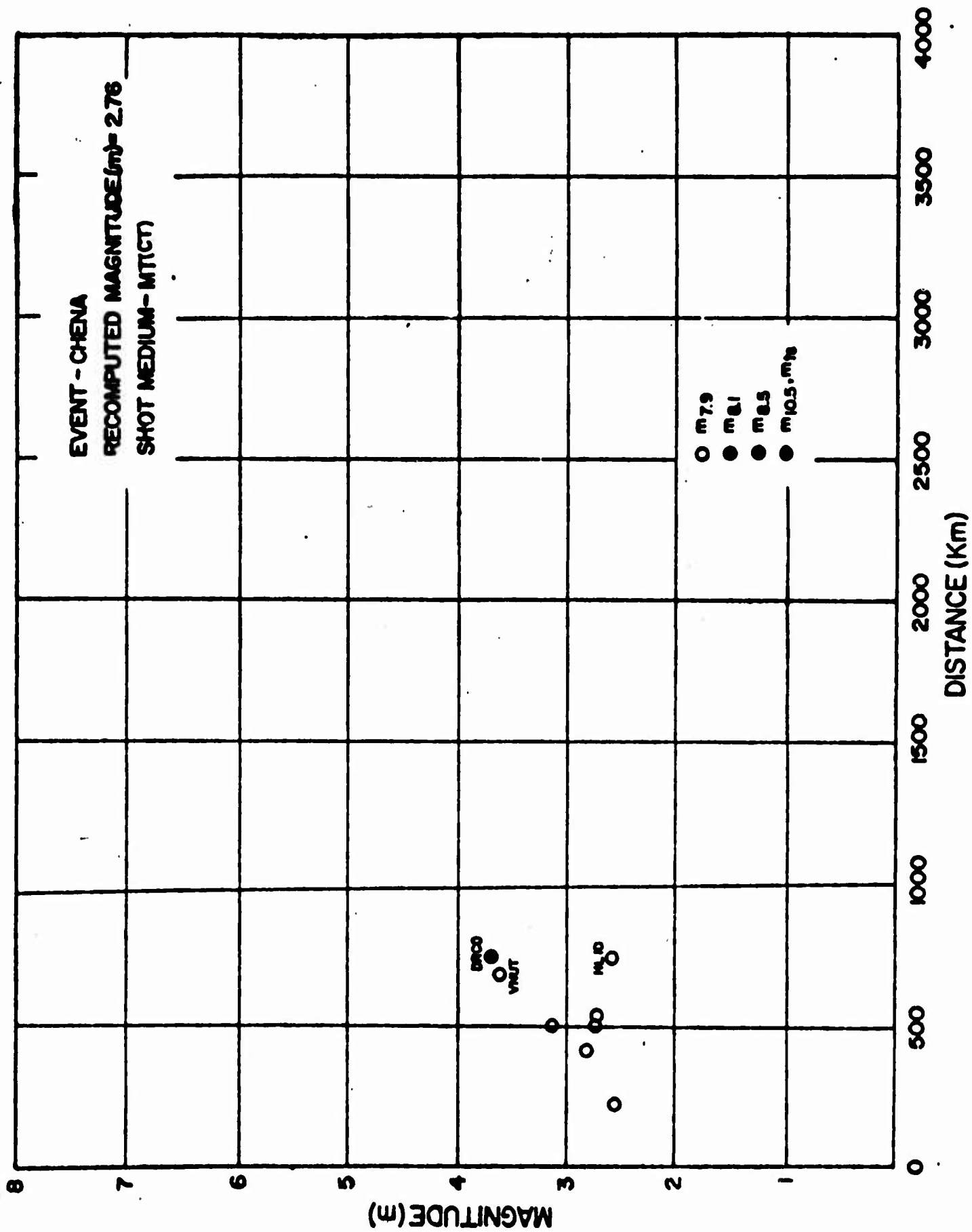


Figure 67
AFTAC/VSC

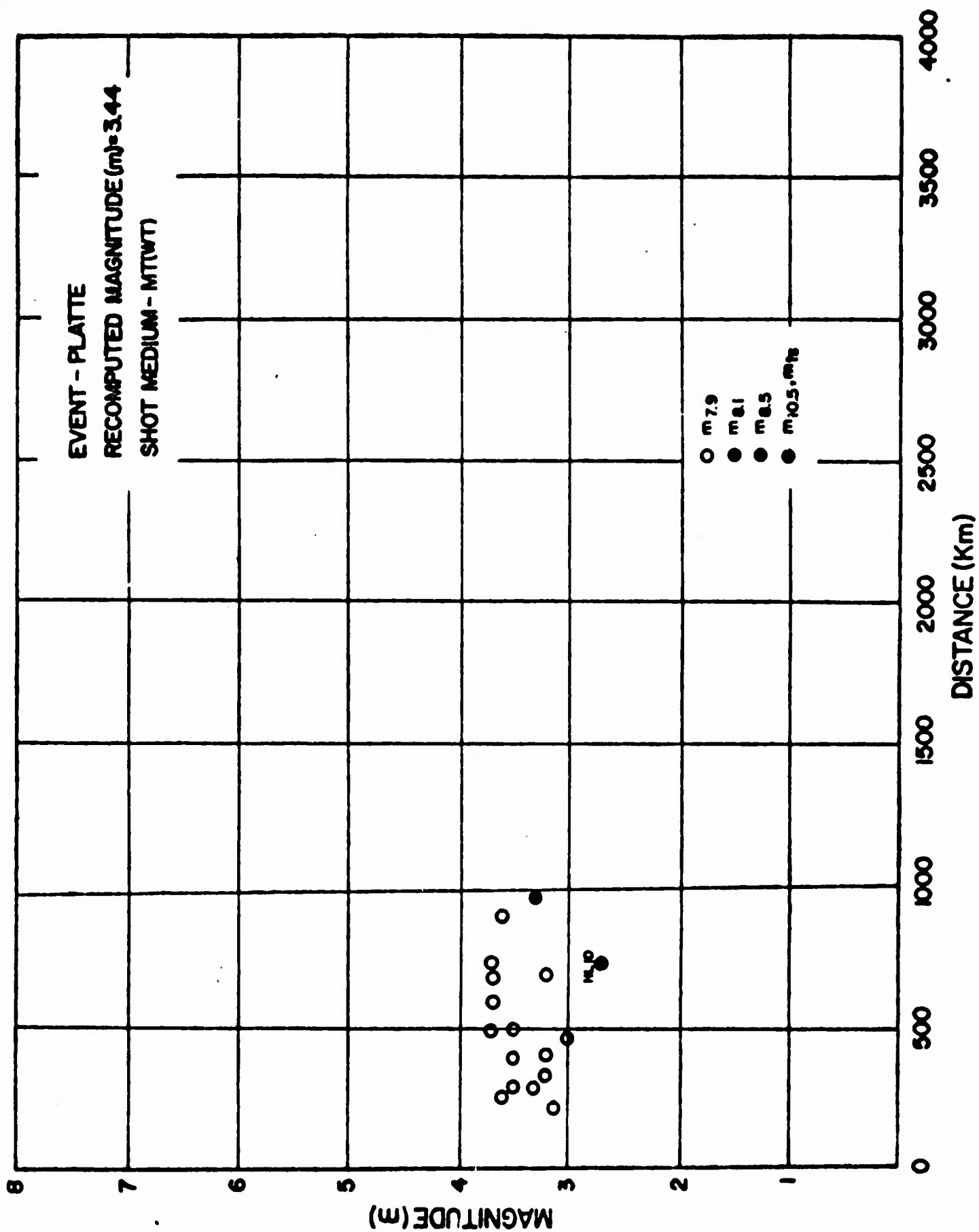


Figure 68
AFTAC/VSC

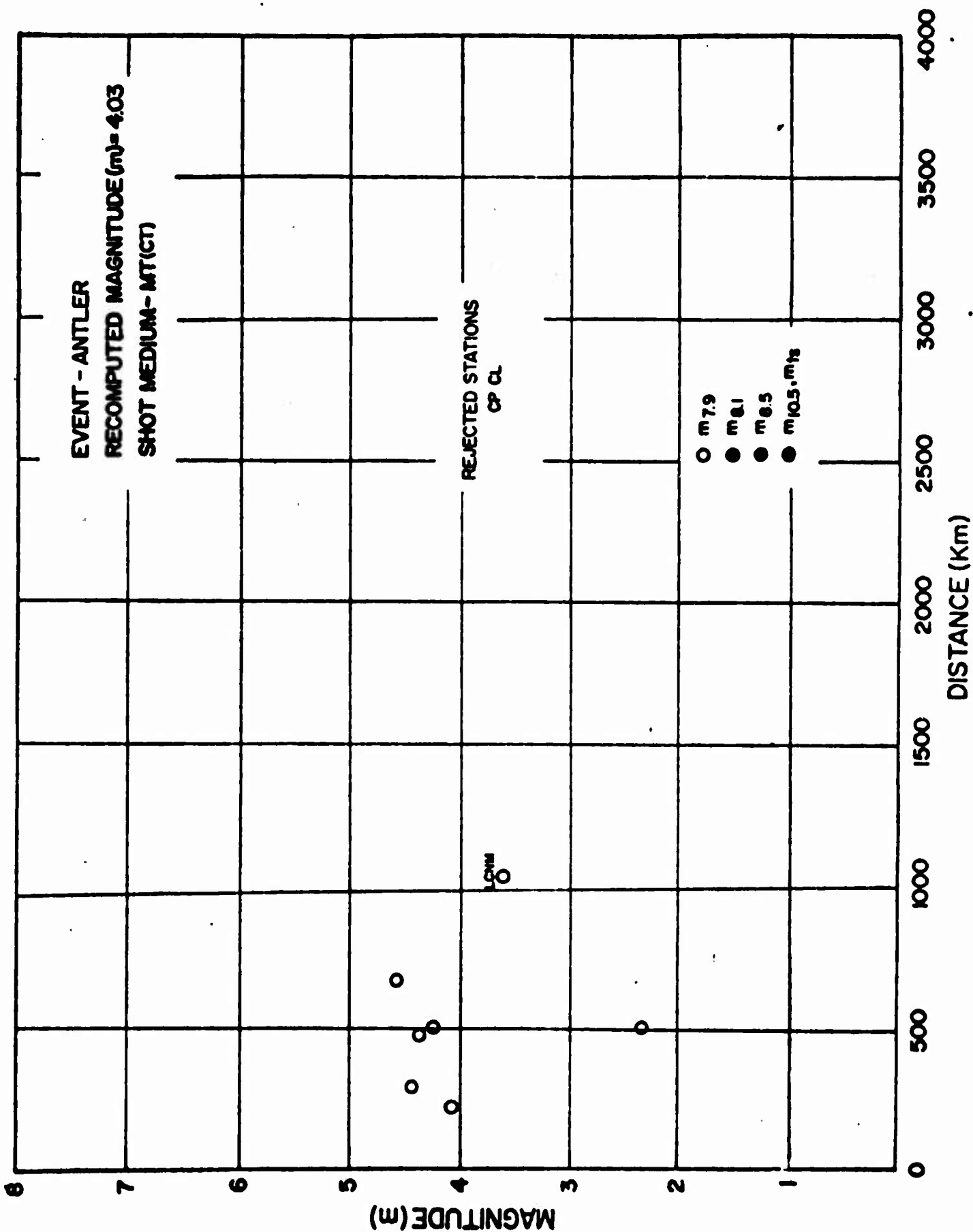


Figure 69
 AFTAC/VSC

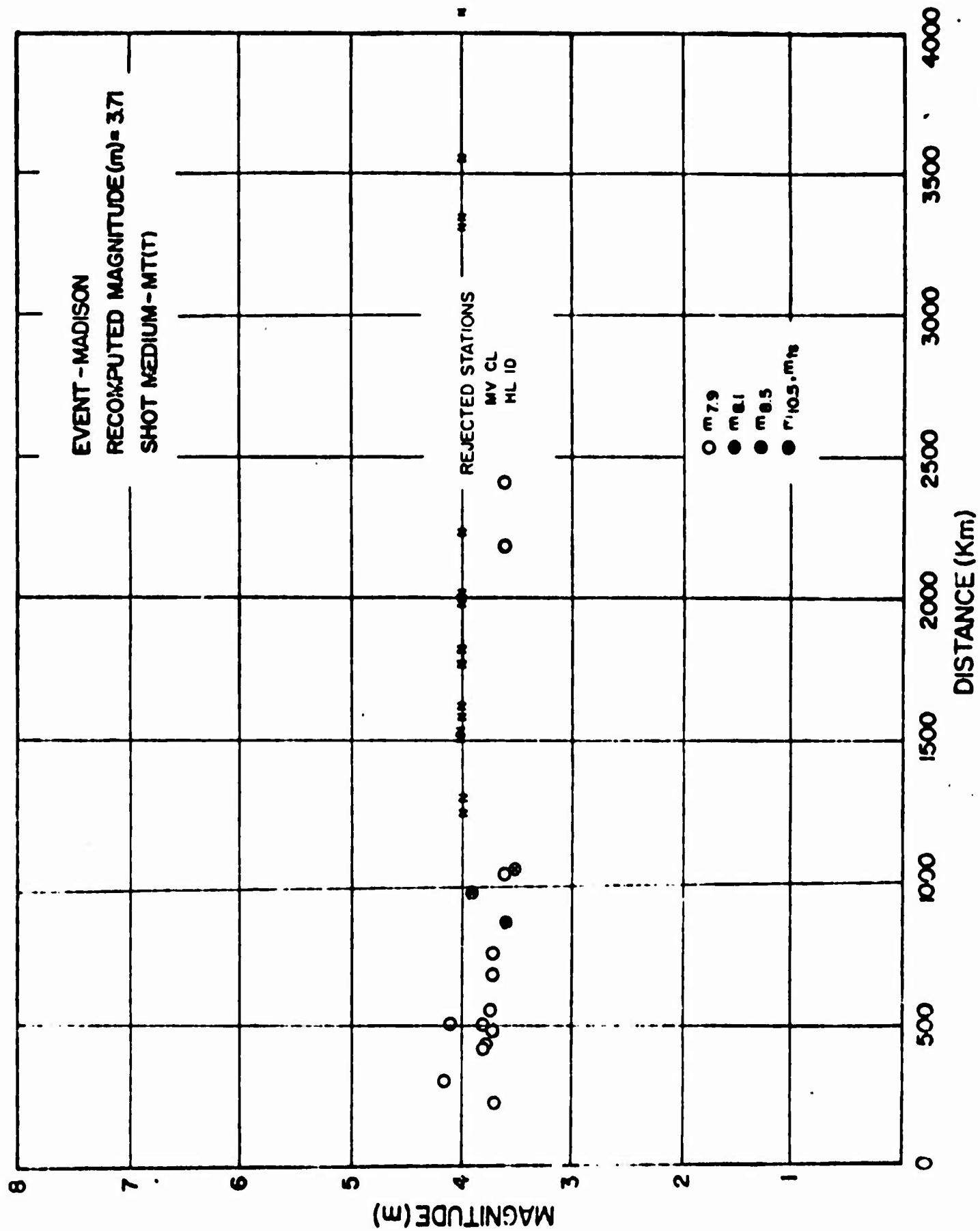


Figure 70
 AFTAC/VSC

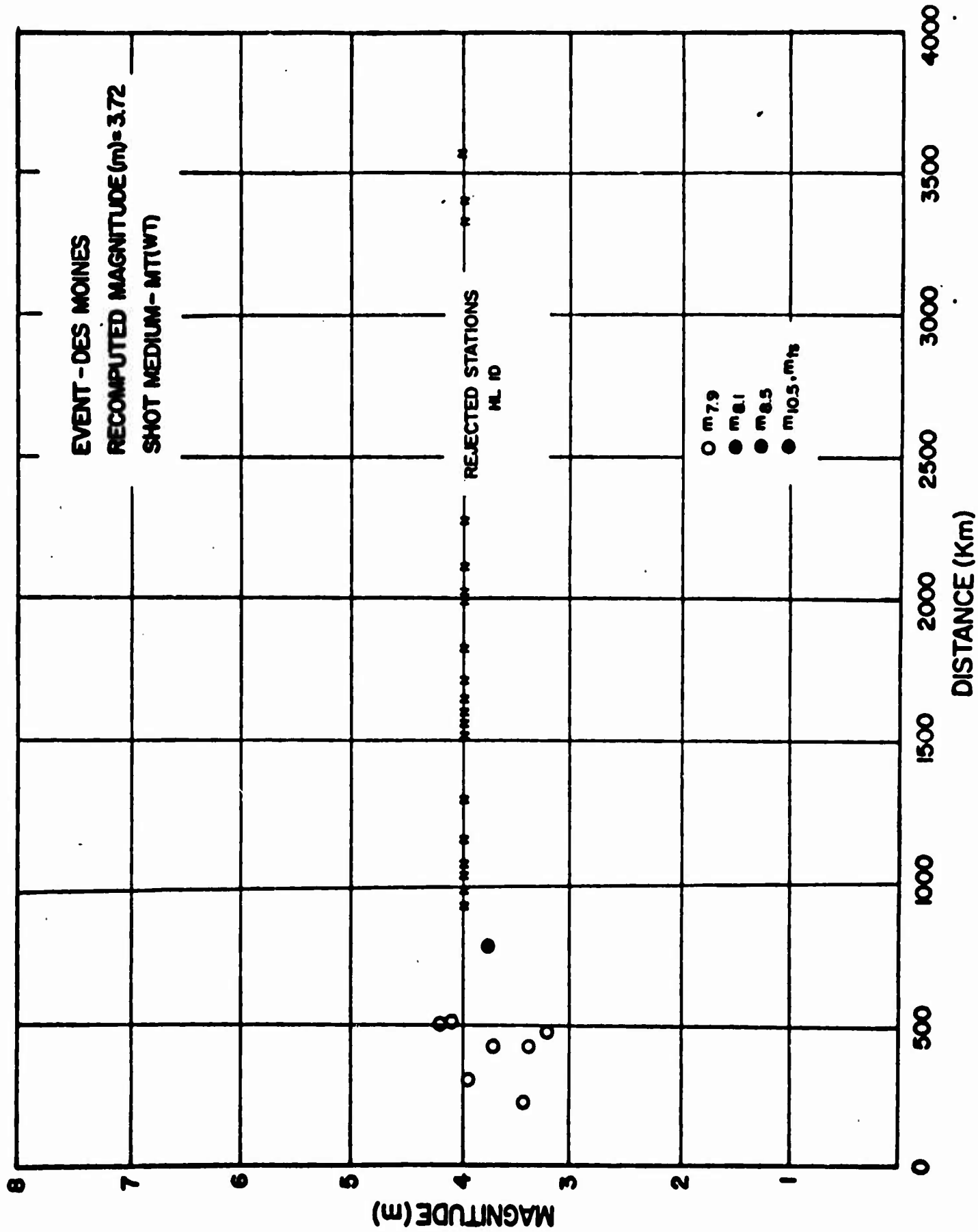


Figure 71
 AFTAC/VSC

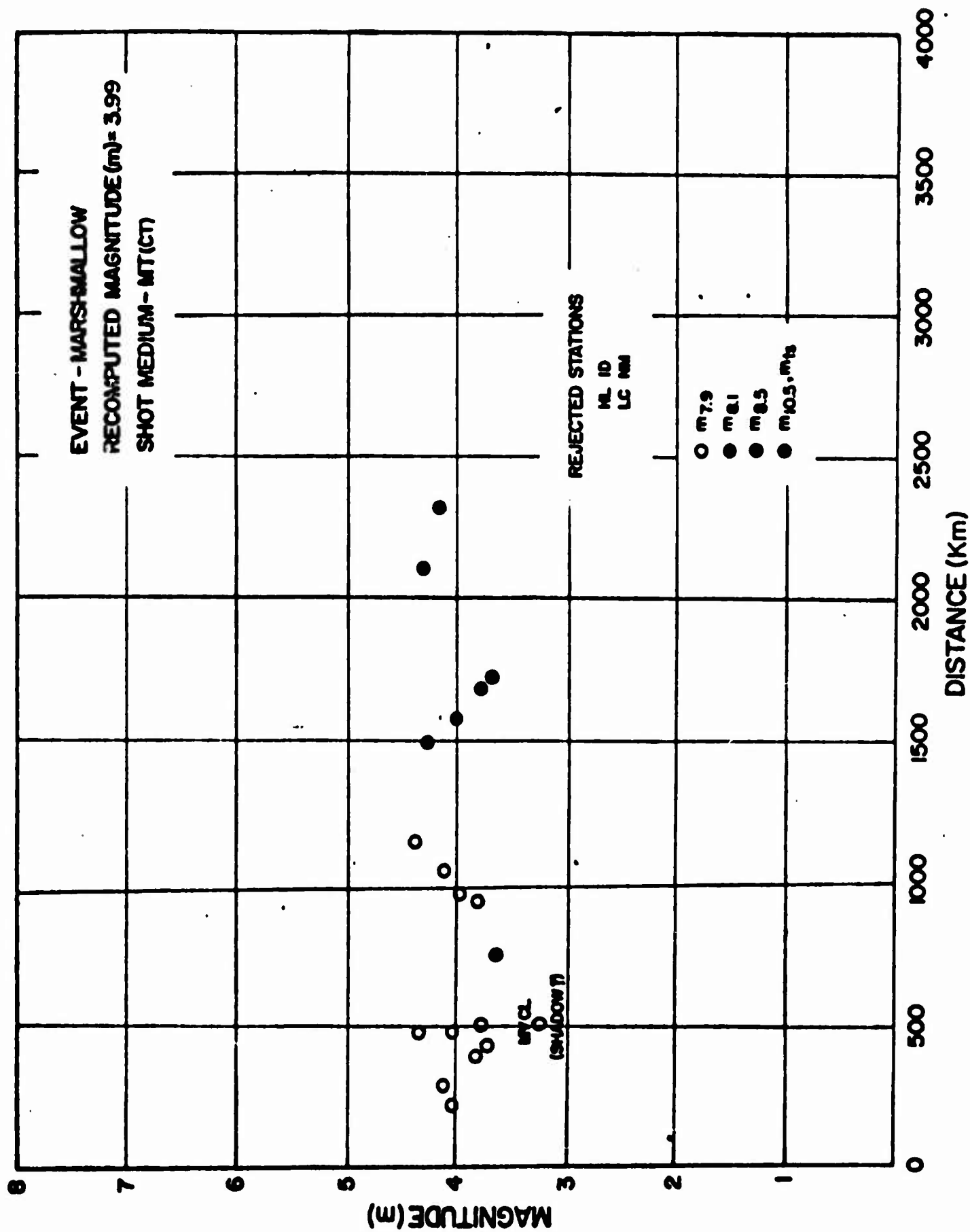
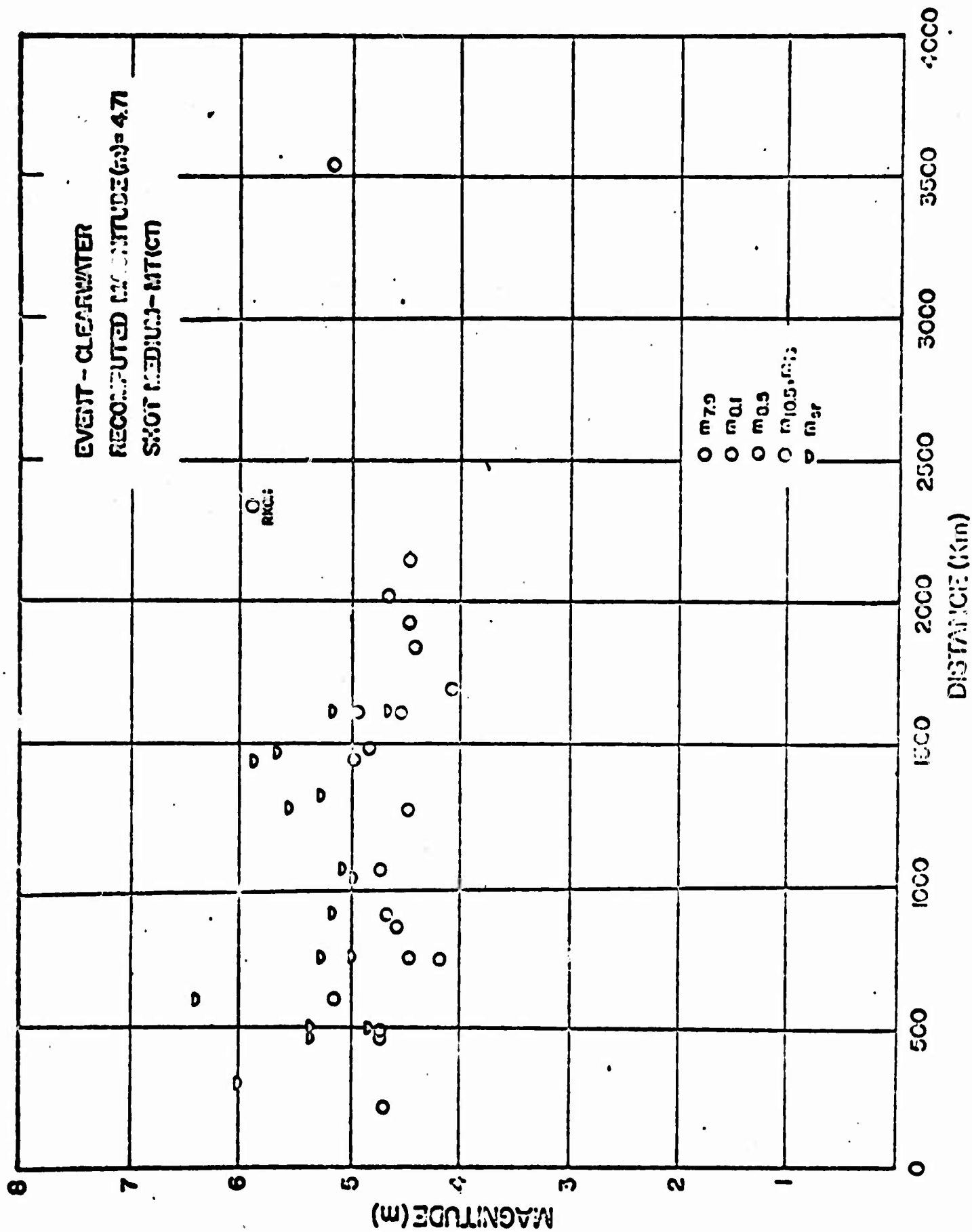
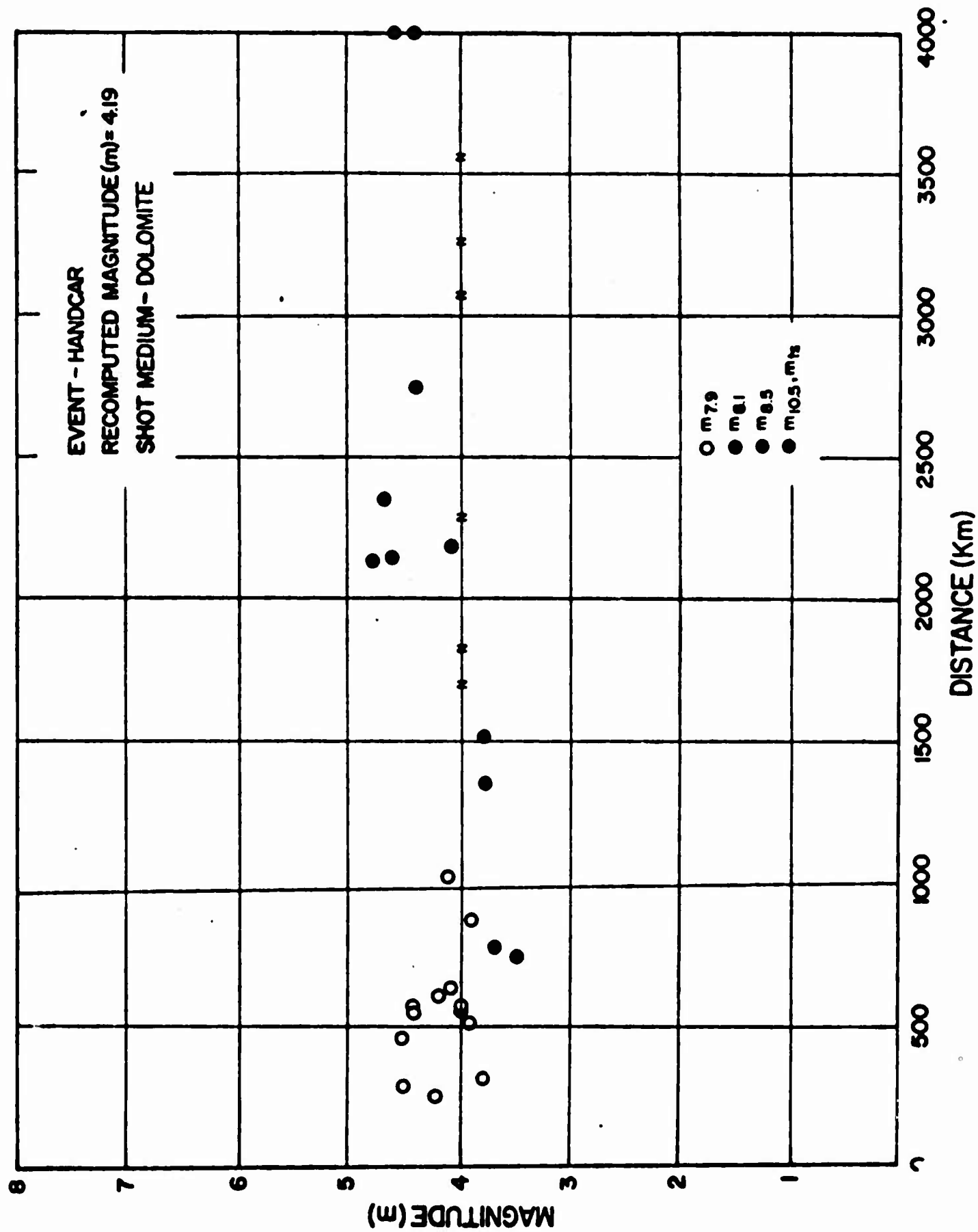


Figure 72
 AFTAC/VSC





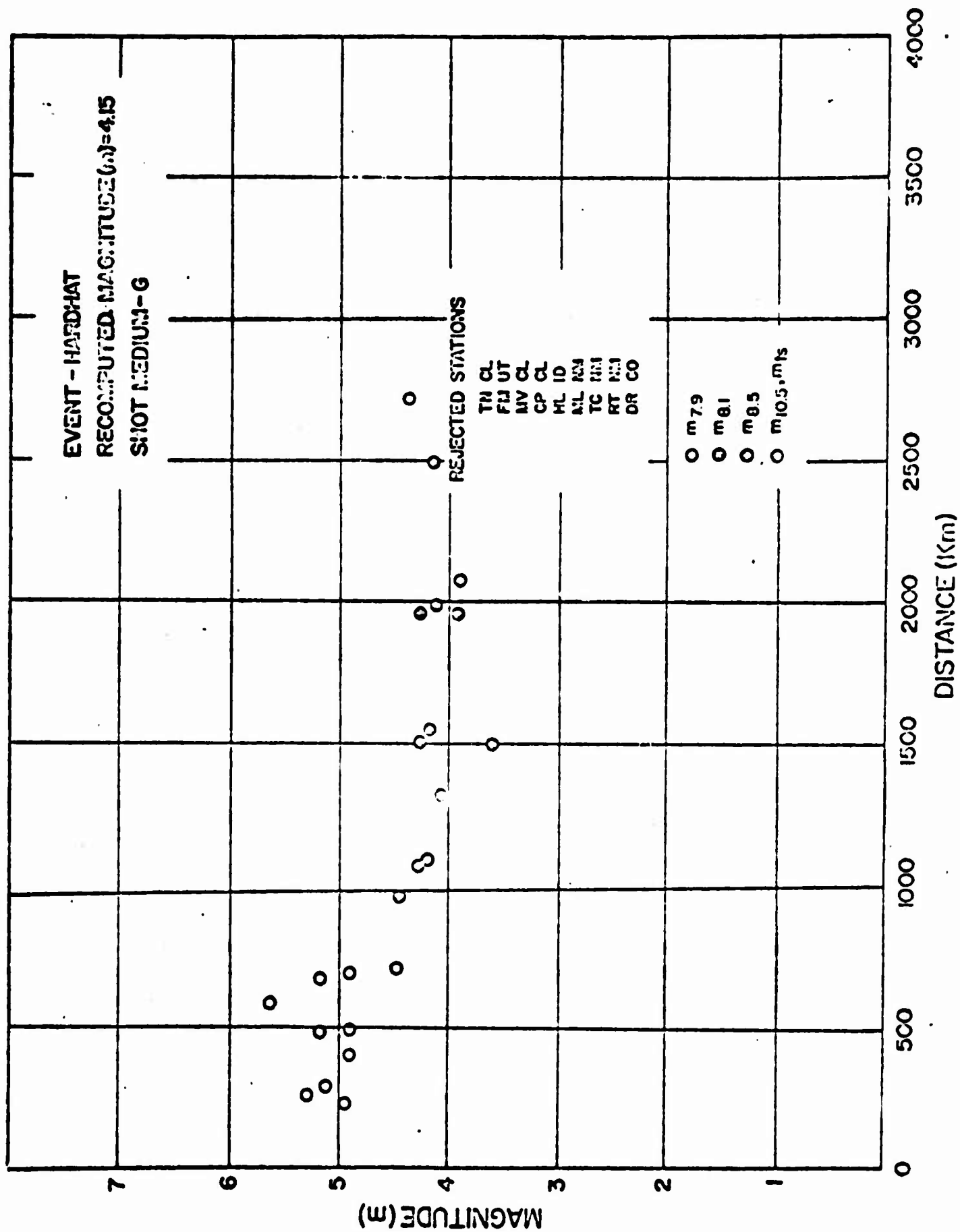


Figure 73
 AFTAC/VSC

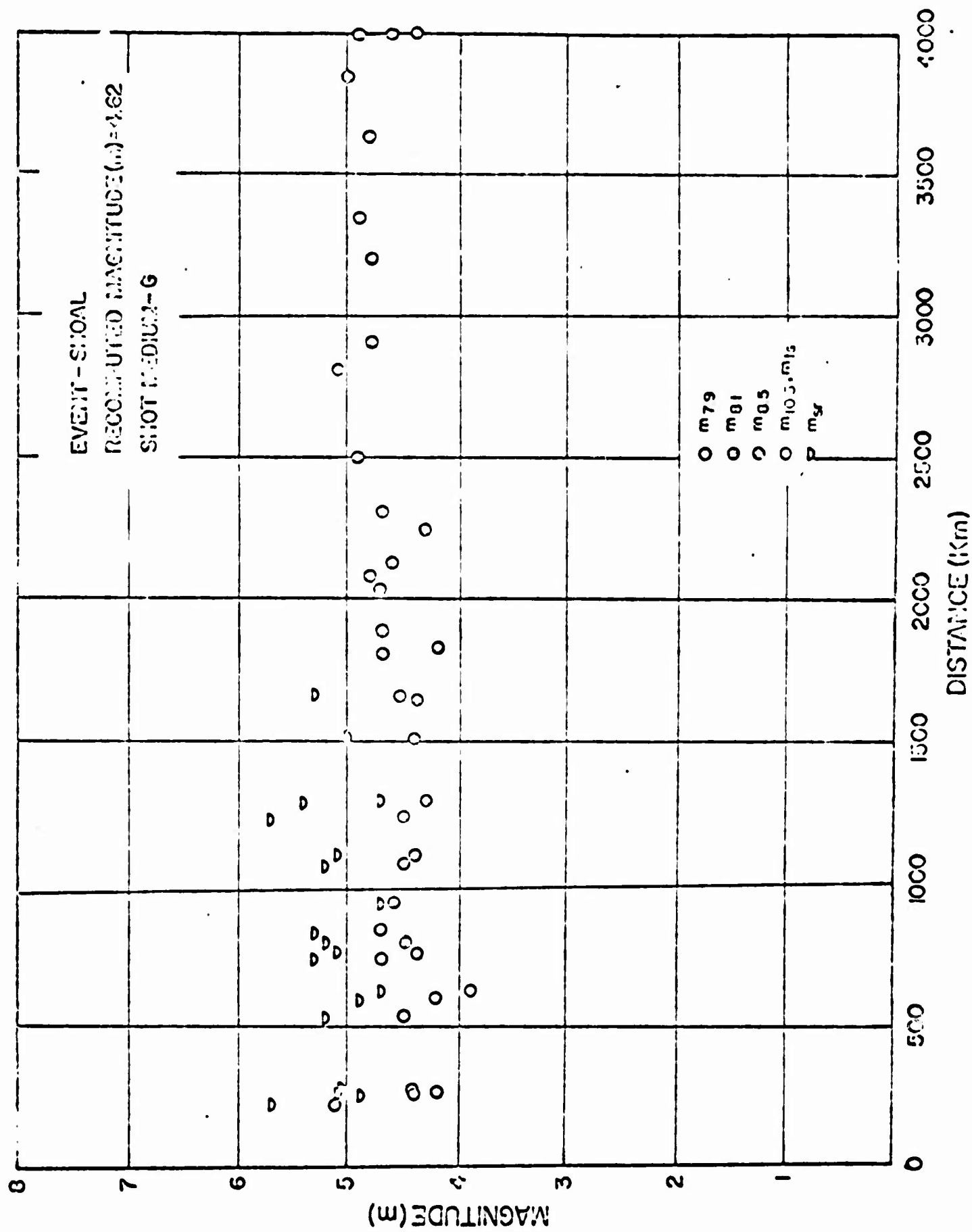


Figure 76
AFTAC/VSC

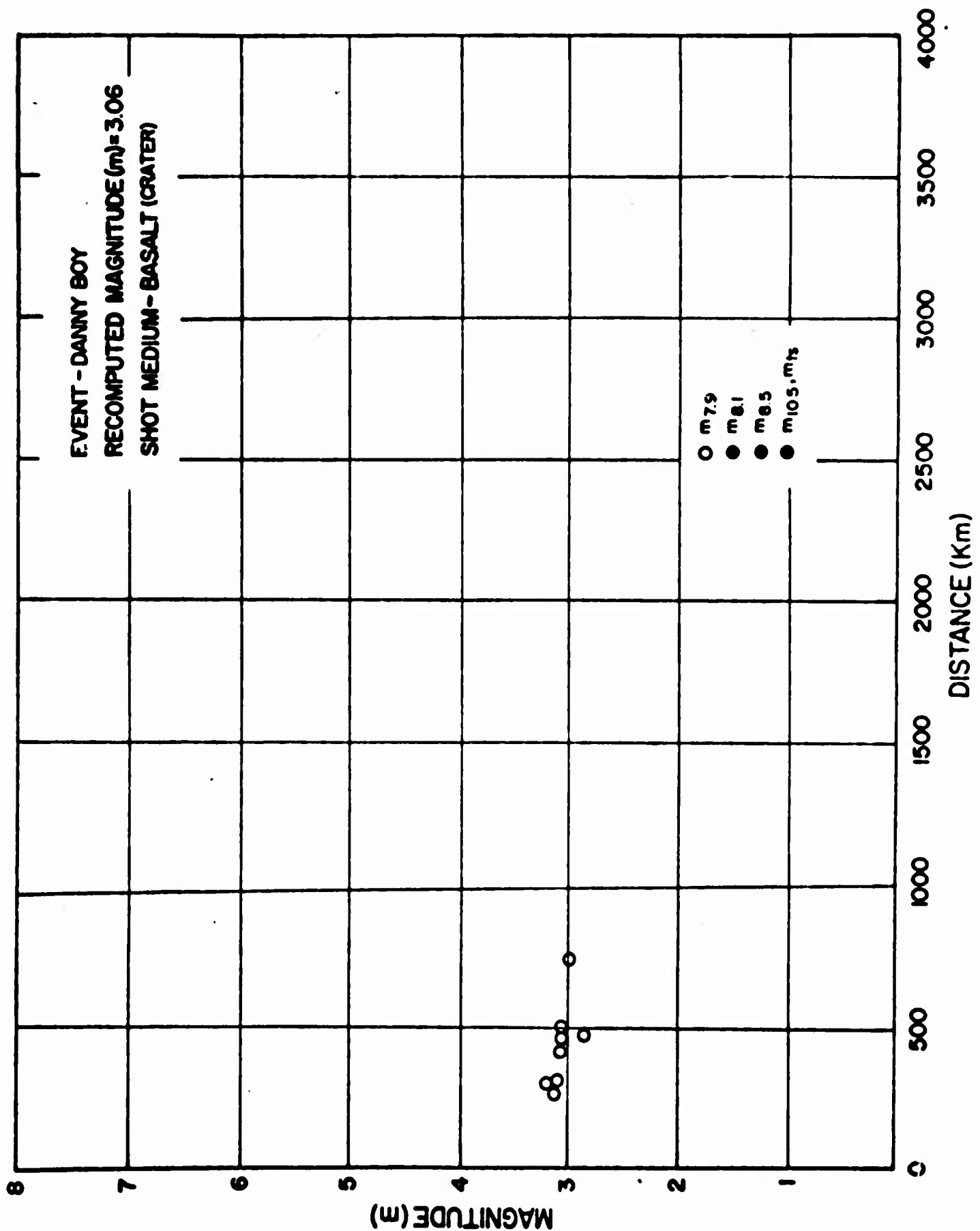


Figure 77
AFTAC/VSC

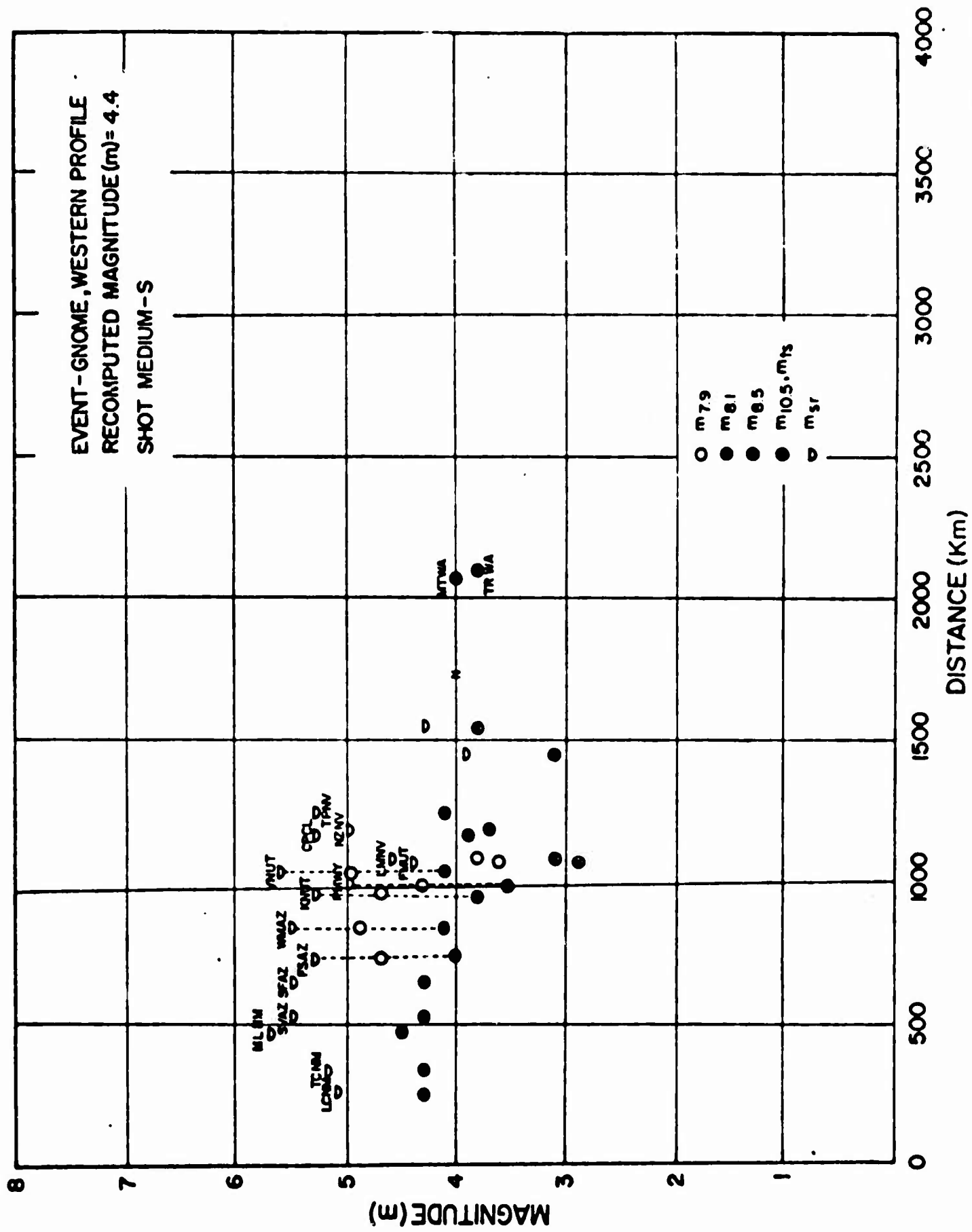


Figure 78

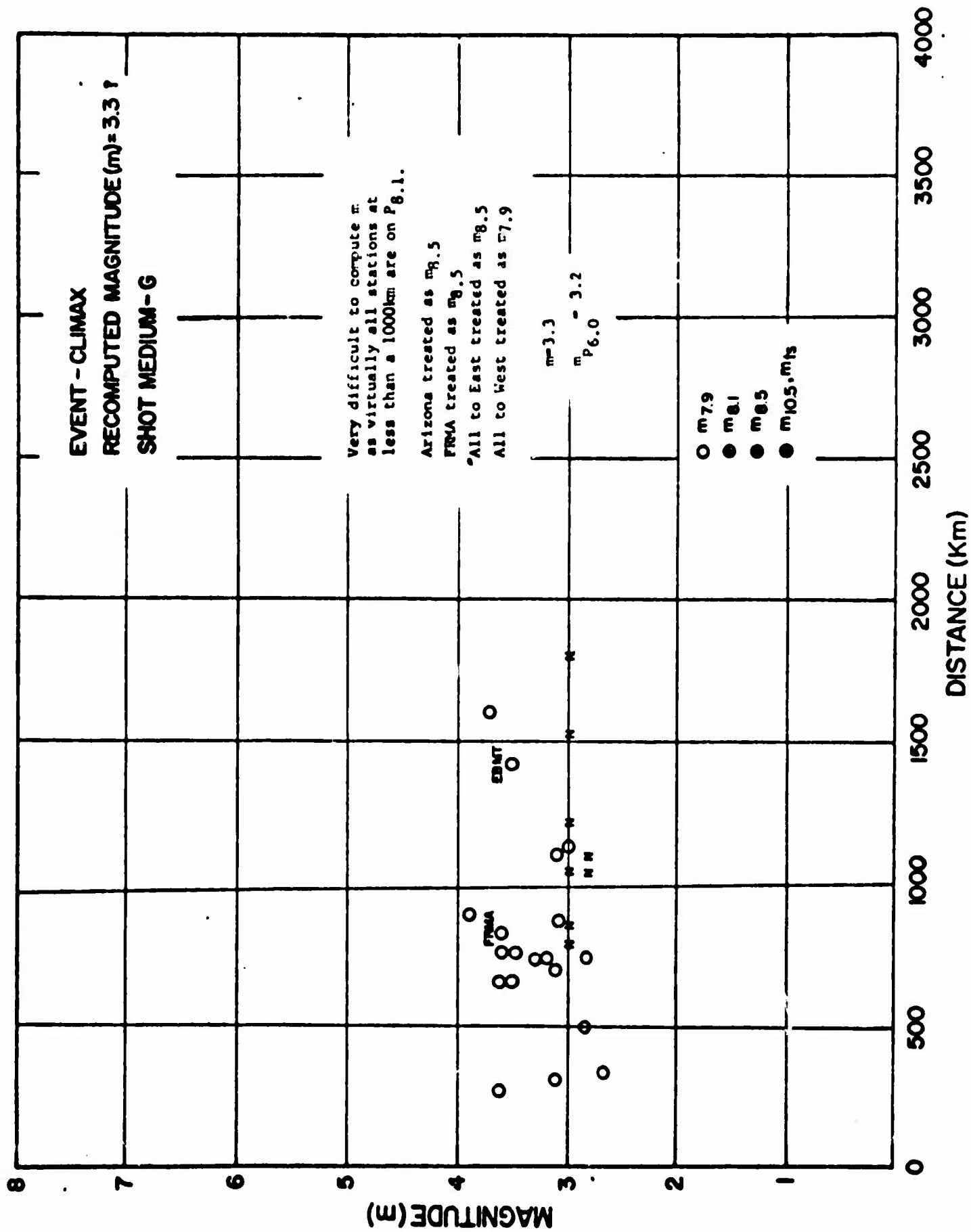


Figure 79
 AFTAC/VSC

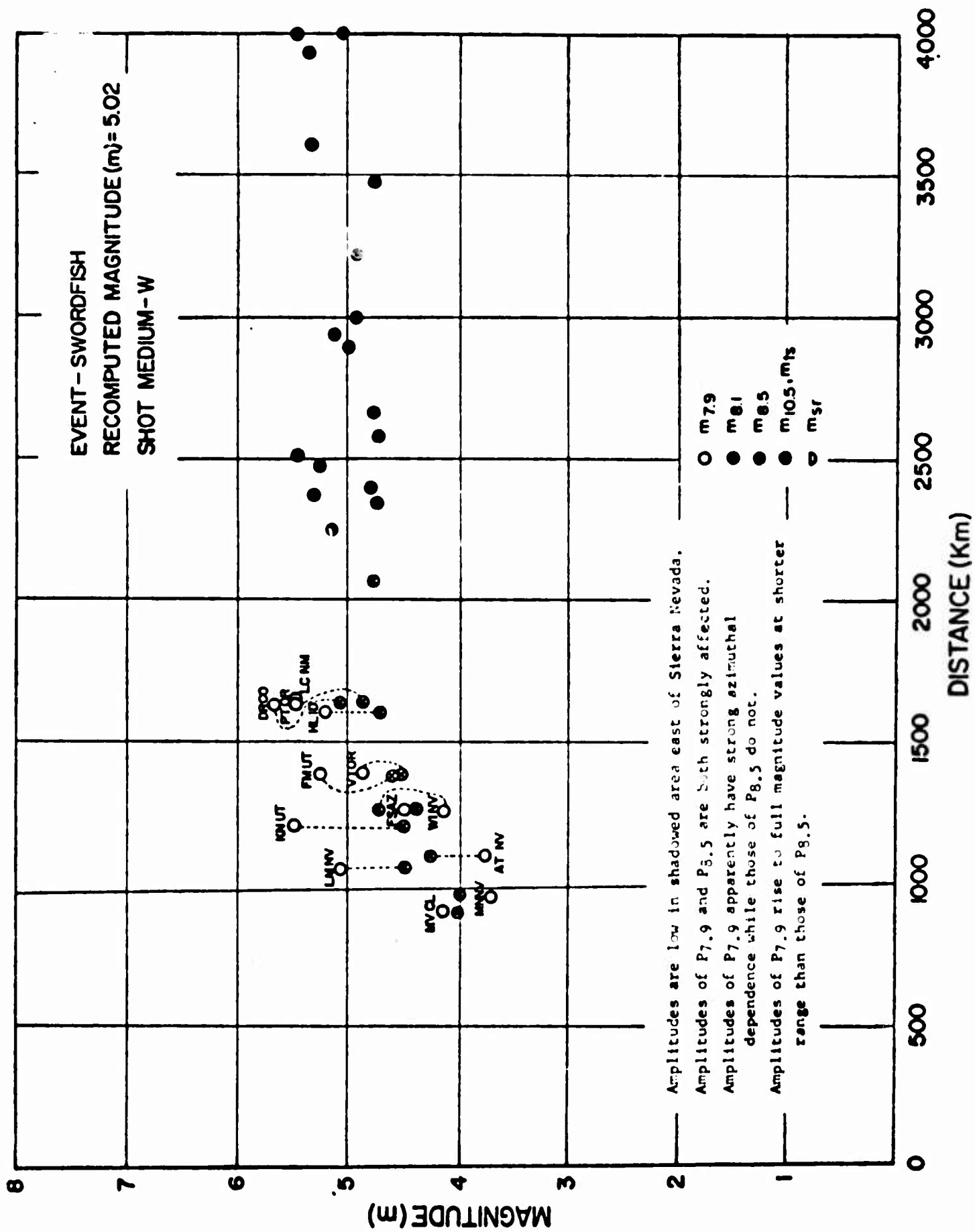


Figure 80
AFTAC/VSC

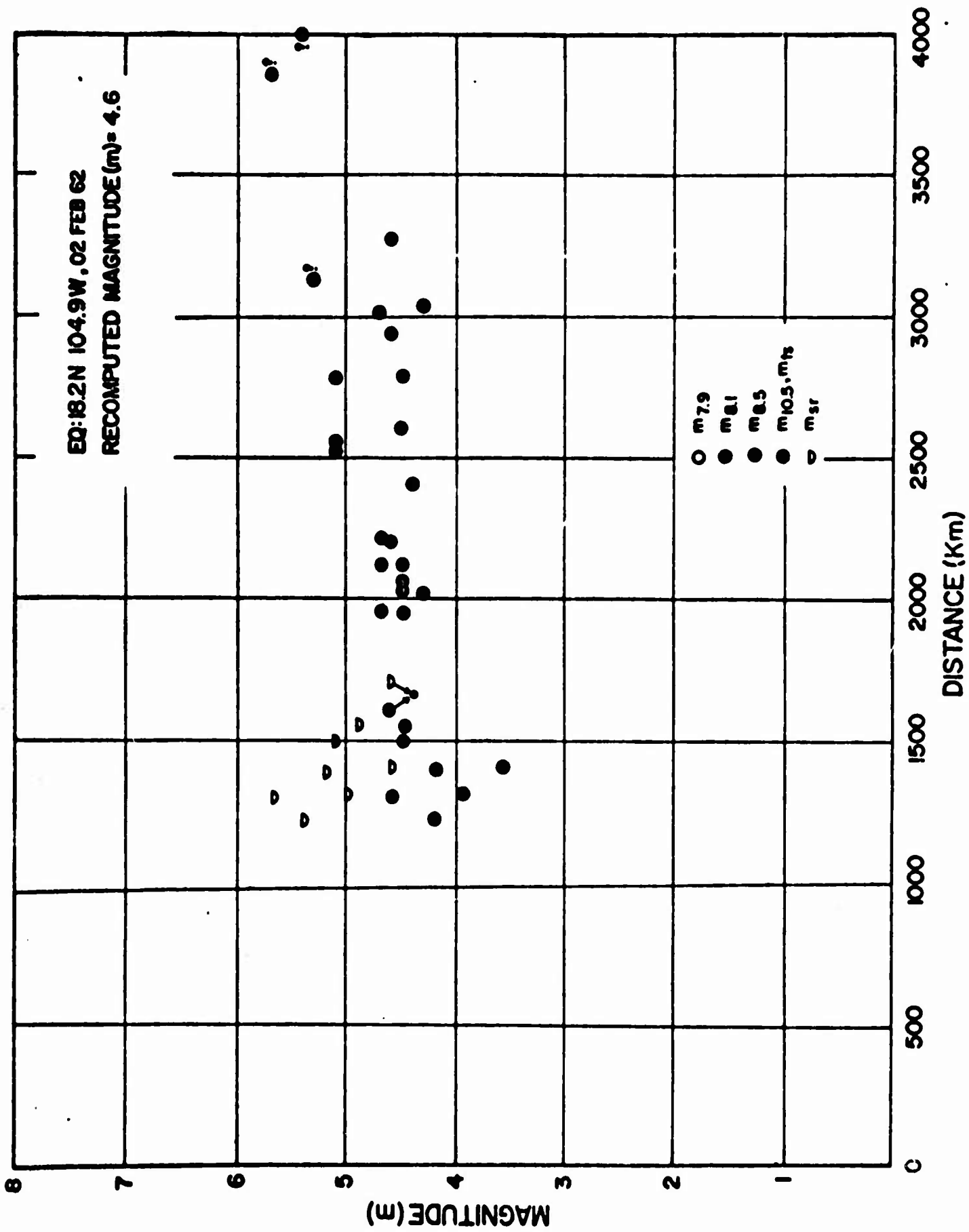


Figure 81
AFTAC/VSC

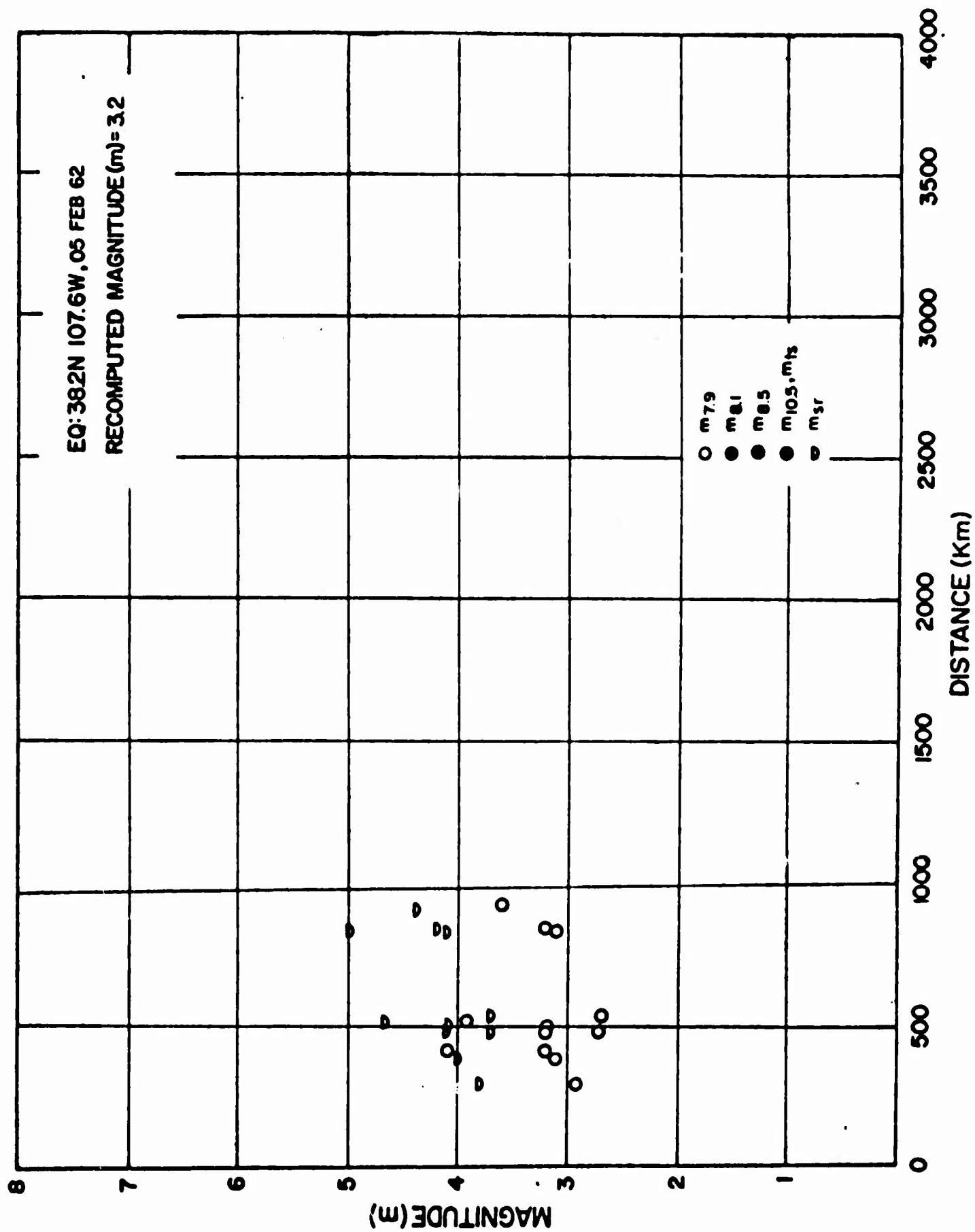


Figure 82
AFTAC/VSC

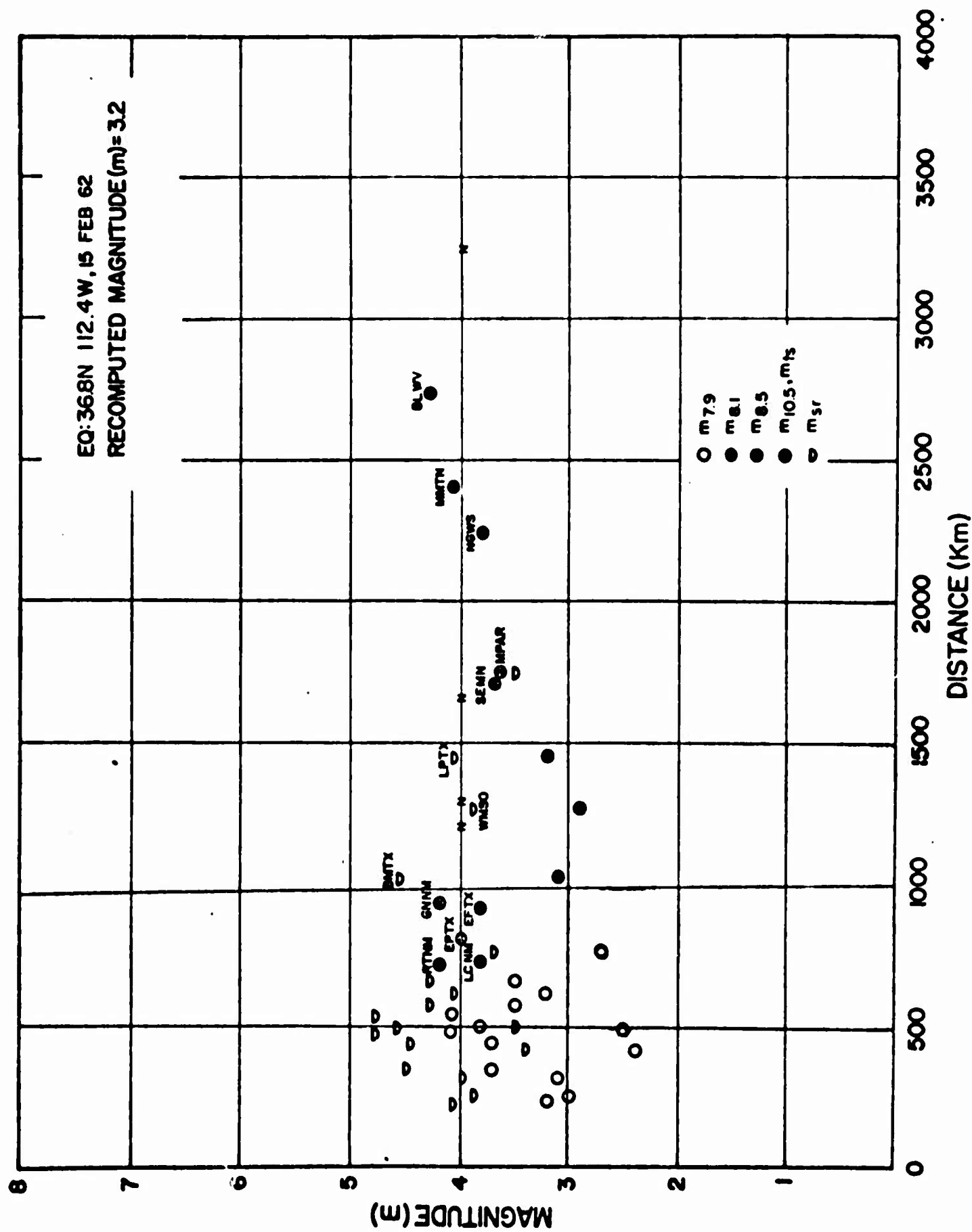
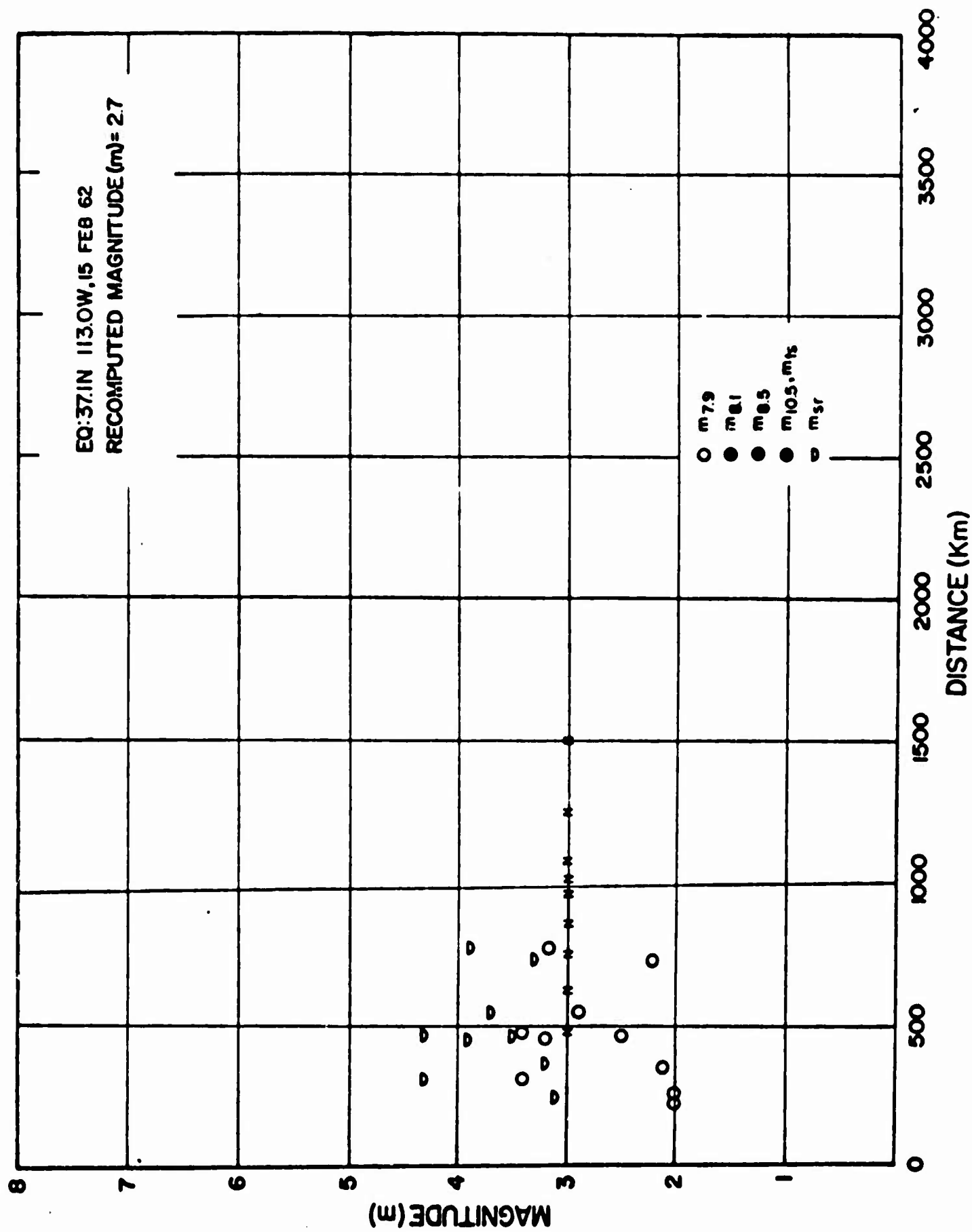


Figure 83
AFTAC/VSC



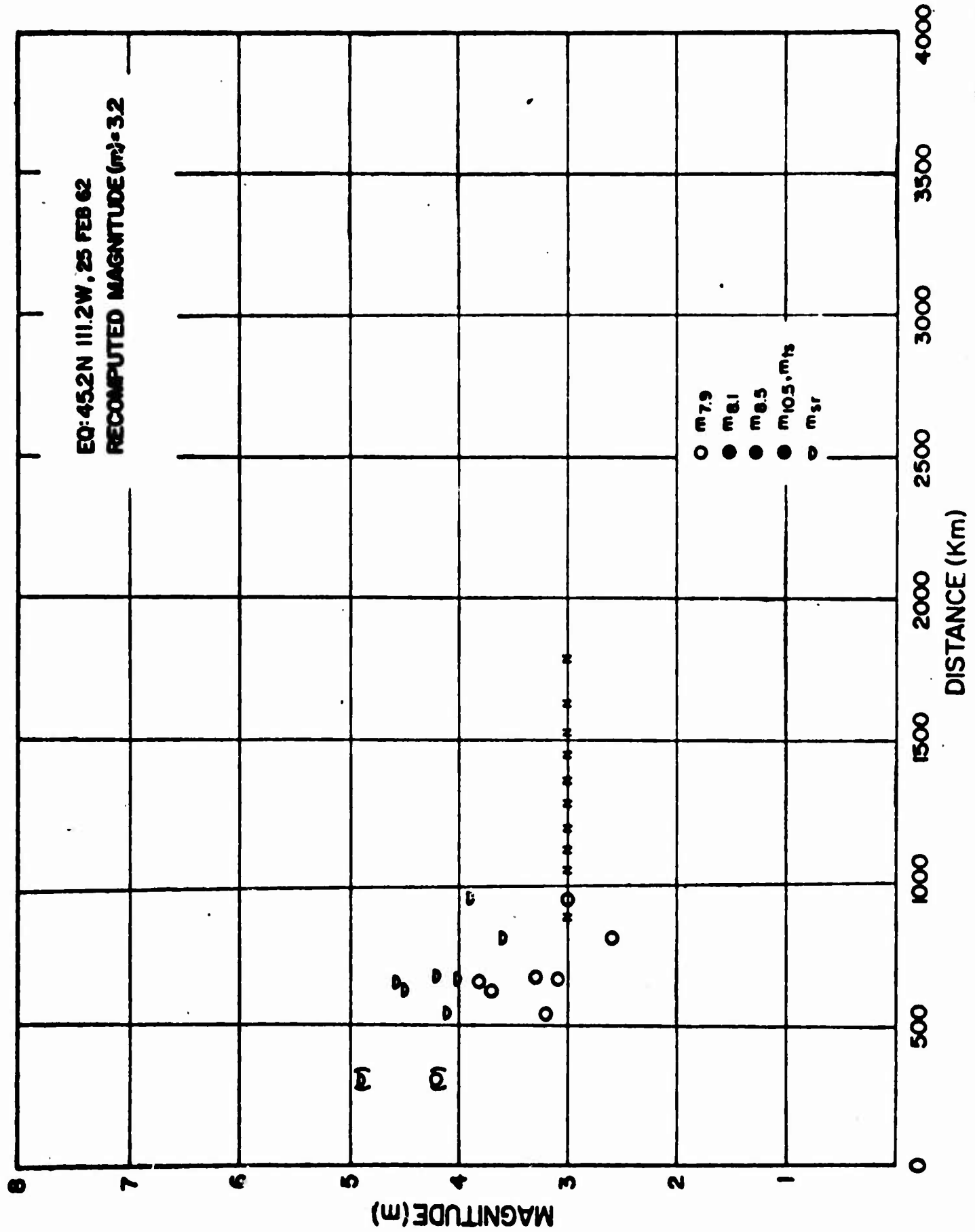
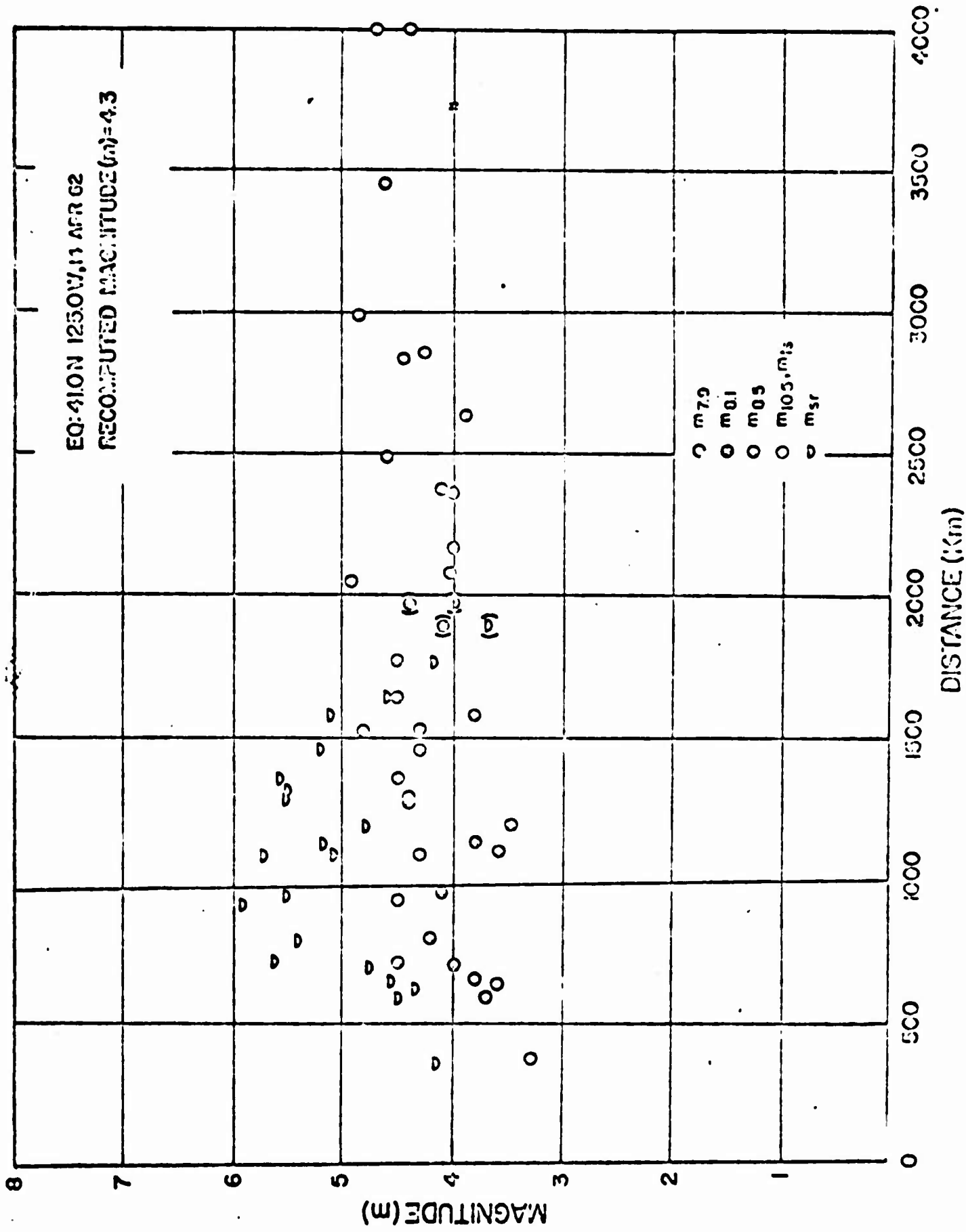


Figure 85
AFTAC/VSC



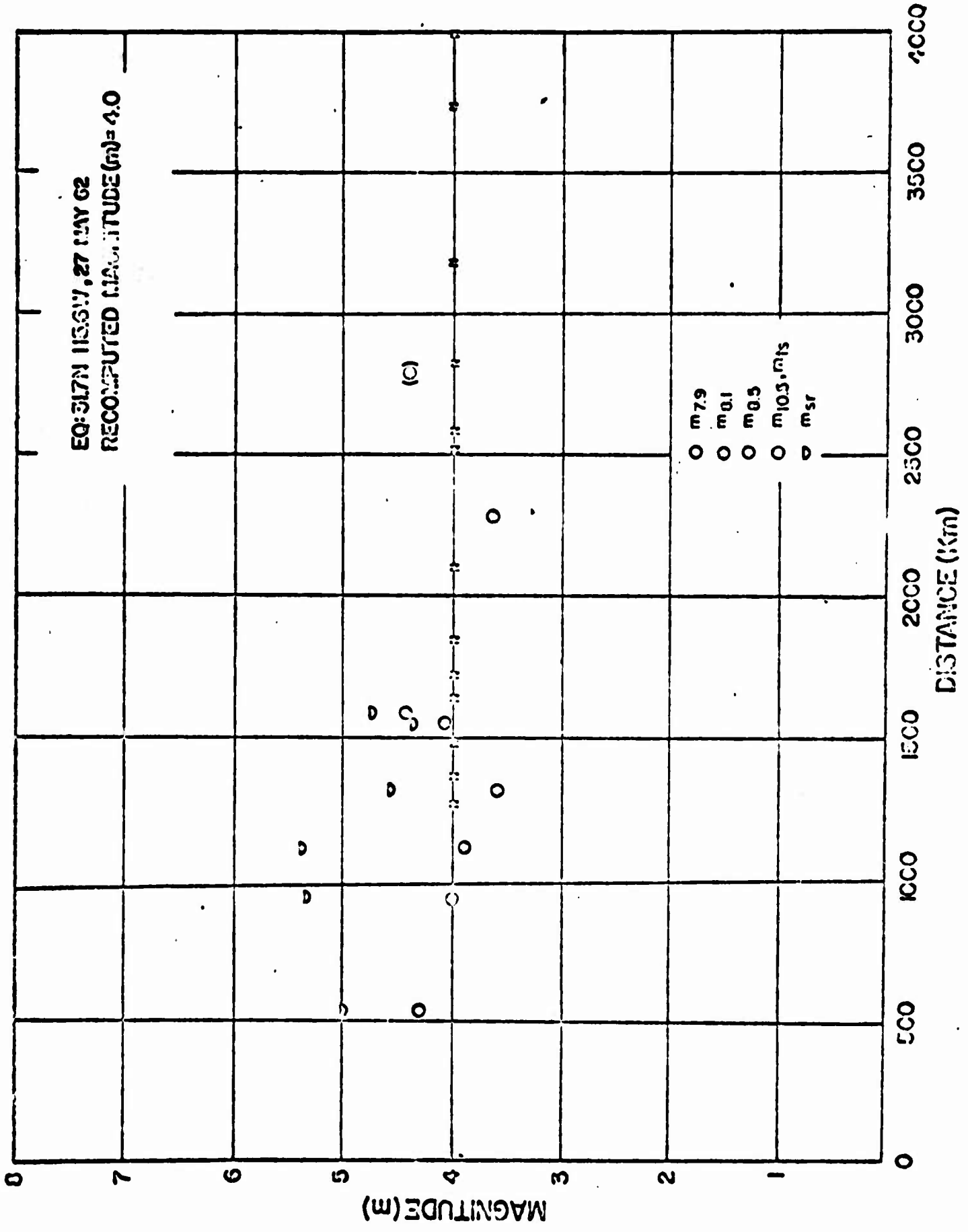
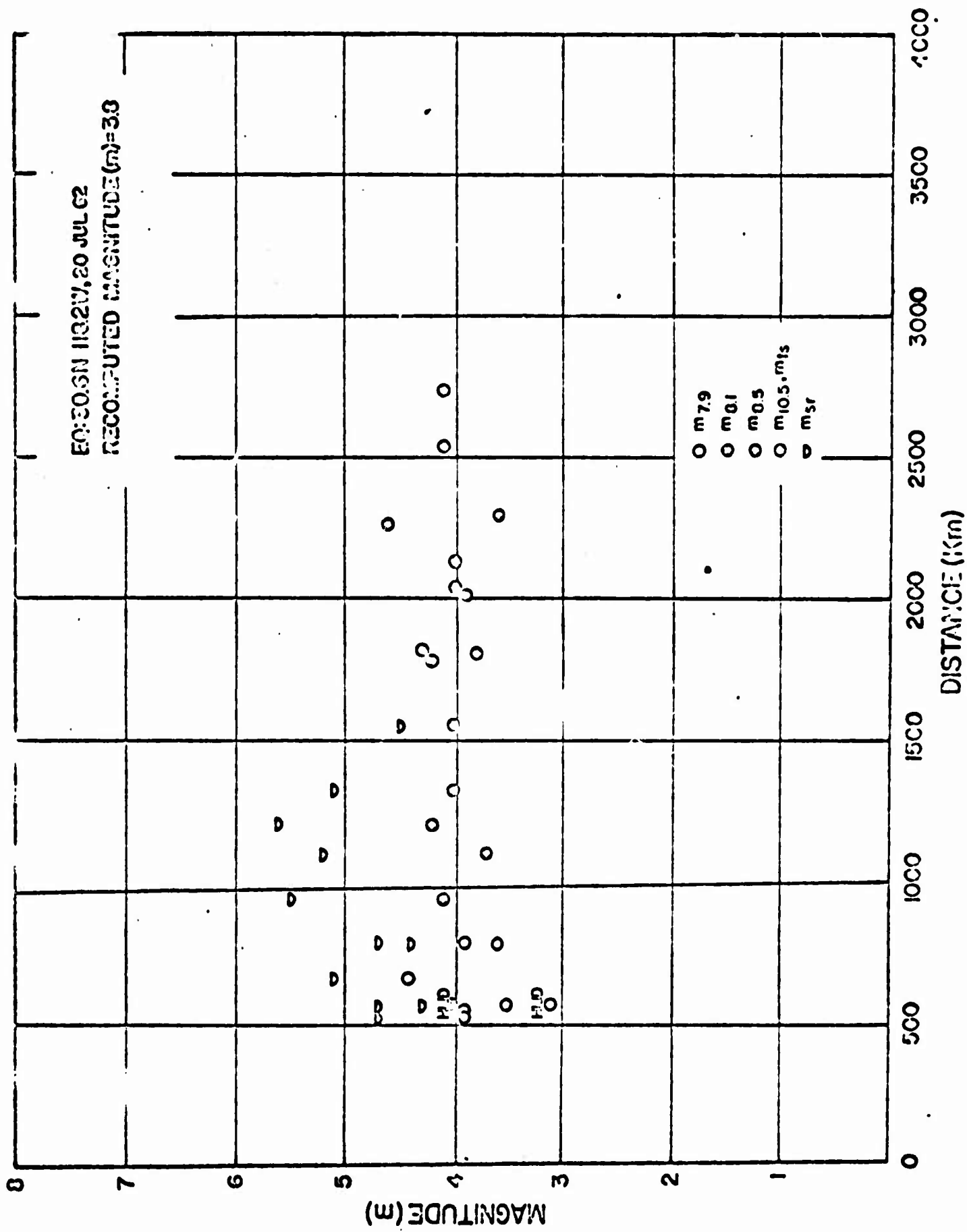


Figure 07
AFTAC/VSC



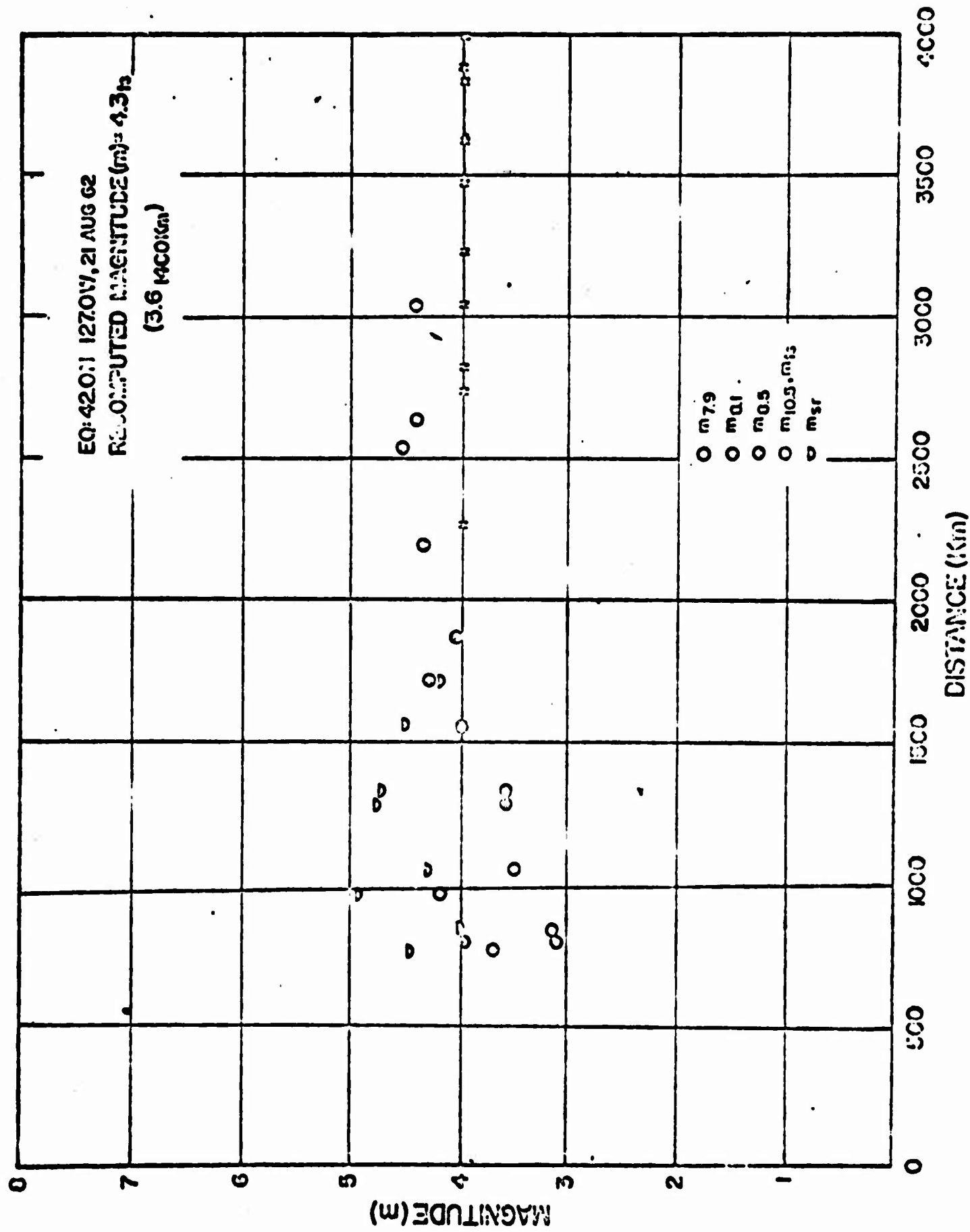


Figure C3
 AFTAC/VSC

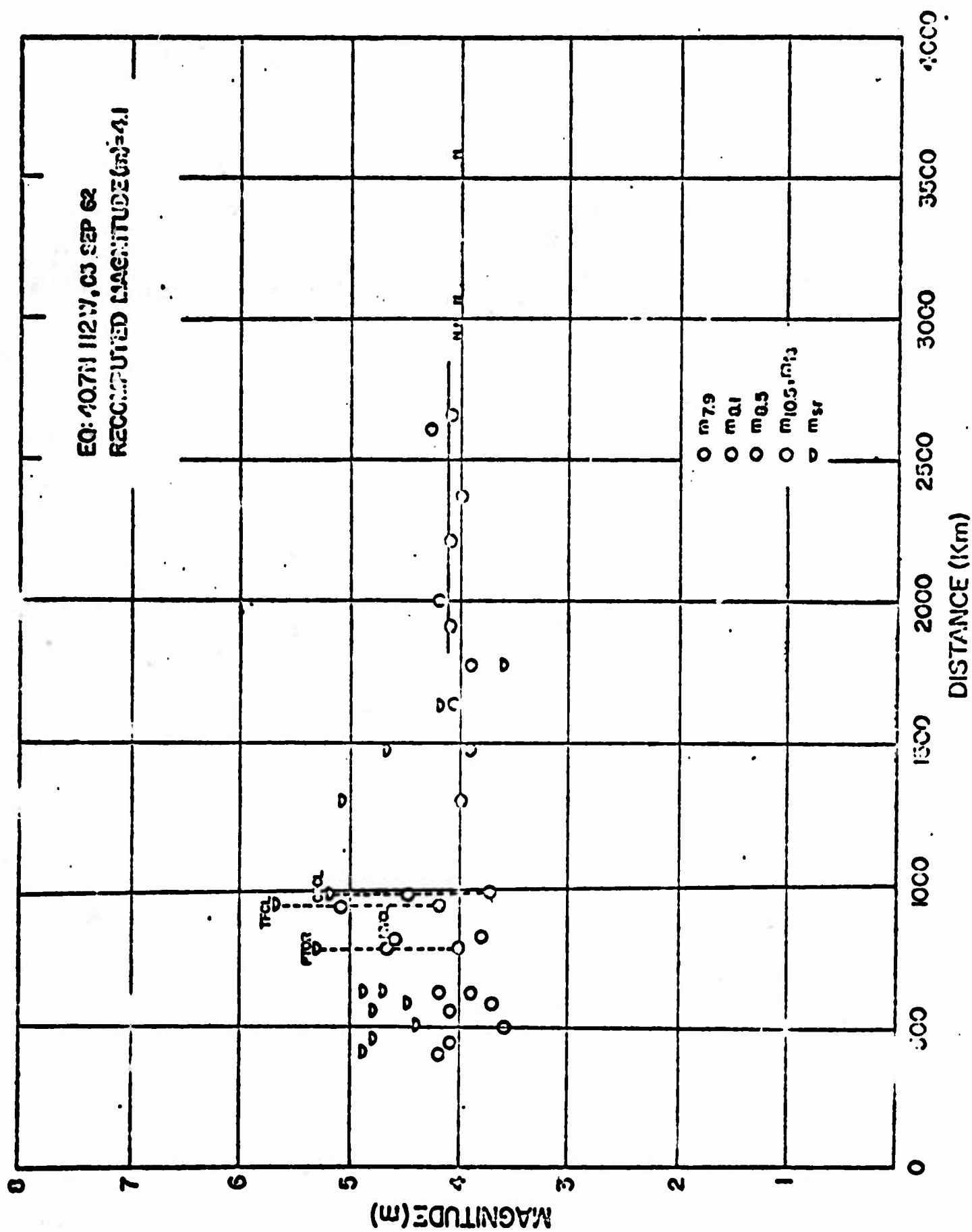


Figure 21
 AFTAC/VSC

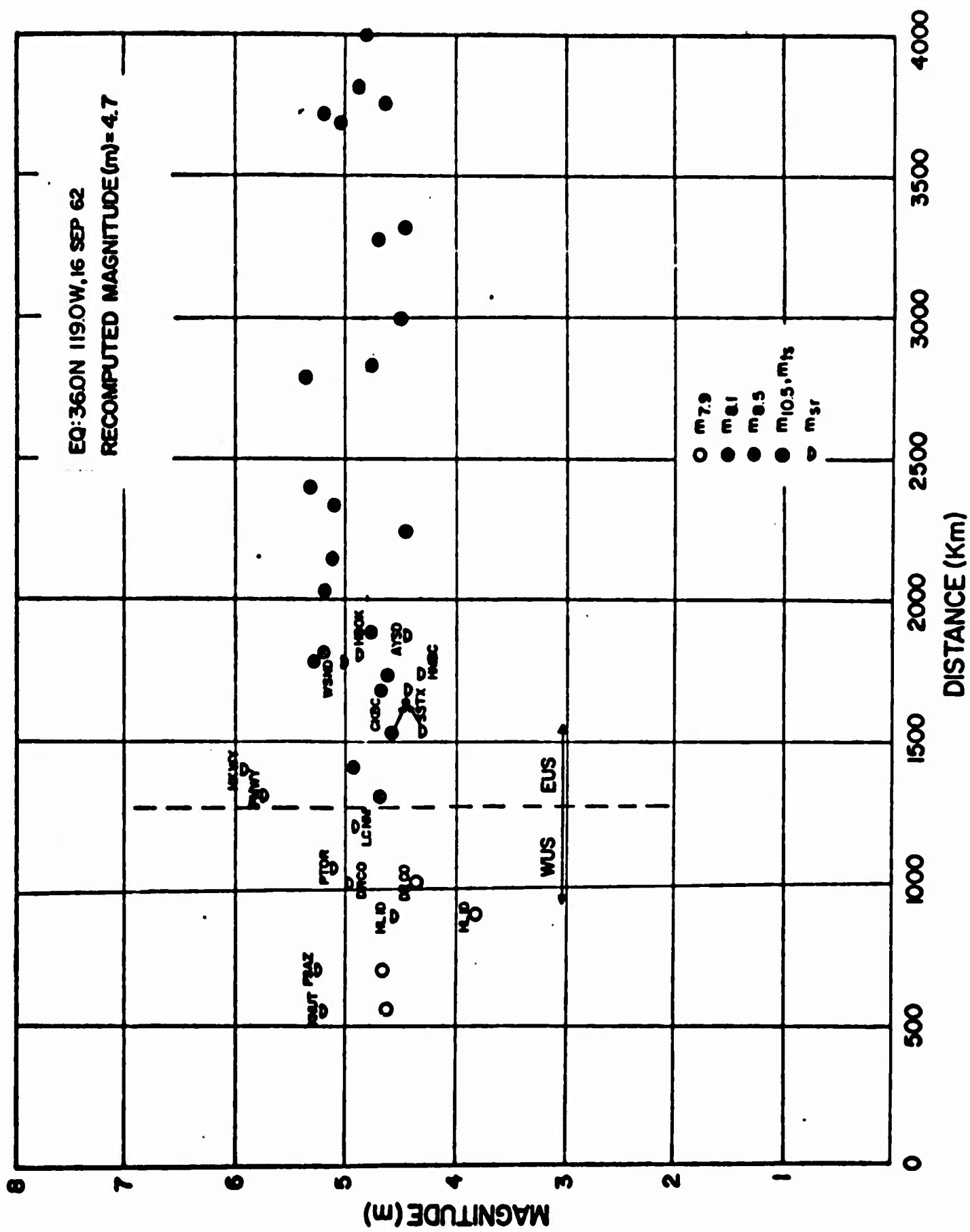


Figure 92
AFTAC/VSC

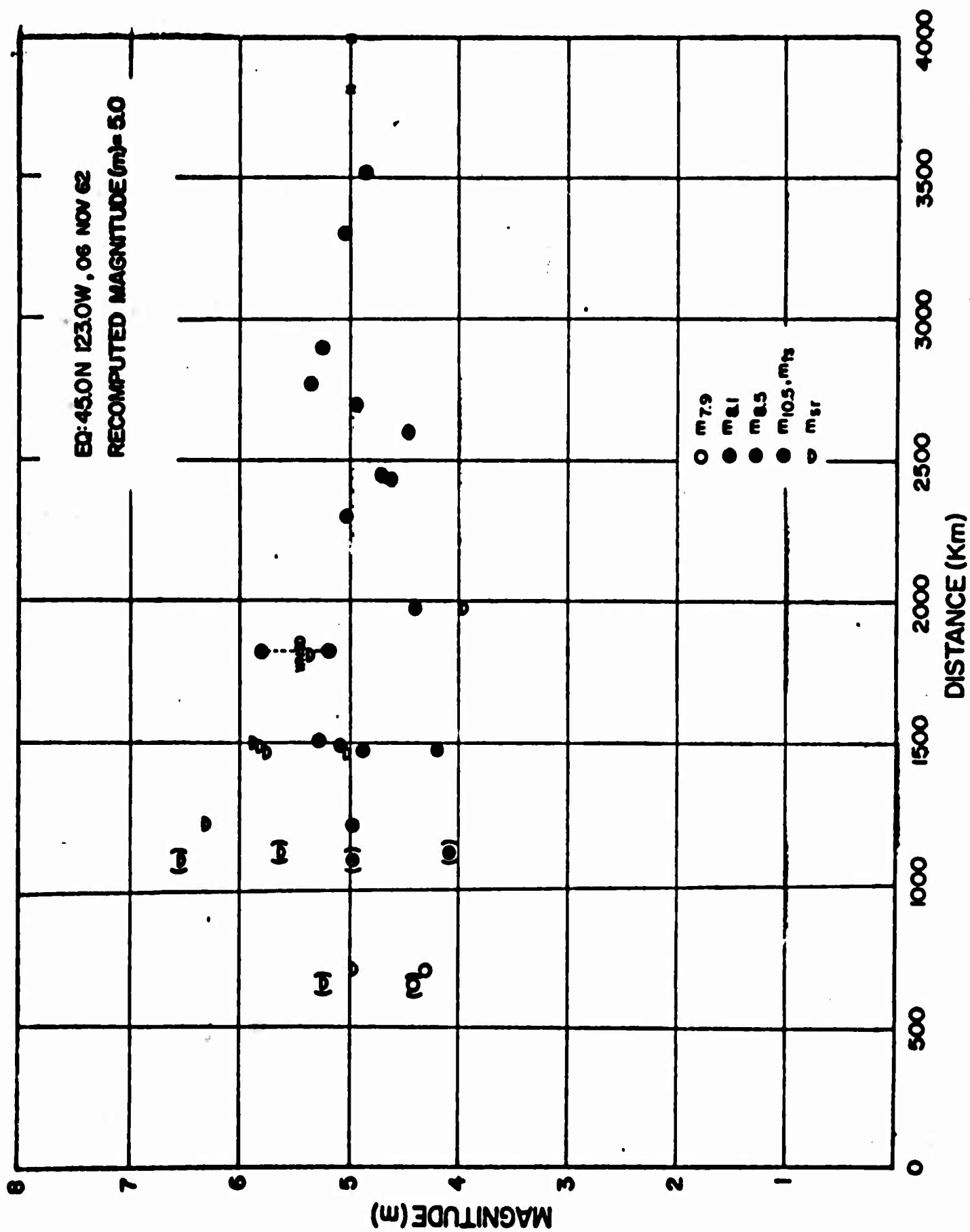


Figure 93
AFTAC/VSC

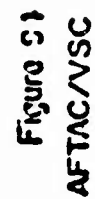


Figure S1
AFTAC/VSC

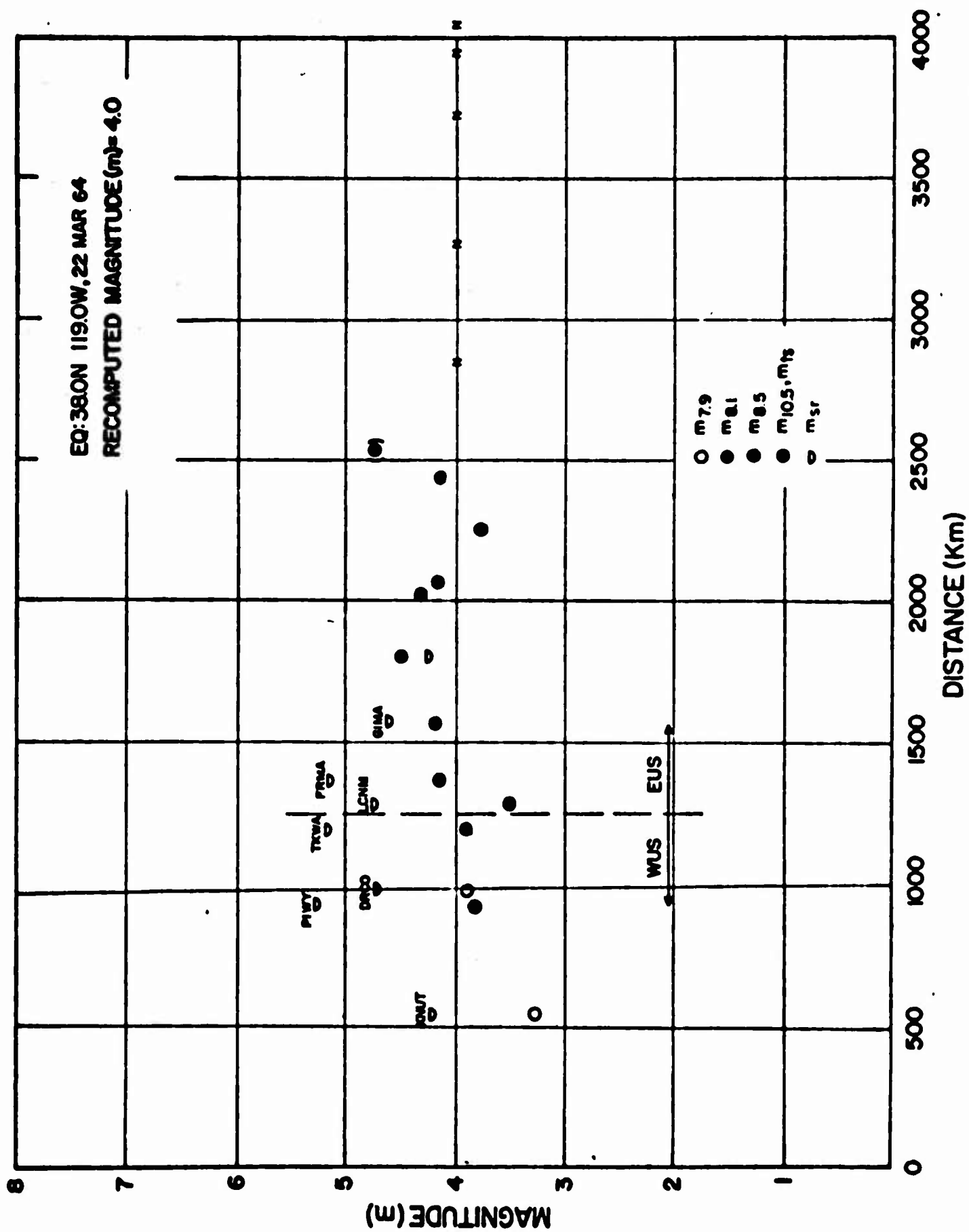
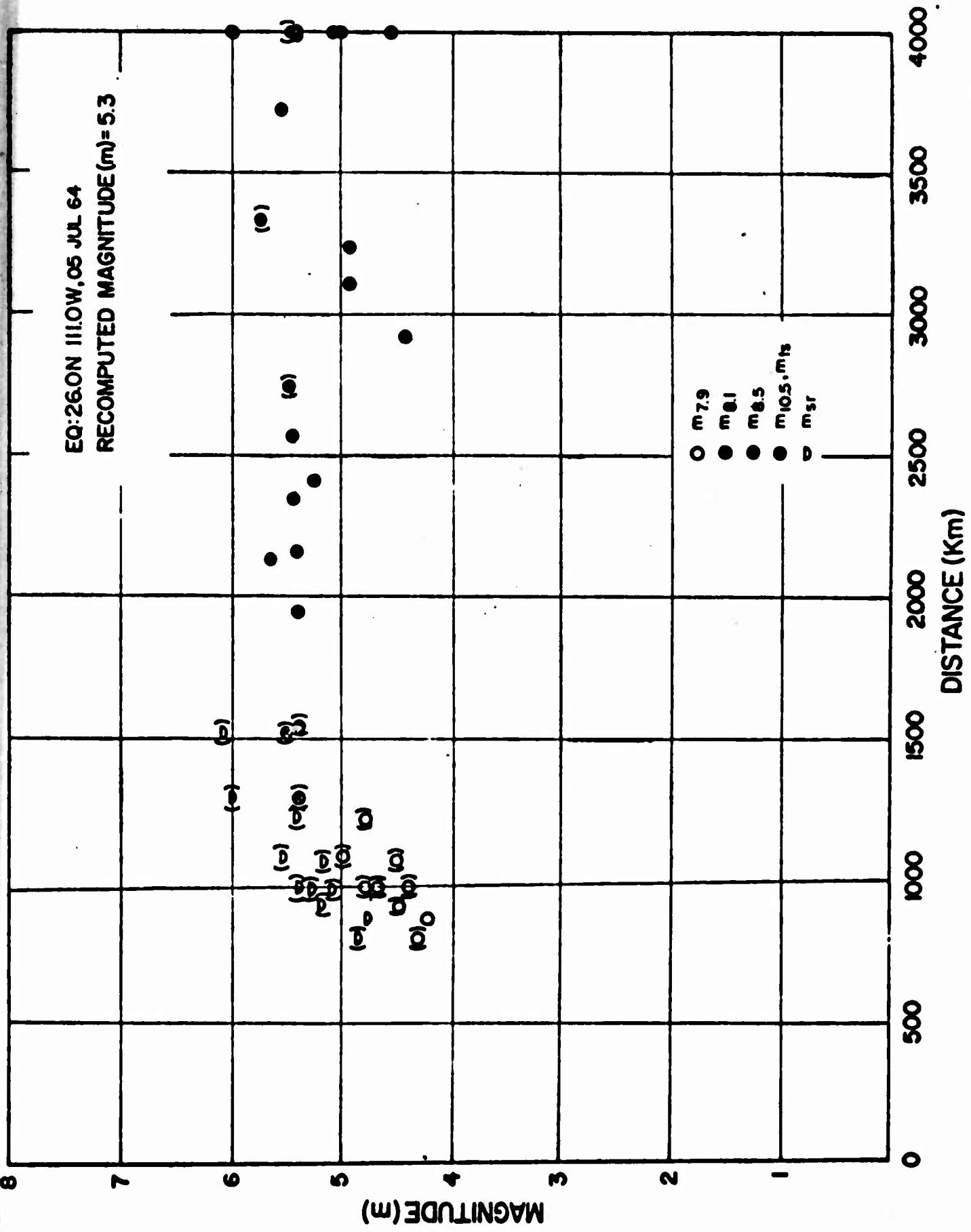


Figure 95
AFTAC/VSC



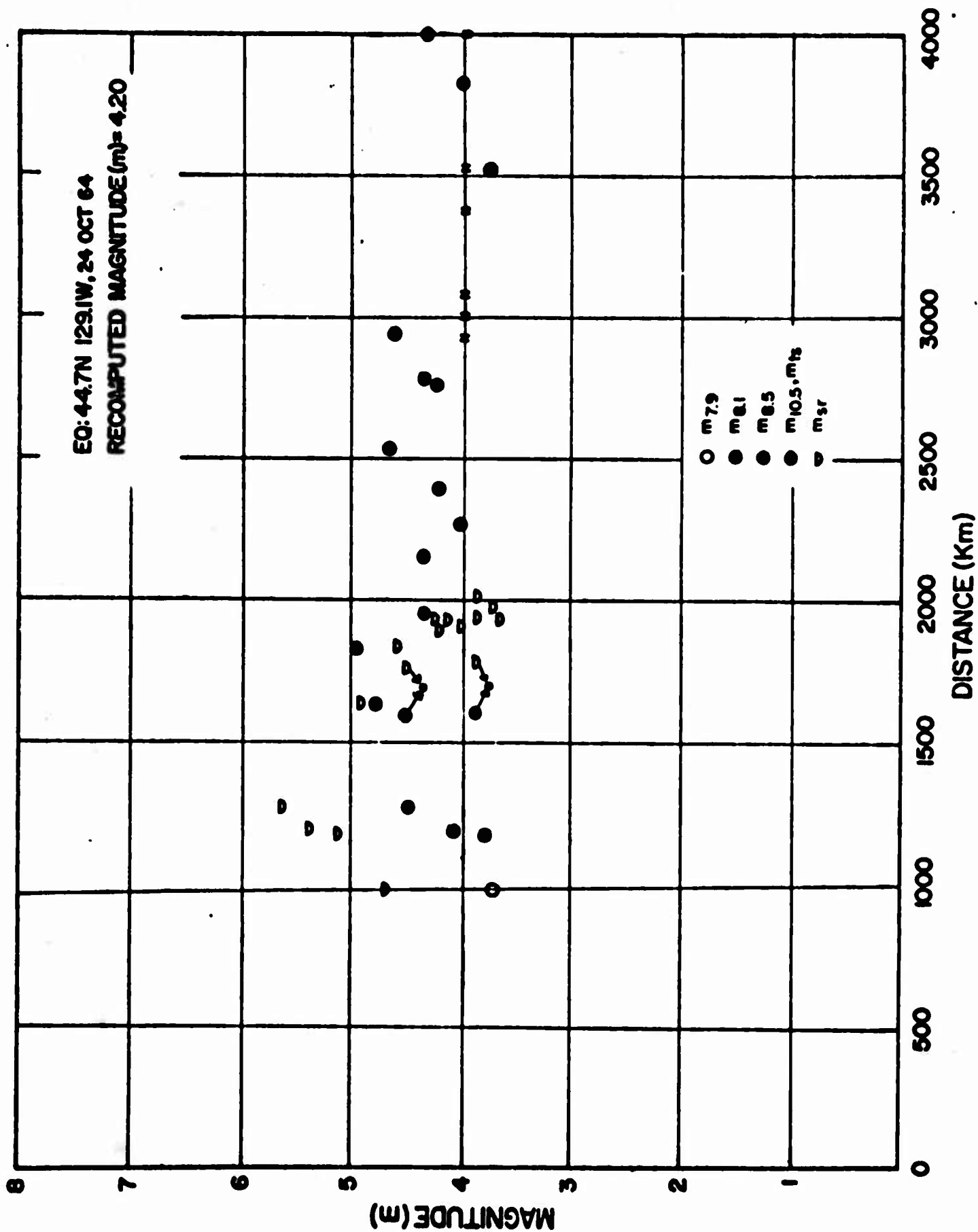


Figure 97
AFTAC/VSC

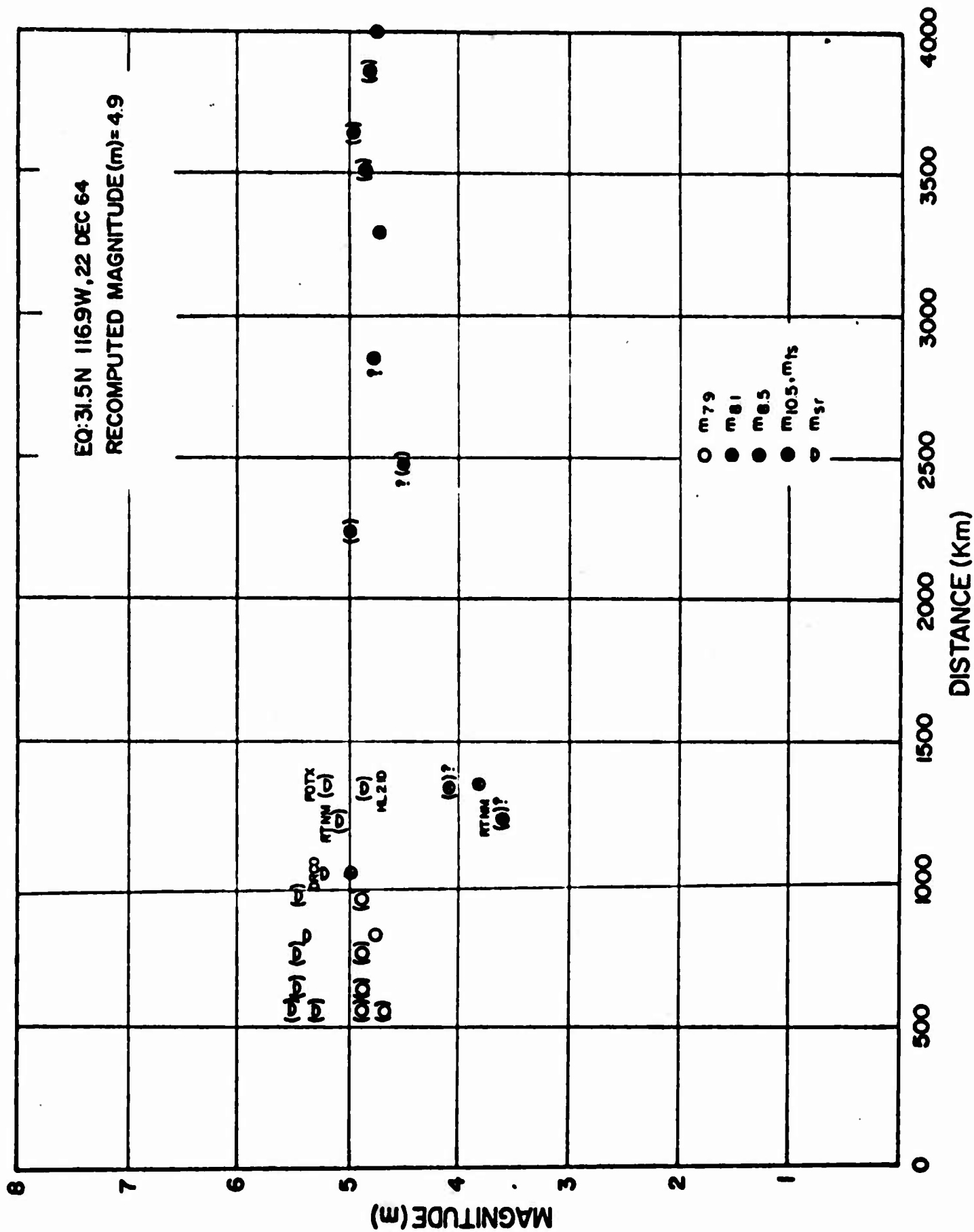


Figure 98
AFTAC/VSC

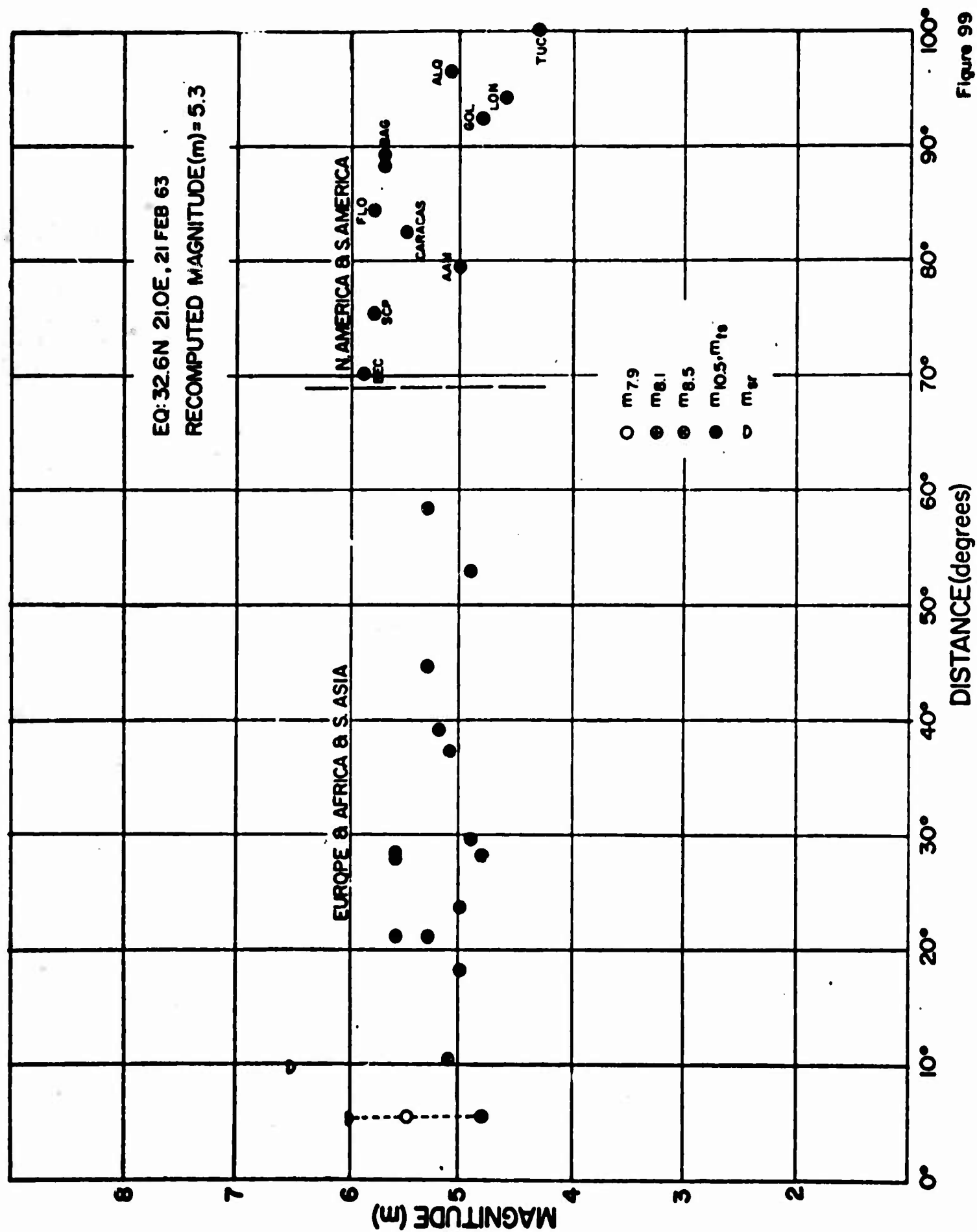


Figure 99
AFTAC/VSC



Figure 100
AFTAC/VSC

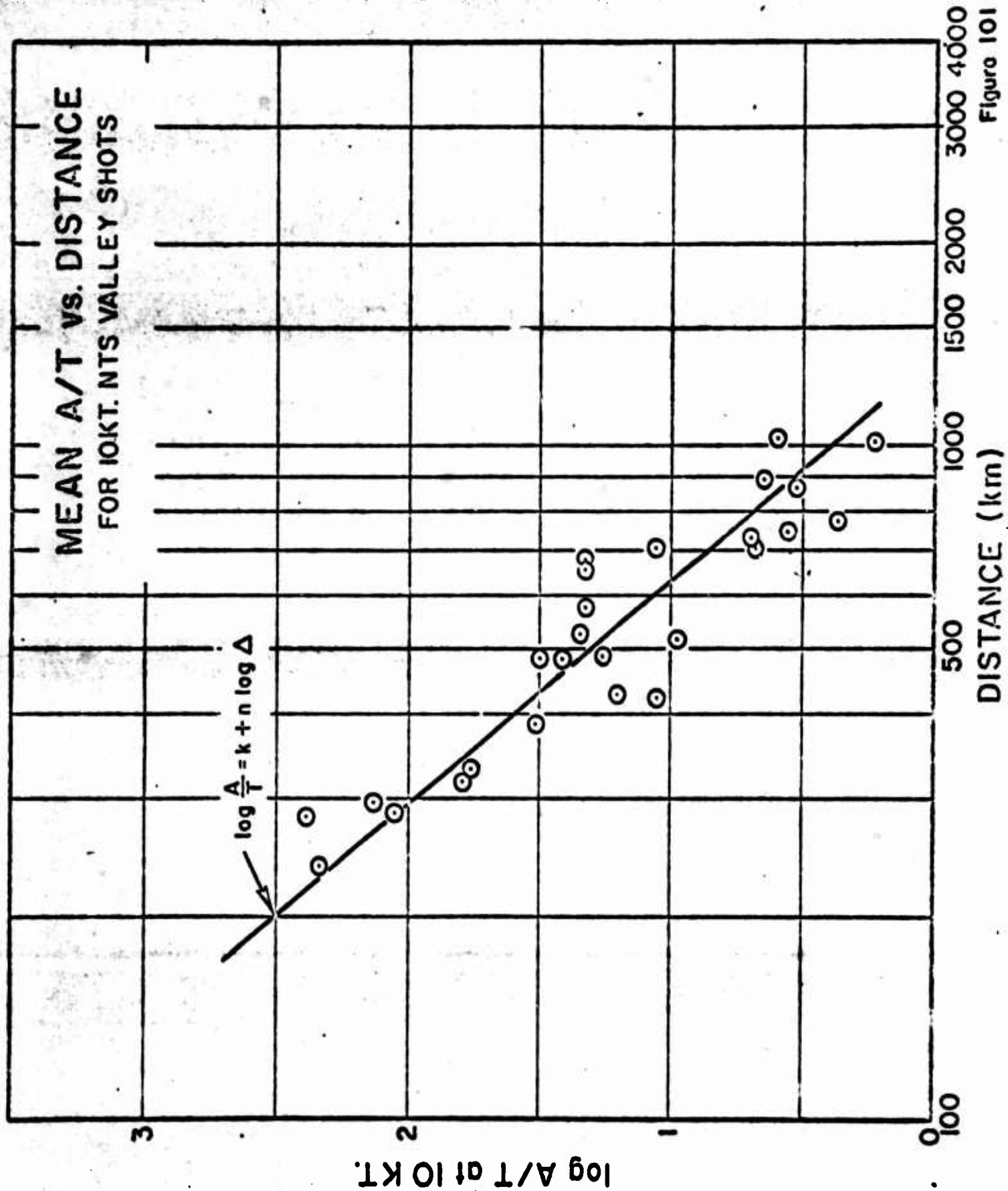
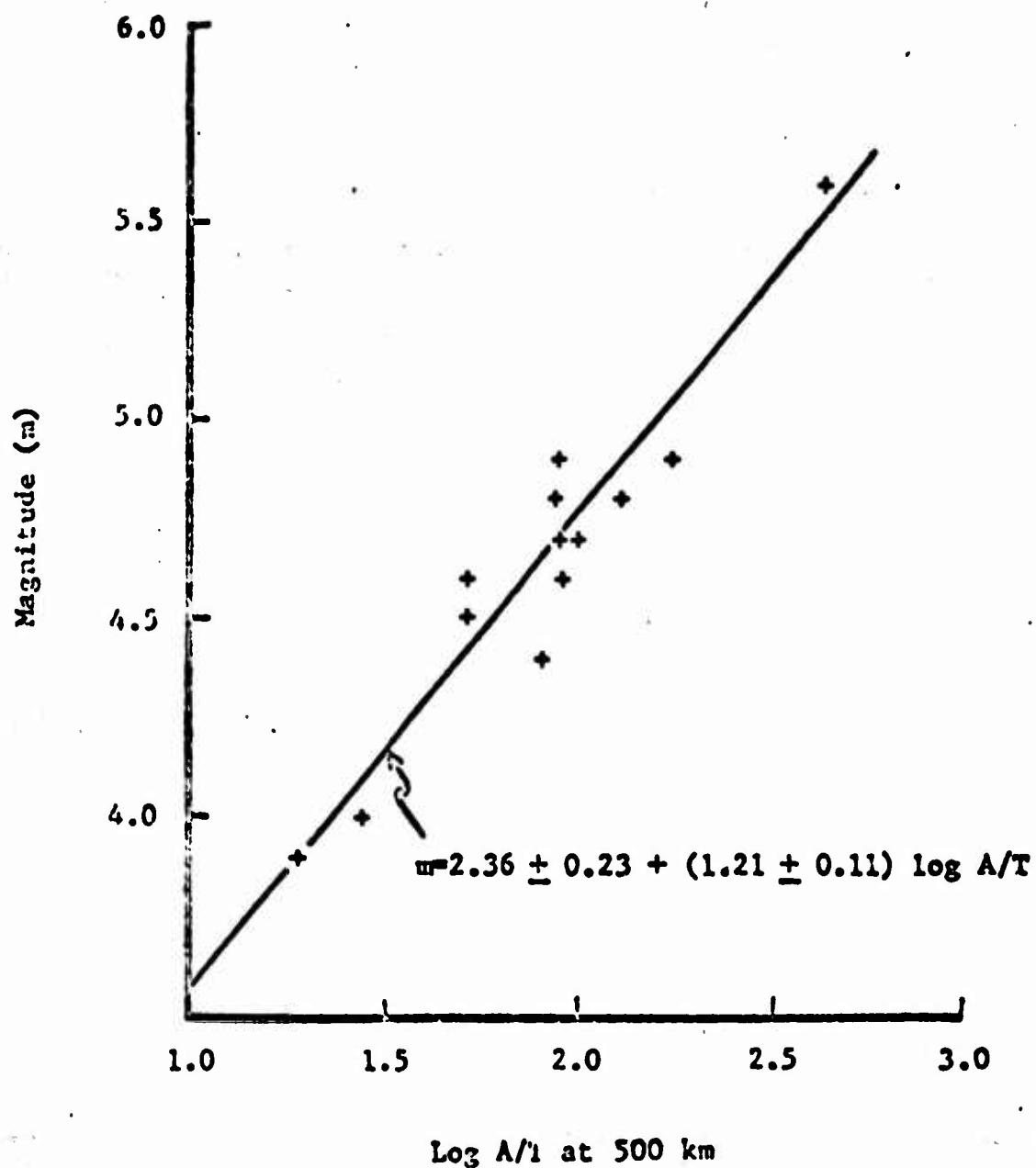


Figure 101

AFTAC/VSC



Magnitude from teleseismic stations (dist. $\geq 16^\circ$)
 versus logarithm of amplitude divided by period
 (A/T) at 500 km, based on nuclear explosions at
 the Nevada Test Site and SHOAL (Fallon, Nevada).

Figure 102
 AFTAC/VSC

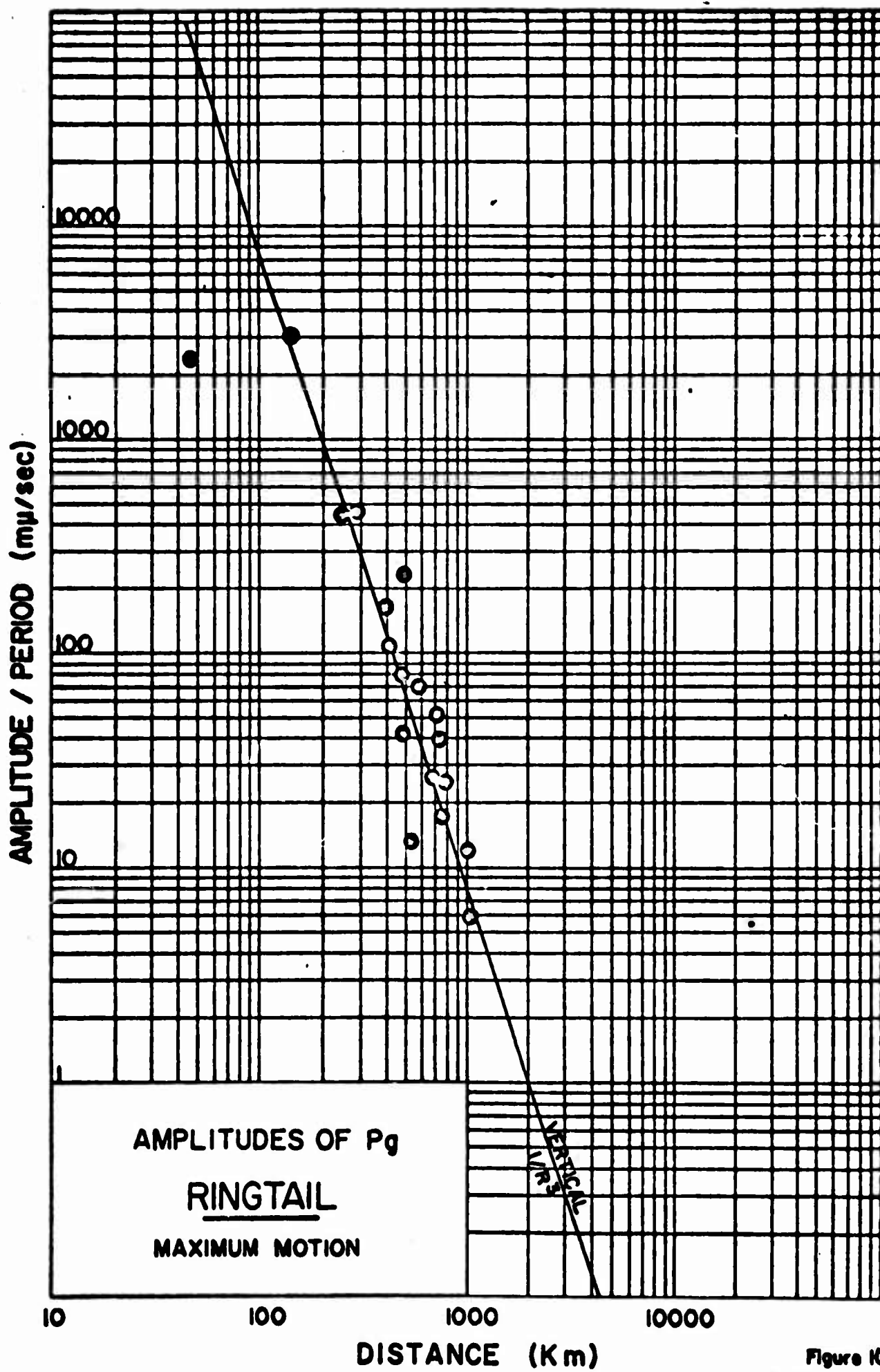


Figure 103
AFTAC/VSC

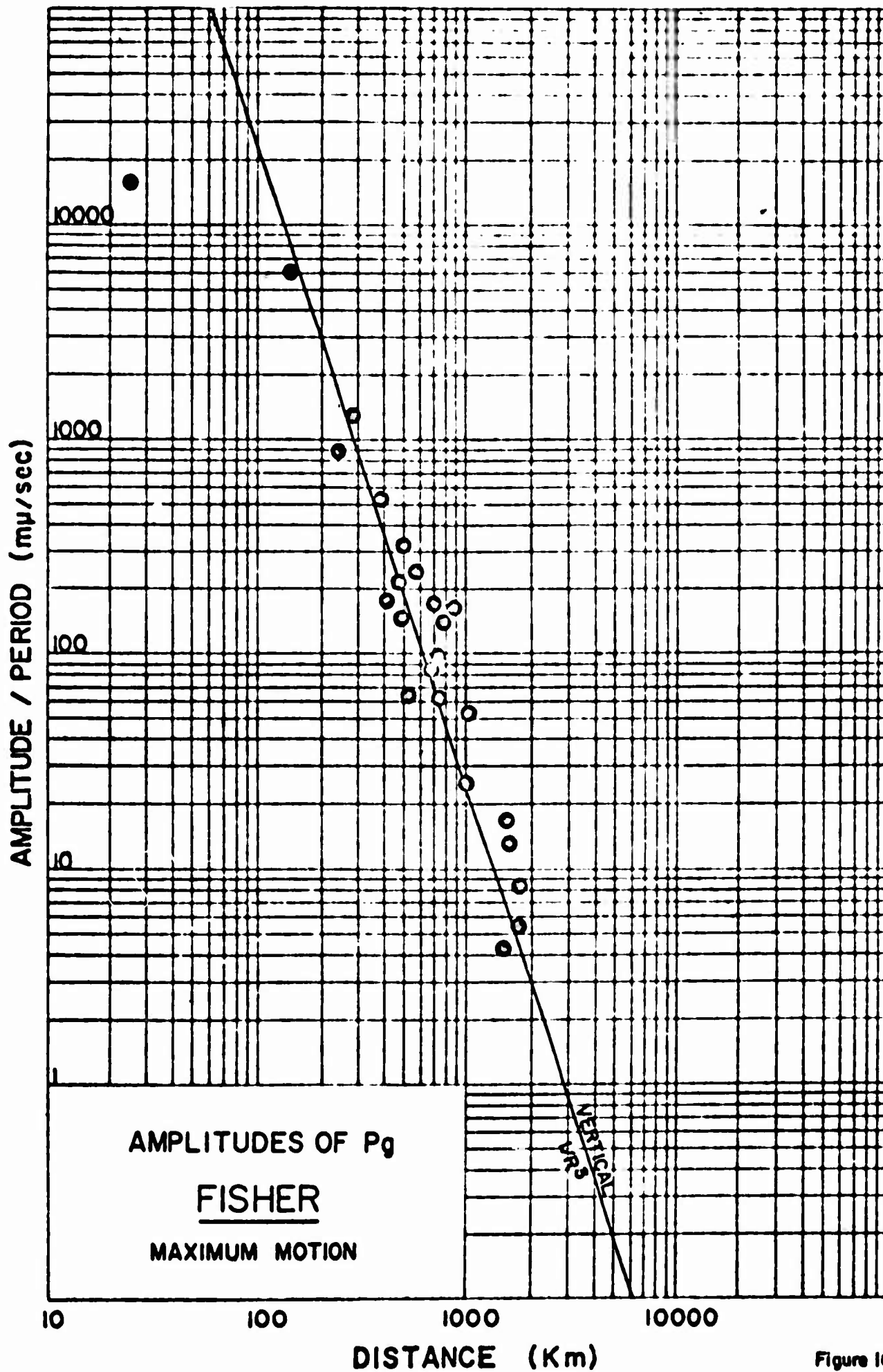


Figure 104
AFTAC/VSC

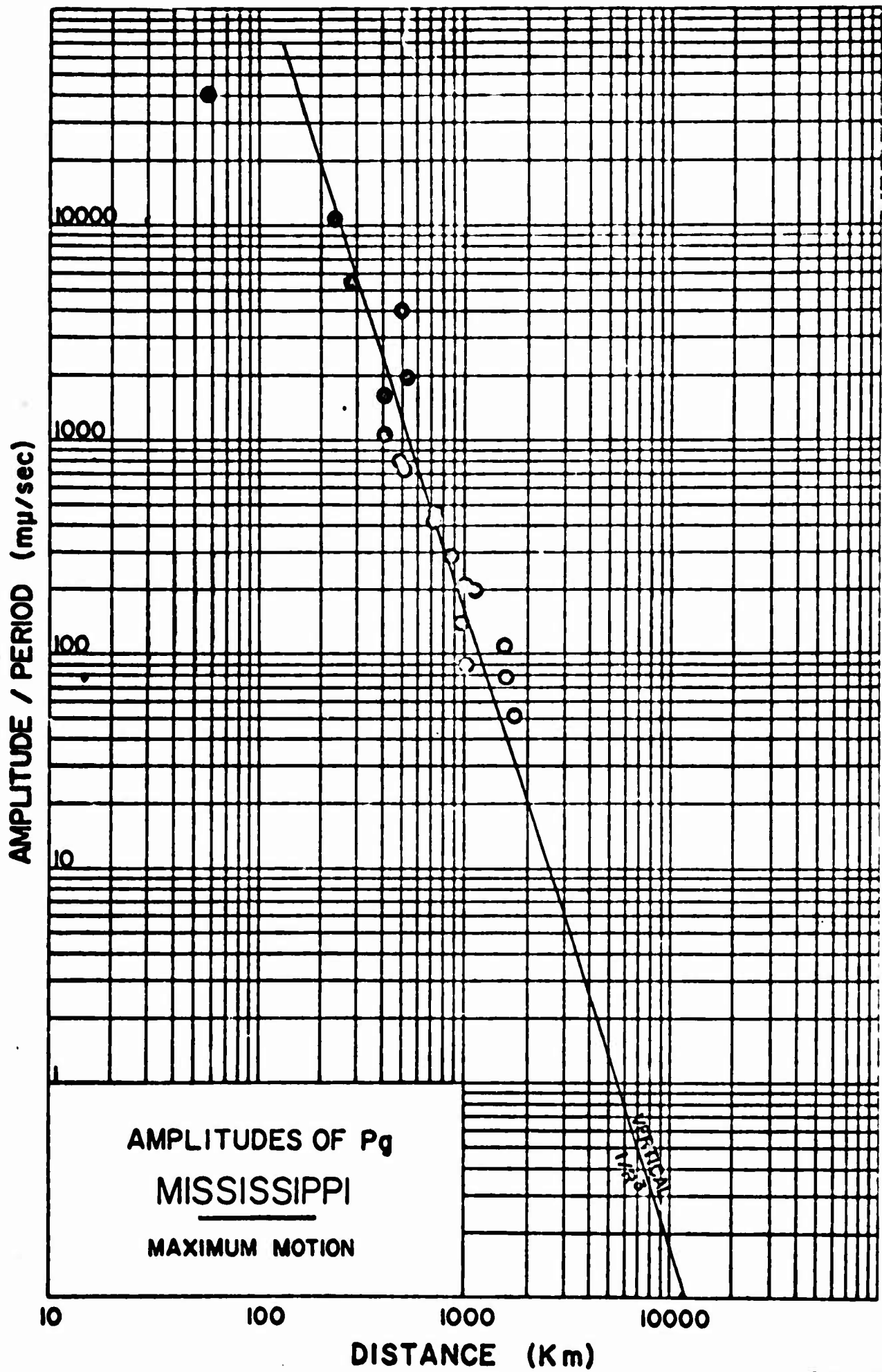


Figure 105
AFTAC/VSC

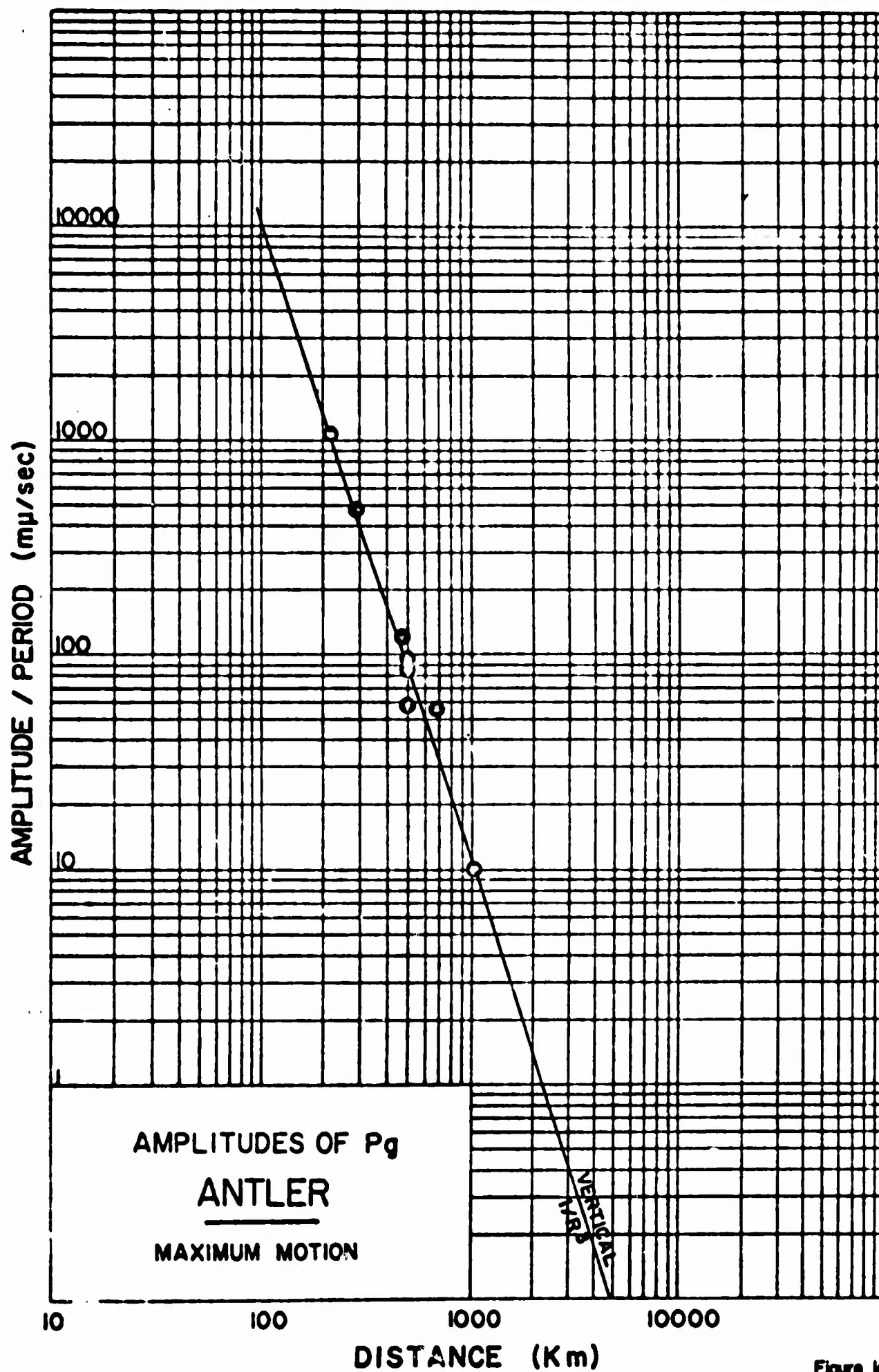


Figure 108
AFTAC/VSC

